

NASA CR-167973
PWA-5594-191



ENERGY EFFICIENT ENGINE

TURBINE INTERMEDIATE CASE AND LOW-PRESSURE TURBINE
COMPONENT TEST HARDWARE DETAILED DESIGN REPORT

by

K. Leach, R. Thulin and D. Howe

UNITED TECHNOLOGIES CORPORATION
Pratt & Whitney Aircraft Group
Commercial Products Division

Prepared for:

NATIONAL AERONAUTICS AND SPACE ADMINISTRATION

Lewis Research Center
Cleveland, OH 44135

Contract NAS3-20646 .

FOREWORD

The Energy Efficient Engine Component Development and Integration Program is being conducted under parallel National Aeronautics and Space Administration contracts to the Pratt & Whitney Aircraft Group, Commercial Products Division and the General Electric Company. The overall project is under the direction of Mr. Carl C. Ciepluch. Mr. John W. Schaefer is the NASA Assistant Project Manager for the Pratt & Whitney Aircraft effort under Contract NAS3-20646, and Mr. M. Vanco is the NASA Project Engineer responsible for the portion of the program described in this report. Mr. William B. Gardner is the Pratt & Whitney Aircraft Program Manager for the Energy Efficient Engine Program. This report was prepared by Mr. K. Leach, Mr. R. Thulin and Mr. D. Howe of Pratt & Whitney Aircraft.

TABLE OF CONTENTS

	<u>Page</u>
SECTION 1.0 SUMMARY	1
SECTION 2.0 INTRODUCTION	3
SECTION 3.0 DESIGN OVERVIEW	5
3.1 Turbine Intermediate Case and Low-Pressure Turbine Concepts	5
3.1.1 Turbine Intermediate Case	5
3.1.2 Low-Pressure Turbine	7
3.2 Predicted Performance	8
SECTION 4.0 INTERMEDIATE CASE AND LOW-PRESSURE TURBINE AERODYNAMIC DESIGN	11
4.1 Aerodynamic Design Parameters	11
4.2 Flowpath and Airfoil Cross Section Definition	12
4.2.1 Intermediate Case Flowpath	12
4.2.2 Intermediate Case Strut Fairing	14
4.2.3 Low-Pressure Turbine Flowpath	18
4.2.4 Turbine Airfoil Definition	20
4.3 Supporting Technology Programs	60
4.3.1 Introduction	60
4.3.2 Transition Duct Model Test Program	60
4.3.3 Low-Pressure Turbine Subsonic Cascade Technology Program	64
4.3.4 Low-Pressure Turbine Boundary Layer Program	68
4.4 Performance Status and Adjustment	81
SECTION 5.0 TURBINE THERMAL-MECHANICAL DESIGN	85
5.1 Mechanical Design Objectives and Goals	85
5.2 Turbine Mechanical Configuration	86
5.2.1 Turbine Rotor Assembly	87
5.2.1.1 Blades	88
5.2.1.1.1 Mechanical Design Features	88
5.2.1.1.2 Structural Analysis	92
5.2.1.2 Disk and Hub Assembly	103
5.2.1.2.1 Mechanical Design Features	103
5.2.1.2.2 Structural Analysis	104
5.2.1.3 Thrust Balance Seal	108
5.2.1.3.1 Mechanical Design Features	108
5.2.1.3.2 Structural Analysis	109
5.2.1.4 Inner Cavity Knife-Edge Seals	109
5.2.1.4.1 Mechanical Design Features	109
5.2.1.4.2 Structural Analysis	109
5.2.1.5 Rotor Shaft Assembly	109
5.2.1.5.1 Mechanical Design Features	109
5.2.1.5.2 Structural Analysis	112

TABLE OF CONTENTS (Cont'd)

5.2.2 Turbine Vane and Case Assembly	114
5.2.2.1 Vanes	114
5.2.2.1.1 Mechanical Design Features	114
5.2.2.1.2 Structural Analysis	120
5.2.2.2 Vane Cases	125
5.2.2.2.1 Mechanical Design Features	125
5.2.2.2.2 Structural Analysis	127
5.2.2.3 Turbine Exhaust Case	132
5.2.2.3.1 Mechanical Design Features	132
5.2.2.3.2 Structural Analysis	132
5.2.2.4 Low-Pressure Turbine Active Clearance Control System	134
5.2.2.4.1 Design Approach	134
5.2.2.4.2 Mechanical Design Features	134
5.2.2.4.3 Clearance Analysis	136
5.2.3 Turbine Intermediate Case	140
5.2.3.1 Mechanical Design Features	140
5.2.3.1.1 Structural Struts	142
5.2.3.1.2 Strut Fairings	144
5.2.3.1.3 Outer Case and Outer Case Heatshield	144
5.2.3.1.4 Engine Mount Lugs	146
5.2.3.1.5 Oil Supply and Scavenge Lines	147
5.2.3.1.6 Thrust Balance Seal Lands	148
5.2.3.2 Structural Analysis	149
5.2.3.2.1 Primary Support Structure Stress and Life Analysis	149
5.2.3.2.2 Strut Fairing Durability Analysis	155
5.2.3.2.3 Thrust Balance Seal Vibration Analysis	162
5.2.4 Low Rotor Critical Speed Analysis	162
5.2.5 Low-Pressure Turbine Secondary Flow System	166
5.2.5.1 System Description	166
5.2.5.2 Low-Pressure Turbine Rotor	167
5.2.5.3 Low-Pressure Turbine Case	175
5.2.5.4 Turbine Intermediate Case	180
5.2.6 Turbine System Weight Summary	187
SECTION 6.0 CONCLUDING REMARKS	189

TABLE OF CONTENTS (Cont'd)

APPENDIXES

APPENDIX A	NASTRAN Stress Analysis	193
APPENDIX B	Turbine Intermediate Case Strut Fairing Platform and Airfoil Deflection Contours	211
APPENDIX C	Turbine Intermediate Case Strut Fairing Airfoil Coordinates	217
APPENDIX D	Low-Pressure Turbine Vane and Blade Airfoil Coordinates	223
APPENDIX E	Low-Pressure Turbine Exit Guide Vane Airfoil Coordinates	263
LIST OF SYMBOLS		271
REFERENCES		275
DISTRIBUTION LIST		277

LIST OF ILLUSTRATIONS

<u>Number</u>	<u>Title</u>	<u>Page</u>
2-1	Program Schedule for Energy Efficient Engine Turbine Intermediate Case and Low-Pressure Turbine Design Efforts	4
3.1-1	Major Components in the Energy Efficient Engine Turbine Section	5
3.1.1-1	Cross-Sectional View of Turbine Intermediate Case	6
3.1.2-1	Cross-Sectional View of Low-Pressure Turbine Component	8
4.2.1-1	Turbine Intermediate Case Flowpath for the Integrated Core/Low Spool and the Preliminary Design Scaled to a 160,135 N (36,000 lbs) Thrust Size	12
4.2.1-2	Intermediate Case Wall Pressure Distribution Profiles, Showing the High Loading of Integrated Core/Low Spool Design	14
4.2.2-1	Incidence Range Capability as a Function of Pressure Loss, Showing Greater Range With 400 Series Foil	15
4.2.2-2	Fairing Aerodynamic Definition for Section 1 -- Integrated Core/Low Spool Intermediate Case	16
4.2.2-3	Fairing Aerodynamic Definition for Section 2 -- Integrated Core/Low Spool Intermediate Case	16
4.2.2-4	Fairing Aerodynamic Definition for Section 3 -- Integrated Core/Low Spool Intermediate Case	17
4.2.2-5	Fairing Aerodynamic Definition for Section 4 -- Integrated Core/Low Spool Intermediate Case	17
4.2.2-6	Strut Fairing Stacking Arrangement	18
4.2.3-1	Low-Pressure Turbine Flowpath	19
4.2.4-1	Effects of Controlled Vortexing Compared to Free Vortexing	23
4.2.4-2	Turbine Inlet Guide Vane Mean Section Aerodynamic Definition and Pressure Distribution	24

LIST OF ILLUSTRATIONS (Cont'd)

<u>Number</u>	<u>Title</u>	<u>Page</u>
4.2.4-3	Turbine Inlet Guide Vane Root and Tip Section Aerodynamic Definitions and Pressure Distributions	25
4.2.4-4	Turbine Second Stage Blade Root and One-Quarter Root Section Aerodynamic Definitions and Pressure Distributions	26
4.2.4-5	Turbine Second Stage Blade Mean Section Aerodynamic Definition and Pressure Distribution	27
4.2.4-6	Turbine Second Stage Blade Tip and One-Quarter Tip Section Aerodynamic Definitions and Pressure Distributions	28
4.2.4-7	Turbine Third Stage Vane Root and One-Quarter Root Section Aerodynamic Definitions and Pressure Distributions	29
4.2.4-8	Turbine Third Stage Vane Mean Section Aerodynamic Definition and Pressure Distribution	30
4.2.4-9	Turbine Third Stage Vane Tip and One-Quarter Tip Section Aerodynamic Definitions and Pressure Distributions	31
4.2.4-10	Turbine Third Stage Blade Root and One-Quarter Root Section Aerodynamic Definitions and Pressure Distributions	32
4.2.4-11	Turbine Third Stage Blade Mean Section Aerodynamic Definition and Pressure Distribution	33
4.2.4-12	Turbine Third Stage Blade Tip and One-Quarter Tip Section Aerodynamic Definitions and Pressure Distributions	34
4.2.4-13	Turbine Fourth Stage Vane Root and One-Quarter Root Section Aerodynamic Definitions and Pressure Distributions	35
4.2.4-14	Turbine Fourth Stage Vane Mean Section Aerodynamic Definition and Pressure Distribution	36
4.2.4-15	Turbine Fourth Stage Vane Tip and One-Quarter Tip Section Aerodynamic Definitions and Pressure Distributions	37

LIST OF ILLUSTRATIONS (Cont'd)

<u>Number</u>	<u>Title</u>	<u>Page</u>
4.2.4-16	Turbine Fourth Stage Blade Root and One-Quarter Root Section Aerodynamic Definitions and Pressure Distributions	38
4.2.4-17	Turbine Fourth Stage Blade Mean Section Aerodynamic Definition and Pressure Distribution	39
4.2.4-18	Turbine Fourth Stage Blade Tip and One-Quarter Tip Section Aerodynamic Definitions and Pressure Distributions	40
4.2.4-19	Turbine Fifth Stage Vane Root and One-Quarter Root Section Aerodynamic Definitions and Pressure Distributions	41
4.2.4-20	Turbine Fifth Stage Vane Mean Section Aerodynamic Definition and Pressure Distribution	42
4.2.4-21	Turbine Fifth Stage Vane Tip and One-Quarter Tip Section Aerodynamic Definitions and Pressure Distributions	43
4.2.4-22	Turbine Fifth Stage Blade Root and One-Quarter Root Section Aerodynamic Definitions and Pressure Distributions	44
4.2.4-23	Turbine Fifth Stage Blade Mean Section Aerodynamic Definition and Pressure Distribution	45
4.2.4-24	Turbine Fifth Stage Blade Tip and One-Quarter Tip Section Aerodynamic Definitions and Pressure Distributions	46
4.2.4-25	Second Stage Turbine Vane Stacking Arrangement	47
4.2.4-26	Second Stage Turbine Blade Stacking Arrangement	47
4.2.4-27	Third Stage Turbine Vane Stacking Arrangement	48
4.2.4-28	Third Stage Turbine Blade Stacking Arrangement	48
4.2.4-29	Fourth Stage Turbine Vane Stacking Arrangement	49
4.2.4-30	Fourth Stage Turbine Blade Stacking Arrangement	49
4.2.4-31	Fifth Stage Turbine Vane Stacking Arrangement	50

LIST OF ILLUSTRATIONS (Cont'd)

<u>Number</u>	<u>Title</u>	<u>Page</u>
4.2.4-32	Fifth Stage Turbine Blade Stacking Arrangement	50
4.2.4-33	Turbine Exit Guide Vane Flowpath for the Integrated Core/Low Spool	51
4.2.4-34	Turbine Exit Guide Vane Cascade Performance Test Results Under a Navy-Sponsored Program (Contract N00019-77-C-0546).	53
4.2.4-35	Turbine Exit Guide Vane Cascade Performance Test Results Under a Navy-Sponsored Program (Contract N00019-77-C-0546).	54
4.2.4-36	Turbine Exit Guide Vane Root Section Aerodynamic Definition and Pressure Distribution	55
4.2.4-37	Turbine Exit Guide Vane 25-Percent Span Section Aerodynamic Definition and Pressure Distribution	56
4.2.4-38	Turbine Exit Guide Vane Mean Section Aerodynamic Definition and Pressure Distribution	57
4.2.4-39	Turbine Exit Guide Vane 75-Percent Span Section Aerodynamic Definition and Pressure Distribution	58
4.2.4-40	Turbine Exit Guide Vane Tip Section Aerodynamic Definition and Pressure Distribution	59
4.2.4-41	Turbine Exit Guide Vane Stacking Arrangement	59
4.3.2-1	Rig Inlet Mass-Averaged Air Angle Spanwise Data	61
4.3.2-2	Strut Exit Mass-Averaged Air Angle Spanwise Data	62
4.3.2-3	Low-Pressure Turbine Inlet Guide Vane Exit Mass-Averaged Air Angle Spanwise Data	62
4.3.2-4	Outer Wall Loading Profile	63
4.3.2-5	Inner Wall Loading Profile	63
4.3.3-1	Loss Versus Incidence for the Low Camber Vane	64
4.3.3-2	Aft-Loaded Transonic Versus Squared-Off Subsonic Airfoil Profiles and Pressure Distributions	66

LIST OF ILLUSTRATIONS (Cont'd)

<u>Number</u>	<u>Title</u>	<u>Page</u>
4.3.3-3	Aft-Loaded Transonic Versus Squared-Off Subsonic Airfoils Predicted Versus Measured Profile Loss Data	67
4.3.3-4	Aft-Loaded Transonic Versus Squared-Off Subsonic Airfoils Predicted Versus Mass-Averaged, Mixed-Out, Mid-Span Losses.	67
4.3.3-5	Aft-Loaded, Heavyweight, Lightweight -- Predicted Versus Profile Loss Over Range of Incidence, Fixed Exit Mach Number (0.72)	69
4.3.3-6	Aft-Loaded, Heavyweight, Lightweight -- Predicted Versus Measured Mass-Averaged Mid-Span Profile Loss at Design Point Incidence, Variable Exit Mach Numbers	69
4.3.4-1	Turbulent Boundary Layer Velocity Profiles Using Dimensionless Parameters	70
4.3.4-2	Comparison of Measured Integral Parameters for the Squared-Off Test Section With Theoretical Predictions	72
4.3.4-3	Comparison of Measured Mean Velocity Profile data (Squared-Off) With Theoretical Predictions	73
4.3.4-4	Comparison of Measured Integral Parameters for the Aft-Loaded Test Section With Theoretical Predictions	74
4.3.4-5	Comparison of Measured Mean Velocity Profile data (Aft-Loaded) With Theoretical Predictions	75
4.3.4-6	Distribution of Boundary Layer Momentum Loss Thickness (Θ), Shape Factor (H), and Skin Friction (C_f)	76
4.3.4-7	Comparison of Measured Total Turbulence Intensity Profiles with Flat Plate Data	78
4.3.4-8	Distribution of Normalized Turbulence Intensity Components in the Fully Turbulent Region of the Squared-Off Test Configuration	78
4.3.4-9	Distribution of Normalized Turbulence Intensity Components in the Transitional Region of the Squared-Off Test Configuration	79

LIST OF ILLUSTRATIONS (Cont'd)

<u>Number</u>	<u>Title</u>	<u>Page</u>
4.3.4-10	Growth of Turbulence Intensity in the Laminar Region of Each Boundary Layer	80
5.2-1	Low-Pressure Turbine Component Mechanical Configuration	86
5.2.1-1	Energy Efficient Engine Low-Pressure Turbine Rotor Assembly	87
5.2.1-2	Low-Pressure Turbine Blade General Characteristics	89
5.2.1-3	Blade-to-Disk Attachment Design Details	90
5.2.1-4	Tip Shroud Design Details	91
5.2.1-5	Low-Pressure Turbine Second Stage Rotor Resonance Diagram	93
5.2.1-6	Low-Pressure Turbine Third Stage Rotor Resonance Diagram	93
5.2.1-7	Low-Pressure Turbine Fourth Stage Rotor Resonance Diagram	94
5.2.1-8	Low-Pressure Turbine Fifth Stage Rotor Resonance Diagram	94
5.2.1-9	Low-Pressure Turbine Fifth Stage Rotor Resonance Diagram Titanium-Aluminum Alloy Blade	95
5.2.1-10	Shrouded Turbine Blade Flutter Analysis	95
5.2.1-11	Second Stage Blade Durability Design Conditions and Calculated Stress (Blade material: PWA 1447, Coating: PWA 73)	97
5.2.1-12	Third Stage Blade Durability Design Conditions and Calculated Stress (Blade material: PWA 655; No coating)	98
5.2.1-13	Fourth Stage Blade Durability Design Conditions and Calculated Stress (Blade material: PWA 655, No coating)	99
5.2.1-14	Fifth Stage Blade Durability Design Conditions and Calculated Stress (Blade material: PWA 655, No coating)	100
5.2.1-15	Energy Efficient Engine Second Blade Transient Strains (Flight Propulsion System)	102

LIST OF ILLUSTRATIONS (Cont'd)

<u>Number</u>	<u>Title</u>	<u>Page</u>
5.2.1-16	Energy Efficient Engine Third Blade Transient Strains (Flight Propulsion System)	102
5.2.1-17	Low-Pressure Turbine Disk and Hub Assembly	103
5.2.1-18	Rotor Metal Temperature Distribution Used in Stress and Life Analysis	105
5.2.1-19	Rotor Stress Summary	106
5.2.1-20	Rotor Low Cycle Fatigue Life Summary	107
5.2.1-21	Low-Pressure Turbine Thrust Balance Seal Assembly	108
5.2.1-22	Low-Pressure Turbine Interstage Inner Cavity Knife-Edge Seals	110
5.2.1-23	Low Rotor Shaft Assembly	111
5.2.1-24	Low Rotor Shaft Front Temperature and Stress Summary	113
5.2.1-25	Low Rotor Shaft Rear Temperature and Stress Summary	113
5.2.2-1	Low-Pressure Turbine Vane and Case Assembly	115
5.2.2-2	Low-Pressure Turbine Vane General Characteristics	116
5.2.2-3	Attachment Scheme Utilized for Third, Fourth, and Fifth Stage Vanes	117
5.2.2-4	Second Vane Support Structure	117
5.2.2-5	Location of Second Vane Chordal Cuts Employed for Attachment Leakage Control	118
5.2.2-6	Low-Pressure Turbine Second Stage Vane Cluster	119
5.2.2-7	Typical Third, Fourth, and Fifth Stage Vane Cluster	119
5.2.2-8	Second Stage Vane Durability Design Conditions and Calculated Stress (Vane material: PWA 1480, Coating: PWA 73)	121
5.2.2-9	Third Stage Vane Durability Design Conditions and Calculated Stress (Vane material: PWA 1455, No coating)	122

LIST OF ILLUSTRATIONS (Cont'd)

<u>Number</u>	<u>Title</u>	<u>Page</u>
5.2.2-10	Fourth Stage Vane Durability Design Conditions and Calculated Stress (Vane material: PWA 655, No coating)	122
5.2.2-11	Fifth Stage Vane Durability Design Conditions and Calculated Stress (Vane material: PWA 655, No coating)	123
5.2.2-12	Energy Efficient Engine Second Vane Transient Strains	124
5.2.2-13	Energy Efficient Engine Third Vane Transient Strains	124
5.2.2-14	Low-Pressure Turbine Case Assembly	126
5.2.2-15	Typical Outer Airseal Configuration	128
5.2.2-16	Low-Pressure Turbine Case, Baffle and Cooling Manifold Materials Summary	129
5.2.2-17	Low-Pressure Turbine Case Temperature Summary at Sea Level Takeoff Hot Day Conditions	130
5.2.2-18	Low-Pressure Turbine Case Stress Summary	131
5.2.2-19	Flight Propulsion System Turbine Exhaust Case Assembly - Preliminary Design	133
5.2.2-20	Integrated Core/Low Spool Turbine Exhaust Case Assembly	133
5.2.2-21	Low-Pressure Turbine Case Active Clearance Control Features	135
5.2.2-22	Low-Pressure Turbine Case Modifications for Flight Propulsion System Active Clearance Control System	137
5.2.2-23	Typical Low-Pressure Turbine Rotor and Case Radial Growth Caused by Centrifugal Force, Thermals, and Pressure	137
5.2.3-1	Turbine Intermediate Case	141
5.2.3-2	Turbine Intermediate Case Structural Strut Details	142
5.2.3-3	Bearing Compartment Axial and Radial Maneuver and Inbalance Loads	143
5.2.3-4	Structural Strut-to-Torque Ring Weldment	143

LIST OF ILLUSTRATIONS (Cont'd)

<u>Number</u>	<u>Title</u>	<u>Page</u>
5.2.3-5	Turbine Intermediate Case Strut Fairing	145
5.2.3-6	Turbine Intermediate Case Outer Case and Outer Case Heatshield Details	145
5.2.3-7	Engine Rear Mount Details	146
5.2.3-8	Routing for Nos. 4-5 Bearing Compartment Oil Supply, Scavenge and Drain Lines	147
5.2.3-9	Turbine Intermediate Case Front and Rear Thrust Balance Seal Lands	148
5.2.3-10	Turbine Intermediate Case Structure Illustrating Complex Geometry	149
5.2.3-11	NASTRAN Model Used to Analyze Nonaxisymmetric Structural Loads	151
5.2.3-12	NASTRAN Model Used to Analyze Axisymmetric Loads	152
5.2.3-13	Bearing Load Diagram and Spring Rates Resulting from NASTRAN Analysis	153
5.2.3-14	Radial and Circumferential Deflections Caused by Thermal Gradients Between Strut and Cases	153
5.2.3-15	Axial Deflections Caused by Thermal Loads and Thrust Balance Pressure Loads	154
5.2.3-16	Location of Minimum Clearance Between Structural Strut and Aerodynamic Fairing	154
5.2.3-17	Structural Strut Stress and Life Summary for Flight Propulsion System and Intergrated Core/Low Spool	156
5.2.3-18	NASTRAN Model Utilized to Conduct Turbine Intermediate Case Strut Fairing Durability Analysis	157
5.2.3-19	Hot-Spot Temperature Profiles Utilized in Strut Fairing Durability Analysis	158
5.2.3-20	Flight Propulsion System Structural Analysis Summary	159
5.2.3-21	Intergrated Core/Low Spool Structural Analysis Summary	159

LIST OF ILLUSTRATIONS (Cont'd)

<u>Number</u>	<u>Title</u>	<u>Page</u>
5.2.3-22	Illustration of Flight Propulsion System Strut Fairing Transient Strain Calculation Procedure	160
5.2.3-23	Summary of Flight Propulsion System Strut Fairing Transient Strains at Maximum Stress Locations	161
5.2.4-1	Low Rotor Bearing Locations	163
5.2.4-2	Rotor-Frame Model Used for Critical Speed Analysis	164
5.2.4-3	Strain Energy Results from Component Preliminary Design Critical Speed Analysis	165
5.2.4-4	Increase in Low-Pressure Turbine Mode Strain Energy as Low Rotor Design Evolved	165
5.2.4-5	Effects on Fan, Low-Pressure Compressor and Shaft Mode Responses Due to the Addition of an Oil-Film Damper to the Number 5 Bearing	166
5.2.4-6	Illustration Showing Effectiveness of Damped Number 5 Bearing in Reducing Low-Pressure Turbine Mode Imbalance Response	167
5.2.4-7	Summary of Critical Speed Analysis Results for Integrated Core/Low Spool and Flight Propulsion System	168
5.2.4-8	Mode Shape for Integrated Core/Low Spool Low-Pressure Turbine Mode -- Damped Number 5 Bearings	168
5.2.4-9	Mode Shape for Integrated Core/Low Spool Fan Mode -- Damped Number 5 Bearing	169
5.2.4-10	Mode Shape for Integrated Core/Low Spool Shaft Mode -- Damped Number 5 Bearing	169
5.2.5-1	Low-Pressure Turbine Secondary Flow System	170
5.2.5-2	Pressure-Balanced Cooling Air Distribution System	172
5.2.5-3	A-Frame Rotor Construction Showing Turbine Rim Cooling Air Flow Distribution	173
5.2.5-4	Disk Rim and 'Wing' Support Structure Cooling Scheme	174

LIST OF ILLUSTRATIONS (Cont'd)

<u>Number</u>	<u>Title</u>	<u>Page</u>
5.2.5-5	Rotor Finite Element Model Showing Temperature Distribution at Steady-State Sea Level Takeoff Hot Day Engine Operating Conditions	174
5.2.5-6	Temperature Versus Time History at Selected Second Stage Low-Pressure Turbine Disk Locations During Severe Engine Power Excursions	176
5.2.5-7	Temperature Versus Time History at Selected Fourth Stage Low-Pressure Turbine Disk Locations During Severe Engine Power Excursions	176
5.2.5-8	Low-Pressure Turbine Case Cooling Flow Distribution System	177
5.2.5-9	Details of Case Hook Cooling Configuration	177
5.2.5-10	Cooling Flow Film Coefficient Variation as a Function of Inner Case-To-Baffle Gap Width	178
5.2.5-11	Comparison of Integrated Core/Low Spool and Flight Propulsion System Low-Pressure Turbine Case Cooling Airflow Distributions	179
5.2.5-12	Design Features Utilized to Thermally Isolate the Inner Case and Case Hooks from the Hot Gaspath	179
5.2.5-13	Case Finite Element Model Showing Temperature Distribution at Steady-State Sea Level Takeoff Hot Day Operating Conditions	181
5.2.5-14	Temperature Distribution at Low-Pressure Turbine Third Vane Attachment at Steady-State Sea Level Takeoff Hot Day Operating Conditions	182
5.2.5-15	Temperature Versus Time History at Selected Second Stage Low-Pressure Turbine Vane/Outer Airseal Locations During Severe Engine Power Excursions	182
5.2.5-16	Temperature Versus Time History at Selected Fourth Stage Low-Pressure Turbine Vane/Outer Airseal Locations During Severe Engine Power Excursions	183
5.2.5-17	Low-Pressure Turbine Second Stage Outer Airseal Radial Deflection with Active Clearance Control in Operation	183

LIST OF ILLUSTRATIONS (Cont'd)

<u>Number</u>	<u>Title</u>	<u>Page</u>
5.2.5-18	Low-Pressure Turbine Fourth Stage Outer Airseal Radial Deflection with Active Clearance Control in Operation	184
5.2.5-19	Turbine Intermediate Case Secondary Flow System	184
5.2.5-20	Integrated Core/Low Spool Turbine Intermediate Case Temperature Map at Sea Level Takeoff Engine Operating Conditions	185
5.2.5-21	Temperature-Time History for Turbine Intermediate Case Torque Box-To-Strut Case Support Structure During Temperature Excursions	186

LIST OF TABLES

<u>Table</u>	<u>Title</u>	<u>Page</u>
3.2-I	Goal Aerodynamic Efficiency	9
4.1-I	Turbine General Aerodynamics	11
4.2.1-I	Intermediate Case Geometry Comparison	13
4.2.2-I	Integrated Core/Low Spool Design	15
4.2..3-I	Airfoil Quantity by Stage	19
4.2.4-I	Low-Pressure Turbine Airfoil Design Summary	21
4.2.4-II	Gas Triangle Summary	22
4.2.4-III	Exit Guide Vane Characteristics	51
4.2.4-IV	Comparison of Navy Foil to Energy Efficient Engine	52
4.5-I	Goal Performance for Low-Pressure Turbine	82
4.5-II	Low-Pressure Turbine Efficiency Update	82
4.5-III	Detail Design Report Status Performance	84
5.1-I	Life Requirements for Major Turbine Subassemblies	85
5.2.1-I	Blade Attachment Stress Summary	96
5.2.1-II	Tip Shroud Stress Summary	96
5.2.1-III	Blade Airfoil Creep Strength Margins	101
5.2.1-IV	Summary of Predicted Blade Lives	101
5.2.1-V	Disk Structural Summary	104
5.2.2-I	Airfoil Stress Summary	120
5.2.2-II	Vane Airfoil Creep Strength Margins	123
5.2.2.-III	Summary of Predicted Vane Lives	125
5.2.2-IV	Case Thickness Requirements for Blade Containment	127
5.2.2-V	Predicted Tailplug Resonant Frequencies	132

LIST OF TABLES (Cont'd)

<u>Table</u>	<u>Title</u>	<u>Page</u>
5.2.2-VI	Active Clearance Control System Cooling Flow Management	138
5.2.2-VII	Energy Efficient Engine Low-Pressure Turbine Blade Tip Clearance Summary	138
5.2.2-VIII	Energy Efficient Engine Low-Pressure Turbine Interstage Seal Clearance Summary	139
5.2.2-IX	Energy Efficient Engine Low-Pressure Turbine Blade Tip Clearance Summary	139
5.2.2-X	Energy Efficient Engine Low-Pressure Turbine Interstage Seal Clearance Summary	140
5.2.3-I	Strut Bolt Stress Summary	157
5.2.3-II	Gas Environment Definition	158
5.2.3-III	Predicted Lives	161
5.2.6-I	Preliminary Weight Summary for Integrated Core/Low Spool Turbine Intermediate Case and Low-Pressure Turbine Component	187

SECTION 1.0 SUMMARY

A four stage low-pressure turbine component has been designed to power the fan and low-pressure compressor system for the Energy Efficient Engine. In conjunction with the low-pressure turbine definition, designs for a turbine intermediate case and an exit guide vane assembly have been also established.

The low-pressure turbine aeromechanical design incorporates numerous advanced features to enhance efficiency, durability and performance retention. The aerodynamic definition is aggressive, considering the large expansion ratio and high inlet swirl. To attain a successful aerodynamic design, several features were incorporated including low loss airfoil designs, counterrotating spools, and a low ratio of through flow to wheel speed (C_x/U).

Additional performance gains are achieved by minimizing endwall losses with the use of flow guides on airfoil platforms, improved interstage sealing and active clearance control. Turbine airfoils are fabricated from high strength/high temperature materials to meet life and durability requirements. The use of these materials negates the requirement for cooling, which contributes substantially to a higher level of performance.

The combined effect of these technology features results in a status component efficiency of 91.3 percent for the flight propulsion system and 90.3 percent for the integrated core/low spool. This represents a 2.3 percent improvement for the flight propulsion system and a 1.3 percent improvement for the integrated low spool relative to the low-pressure turbine component in the reference base engine. This prediction for the flight propulsion system is slightly below the efficiency goal of 91.5 percent mainly because of maneuver deflections, which are calculated to require greater blade tip clearances than goal values. Calculated life of major parts meets or exceeds design goals.

Separate from the turbine module is the exit guide vane assembly. The exit guide vanes are designed to present the mixer with a low Mach number, zero swirl gas stream. This component is designed for low loss performance with a predicted total loss of 0.9 percent $\Delta P_T/P_T$.

The turbine intermediate case is a compact configuration, containing eleven structural struts to support the number 4 and 5 bearing compartment. The struts are encased by aerodynamically-shaped fairings that turn the gas flow 5 degrees to provide the low-pressure turbine inlet with the proper flow field. A pressure loss of 0.7 percent $\Delta P_T/P_T$, which is consistent with the goal, is predicted for the intermediate case designed for a future flight propulsion system. However, duct pressure loss is expected to be 1.5 percent $\Delta P_T/P_T$ for the integrated core/low spool because of geometry differences to maintain aerodynamic compatibility with the low-pressure turbine.

The low-pressure turbine, exit guide vane and intermediate case designs are a positive step towards improving engine fuel efficiency on a component level. Many of the technology advancements in the areas of aerodynamics, structures and materials are universally applicable to any engine of the next generation. Technology verification is the next step, and this will be accomplished during the scheduled integrated core/low spool test program.

SECTION 2.0 INTRODUCTION

The Energy Efficient Engine Component Development and Integration Program, sponsored by the National Aeronautics and Space Administration, is directed towards demonstrating the technology required to achieve greater fuel efficiency for future commercial gas-turbine engines. The overall program goals include a reduction in fuel consumption of at least 12 percent and a reduction in direct operating cost of at least 5 percent relative to a Pratt & Whitney Aircraft JT9D-7A base engine. To demonstrate the technology required to achieve these goals, the program currently consists of three active tasks. These include:

- Task 1 Flight Propulsion System Analysis, Design and Integration
- Task 2 Component Analysis, Design and Development
- Task 4 Integrated Core/Low Spool Design, Fabrication and Test

Under Task 2 of the program, two major accomplishments have been the design of the turbine intermediate case and the low-pressure turbine component. These components utilize technology advancements in the areas of aerodynamics materials and structure-mechanics to meet the requirements for the integrated core/low spool as well as a future flight propulsion system. The program schedule for the design of the turbine intermediate case and low-pressure turbine system, including supporting technology programs, is shown in Figure 2-1.

This report presents a comprehensive description of the aerodynamic and thermal-mechanical designs of the intermediate case and low-pressure turbine components. The following section, Section 3, provides an overview of the component designs and the predicted performance. Section 4 contains the details of the aerodynamic designs, and Section 5 presents a discussion of the thermal-mechanical designs. Concluding remarks are presented in Section 6.

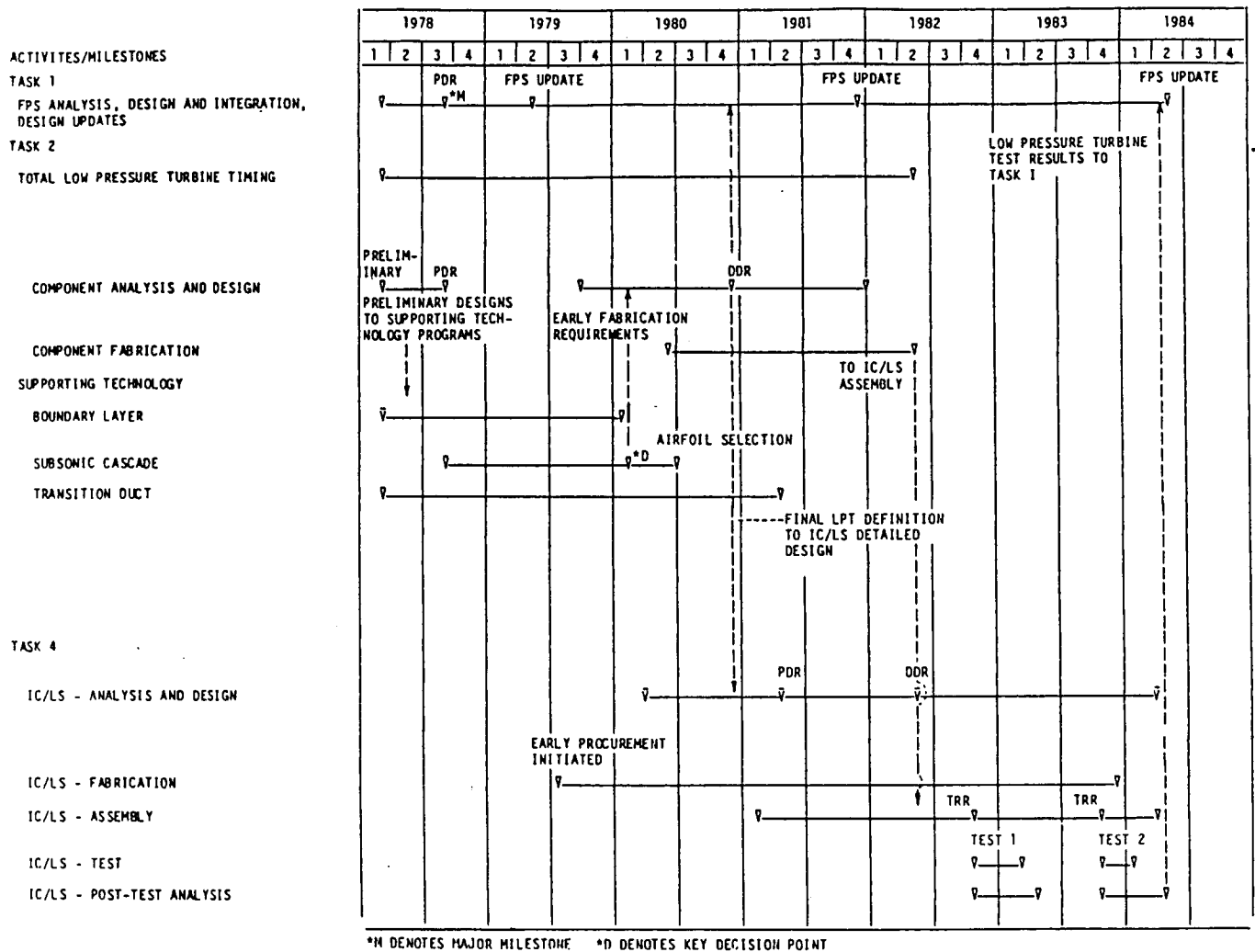


Figure 2-1

Program Schedule for Energy Efficient Engine Turbine Intermediate Case and Low-Pressure Turbine Design Efforts

SECTION 3.0 DESIGN OVERVIEW

3.1 TURBINE INTERMEDIATE CASE AND LOW-PRESSURE TURBINE CONCEPTS

A cross-sectional view of the turbine intermediate case, low-pressure turbine and exit guide vane, as integrated in the turbine section of the Pratt & Whitney Aircraft Energy Efficient Engine, is shown in Figure 3.1-1. The principal design goals include a turbine efficiency of 91.5 percent, an intermediate case pressure loss of 0.7 percent $\Delta P_T/P_T$ and an exit guide vane pressure loss of 0.9 percent $\Delta P_T/P_T$.

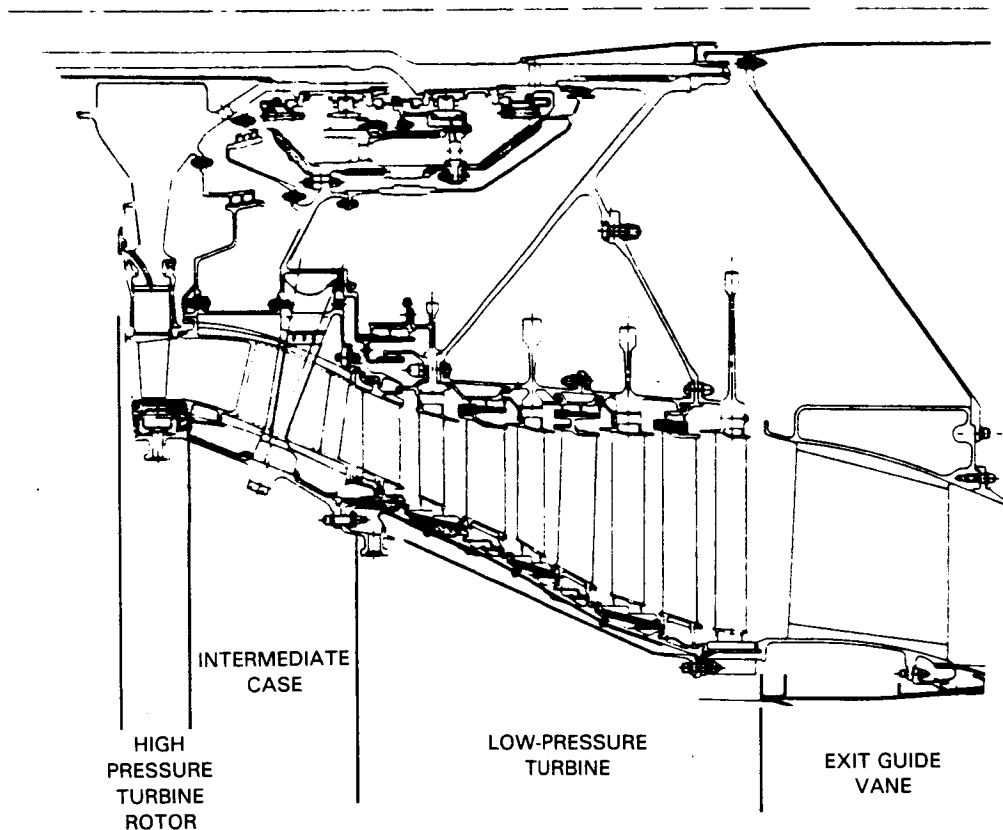


Figure 3.1-1 Major Components in the Energy Efficient Engine Turbine Section

3.1.1 Turbine Intermediate Case

In the Energy Efficient Engine design, the turbine intermediate case provides the gaspath transition between the high-pressure turbine exit and the low-pressure turbine inlet. It also provides a frame for the turbine rotor supports and rear engine mounts. This arrangement permits use of a straddle mounted, or simply-supported, high-pressure rotor system for improved clearance control. Another advantage is that the number 4 and 5 bearing compartment can be located after the high-pressure turbine disk in a less severe thermal environment.

However, the intermediate case introduces certain technical challenges that have been addressed during the design process. These include: (1) high gaspath temperatures which can cause excessive thermal stresses and distortion resulting in limited life; (2) strut fairing airfoil size constraints that limit the internal passage volume available for the structural struts and oil service lines; and (3) high thrust balance loads on the support structure, causing high bending stresses.

A cross-sectional view of the turbine intermediate case is shown in Figure 3.1.1-1. The design is compact and minimizes pressure loss resulting from excessive boundary layer formation and local separation.

Structural support for the number 4 and 5 bearing compartment is provided by eleven support struts. To minimize blockage and pressure loss, the struts are encased by aerodynamically-shaped fairings. Oil supply and scavenge tubes to the bearing compartment are routed through hollow fairings in the cavity just forward of the strut leading edge. These lines are fully insulated for protection from the high temperature environment. Also, the struts are cooled with a small percentage of high-pressure compressor bleed air.

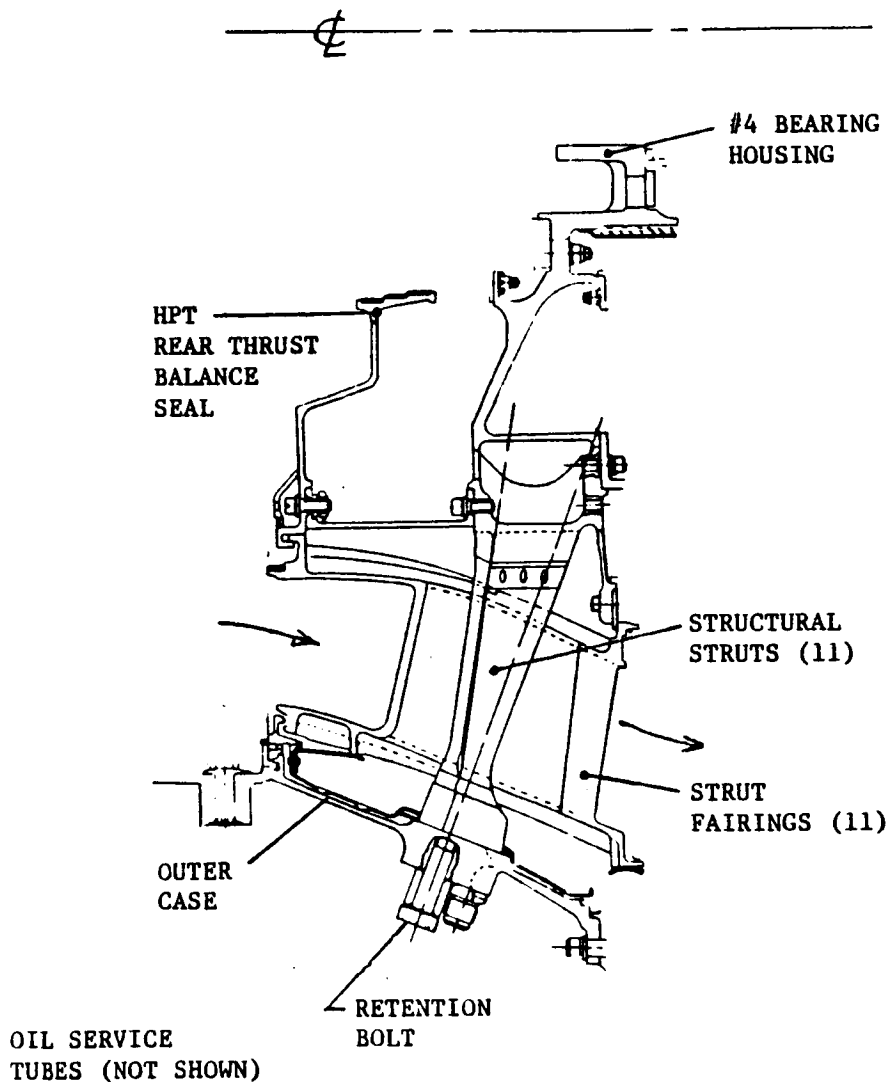


Figure 3.1.1-1 Cross-Sectional View of Turbine Intermediate Case

3.1.2 Low-Pressure Turbine

The low-pressure turbine is a highly loaded four-stage design. The turbine for a future flight propulsion system is shown in Figure 3.1.2-1 and has several features to minimize leakage, improve aerodynamics and reduce weight. Some of these features are:

- o Double wall case construction with case-tied outer air seals and an internal active clearance control system for controlling blade tip clearances
- o Accomplishing the required expansion ratio (5.5) in four stages rather than five, thereby reducing component weight
- o Increased velocity ratio ($V_m = 0.468$) compared to the reference base engine coupled with a low ratio of through flow velocity to wheel speed (C_x/U) for improved aerodynamic performance
- o Low loss aft-loaded airfoils with elliptical leading edges
- o Controlled vortexing to reduce root section aerodynamic losses
- o Stepped labyrinth inner air seals in the third through fifth stages, and case-tied knife-edge inner air seals (thrust balance seals) in the second stage to control leakage
- o Blade leading and trailing edge flow guides to minimize cavity recirculation losses

In addition, the low-pressure turbine is counter rotating relative to the high-pressure turbine to enhance aerodynamic performance by reducing turning losses in the second stage vane. Performance is further improved by the elimination of cooling in the second stage through the use of high strength and high temperature capability materials for the airfoils. The combined effect of all these features translates into a low-pressure turbine efficiency benefit of 2.3 percent for the Energy Efficient Engine flight propulsion system relative to the reference base engine.

Separate from the turbine module is the turbine exit guide vane assembly, which is designed to present the mixer with a low Mach number, zero swirl gas stream. The vanes are a hollow, welded construction in the flight propulsion system. Solid castings are used, however, in the integrated core/low spool as a cost saving feature.

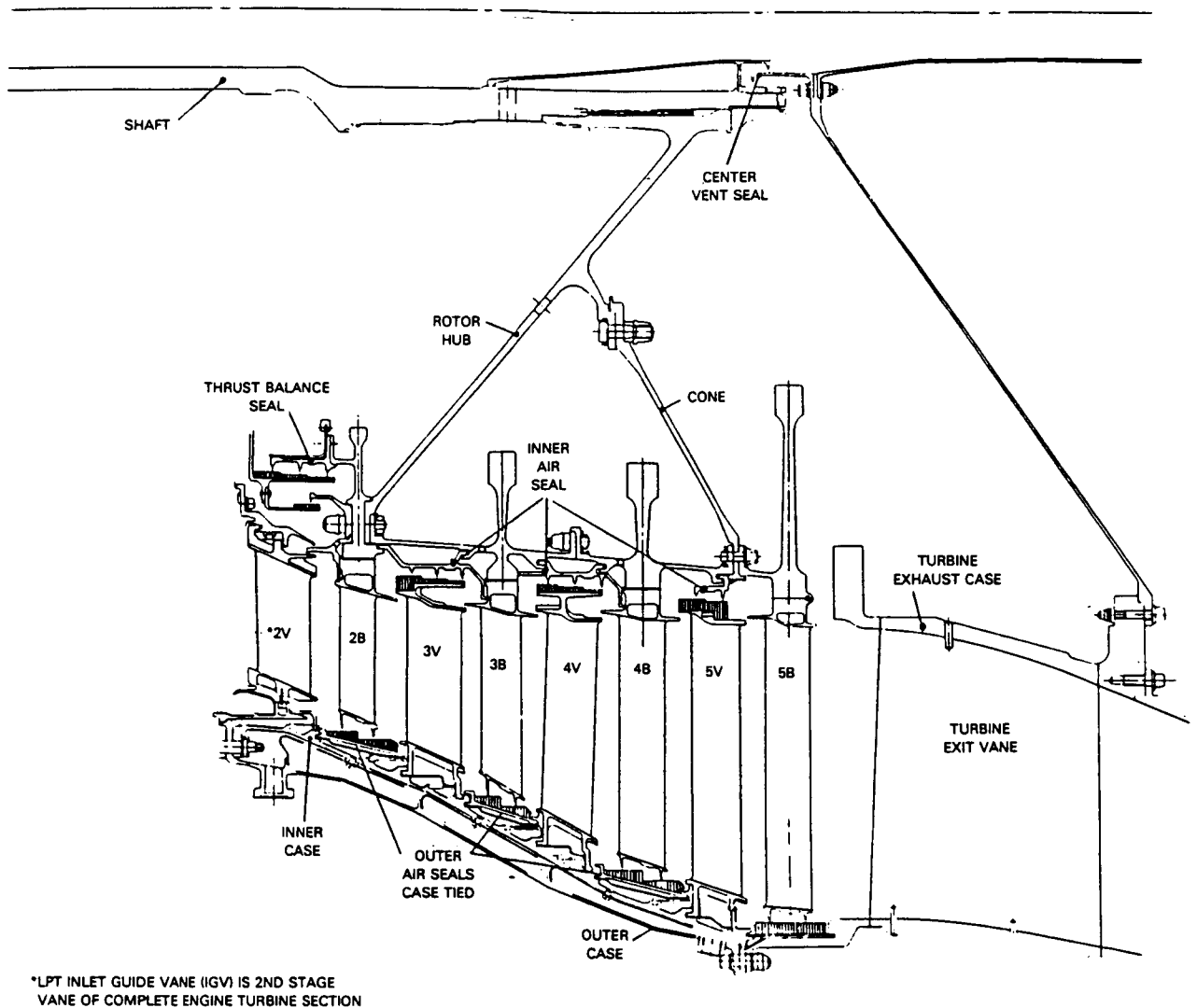


Figure 3.1.2-1 Cross-Sectional View of Low-Pressure Turbine Component

3.2 PREDICTED AERODYNAMIC PERFORMANCE

Aerodynamic studies conducted prior to detailed mechanical design confirmed that the initially established goal of 0.7 percent $\Delta P_T/P_T$ loss for the turbine intermediate case in the flight propulsion system could be attainable. Similar studies conducted for the integrated core/low spool predicted that loss would be 1.5 percent $\Delta P_T/P_T$ because of geometry differences necessary to maintain aerodynamic compatibility with the low-pressure turbine. This loss level is consistent with the integrated core/low spool goal of 1.5 percent $\Delta P_T/P_T$.

The turbine intermediate case structural struts are designed for a 15,000 hour life for the flight propulsion system and 50 hours of hot time for the integrated core/low spool.

The goal performance of the low-pressure turbine component is summarized in Table 3.2-I. The items of improvement relative to the reference base engine are indicated. Studies conducted prior to completion of the mechanical design indicated that flight propulsion system aerodynamic efficiency would surpass the goal if the clearances assumed could be maintained. An updated performance prediction (status) after completion of the mechanical design is presented in Section 4.5, Performance Status and Adjustment.

Turbine life predictions for the flight propulsion system are consistent with the goals of 15,000 hours or 3300 missions for the airfoils and 30,000 hours or 20,000 missions for the disks, hubs, shaft and static structure. For the integrated core/low spool, life estimates exceed the goal of at least 50 hours of hot time operation or 1000 cycles.

TABLE 3.2-I
GOAL AERODYNAMIC EFFICIENCY
(Aerodynamic Design Point)

Reference Base Engine	89.0%
Increased Velocity Ratio	+0.3
Improved Aerodynamic Benefits	+1.0
Reduced Clearance and Flow Guides	+1.2
TOTAL	91.5%

Assumptions:

- (1) 0.051 cm (0.020 in) Clearance for Inner Seals
- (2) 0.051 cm (0.020 in) Clearance for Outer Blade Tip Seals
- (3) 0.152 cm (0.060 in) Clearance on Flow Guides
- (4) No Instrumentation

SECTION 4.0
INTERMEDIATE CASE AND LOW-PRESSURE TURBINE AERODYNAMIC DESIGN

4.1 AERODYNAMIC DESIGN PARAMETERS

The aerodynamic definition of the intermediate case and low-pressure turbine components was based on a series of analyses to establish the flowpath, airfoil contours and flow characteristics to achieve the highest level of performance within the constraints of the basic mechanical configuration. In addition, the final designs were influenced largely by the results obtained from supporting technology programs which were in progress concurrent with the design process.

The general parameters governing the aerodynamic design of the intermediate case and low-pressure turbine are presented in Table 4.1-I. The values listed in this table are for the aerodynamic design point of the integrated core/low spool.

TABLE 4.1-I
TURBINE GENERAL AERODYNAMICS
(At Aerodynamic Design Point)

INTERMEDIATE CASE

Annulus Area Ratio	1.57
Effective Area Ratio	1.42
$\alpha_2 - \alpha_2$ Free Vortex, (deg)	5
$\Delta P_T/P_T$, (%)	1.5

LOW-PRESSURE TURBINE

Stages	4
Rotation	Counter
Speed (rpm)	3902.0
Inlet Total Pressure, Pa (psia)	319,229.2 (46.3)
Inlet Total Temperature, K (°R)	1161 (2090)
Inlet Corrected Flow, $W \sqrt{T/P_t}$	69.342
Exit Corrected Flow, $W \sqrt{T/P_t}$	323.17
Pressure Ratio	5.51
ΔH , (Btu/sec)	12760.0
Mean Velocity Ratio	0.468
Work Factor, ($\Delta h/u^2$)	2.28
Average Flow Coefficient, C_x/u	0.76
Work Split, %	23/24/26/27
Mean Reaction	.45/.45/.45/.46
Goal Clearances, cm(in)	0.051 (0.020)
Goal Efficiency Split, %	90/88.9/90.4/90.9
Goal Overall Efficiency, %	91.5

4.2 FLOWPATH AND AIRFOIL CROSS SECTION DEFINITION

4.2.1 Intermediate Case Flowpath

The basic flowpath of the turbine intermediate case for the Energy Efficient Engine required certain modifications in the integrated core/low spool to maintain aerodynamic compatibility with the low-pressure turbine component. Figure 4.2.1-1 shows a comparison of the final flowpath for the integrated core/low spool and the preliminary flowpath established during the earlier part of the program, but scaled to the current thrust size of 160,135 N (36,000 lb). A further comparison of the geometric differences of the two designs is provided in Table 4.2.1-I. As indicated, several major differences are apparent because of the requirements of the integrated/core low spool design.

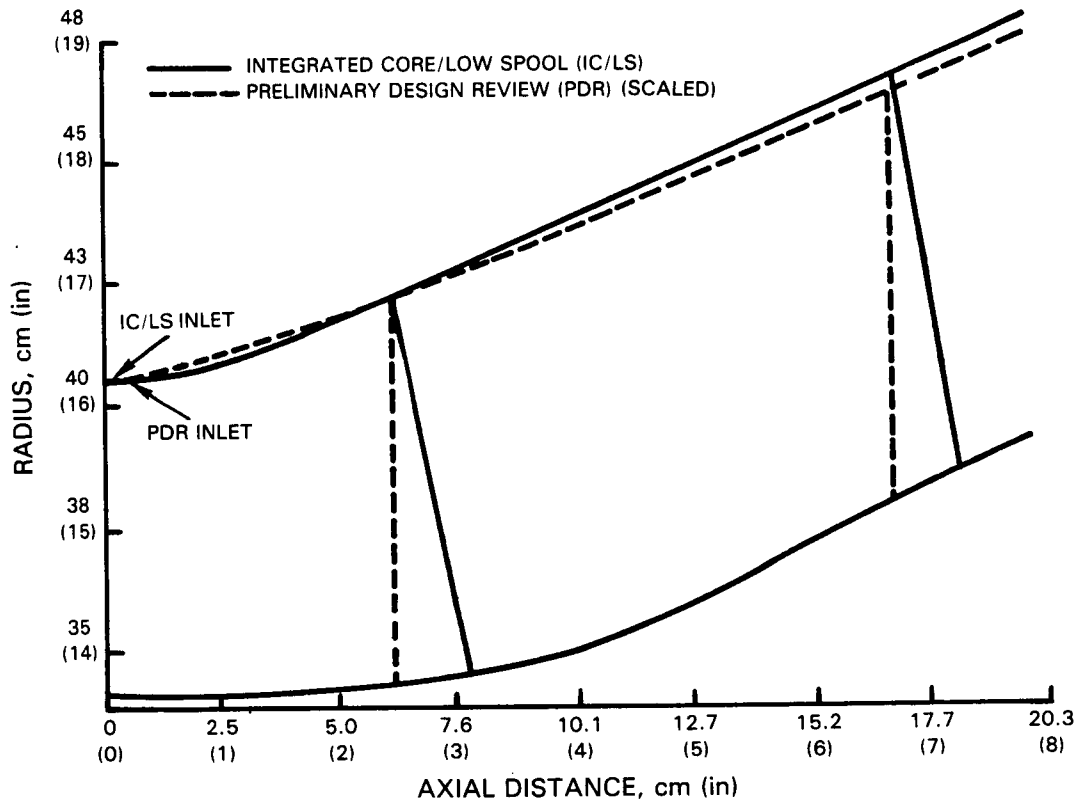


Figure 4.2.1-1 Turbine Intermediate Case Flowpath for the Integrated Core/Low Spool and the Preliminary Design Scaled to a 160,135 N (36,000 lb) Thrust Size

The increase in corrected flow of the integrated core/low spool cycle compared to the flight propulsion system cycle dictated a 5 percent increase in the intermediate case exit annulus area. Also, the intermediate case support strut was changed from a nonworking to a working airfoil, turning the gas flow 5 degrees back towards axial. These modifications provide the proper inlet flowfield to the low-pressure turbine in the integrated core/low spool. In addition, to obtain proper case stiffness, the posture of the support strut was

TABLE 4.2.1-1
INTERMEDIATE CASE GEOMETRY COMPARISON

<u>DUCT</u>	<u>Preliminary Design</u>	<u>Integrated Core/ Low Spool</u>
Length, cm (in)	21.0 (8.2) (7.7 scaled)	19.8 (7.8)
L/H	3.0	3.0
Ann. Area Ratio	1.50	1.57
Eff. Area Ratio	1.26	1.42
Duct Exit Gas Angle (deg)		
Hub	30	35
Midspan	36	39
Tip	33	40
Duct Exit Mach No.		
Hub	0.50	0.40
Midspan	0.44	0.39
Tip	0.41	0.30
<u>STRUT</u>	<u>NONWORKING</u>	<u>WORKING</u>
No. of Foils	14	11
Type	65C/A	400
$\alpha 2 - \alpha 2$ Free Vortex, deg	0	5

changed by canting it tangentially approximately 11 degrees opposite rotation and shifting the sections axially rearward. Finally, the fairing cross section was changed from a 65 circular arc to a 400 series airfoil to increase the incidence range. The width of the fairing was set by the area required for adequate oil scavenging from the number 4 and 5 bearing compartment.

For high-pressure turbine blade structural considerations, the flowpath length was increased 0.2 cm (0.1 in) for a final duct length of 19.8 cm (7.8 in). Moreover, the number of fairings was reduced from 14 to 11 to preclude vibratory excitation of the high-pressure turbine blade precipitated by a passing frequency.

Overall, the net effect of these changes is a more aggressive flowpath design, as indicated in Figure 4.2.1-2 by the considerably higher level of diffusion, with an attendant higher system pressure loss. This loading is achievable, as demonstrated by the results of a Transition Duct Model Test Program (Ref.1) (Section 4.3.2). The estimated total duct pressure loss for the integrated core/low spool is 1.5 percent $\Delta P_T/P_T$.

For the flight propulsion system, however, the intermediate case flowpath retains many of the features in the original definition to achieve the goal pressure loss of 0.7 percent. These include maintaining an exit annulus area ratio of 1.50, which is 5 percent lower than that established for the integrated core/low spool, and a free vortex (nonworking) type fairing.

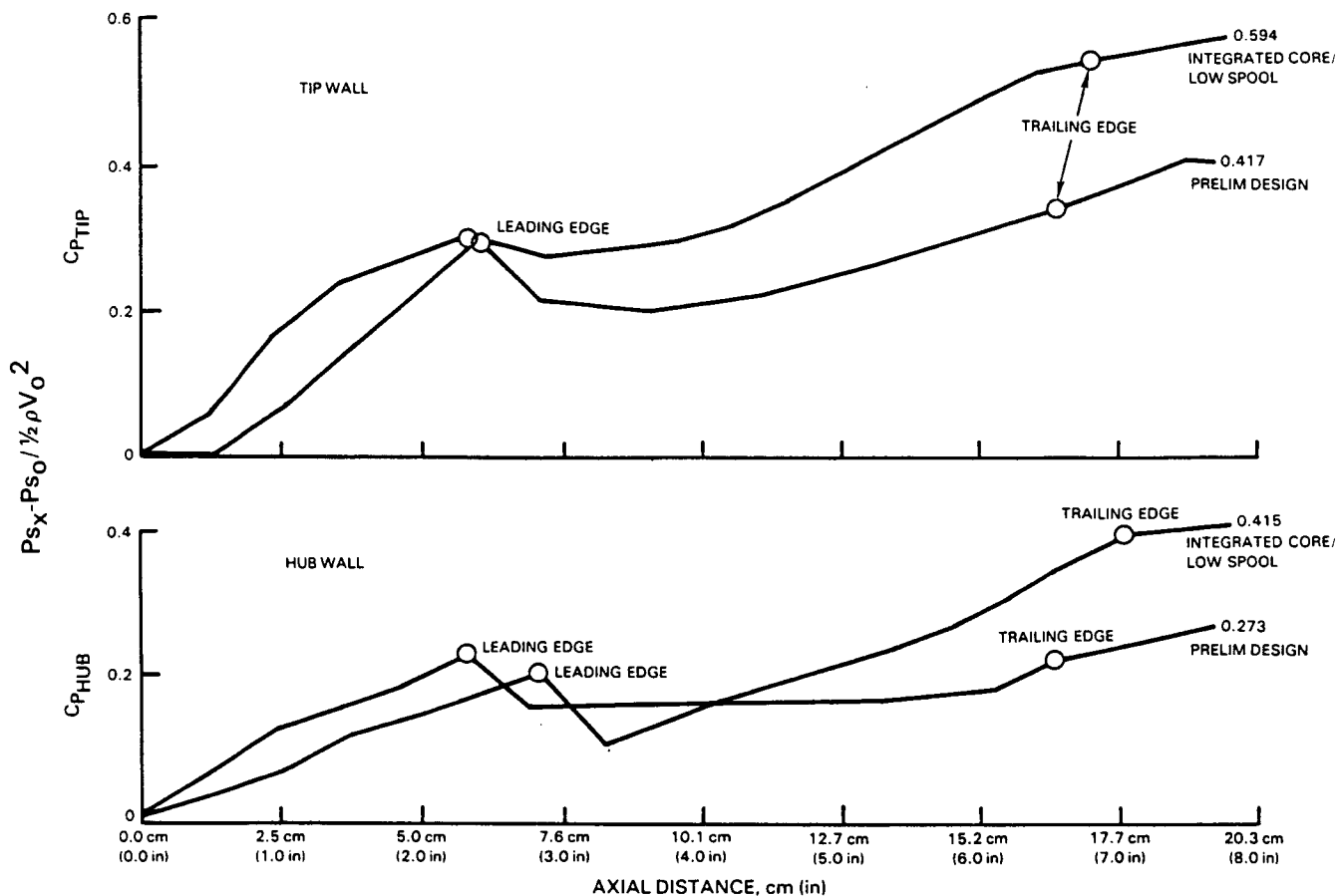


Figure 4.2.1-2 Intermediate Case Wall Pressure Distribution Profiles, Showing the High Loading of Integrated Core/Low Spool Design

4.2.2 Intermediate Case Strut Fairing

The fairing, which encases the structural strut, is a standard 400 series airfoil. The definition was established on the basis of airfoil thickness, length and leading and trailing edge radii. Also, as shown in Figure 4.2.2-1, a 400 series airfoil offers a larger incidence range with only a slight compromise in pressure loss in comparison with other airfoil series.

The main criteria governing the fairing aerodynamic design were thickness and flow turning. To accommodate the structural strut, the thickness was established at 2.54 cm (1.0 in). Flow turning, as discussed earlier, was determined at 5 degrees to satisfy low-pressure turbine aerodynamics in the integrated core/low spool. Axial spacing as well as the canted posture of the fairing were dictated by structural requirements.

A summary of the final fairing definition is contained in Table 4.2.2-I. Also, Figures 4.2.2-2 through 4.2.2-5 present corresponding pressure distributions and section aerodynamics for each of the four radial sections identified in Table 4.2.2-I. Figure 4.2.2-6 shows the stacking arrangement of the fairing.

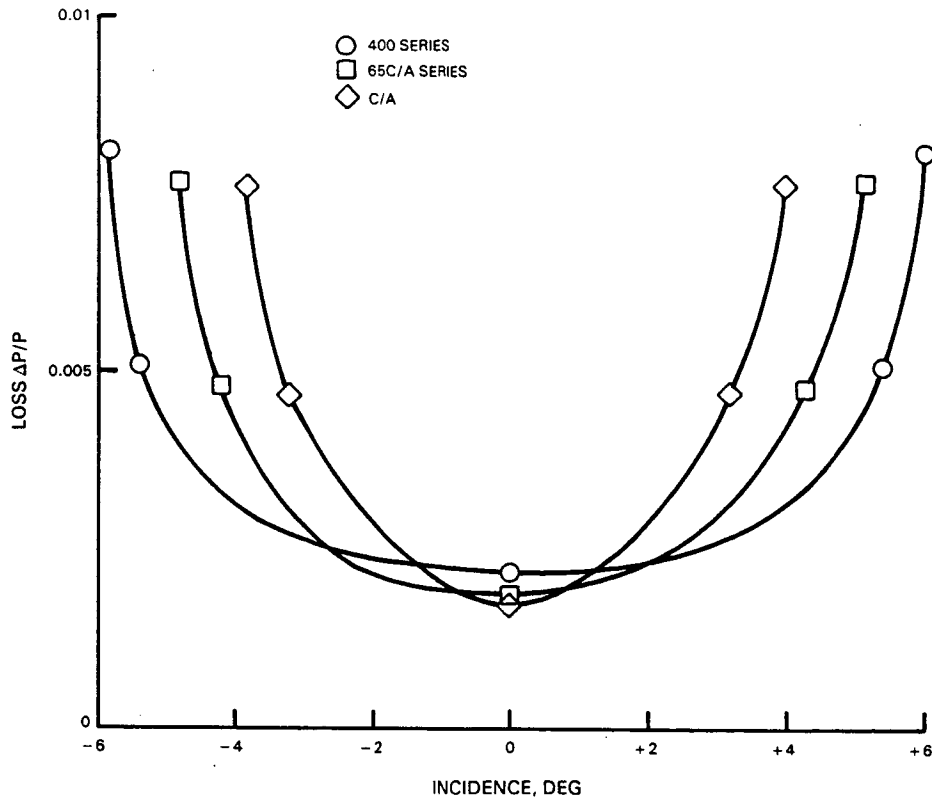


Figure 4.2.2-1 Incidence Range Capability as a Function of Pressure Loss, Showing Greater Range With 400 Series Foil

TABLE 4.2.2-I
 INTEGRATED CORE/LOW SPOOL DESIGN
 Transition Duct Strut Fairing Design

Section (Planar)	1	2	3	4
Radius, cm(in)	35.003(13.781)	39.187(15.428)	42.735(16.825)	47.444(18.679)
Foil Type	400	400	400	400
Number of Foils	11	11	11	11
Axial Chord, cm(in)	10.97(4.32)	11.25(4.43)	11.50(4.53)	11.78(4.64)
Actual Chord, cm(in)	20.39(8.03)	17.29(6.81)	15.59(6.14)	14.93(5.88)
Maximum Thickness, cm(in)	2.5(1.0)	2.5(1.0)	2.5(1.0)	2.5(1.0)
Gap/Chord	0.98	1.29	1.59	1.82
Inlet Metal Angle,	150.2	144.5	138.7	131.6
Inlet Gas angle,	148.5	142.5	141.8	148.1
Inlet Mach Number	0.51	0.50	0.48	0.43
Exit Metal Angle,	33.4	44.1	51	54.9
Exit Gas Angle,	31.9	35.3	38.4	42.4
Exit Mach Number	0.37	0.40	0.40	0.31

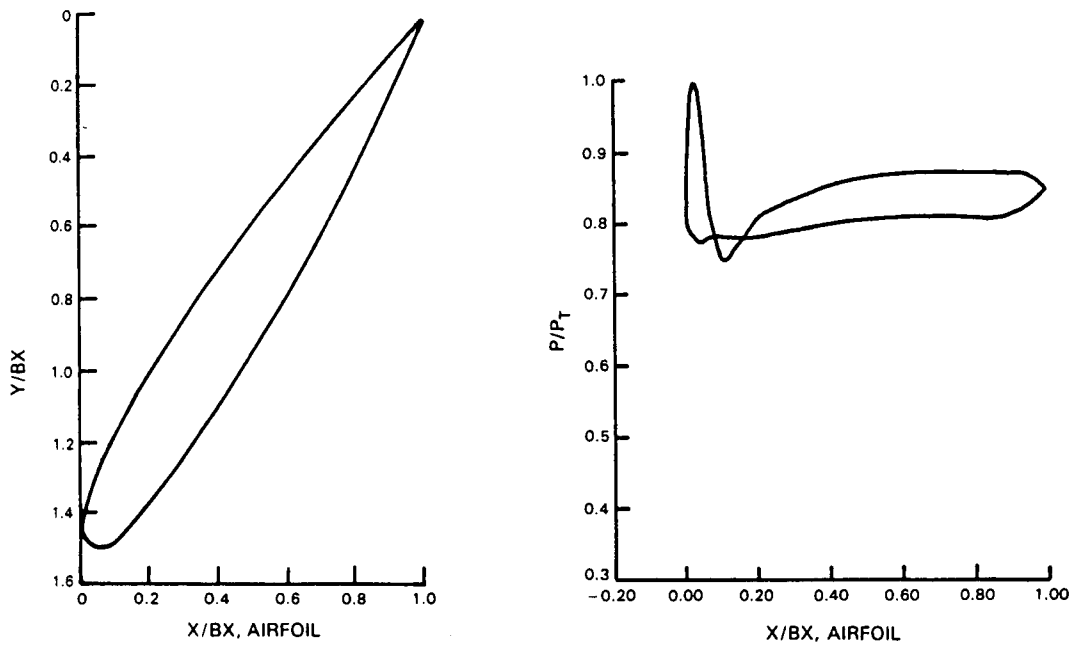


Figure 4.2.2-2 Fairing Aerodynamic Definition for Section 1 -- Integrated Core/Low Spool Intermediate Case

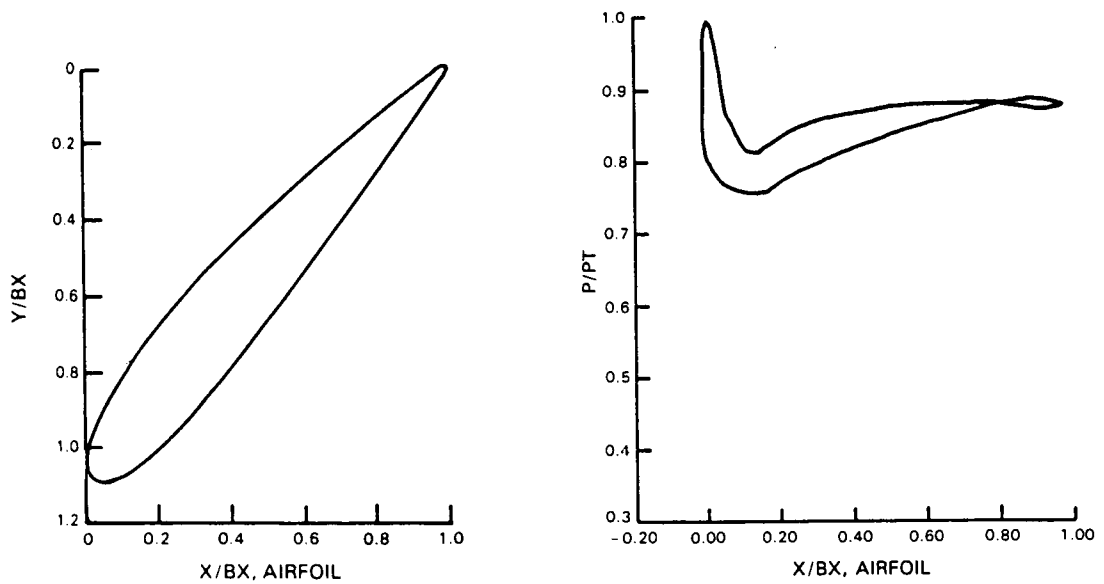


Figure 4.2.2-3 Fairing Aerodynamic Definition for Section 2 -- Integrated Core/Low Spool Intermediate Case

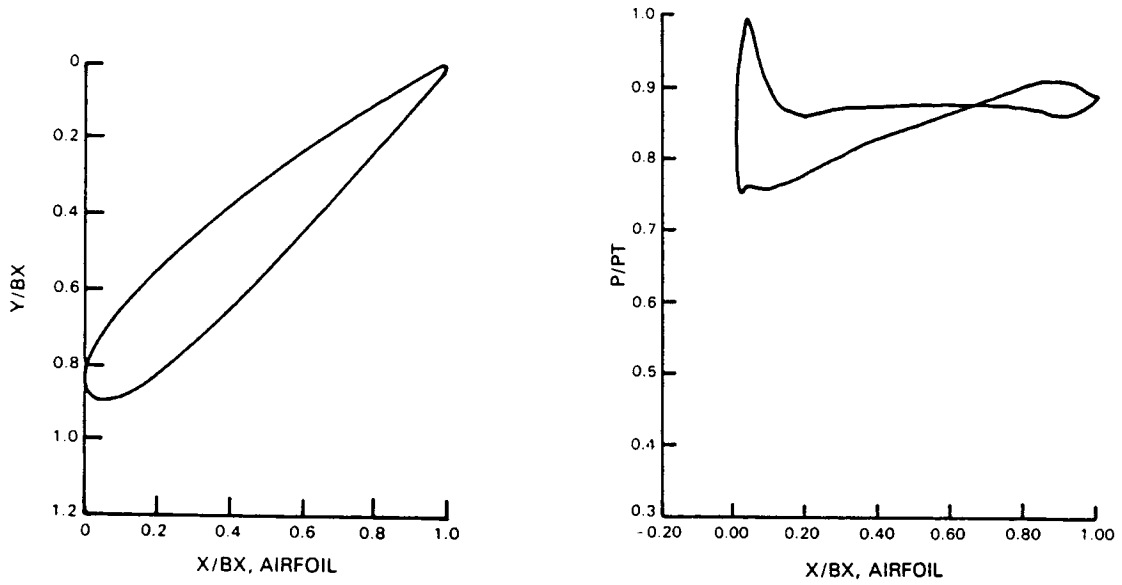


Figure 4.2.2-4 Fairing Aerodynamic Definition for Section 3 -- Integrated Core/Low Spool Intermediate Case

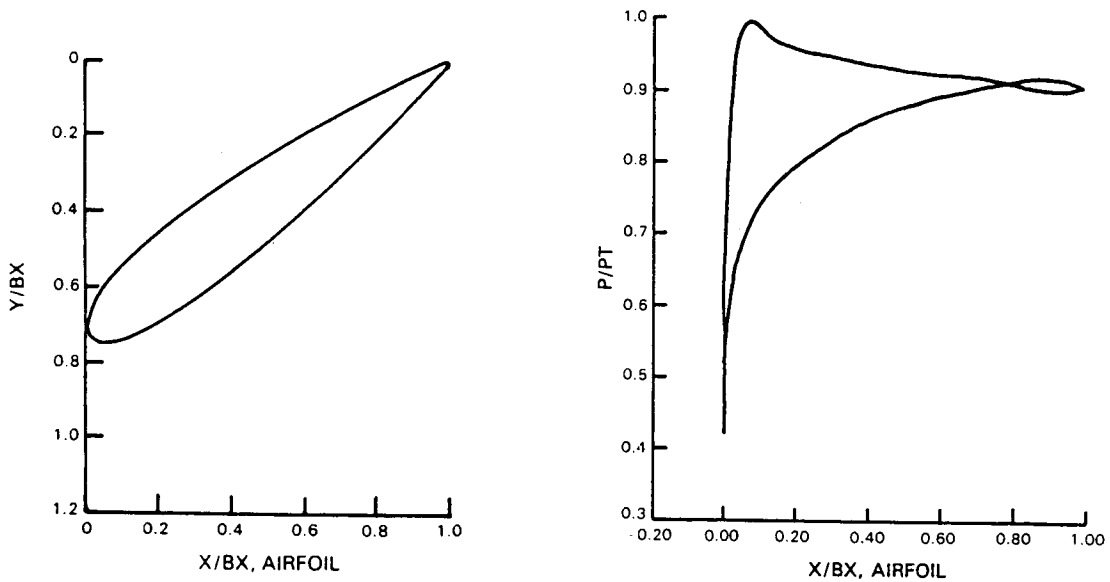


Figure 4.2.2-5 Fairing Aerodynamic Definition for Section 4 -- Integrated Core/Low Spool Intermediate Case

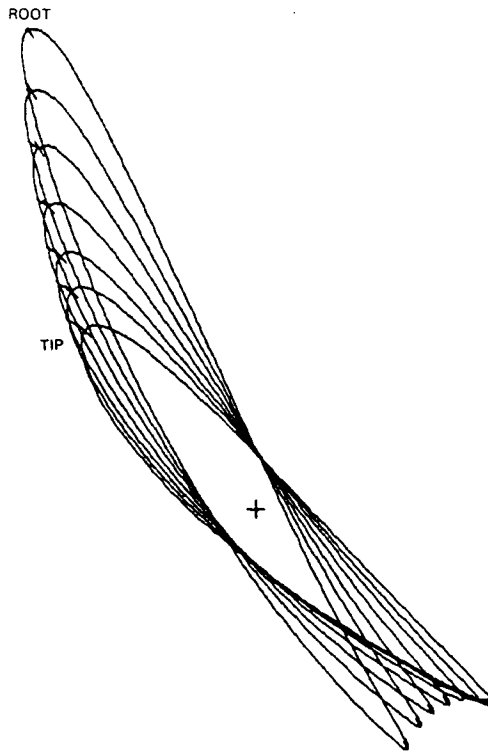


Figure 4.2.2-6 Strut Fairing Stacking Arrangement

4.2.3 Low-Pressure Turbine Flowpath

The low-pressure turbine flowpath evolved from a series of iterative design analyses. The final definition, as presented in Figure 4.2.3-1, is sized for a thrust of 160,135 N (36,000 lb), consistent with the integrated core/low spool.

As shown in Figure 4.2.3-1, the turbine flowpath, from the inlet to the exit of the last or fifth-stage blade, is 61.23 cm (24.12 in) in length with a maximum elevation of 65.93 cm (25.96 in). The axial gap between stages is sufficient for the incorporation of flow guides and allows adequate margin to preclude clashing that may result from pressure load deflections on the airfoils, vibratory deflections and mechanical tolerances. Flow guides are extensions of the airfoil platforms and serve to minimize cavity recirculation losses.

The four turbine stages contain a total of 756 airfoils. A delineation of the number of airfoils for each stage is presented in Table 4.2.3-I. All airfoils are a high aspect ratio and designed for low loss. Turbine blades in all stages are tip shrouded.

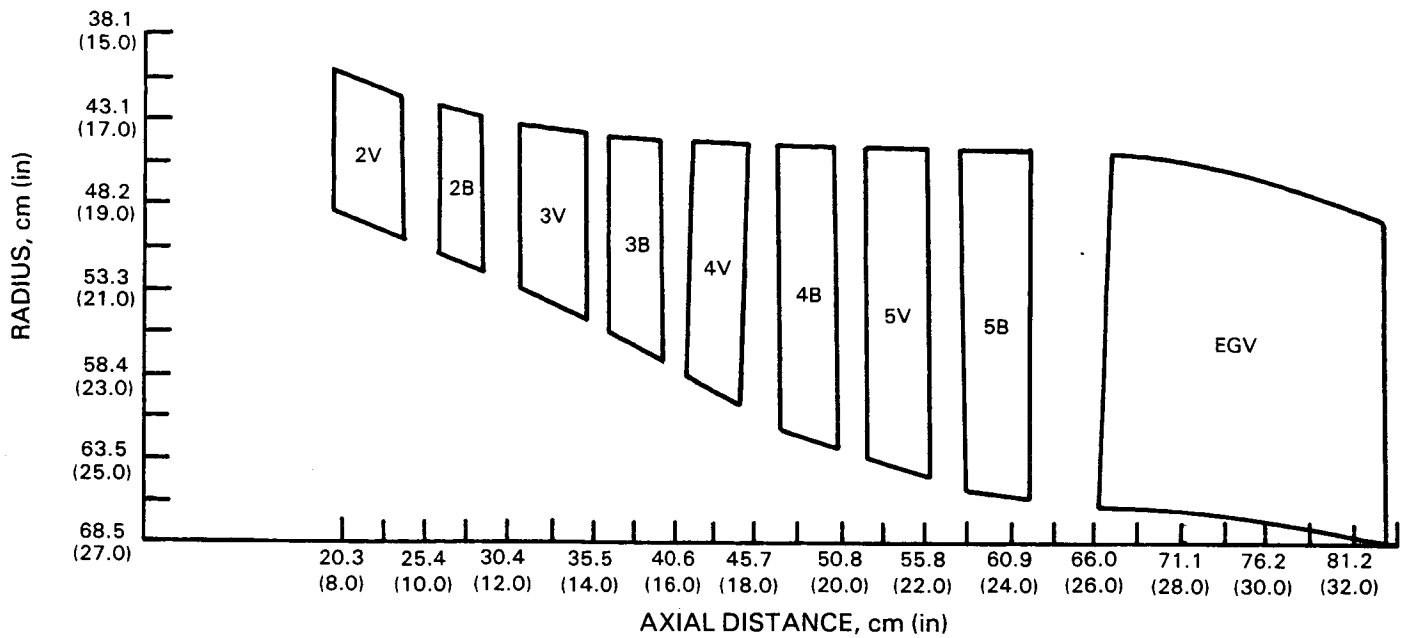


Figure 4.2.3-1 Low-Pressure Turbine Flowpath

TABLE 4.2.3-I
AIRFOIL QUANTITY BY STAGE

Second Stage*	
Vanes	54
Blades	120
Third Stage	
Vanes	72
Blades	96
Fourth Stage	
Vanes	84
Blades	100
Fifth Stage	
Vanes	108
Blades	122
Total	756

* The low-pressure turbine inlet guide vane is the same as the second-stage vane in the complete Energy Efficient Engine turbine section.

In terms of component aerodynamics, the turbine is characterized by a high expansion ratio (5.5) compared to the number of stages, a low mean velocity ratio (0.468) and a low ratio of throughflow to wheel speed (C_x/U) (0.76). Also, the low-pressure turbine is counterrotating in relation to the single-stage high-pressure turbine. This results in a low camber inlet guide vane for improved performance. Airfoils in the remaining stages have a high level of turning. The rotating stages are defined with a reaction level of 45, 45, 45 and 46 percent to enhance efficiency, and the turbine stage work split is defined at 23, 24, 26 and 27 percent, respectively. These levels provide both an optimum efficiency and exit guide vane loss level.

The addition of the turbine exit guide vane increases the flowpath length by 21.59 cm (8.5 in) for a total length of 82.85 cm (32.62 in). The radius is increased by 2.74 cm (1.08 in) for a total height of 68.68 cm (27.04 in). There is a total of 30 turbine exit guide vanes. Endwall contours are defined for compatibility with the internal exhaust mixer. The airfoil is also contoured to present the mixer with an acceptable inlet Mach number and zero swirl.

The adaptation of the turbine flowpath designed for the integrated core/low spool to the flight propulsion system would conceptually require only one minor modification. This would entail a 5 percent reduction in the turbine inlet annulus area to accommodate the lower inlet corrected flow of the flight propulsion system cycle. The revised flowpath would also necessitate a slight change to the airfoils.

4.2.4 Turbine Airfoil Definition

The turbine airfoils are comprised of individually designed sections. Contours and performance characteristics were defined with the use of Pratt & Whitney Aircraft's analytical techniques used specifically for designing turbine airfoils. Basically, a streamline computer design simulation generated the radial aerodynamic environment. This information served as input to the interactive airfoil design system for definition of the external contour. Analyses were then performed to ascertain pressure distribution and boundary layer characteristics. On the basis of these results, iterations of the airfoil shape were made to optimize performance. In addition, boundary layer and plane cascade tests, conducted as part of the Low-Pressure Turbine Subsonic Cascade Technology Program (Ref.2) and Boundary Layer Technology Program (Ref.3), were instrumental in substantiating the selected airfoil contours. Salient results from these programs are summarized in Sections 4.3.3 and 4.3.4 of this report.

Pertinent characteristics of the final airfoil designs are presented in Table 4.2.4-I. Velocity triangle data are summarized in Table 4.2.4-II. The velocity triangles were established using a controlled vortex philosophy. In this manner, vane trailing edge root sections were opened and the trailing edge tip sections were closed. This maintains the meanline aerodynamics, while reducing the turning done by the blade root sections and increasing the blade root reactions. The change in root section aerodynamics produces a reduction in endwall loss generation, thus increasing efficiency. Figure 4.2.4-1 shows an example of the effects produced by controlled vortexing in comparison to a free vortex design for the turbine fourth stage. Fifth-stage blade vortexing was set to achieve reasonable load factors for the turbine exit guide vane.

Besides controlled vortexing, the airfoils are designed with an elliptical leading edge to provide a uniform pressure distribution.

Of particular importance, the Low-Pressure Turbine Subsonic Cascade Technology Program verified the choice of blade and vane contours needed to obtain low loss characteristics as well as defined the characteristics of the low camber inlet guide vane. Results showed that an airfoil that continuously accelerates the flow on the suction surface to the region of the gaging point can provide an approximate 18 percent reduction in profile loss compared to an airfoil which achieves maximum velocity further forward on the suction surface. These lower loss airfoils, termed "aft loaded" because of the shape of the pressure distribution curve, were selected for the turbine design. Furthermore, the

Subsonic Cascade Program evaluated the performance and loss characteristics of the unique low camber inlet guide vane over a range of inlet angles. At design conditions, measured profile losses and secondary losses were 0.54 and 0.56 percent $\Delta P_T/P_T$, respectively. The vanes also showed a negative incidence range of 8 degrees, as defined by the point where the loss level is 50 percent above the design point loss.

Figures 4.2.4-2 through 4.2.4-24 present airfoil contours of different vane and blade sections in each stage. These figures also summarize the section aerodynamics and contain the static pressure distribution. Figures 4.2.4-25 through 4.2.4-32 show the stacking arrangements of the airfoil in each stage.

TABLE 4.2.4-I
LOW-PRESSURE TURBINE AIRFOIL DESIGN SUMMARY

Second-Stage Vane	
Trailing Edge Span, cm (in)	8.76(3.45)
Trailing Edge Hub/Tip Ratio	0.826
Aspect Ratio	2.203
Second-Stage Blade	
Trailing Edge Span, cm (in)	9.45 (3.724)
Trailing Edge Hub/Tip Ratio	0.820
Aspect Ratio	3.545
Third-Stage Vane	
Trailing Edge Span, cm (in)	11.282(4.442)
Trailing Edge Hub/Tip Ratio	0.796
Aspect Ratio	2.759
Third-Stage Blade	
Trailing Edge Span, cm (in)	13.314(5.242)
Trailing Edge Hub/Tip Ratio	0.770
Aspect Ratio	4.339
Fourth-Stage Vane	
Trailing Edge Span, cm (in)	15.946(6.278)
Trailing Edge Hub/Tip Ratio	0.737
Aspect Ratio	4.282
Fourth-Stage Blade	
Trailing Edge Span, cm (in)	18.224(7.175)
Trailing Edge Hub/Tip Ratio	0.711
Aspect Ratio	5.400
Fifth-Stage Vane	
Trailing Edge Span, cm (in)	19.913(7.840)
Trailing Edge Hub/Tip Ratio	0.693
Aspect Ratio	5.433
Fifth-Stage Blade	
Trailing Edge Span, cm (in)	20.863(8.214)
Trailing Edge Hub/Tip Ratio	0.684
Aspect Ratio	6.285

TABLE 4.2.4-II
GAS TRIANGLE SUMMARY
(Aerodynamic Design Point)

	Inlet Angle	Exit Angle	Inlet Mach No.	Exit Mach No.	Gas Turning	Convergence	V_{exit}/V_{inlet}
IGV							
R	144.3°	26.6°	0.396	0.666	9.1°	1.43	1.65
M	141.3°	24.2°	0.394	0.658	14.5°	1.47	1.64
T	139.4°	21.7°	0.306	0.534	19.0°	1.53	1.73
B2							
R	43.9°	23.0°	0.433	0.614	113.2°	1.27	1.40
1/4R	41.4°	24.2°	0.422	0.638	114.4°	1.34	1.48
M	40.7°	25.9°	0.394	0.620	113.3°	1.42	1.58
1/4T	42.9°	27.6°	0.335	0.580	109.5°	1.51	1.70
T	50.2°	28.7°	0.256	0.543	101.2°	1.78	2.09
V3							
R	36.0°	30.3°	0.350	0.601	113.6°	1.44	1.69
1/4R	41.7°	24.2°	0.373	0.648	114.0°	1.48	1.70
M	47.6°	22.8°	0.350	0.656	109.6°	1.61	1.85
1/4T	54.4°	22.2°	0.307	0.631	103.3°	1.80	2.00
T	59.3°	21.9°	0.266	0.590	98.8°	1.90	2.17
B3							
R	53.5°	23.5°	0.380	0.645	102.9°	1.42	1.67
1/4R	42.4°	23.2°	0.383	0.679	114.5°	1.47	1.73
M	41.7°	22.7°	0.365	0.665	115.7°	1.56	1.78
1/4T	44.7°	22.1°	0.324	0.629	113.3°	1.72	1.90
T	49.9°	21.7°	0.278	0.599	108.5°	1.83	2.12
V4							
R	37.5°	28.9°	0.368	0.647	113.6°	1.41	1.72
1/4R	40.1°	22.4°	0.391	0.700	117.5°	1.48	1.79
M	42.9°	21.2°	0.357	0.689	115.9°	1.62	1.88
1/4T	47.5°	20.3°	0.309	0.644	112.2°	1.75	2.03
T	52.4°	19.6°	0.279	0.598	108.0°	1.88	2.10
B4							
R	49.2°	22.1°	0.397	0.692	108.7°	1.40	1.70
1/4R	38.9°	22.1°	0.401	0.738	118.9°	1.49	1.79
M	40.9°	22.2°	0.359	0.689	116.9°	1.64	1.87
1/4T	46.7°	22.4°	0.286	0.649	110.9°	2.03	2.21
T	55.5°	22.5°	0.228	0.643	101.9°	2.28	2.76
V5							
R	37.2°	32.4°	0.409	0.685	110.5°	1.36	1.63
1/4R	39.4°	27.3°	0.426	0.728	113.3°	1.42	1.66
M	45.6°	22.6°	0.348	0.736	111.8°	1.70	2.05
1/4T	53.9°	22.6°	0.297	0.704	103.5°	1.89	2.29
T	57.8°	22.6°	0.289	0.648	99.7°	1.87	2.19
B5							
R	55.3°	37.3°	0.450	0.784	87.5°	1.35	1.69
1/4R	48.9°	28.8°	0.439	0.818	102.3°	1.43	1.79
M	44.7°	25.5°	0.385	0.791	108.9°	1.60	1.98
1/4T	52.0°	27.0°	0.325	0.770	101.0°	1.86	2.28
T	62.7°	29.5°	0.263	0.741	87.8°	2.0	2.72
EGV							
R	55.7°	90.0°	0.515	0.396	34.3°		
1/4R	47.9°	90.0°	0.507	0.373	42.1°		
M	50.1°	90.0°	0.441	0.350	39.9°		
1/4T	58.1°	90.0°	0.405	0.366	31.9°		
T	67.9°	90.0°	0.415	0.390	22.1°		

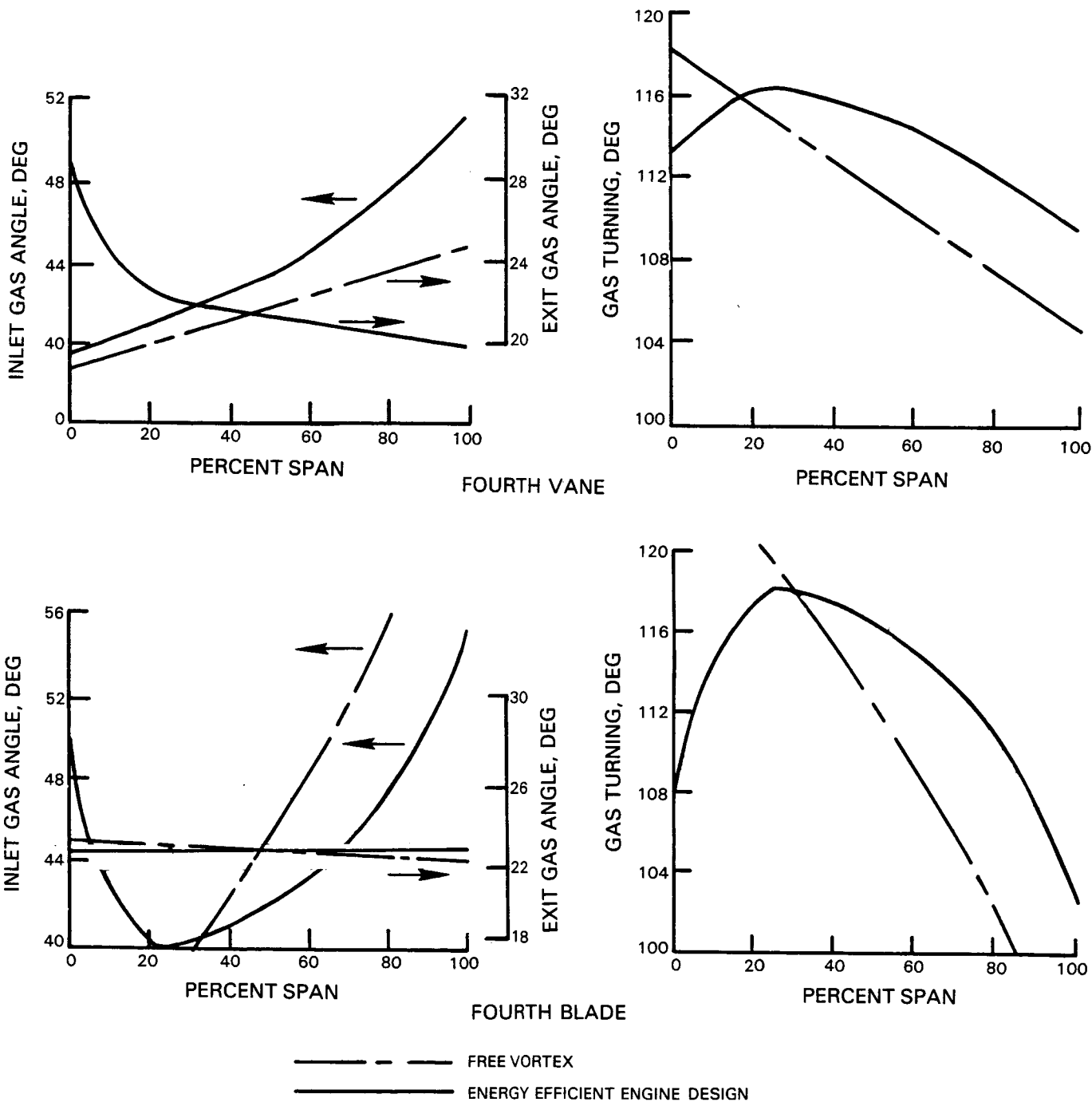
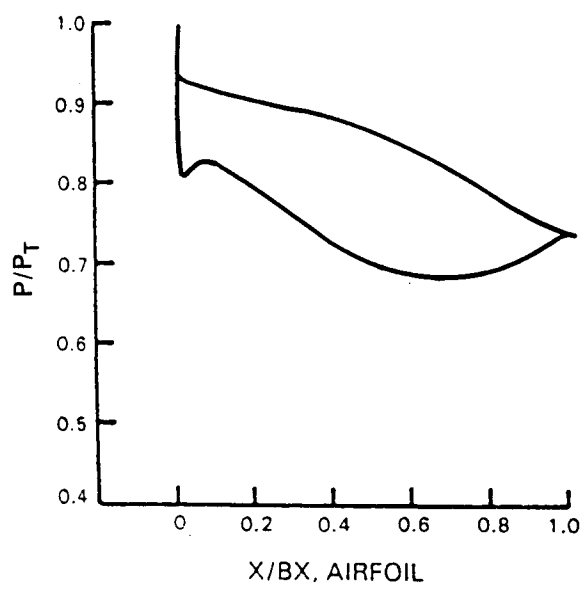
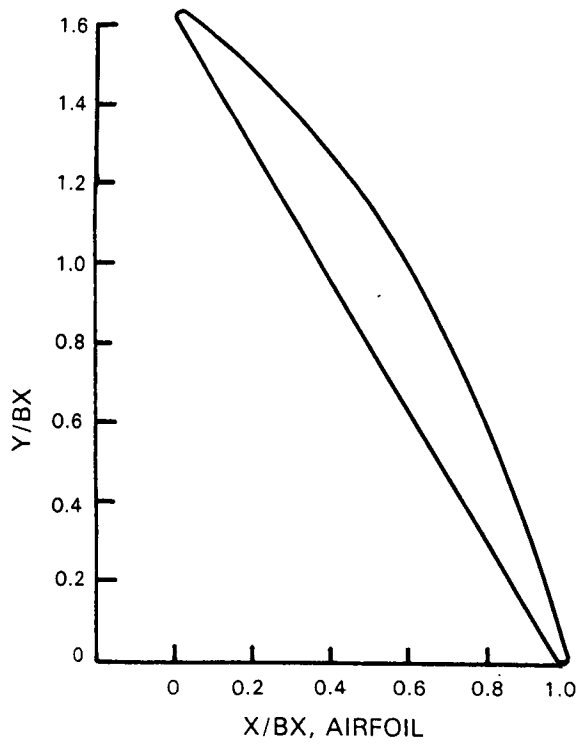
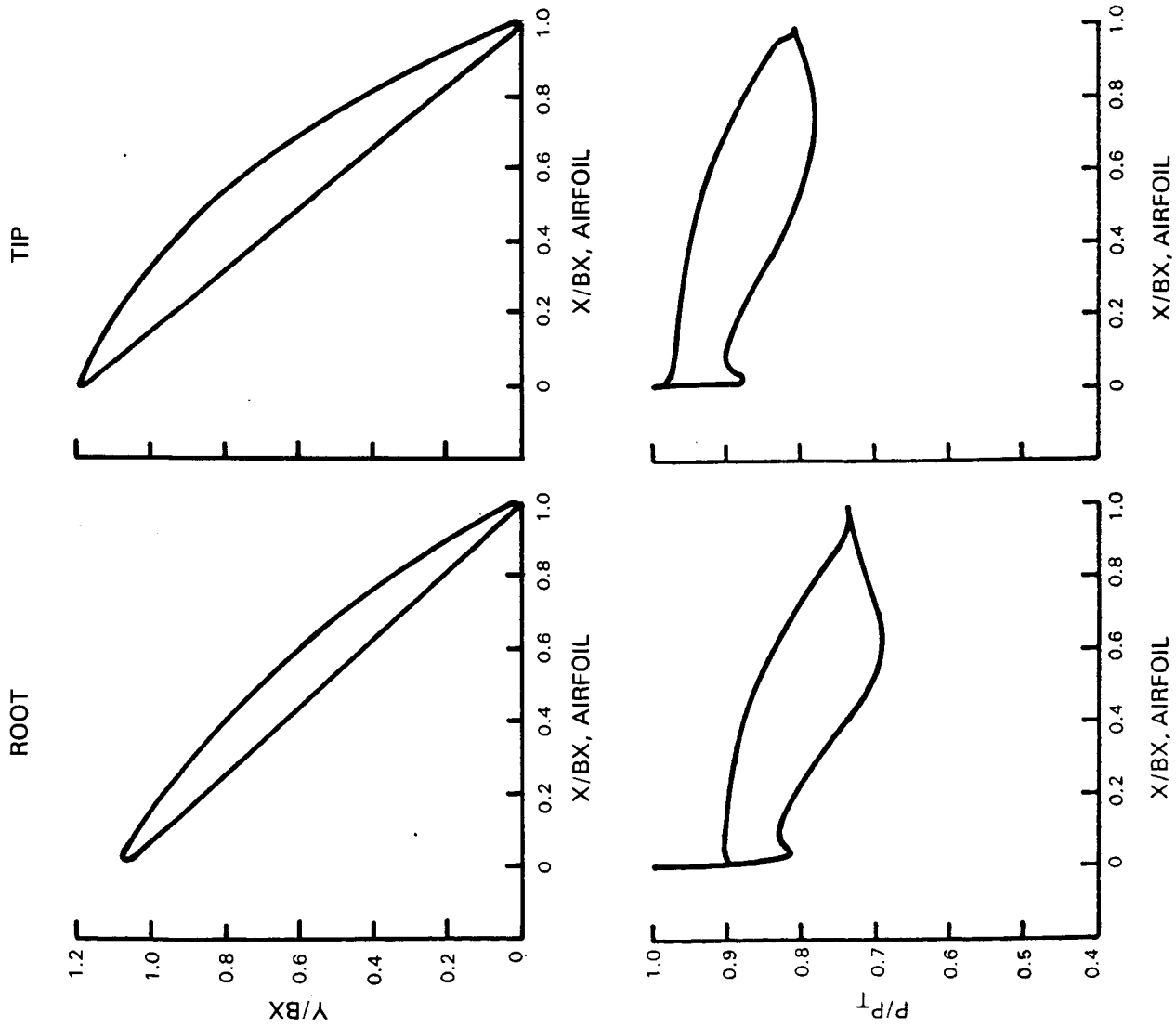


Figure 4.2.4-1 Effects of Controlled Vortexing Compared to Free Vortexing



RADIUS cm (in)	46.012 (18.115)
INLET METAL ANGLE	137.5°
EXIT METAL ANGLE	24.4°
AXIAL CHORD cm (in)	3.975 (1.565)
FOILS	54.
SOLIDITY (bx)	.743
ELLIPSE RATIO	4/1
CHORD cm (in)	7.244 (2.852)
INLET GAS ANGLE	140.5°
EXIT GAS ANGLE	24.2°
INLET MACH NO.	.378
EXIT MACH NO.	.657
INCIDENCE	-2.95°
MMAX	.753
ΔP/Q T.E.	.229

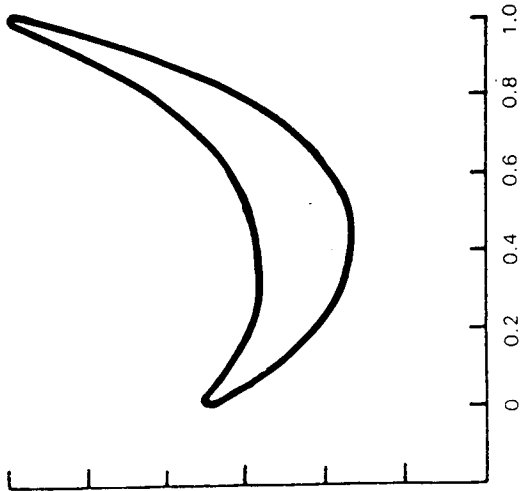
Figure 4.2.4-2 Turbine Inlet Guide Vane Mean Section Aerodynamic Definition and Pressure Distribution



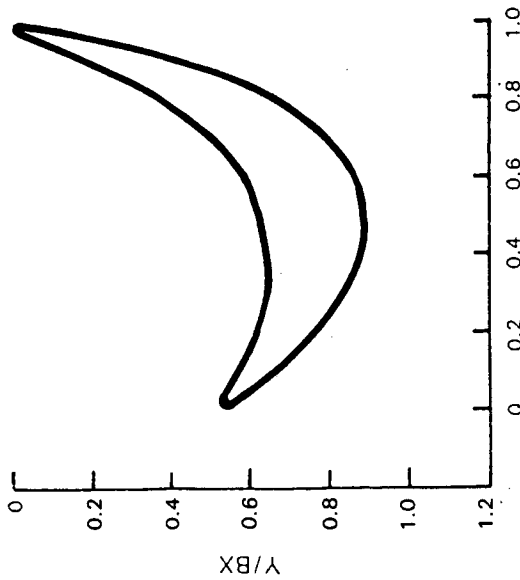
	ROOT	TIP
RADIUS, cm (in)	41.630 (16.390)	50.393 (19.840)
INLET METAL ANGLE	140.0°	136.0°
EXIT METAL ANGLE	26.6°	21.7°
AXIAL CHORD, cm (in)	3.992 (1.572)	3.964 (1.561)
FOILS	54	54
SOLIDITY (bx)	0.824	0.676
ELLIPSE RATIO	4/1	4/1
CHORD, cm (in)	7.117 (2.802)	7.688 (3.027)
INLET GAS ANGLE	142.9°	138.4°
EXIT GAS ANGLE	26.6°	21.7°
INLET MN	0.403	0.249
EXIT MN	0.666	0.534
INCIDENCE	-2.9°	-2.4°
M _{MAX.}	0.757	0.602
ΔP/Q T.E.	0.177	0.131

Figure 4.2.4-3 Turbine Inlet Guide Vane Root and Tip Section Aerodynamic Definitions and Pressure Distributions

1/4 ROOT



ROOT



	ROOT	1/4 ROOT
RADIUS, cm (in)	43.032 (16.942)	45.397 (17.873)
INLET METAL ANGLE	38.6°	36.5°
EXIT METAL ANGLE	23.1°	24.2°
AXIAL CHORD, cm (in)	2.66 (1.05)	2.66 (1.05)
FOILS	120	120
SOLIDITY (bx)	1.18	1.12
ELLIPSE RATIO	4/1	4/1
CHORD, cm (in)	2.862 (1.127)	2.885 (1.136)
INLET GAS ANGLE	42.5°	40.7°
EXIT GAS ANGLE	23.0°	24.3°
INLET MN	0.430	0.413
EXIT MN	0.615	0.638
INCIDENCE	-4.0°	-4.2°
M _{MAX}	0.795	0.838
ΔP/Q T.E.	0.327	0.388

RADIUS, cm (in)
 INLET METAL ANGLE
 EXIT METAL ANGLE
 AXIAL CHORD, cm (in)
 FOILS
 SOLIDITY (bx)
 ELLIPSE RATIO
 CHORD, cm (in)
 INLET GAS ANGLE
 EXIT GAS ANGLE
 INLET MN
 EXIT MN
 INCIDENCE
 M_{MAX}
 ΔP/Q T.E.

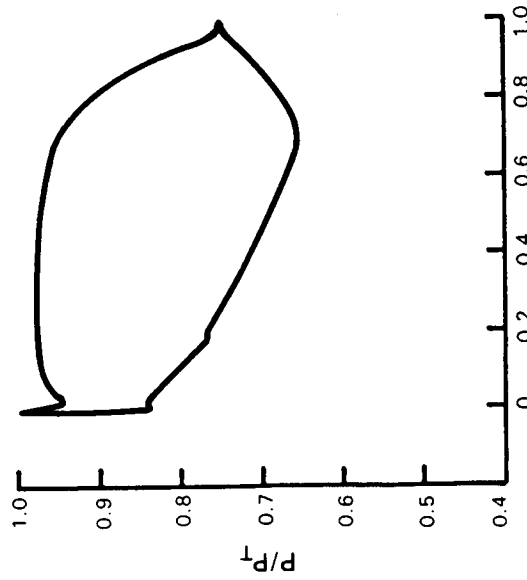
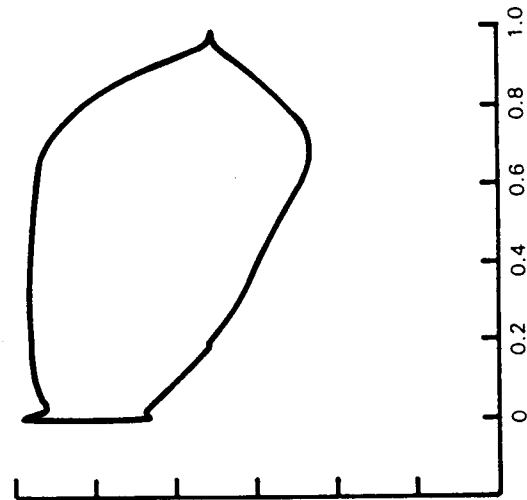
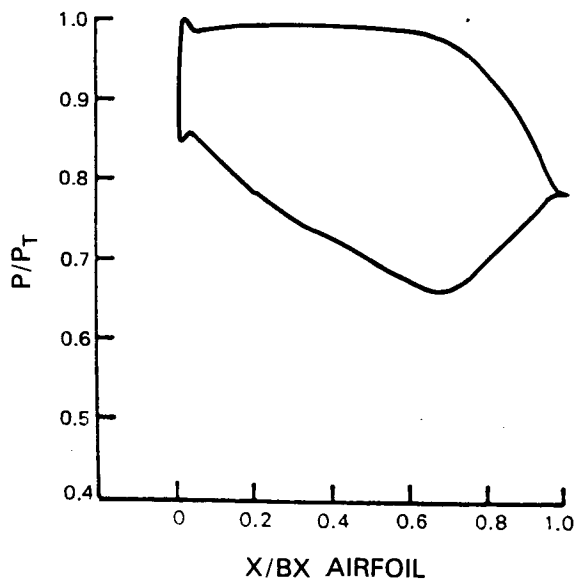
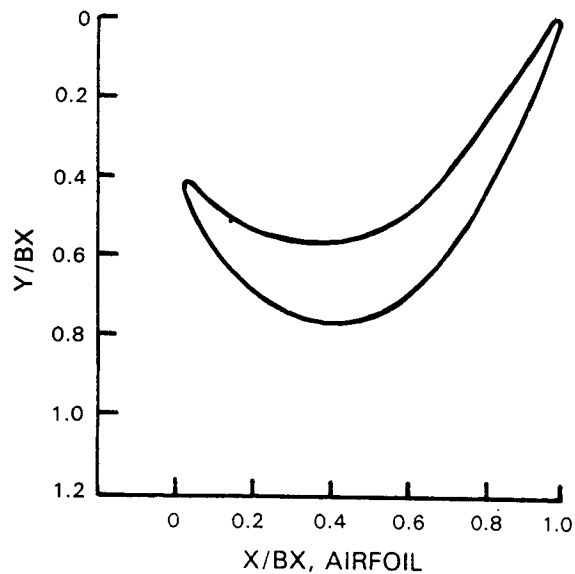


Figure 4.2.4-4 Turbine Second Stage Blade Root and One-Quarter Root Section Aerodynamic Definitions and Pressure Distributions



RADIUS cm (in)	47.759 (18.803)
INLET METAL ANGLE	36.4°
EXIT METAL ANGLE	25.2°
AXIAL CHORD cm (in)	2.66 (1.05)
FOILS	120.
SOLIDITY (bx)	1.07
ELLIPSE RATIO	4/1
CHORD cm (in)	2.943 (1.159)
INLET GAS ANGLE	41.0°
EXIT GAS ANGLE	25.7°
INLET M _n	.378
EXIT M _n	.624
INCIDENCE	-4.6°
M _{MAX}	.834
Δ P/Q T.E.	.418

Figure 4.2.4-5 Turbine Second Stage Blade Mean Section Aerodynamic Definition and Pressure Distribution

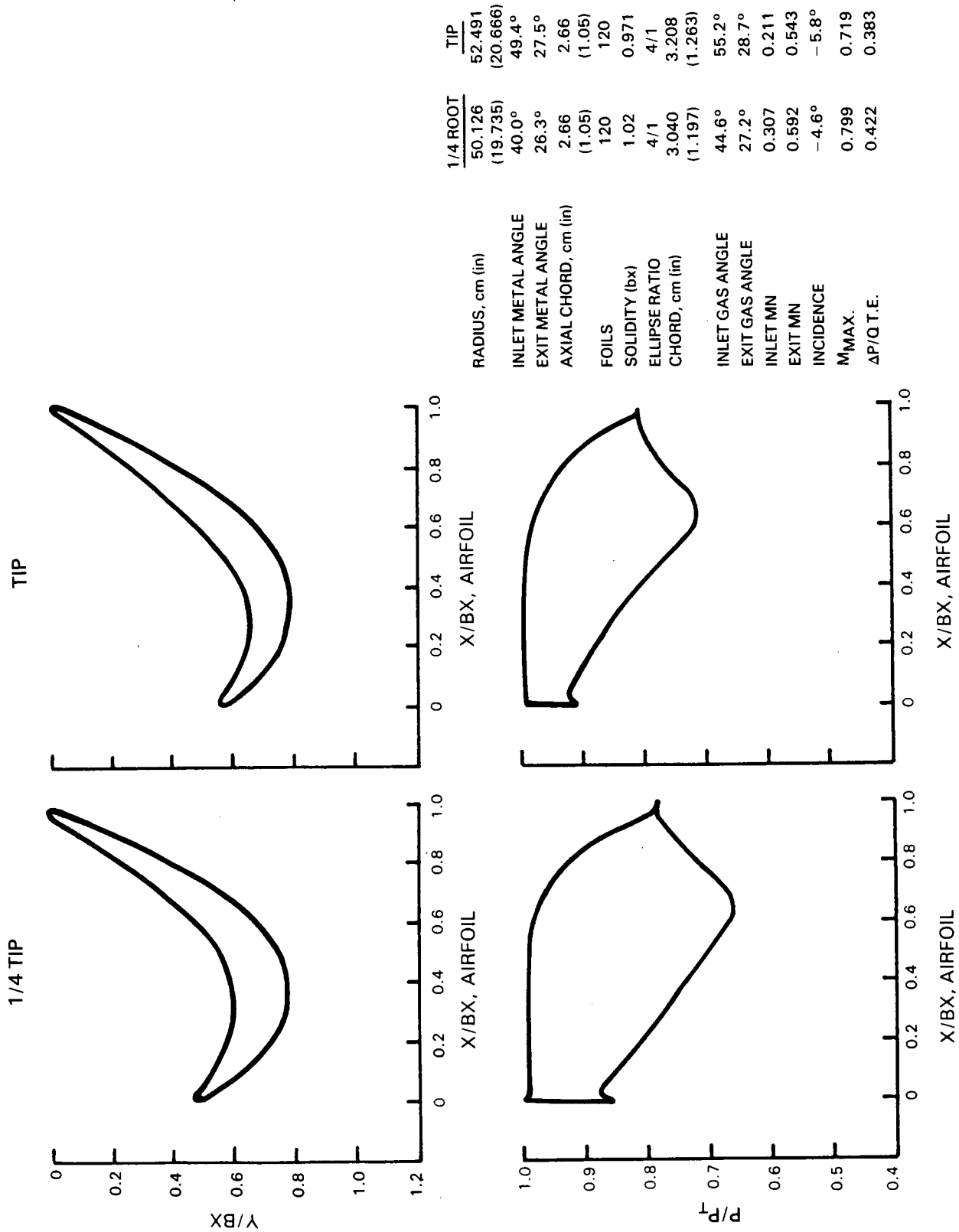
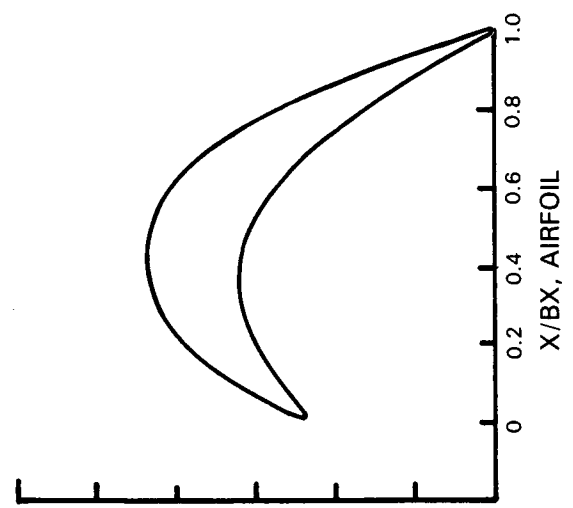
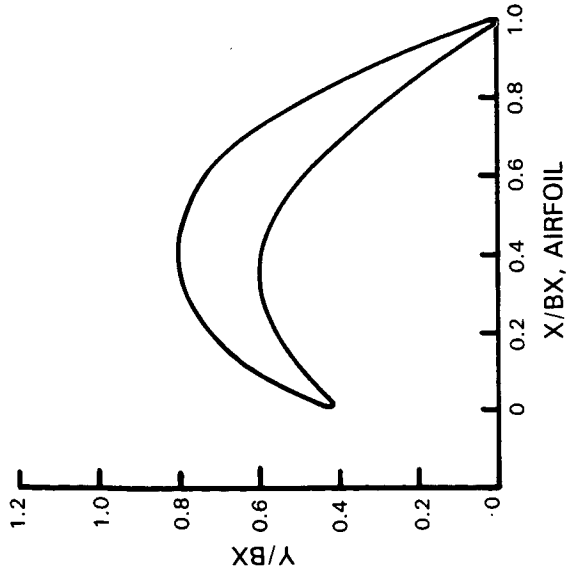


Figure 4.2.4-6 Turbine Second Stage Blade Tip and One-Quarter Tip Section Aerodynamic Definitions and Pressure Distributions

1/4 ROOT



ROOT



	ROOT	1/4 ROOT
RADIUS, cm (in)	44.081 (17.355)	46.901 (18.465)
INLET METAL ANGLE	32.7°	37.2°
EXIT METAL ANGLE	27.7°	21.5°
AXIAL CHORD, cm (in)	4.08 (1.61)	4.08 (1.61)
FOILS	72.0	72.0
SOLIDITY (bx)	1.06	1.00
ELLIPSE RATIO	4/1	4/1
CHORD, cm (in)	4.394 (1.730)	4.587 (1.806)
INLET GAS ANGLE	37.6°	43.6°
EXIT GAS ANGLE	30.3°	23.7°
INLET MN	0.360	0.372
EXIT MN	0.601	0.653
INCIDENCE	-4.9°	-6.4°
M _{MAX.}	0.831	0.913
ΔP/Q.T.E.	0.402	0.469

RADIUS, cm (in)
 INLET METAL ANGLE
 EXIT METAL ANGLE
 AXIAL CHORD, cm (in)
 FOILS
 SOLIDITY (bx)
 ELLIPSE RATIO
 CHORD, cm (in)
 INLET GAS ANGLE
 EXIT GAS ANGLE
 INLET MN
 EXIT MN
 INCIDENCE
 M_{MAX.}
 ΔP/Q.T.E.

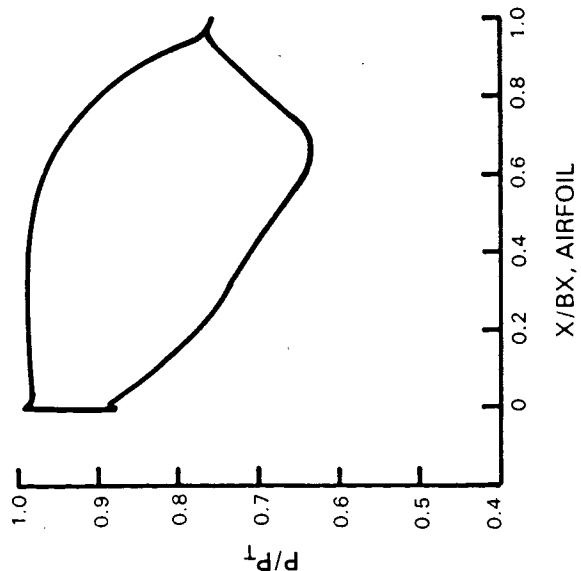
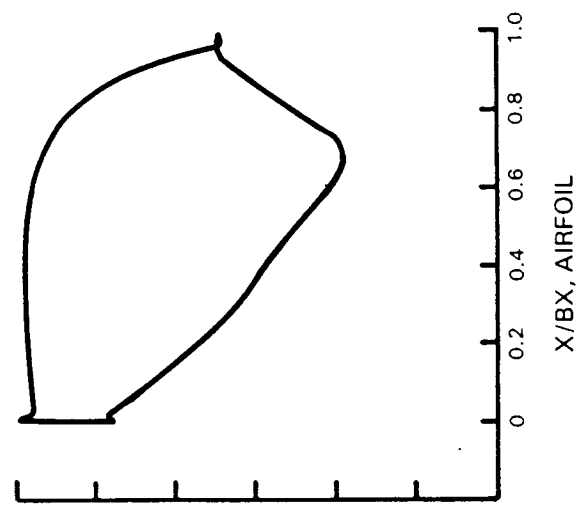
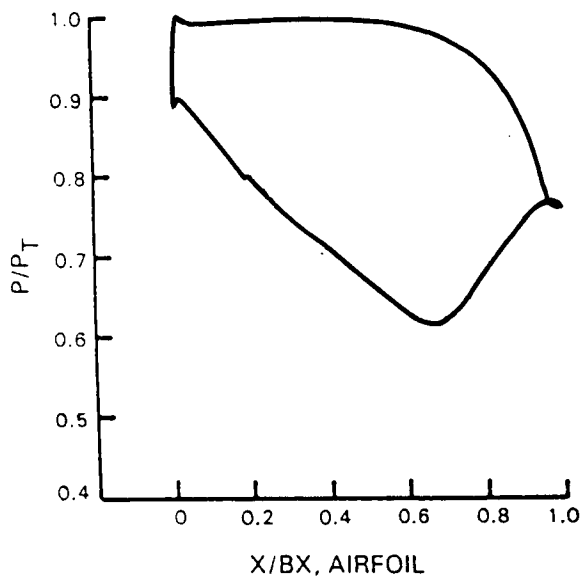
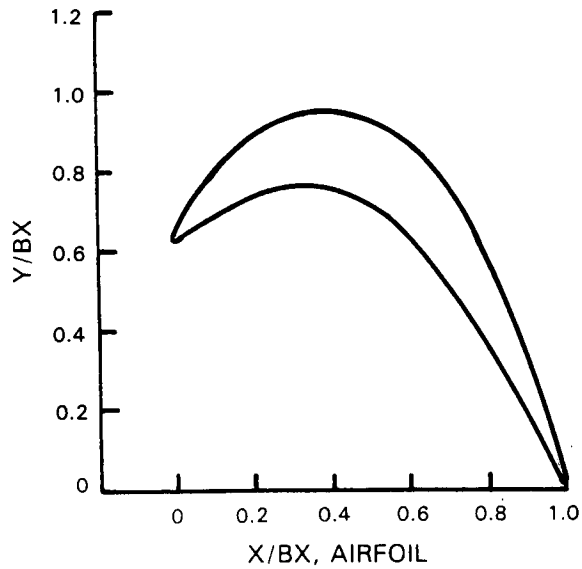


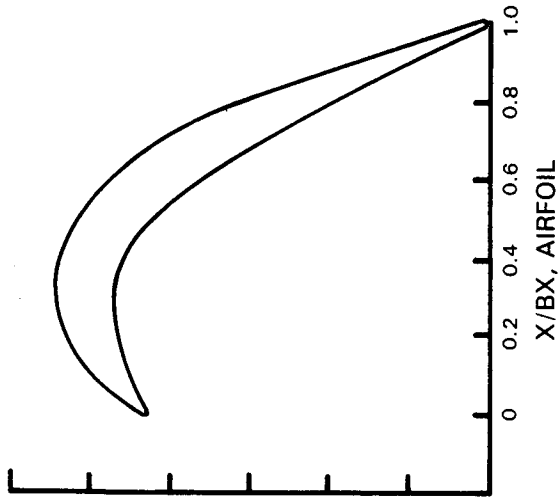
Figure 4.2.4-7 Turbine Third Stage Vane Root and One-Quarter Root Section Aerodynamic Definitions and Pressure Distributions



RADIUS cm (in)	49.68 (19.56)
INLET METAL ANGLE	41.7°
EXIT METAL ANGLE	21.0°
AXIAL CHORD cm (in)	4.08 (1.61)
FOILS	72.
SOLIDITY (bx)	.942
ELLIPSE RATIO	4/1
CHORD cm (in)	4.831 (1.902)
INLET GAS ANGLE	49.5°
EXIT GAS ANGLE	22.9°
INLET M _n	.337
EXIT M _n	.657
INCIDENCE	-7.9°
M _{MAX}	.912
ΔP/Q T.E.	.466

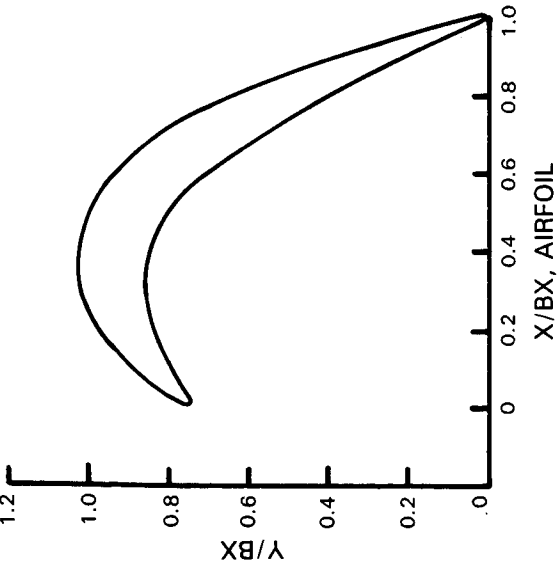
Figure 4.2.4-8 Turbine Third Stage Vane Mean Section Aerodynamic Definition and Pressure Distribution

TIP



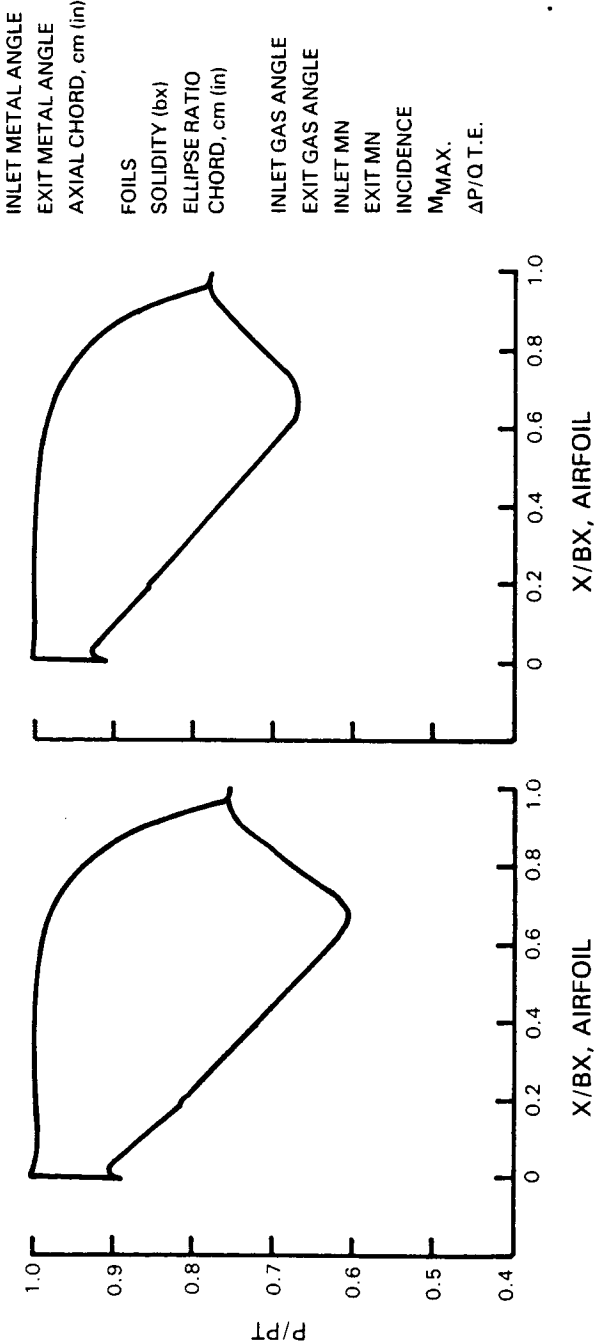
X/BX, AIRFOIL

1/4 TIP



X/BX, AIRFOIL

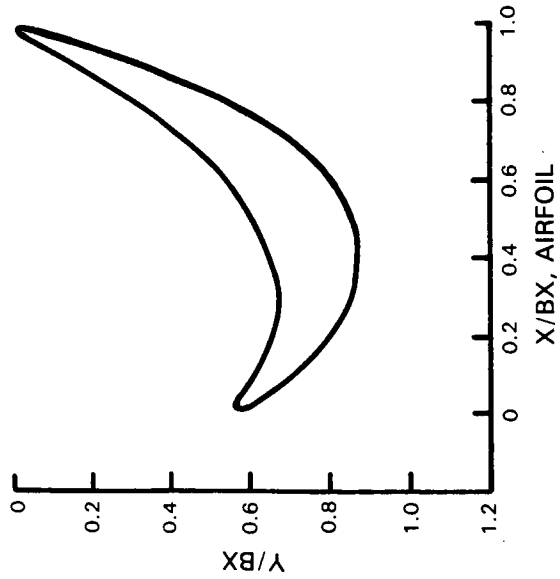
RADIUS, cm (in)	1/4 TIP	TIP
INLET METAL ANGLE	52.542 (20.686)	55.364 (21.797)
EXIT METAL ANGLE	47.7°	52.2°
AXIAL CHORD, cm (in)	20.5°	19.8°
FOILS	4.08	4.08
SOLIDITY (bx)	(1.61)	(1.61)
ELLIPSE RATIO	72.0	72.0
CHORD, cm (in)	0.892	0.846
INLET GAS ANGLE	4/1	4/1
EXIT GAS ANGLE	5.123	5.471
INLET MN	(2.017)	(2.154)
EXIT MN	57.0°	63.0°
INCIDENCE	22.4°	21.9°
M _{MAX.}	0.288	0.225
ΔP/Q.T.E.	0.638	0.590
	-9.4°	-10.9°
	0.878	0.778
	0.451	0.373



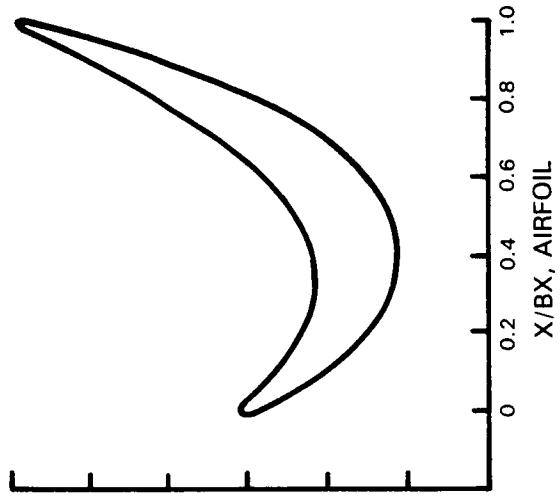
X/BX, AIRFOIL

Figure 4.2.4-9 Turbine Third Stage Vane Tip and One-Quarter Tip Section Aerodynamic Definitions and Pressure Distributions

ROOT



1/4 ROOT



ROOT	1/4 ROOT
44.533	47.863
(17.533)	(18.844)
43.7°	34.2°
21.5°	21.0°
3.07	3.07
(1.21)	(1.21)
96.0	96.0
1.05	0.98
3/1	3/1
3.515	3.477
(1.384)	(1.369)
51.9°	41.0°
23.5°	23.1°
0.381	0.380
0.645	0.678
-8.3°	-6.8°
0.878	0.907
0.378	0.414

RADIUS, cm (in)

INLET METAL ANGLE

EXIT METAL ANGLE

AXIAL CHORD, cm (in)

FOILS

SOLIDITY (bx)

ELLIPSE RATIO

CHORD, cm (in)

INLET GAS ANGLE

EXIT GAS ANGLE

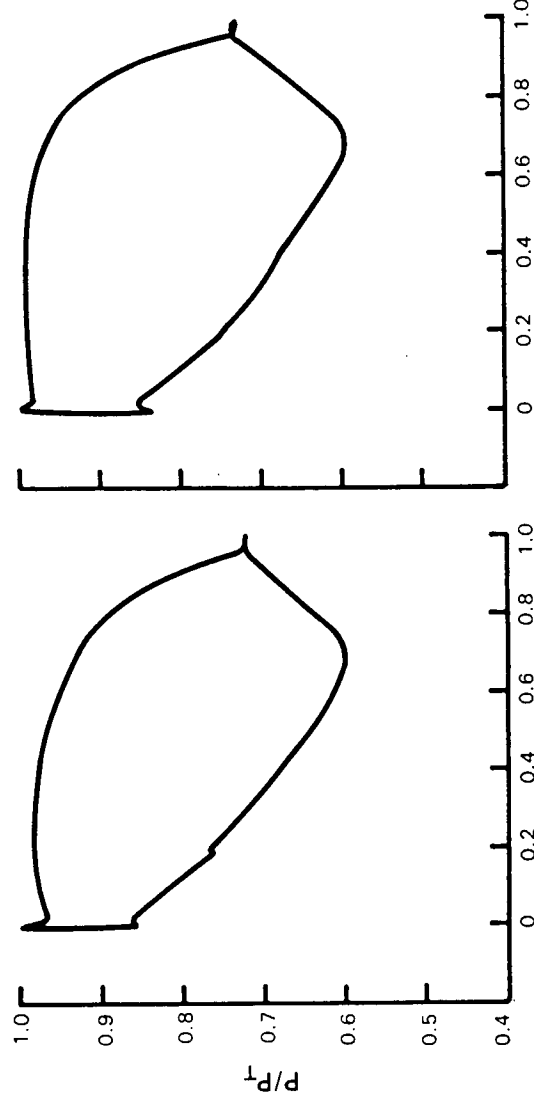
INLET MN

EXIT MN

INCIDENCE

M_{MAX}

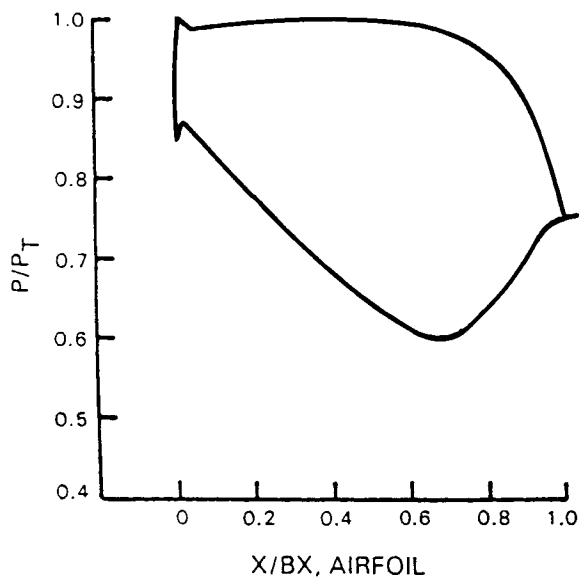
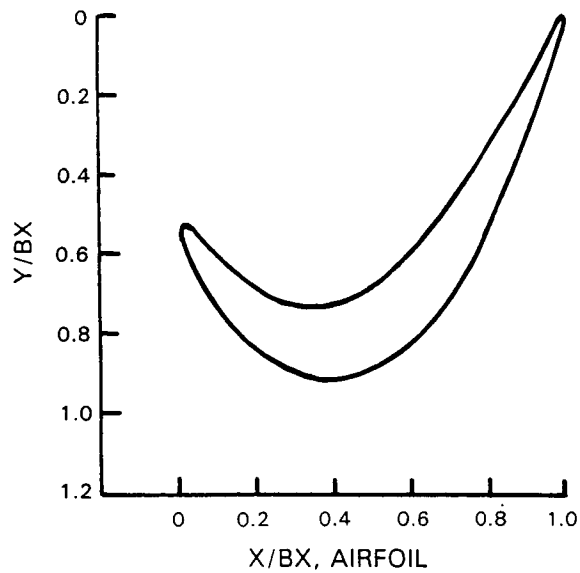
$\Delta P/Q.T.E.$



X/BX, AIRFOIL

X/BX, AIRFOIL

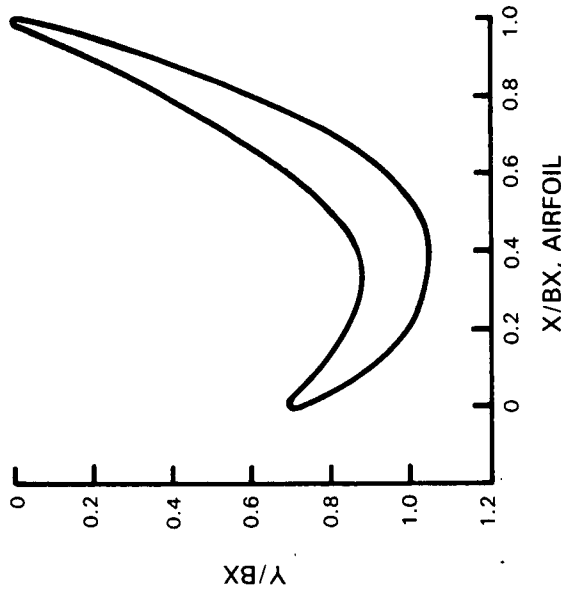
Figure 4.2.4-10 Turbine Third Stage Blade Root and One-Quarter Root Section Aerodynamic Definitions and Pressure Distributions



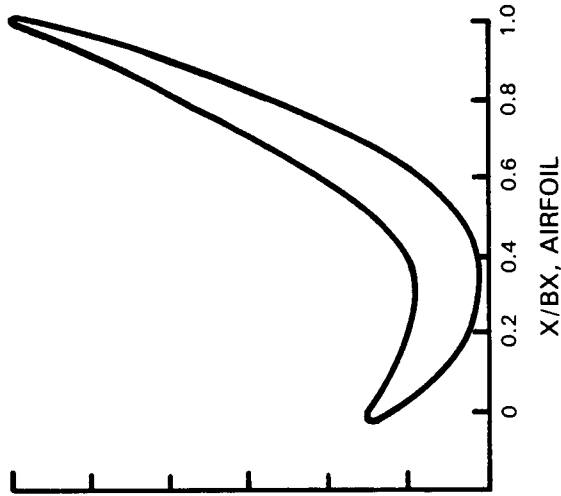
RADIUS cm (in)	51.191(20.154)
INLET METAL ANGLE	35.2°
EXIT METAL ANGLE	20.6°
AXIAL CHORD cm (in)	3.068 (1.208)
FOILS	96.
SOLIDITY (bx)	.916
ELLIPSE RATIO	3/1
CHORD cm (in)	3.550 (1.398)
INLET GAS ANGLE	42.2°
EXIT GAS ANGLE	22.7°
INLET MN	.355
EXIT MN	.666
INCIDENCE	-7.1°
M _{MAX}	.918
ΔP/Q T.E.	.465

Figure 4.2.4-11 Turbine Third Stage Blade Mean Section Aerodynamic Definition and Pressure Distribution

1/4 TIP



TIP



1/4 TIP	TIP
54.521 (21.465)	57.696 (22.715)
37.5°	45.4°
20.1°	19.7°
3.07 (1.21)	3.07 (1.21)
96.0	96.0
0.86	0.81
3/1	3/1
3.741 (1.473)	4.076 (1.608)
46.2°	55.4°
22.2°	21.7°
0.309	0.242
0.636	0.599
-8.7°	-10.0°
0.892	0.811
0.473	0.404

RADIUS, cm (in)
 INLET METAL ANGLE
 EXIT METAL ANGLE
 AXIAL CHORD, cm (in)
 FOILS
 SOLIDITY (bx)
 ELLIPSE RATIO
 CHORD, cm (in)
 INLET GAS ANGLE
 EXIT GAS ANGLE
 INLET MN
 EXIT MN
 INCIDENCE
 M_{MAX}
 $\Delta P/Q.T.E.$

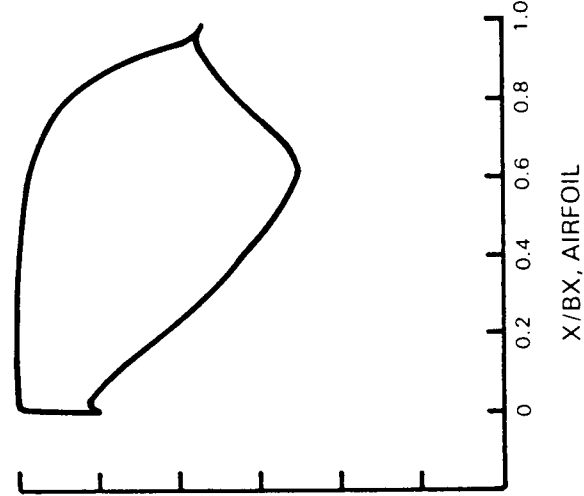
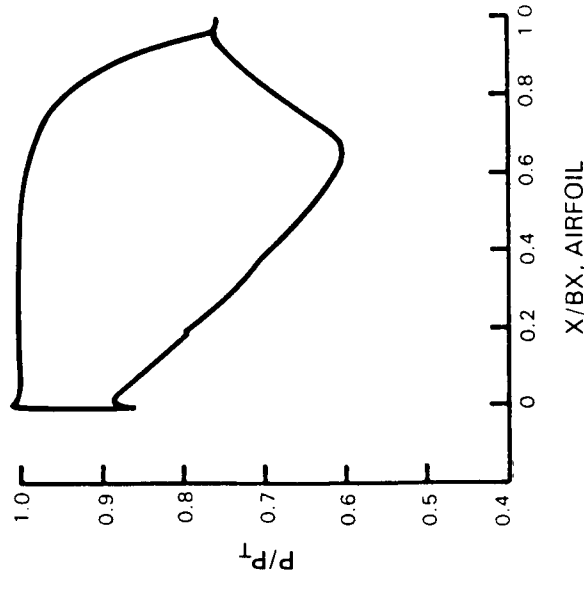
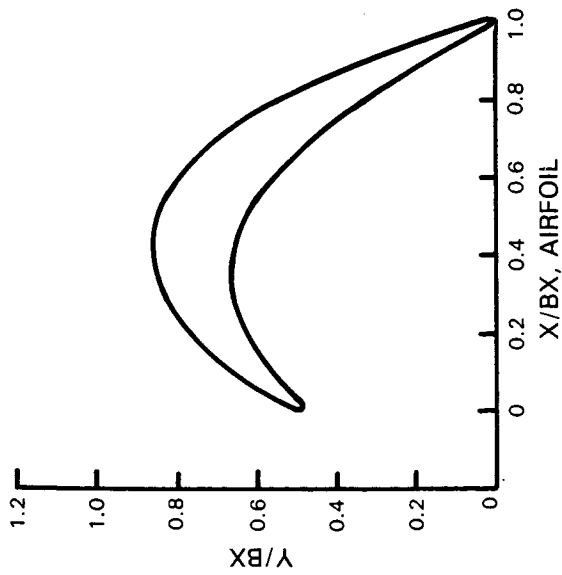
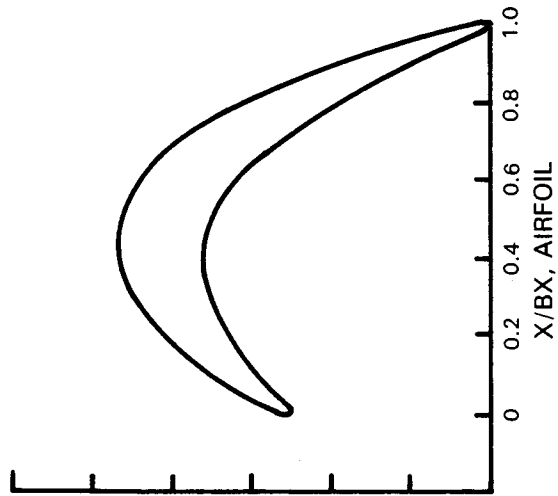


Figure 4.2.4-12 Turbine Third Stage Blade Tip and One-Quarter Tip Section Aerodynamic Definitions and Pressure Distributions

ROOT



1/4 ROOT



	ROOT	1/4 ROOT
RADIUS, cm (in)	44.726 (17.609)	48.7133 (19.1785)
INLET METAL ANGLE	34.2°	36.1°
EXIT METAL ANGLE	26.6°	19.8°
AXIAL CHORD, cm (in)	3.73 (1.47)	3.73 (1.47)
FOILS	84.0	84.0
SOLIDITY (bx)	1.11	1.02
ELLIPSE RATIO	4/1	4/1
CHORD, cm (in)	4.030 (1.587)	4.140 (1.630)
INLET GAS ANGLE	37.7°	40.8°
EXIT GAS ANGLE	28.9°	22.1°
INLET MN	0.370	0.384
EXIT MN	0.648	0.700
INCIDENCE	-3.5°	-4.7°
M _{MAX}	0.864	0.923
ΔP/Q T.E.	0.346	0.40

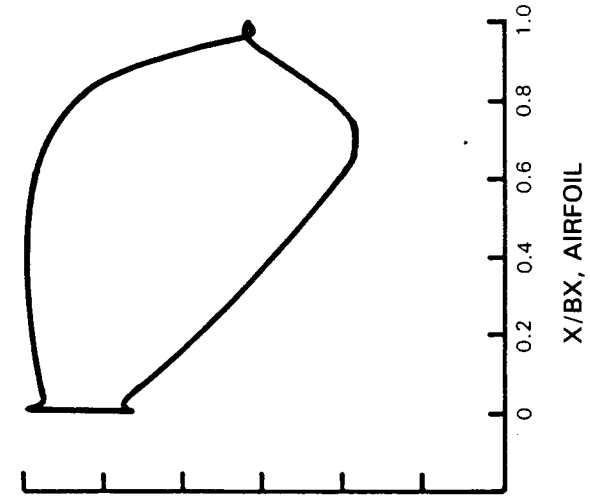
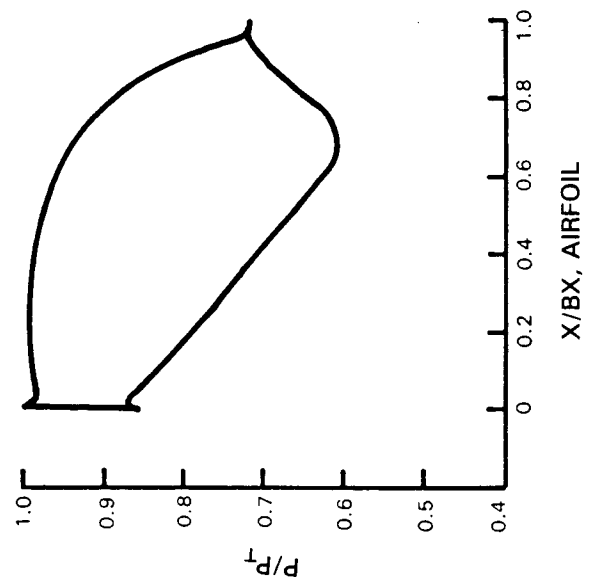
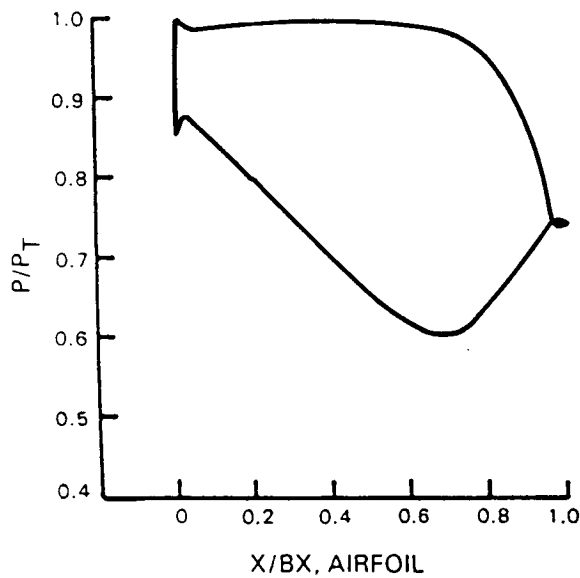
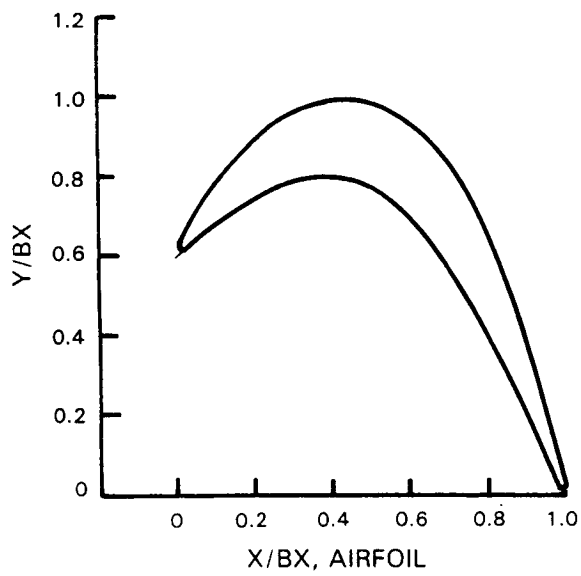


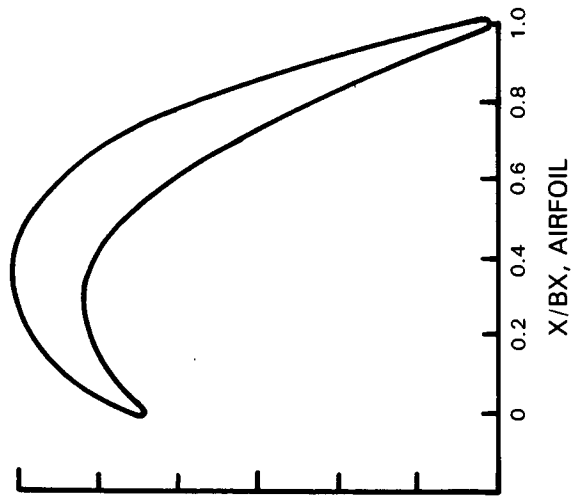
Figure 4.2.4-13 Turbine Fourth Stage Vane Root and One-Quarter Root Section Aerodynamic Definitions and Pressure Distributions



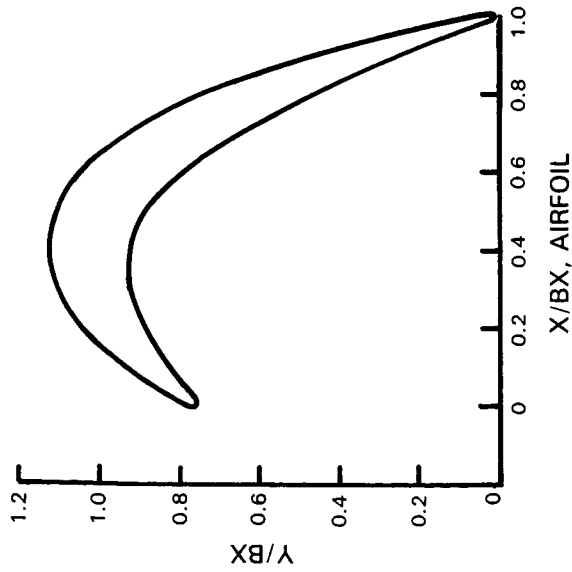
RADIUS cm (in)	52.699 (20.748)
INLET METAL ANGLE	38.7°
EXIT METAL ANGLE	18.9°
AXIAL CHORD cm (in)	3.73 (1.47)
FOILS	84
SOLIDITY (bx)	.9445
ELLIPSE RATIO	4/1
CHORD cm (in)	4.328 (1.704)
INLET GAS ANGLE	43.6°
EXIT GAS ANGLE	21.2°
INLET M _n	.362
EXIT M _n	.690
INCIDENCE	-4.9°
M _{MAX}	.925
ΔP/Q T.E.	.428

Figure 4.2.4-14 Turbine Fourth Stage Vane Mean Section Aerodynamic Definition and Pressure Distribution

TIP



1/4 TIP



	1/4 TIP	TIP
RADIUS, cm (in)	56.6864 (22.3175)	60.672 (23.887)
INLET METAL ANGLE	39.5°	39.5°
EXIT METAL ANGLE	18.2°	17.5°
AXIAL CHORD, cm (in)	3.73 (1.47)	3.73 (1.47)
FOILS	84.0	84.0
SOLIDITY (bx)	0.877	0.819
ELLIPSE RATIO	4/1	4/1
CHORD, cm (in)	4.582 (1.804)	4.909 (1.933)
INLET GAS ANGLE	48.7°	56.0°
EXIT GAS ANGLE	20.4°	19.6°
INLET MN	0.301	0.249
EXIT MN	0.653	0.600
INCIDENCE	-9.2°	-16.5°
M _{MAX}	0.876	0.791
ΔP/Q.T.E.	0.424	0.390

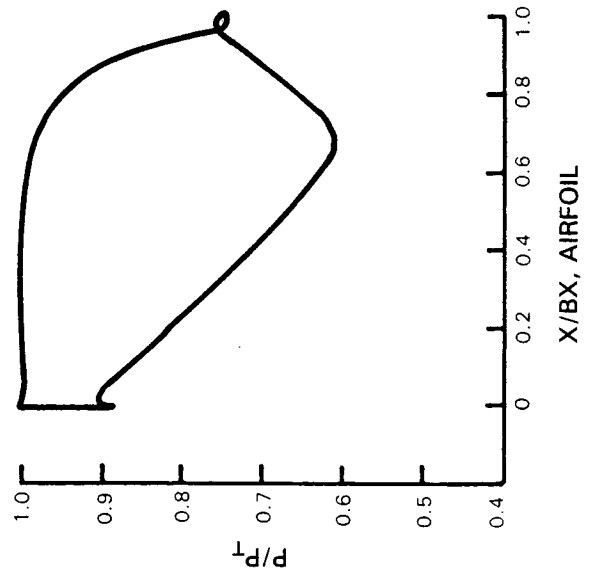
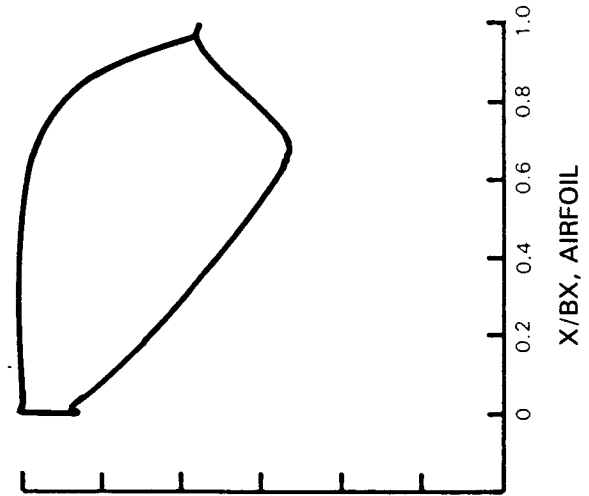


Figure 4.2.4-15 Turbine Fourth Stage Vane Tip and One-Quarter Tip Section Aerodynamic Definitions and Pressure Distributions

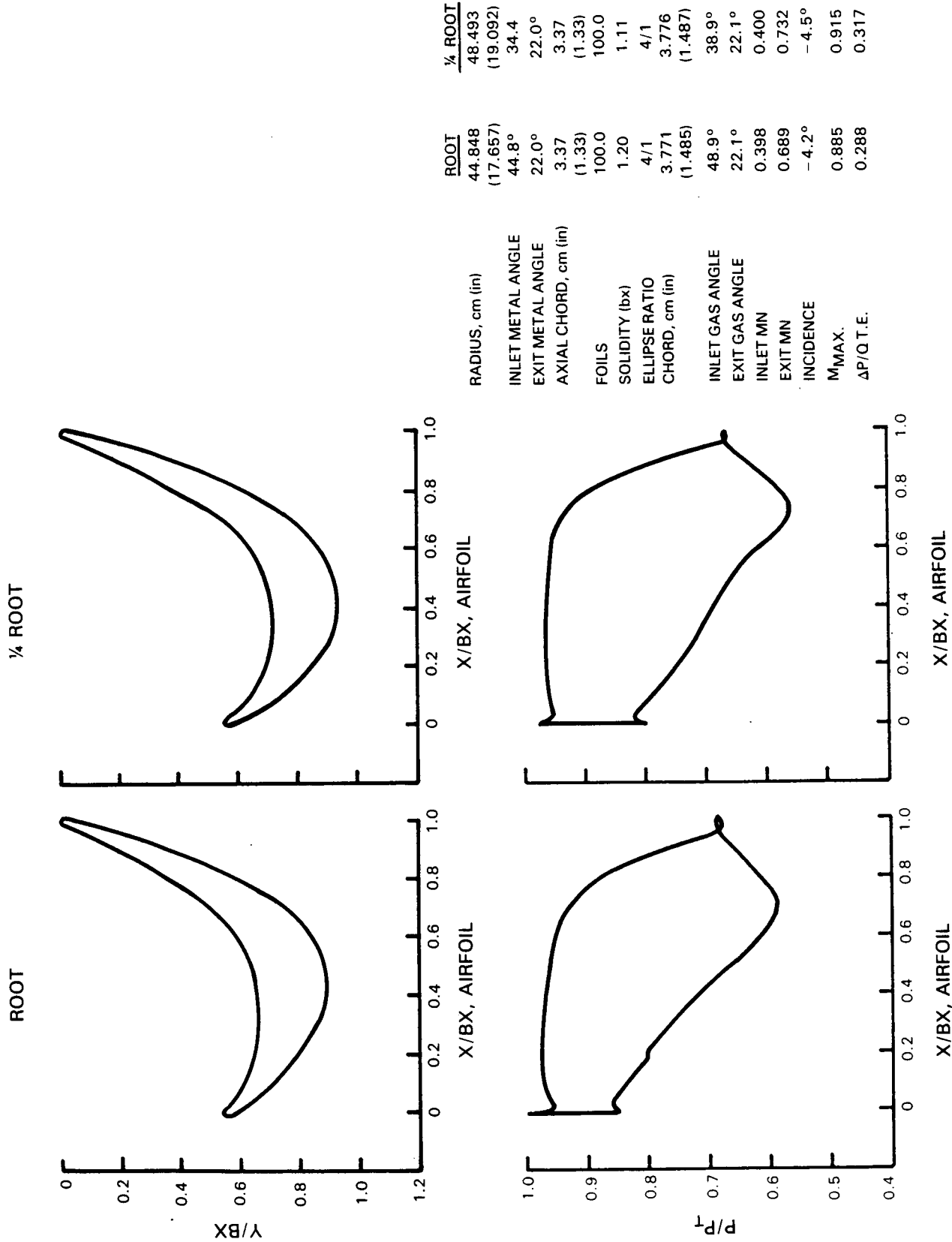
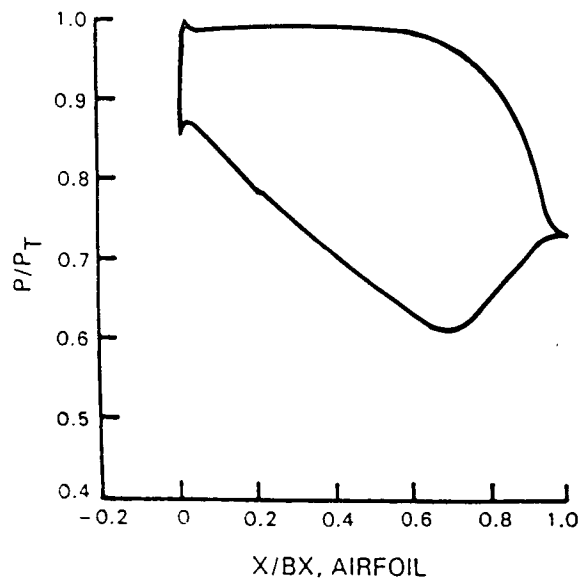
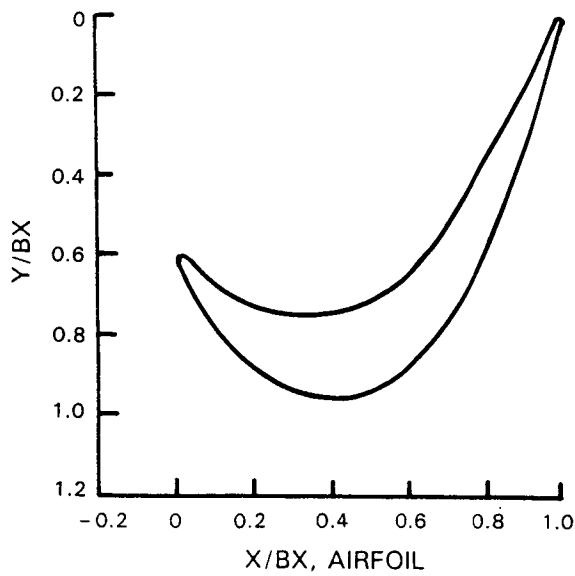


Figure 4.2.4-16 Turbine Fourth Stage Blade Root and One-Quarter Root Section Aerodynamic Definitions and Pressure Distributions



RADIUS cm (in)	53.962 (21.245)
INLET METAL ANGLE	33.8°
EXIT METAL ANGLE	22.1°
AXIAL CHORD cm (in)	3.37 (1.33)
FOILS	100.
SOLIDITY (bx)	.9954
ELLIPSE RATIO	4/1
CHORD cm (in)	3.934 (1.549)
INLET GAS ANGLE	41.5°
EXIT GAS ANGLE	22.2°
INLET M _n	.350
EXIT M _n	.696
INCIDENCE	-7.6°
M _{MAX.}	.902
ΔP/Q T.E.	.386

Figure 4.2.4-17 Turbine Fourth Stage Blade Mean Section Aerodynamic Definition and Pressure Distribution

TIP

1/4 TIP

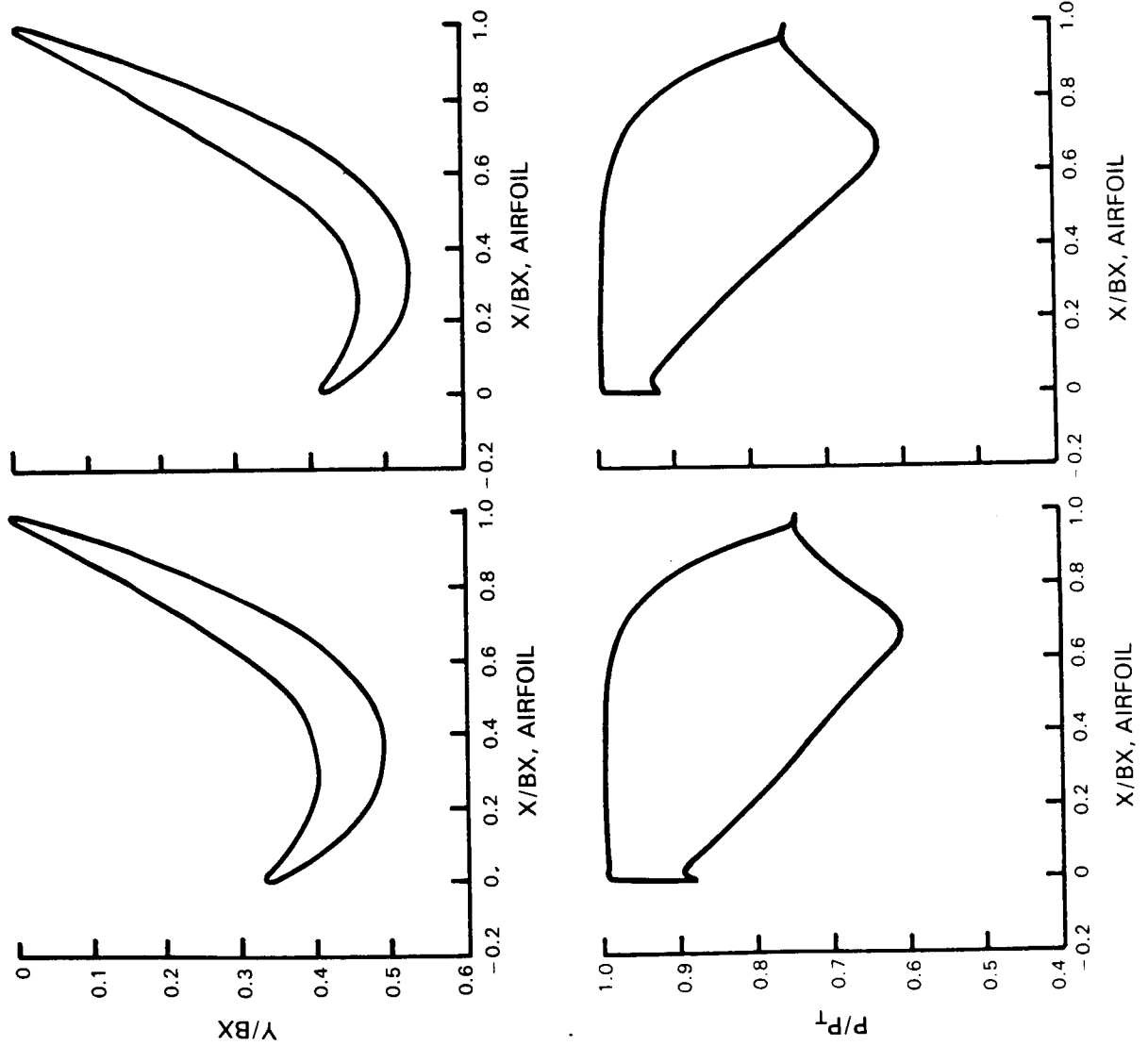
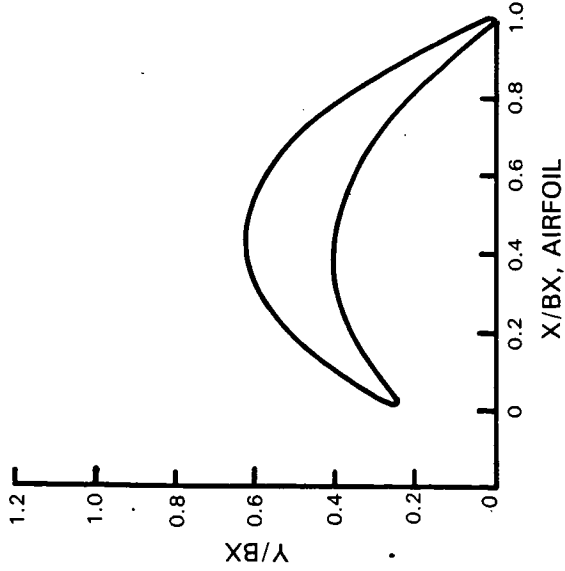
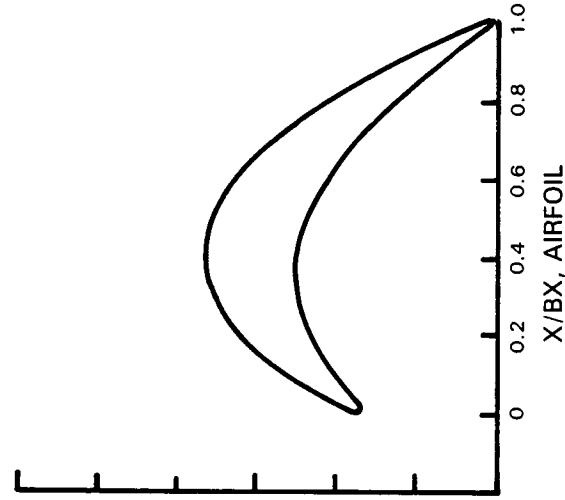


Figure 4.2.4-18 Turbine Fourth Stage Blade Tip and One-Quarter Tip Section Aerodynamic Definitions and Pressure Distributions

ROOT



1/4 ROOT



ROOT	1/4 ROOT
44.95	49.93
(17.70)	(19.66)
38.1°	38.9
30.2°	25.9°
3.65	3.65
(1.44)	(1.44)
108.0	108.0
FOILS	FOILS
1.40	1.26
4/1	4/1
3.776	3.939
(1.487)	(1.551)
INLET GAS ANGLE	INLET GAS ANGLE
37.2°	39.9°
EXIT GAS ANGLE	EXIT GAS ANGLE
32.4°	26.5°
INLET MN	INLET MN
0.407	0.417
EXIT MN	EXIT MN
0.688	0.732
INCIDENCE	INCIDENCE
+1.0°	-1.0°
MMAX.	MMAX.
0.893	0.941
ΔP/Q T.E.	ΔP/Q T.E.
0.357	0.362

RADIUS, cm (in)
 INLET METAL ANGLE
 EXIT METAL ANGLE
 AXIAL CHORD, cm (in)
 FOILS
 SOLIDITY (bx)
 ELLIPSE RATIO
 CHORD, cm (in)
 INLET GAS ANGLE
 EXIT GAS ANGLE
 INLET MN
 EXIT MN
 INCIDENCE
 MMAX.
 ΔP/Q T.E.

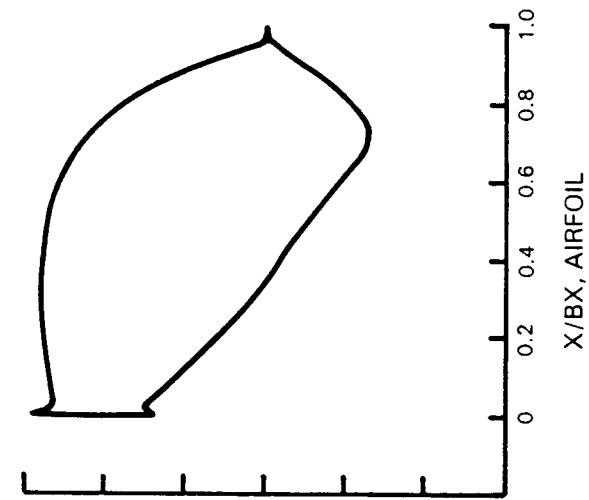
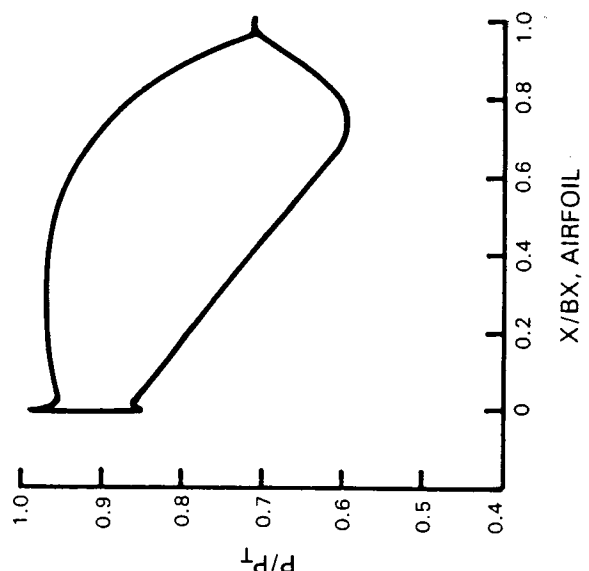
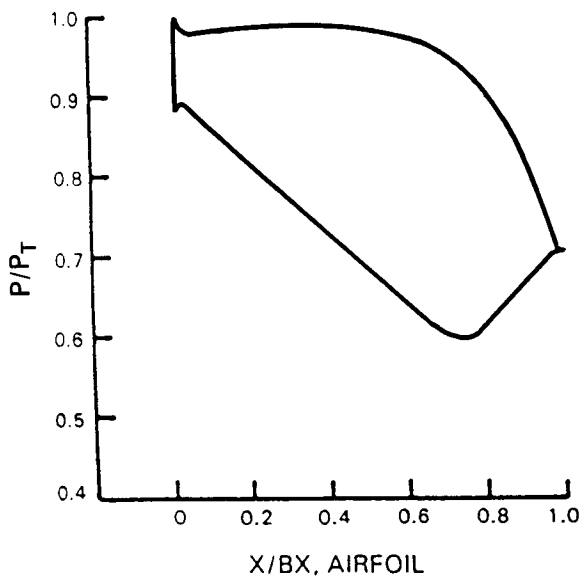
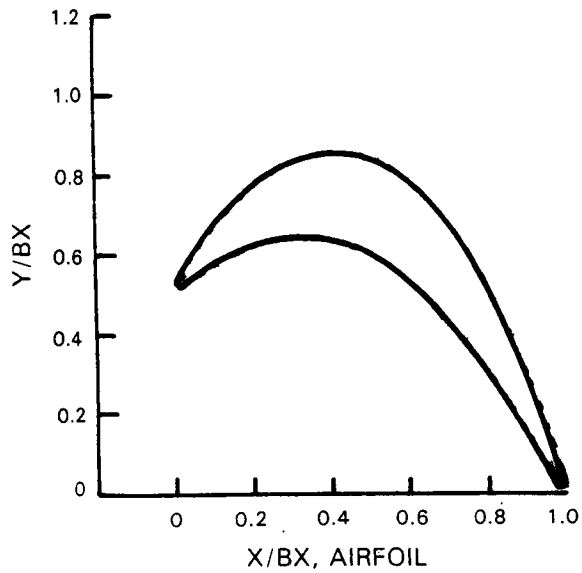


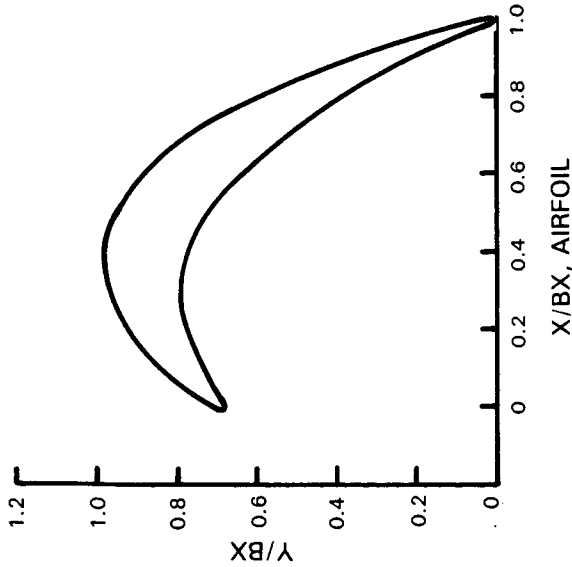
Figure 4.2.4-19 Turbine Fifth Stage Vane Root and One-Quarter Root Section Aerodynamic Definitions and Pressure Distributions



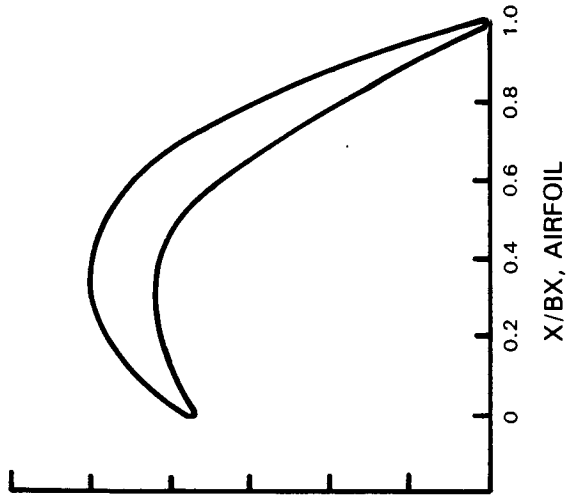
RADIUS cm (in)	54.91 (21.62)
INLET METAL ANGLE	42.0°
EXIT METAL ANGLE	22.6°
AXIAL CHORD cm (in)	3.65 (1.44)
FOILS	108.
SOLIDITY (bx)	1.148
ELLIPSE RATIO	4/1
CHORD cm (in)	4.155 (1.636)
INLET GAS ANGLE	45.4°
EXIT GAS ANGLE	22.7°
INLET M _n	.350
EXIT M _n	.736
INCIDENCE	-3.4°
M _{MAX}	.919
ΔP/Q T.E.	.336

Figure 4.2.4-20 Turbine Fifth Stage Vane Mean Section Aerodynamic Definition and Pressure Distribution

1/4 TIP



TIP



	1/4 TIP	TIP
RADIUS, cm (in)	59.89 (23.58)	64.87 (25.54)
INLET METAL ANGLE	48.0°	53.1°
EXIT METAL ANGLE	21.2°	20.6°
AXIAL CHORD, cm (in)	3.65 (1.44)	3.65 (1.44)
FOILS	108.0	108.0
SOLIDITY (bx)	1.05	0.971
ELLIPSE RATIO	4/1	4/1
CHORD, cm (in)	4.409 (1.736)	4.620 (1.819)
INLET GAS ANGLE	53.0°	58.6°
EXIT GAS ANGLE	22.4°	22.6°
INLET MN	0.301	0.289
EXIT MN	0.712	0.646
INCIDENCE	-5.1°	-5.5°
M _{MAX.}	0.896	0.850
ΔP/Q.T.E.	0.336	0.357

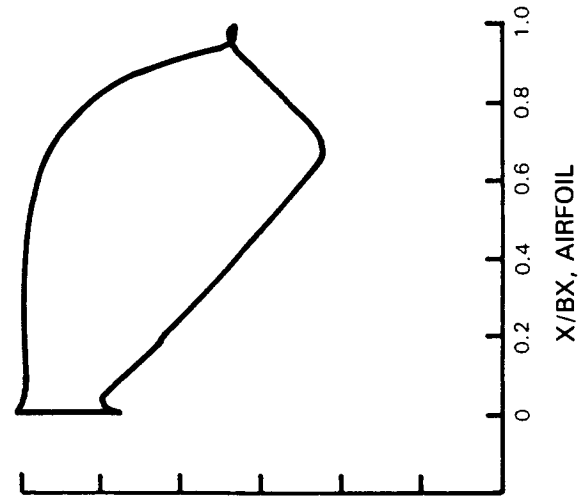
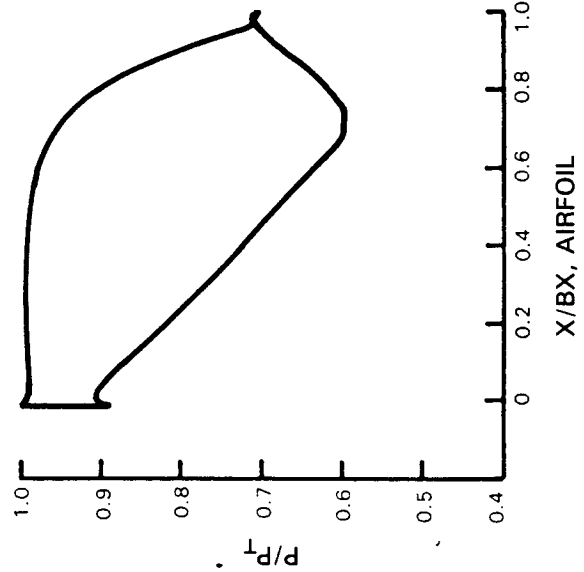
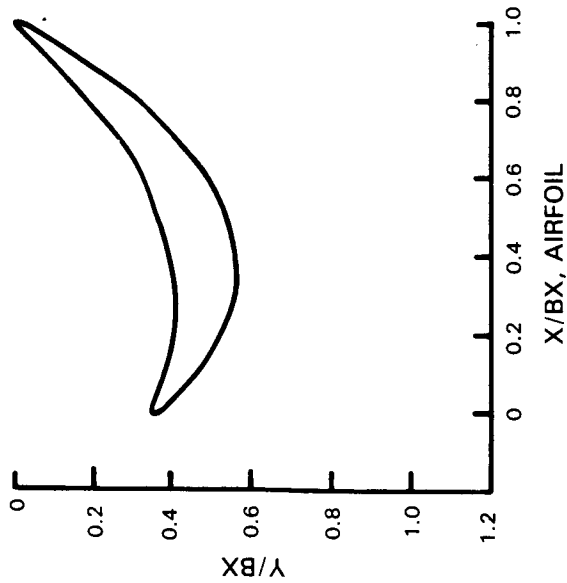
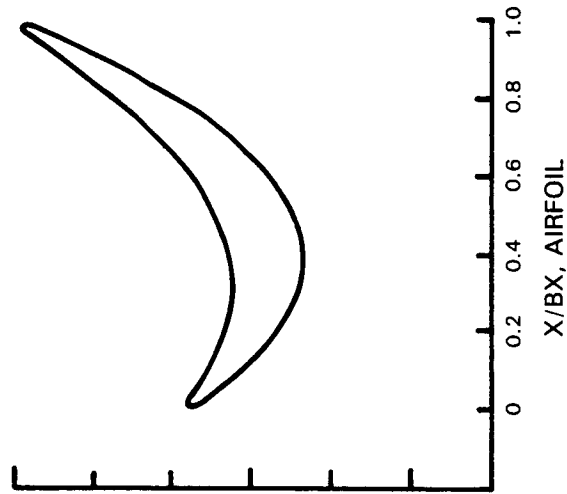


Figure 4.2.4-21 Turbine Fifth Stage Vane Tip and One-Quarter Tip Section Aerodynamic Definitions and Pressure Distributions

ROOT



1/4 ROOT



ROOT	1/4 ROOT
45.069 (17.744)	50.284 (19.797)
54.4°	45.8
35.3°	28.0°
3.53 (1.39)	3.42 (1.35)
122.0	122.0
1.52	1.32
4/1	4/1
3.713 (1.462)	3.726 (1.467)
55.1°	47.7°
37.3°	28.1°
0.453	0.491
0.786	0.817
-0.7°	-1.9°
1.046	1.028
0.379	0.335

RADIUS, cm (in)
 INLET METAL ANGLE
 EXIT METAL ANGLE
 AXIAL CHORD, cm (in)
 FOILS
 SOLIDITY
 ELLIPSE RATIO
 CHORD, cm (in)
 INLET GAS ANGLE
 EXIT GAS ANGLE
 INLET MN
 EXIT MN
 INCIDENCE
 M_{MAX}
 $\Delta P/Q.T.E.$

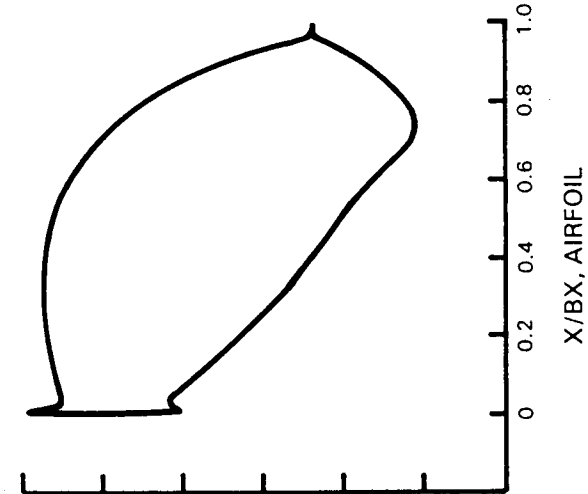
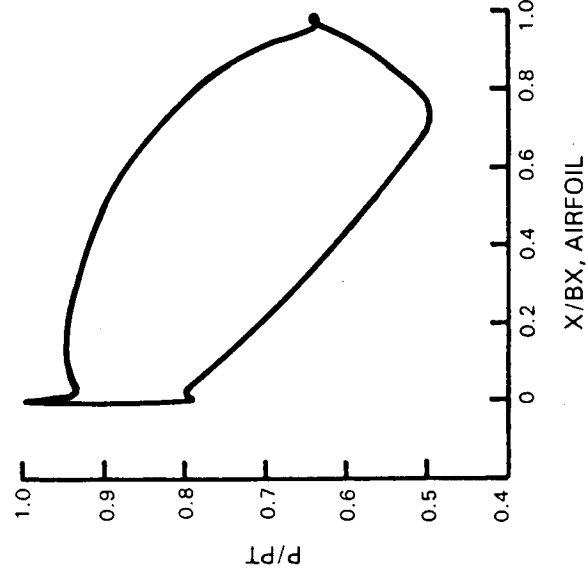
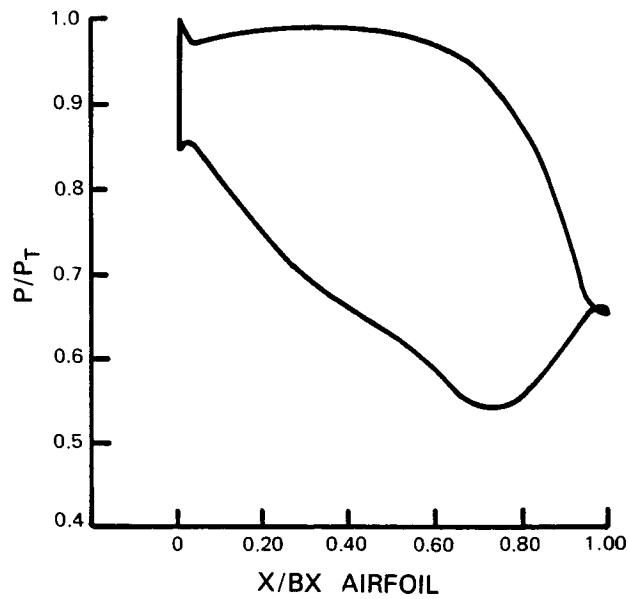
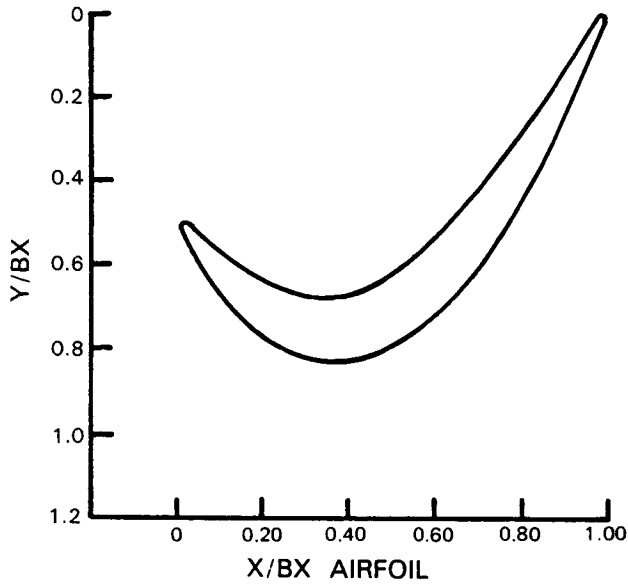


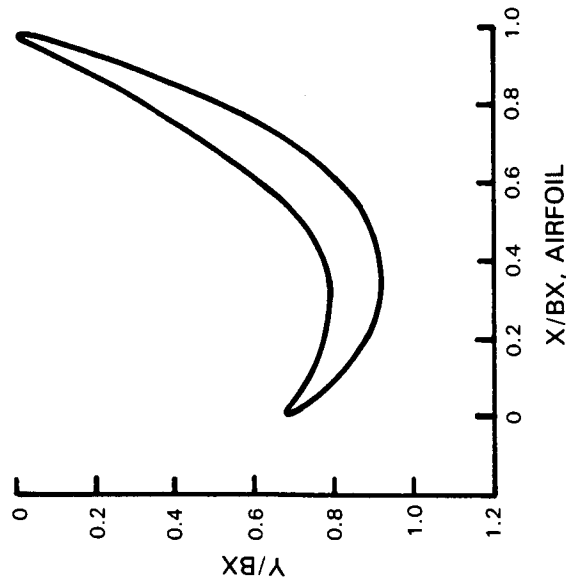
Figure 4.2.4-22 Turbine Fifth Stage Blade Root and One-Quarter Root Section Aerodynamic Definitions and Pressure Distributions



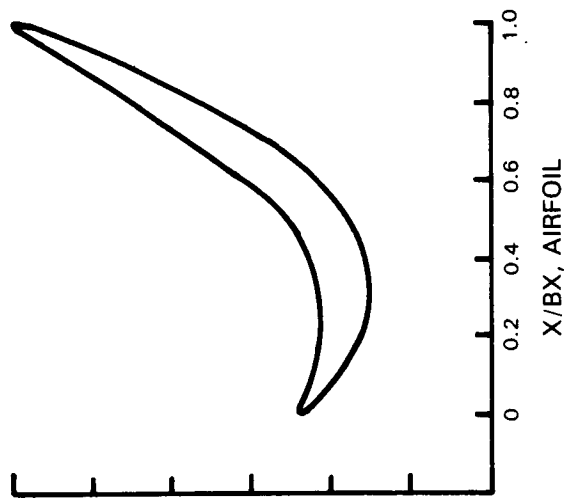
RADIUS cm (in)	55.501 (21.851)
INLET METAL ANGLE	40.2°
EXIT METAL ANGLE	25.5°
AXIAL CHORD cm (in)	3.32 (1.31)
FOILS	122
SOLIDITY (bx)	1.161
ELLIPSE RATIO	4/1
CHORD cm (in)	3.759 (1.480)
INLET GAS ANGLE	44.9°
EXIT GAS ANGLE	25.7°
INLET M _n	.384
EXIT M _n	.795
INCIDENCE	-4.7°
M MAX	.986
ΔP/Q T.E.	.322

Figure 4.2.4-23 Turbine Fifth Stage Blade Mean Section Aerodynamic Definition and Pressure Distribution

1/4 TIP



TIP



	1/4 TIP	TIP
RADIUS, cm (in)	60.716 (23.904)	65.933 (25.958)
INLET METAL ANGLE	46.5°	59.6
EXIT METAL ANGLE	24.5°	27.1°
AXIAL CHORD, cm (in)	3.32 (1.31)	3.32 (1.31)
FOILS	122.0	122.0
SOLIDITY (bx)	1.06	0.977
ELLIPSE RATIO	4/1	4/1
CHORD, cm (in)	3.929 (1.547)	4.094 (1.612)
INLET GAS ANGLE	50.7°	63.9°
EXIT GAS ANGLE	26.2°	29.5°
INLET MN	0.332	0.254
EXIT MN	0.774	0.734
INCIDENCE	-4.2°	-4.2°
M _{MAX}	1.00	0.984
ΔP/Q T.E.	0.373	0.375

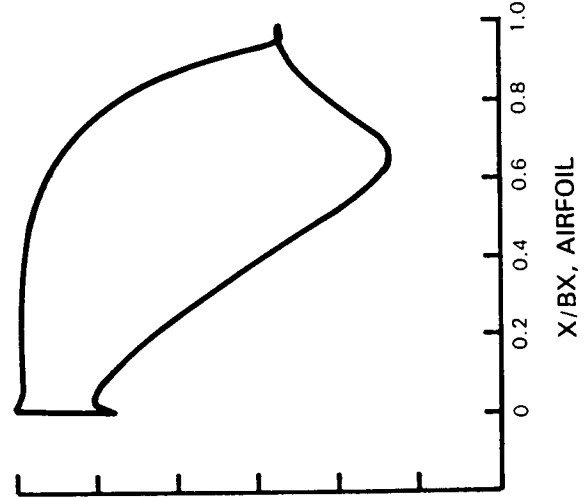
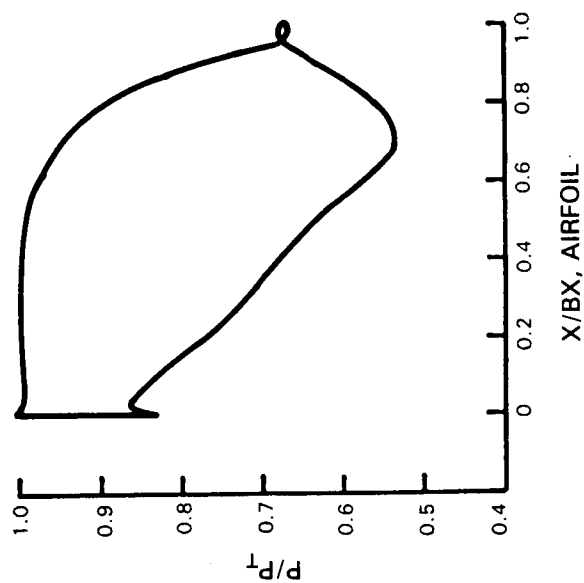


Figure 4.2.4-24 Turbine Fifth Stage Blade Tip and One-Quarter Tip Section Aerodynamic Definitions and Pressure Distributions

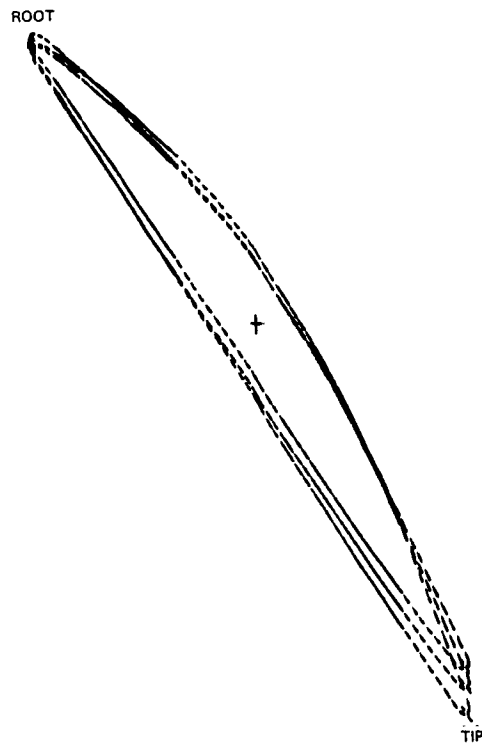


Figure 4.2.4-25 Second Stage Turbine Vane Stacking Arrangement

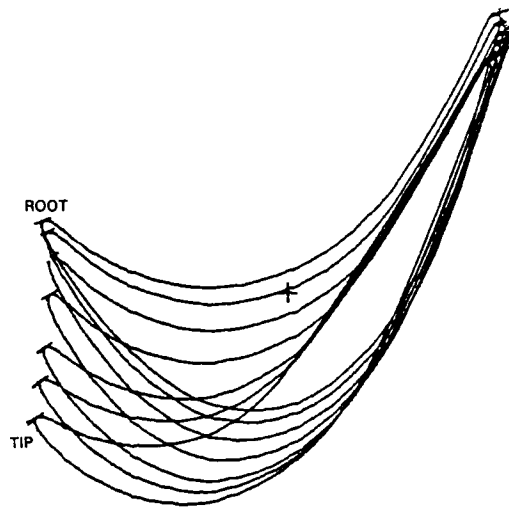


Figure 4.2.4-26 Second Stage Turbine Blade Stacking Arrangement

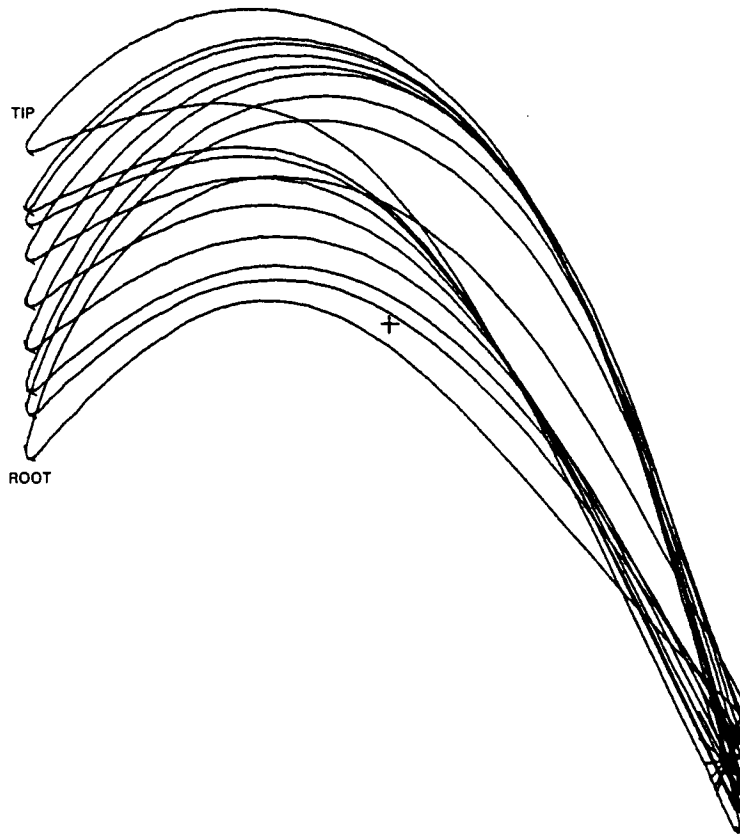


Figure 4.2.4-27 Third Stage Turbine Vane Stacking Arrangement

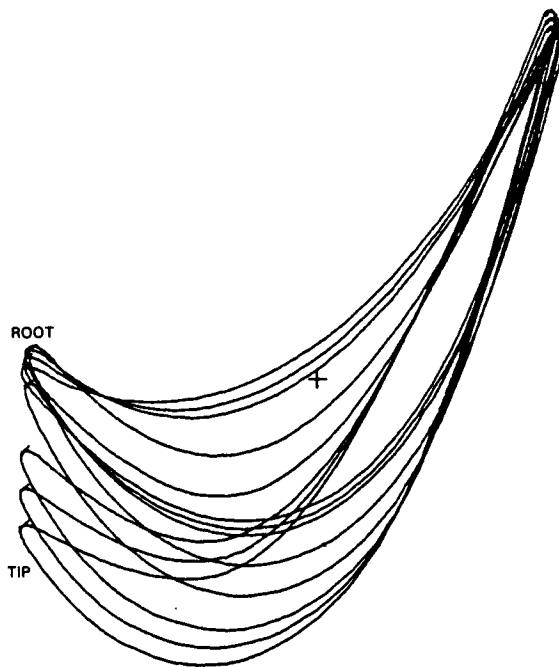


Figure 4.2.4-28 Third Stage Turbine Blade Stacking Arrangement

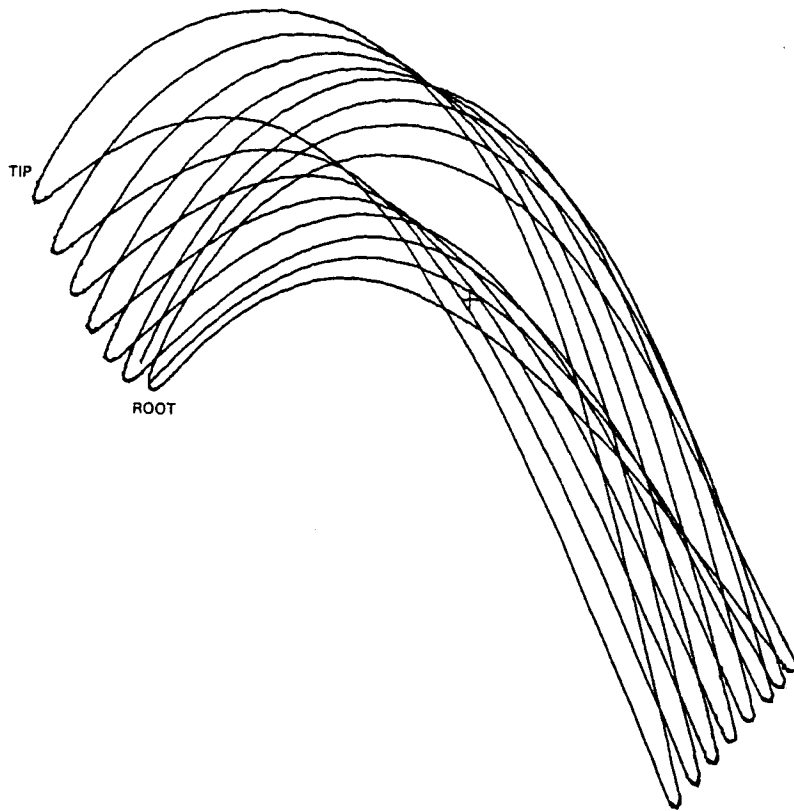


Figure 4.2.4-29 Fourth Stage Turbine Vane Stacking Arrangement

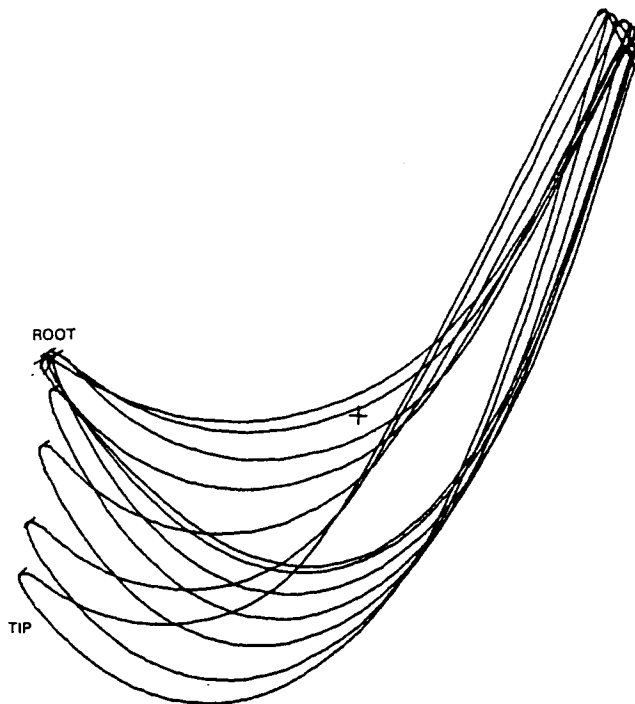


Figure 4.2.4-30 Fourth Stage Turbine Blade Stacking Arrangement

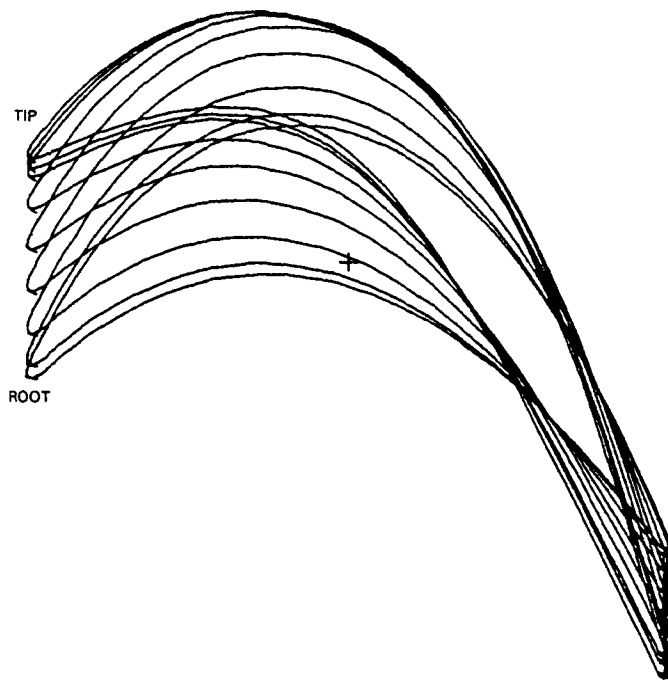


Figure 4.2.4-31 Fifth Stage Turbine Vane Stacking Arrangement

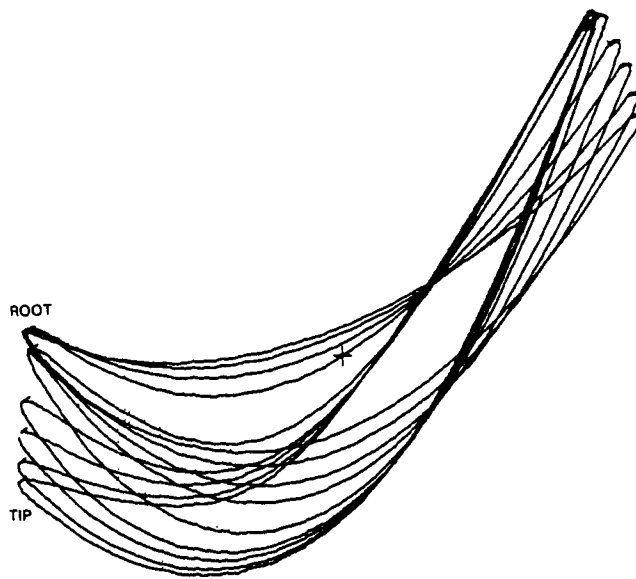


Figure 4.2.4-32 Fifth Stage Turbine Blade Stacking Arrangement

The turbine exit guide vane is designed to present the exhaust mixer with a low Mach number and zero swirl flow field. Figure 4.2.4-33 shows the aerodynamic definition of the exit guide vane, and Table 4.2.4-III presents a summary of the design characteristics at the aerodynamic design point.

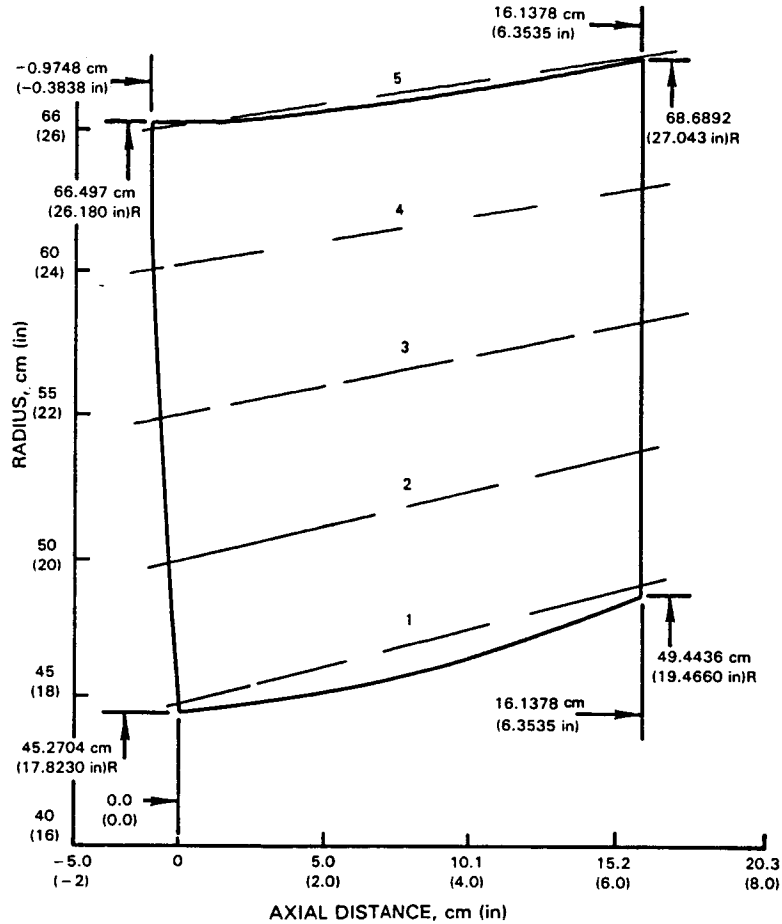


Figure 4.2.4-33 Turbine Exit Guide Vane Flowpath for the Integrated Core/Low Spool

TABLE 4.2.4-III
EXIT GUIDE VANE AERODYNAMIC CHARACTERISTICS
(Planar Sections)
Integrated Core/Low Spool - Aerodynamic Design Point
10,668 m (35,000 ft) 0.8 Mn

	1	2	3	4	5
Radius LE, cm (in)	45.270 (17.823)	50.505 (19.884)	55.740 (21.945)	60.972 (24.005)	66.207 (26.066)
Radius TE, cm(in)	49.443 (19.466)	54.254 (21.360)	59.067 (23.255)	63.878 (25.149)	68.689 (27.043)
Inlet Gas Angle, deg	55.67	47.6	49.5	54.4	66.8
Exit Gas Angle, deg	90.0	90.0	90.0	90.0	90.0
Inlet M_N	0.516	0.503	0.452	0.410	0.412
Exit M_N	0.395	0.372	0.350	0.366	0.386
Incidence, deg	-5.5	-4.5	-4.5	-4.0	-3.5
Deviation, deg	0	3.3	5.9	6.9	5.8
Gap/chord	0.598	0.644	0.701	0.762	0.826
Diffusion Factor*	0.33	0.455	0.465	0.390	0.250
RE _{bact} @ inlet	2.86×10^5	3.0×10^5	2.88×10^5	2.65×10^5	2.51×10^5
Chord, cm (in)	17.310 (6.815)	17.650 (6.949)	17.642 (6.946)	17.559 (6.913)	17.421 (6.859)

*"D" Factor = $1 - \frac{C_2}{C_1} + \frac{\Delta C_u}{2C_1}$ /bact

To establish the definition of the exit guide vane, a controlled diffusion design approach was used to ensure an attached boundary layer and attain the desired gas exit angle. This approach was successfully verified during cascade testing conducted under a Navy-sponsored program (Contract N00019-77-C-0546). Table 4.2.4-IV shows the similarity in design parameters between the Energy Efficient Engine and Navy exit guide vane configurations. Figures 4.2.4-34 and -35 present test results acquired under this program and show the excellent agreement between predicted and measured pressure distribution and gas exit angle. It is also noteworthy to point out the large incidence range that exists at the inlet Mach number levels (0.4 to 0.6) of the Energy Efficient Engine.

The final aerodynamic definition of the exit guide vane is shown in Figures 4.2.4-36 through -40. These figures show airfoil contours and pressure distributions for the five sections identified in Table 4.2.4-III. The stacking arrangement of the exit guide vane is presented in Figure 4.2.4-41.

TABLE 4.2.4-IV
COMPARISON OF NAVY FOIL TO ENERGY EFFICIENT ENGINE

	<u>Navy (Design Point)</u>	<u>Energy Efficient Engine Radius TE = 54.254 (21.360 in) (Design Point)</u>
Inlet Mach	0.763	0.503
Exit Mach	0.529	0.372
Inlet Gas Angle	46.8°	47.6°
Exit Gas Angle	90.0°	90.0°
Gap Chord Ratio	0.70	0.62
Gas Tunning	43.2°	42.4°

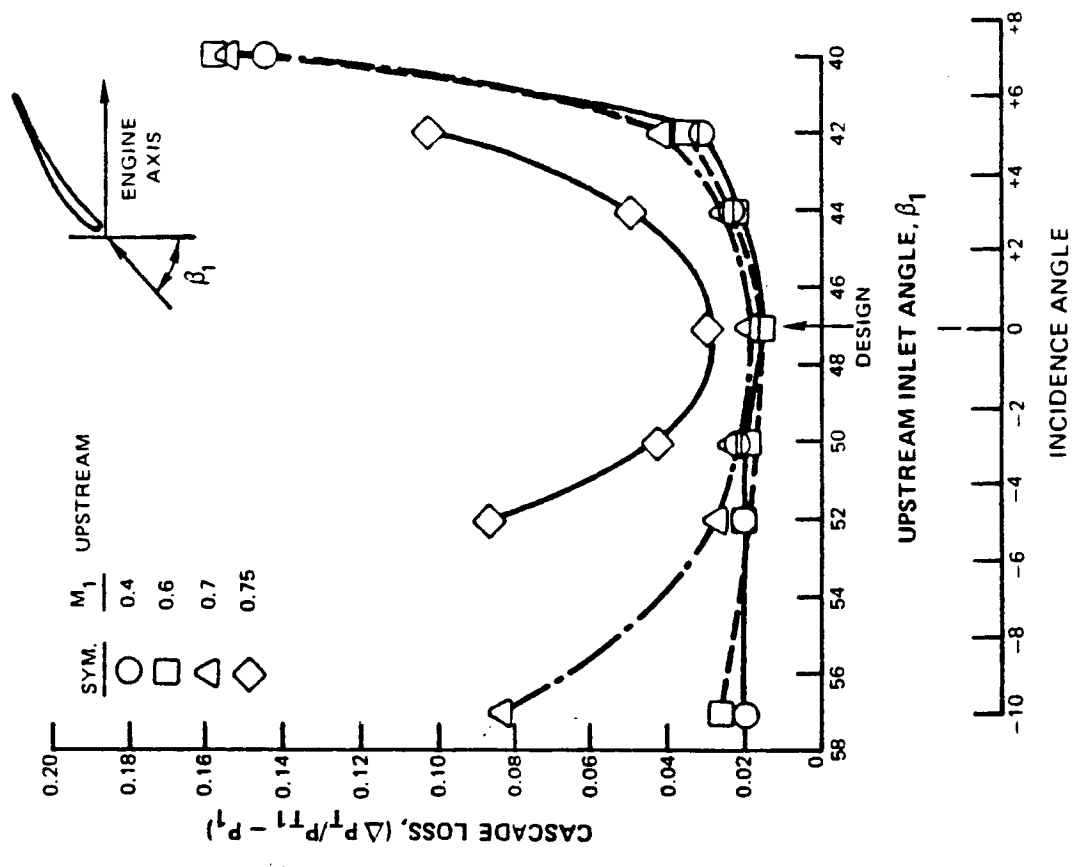
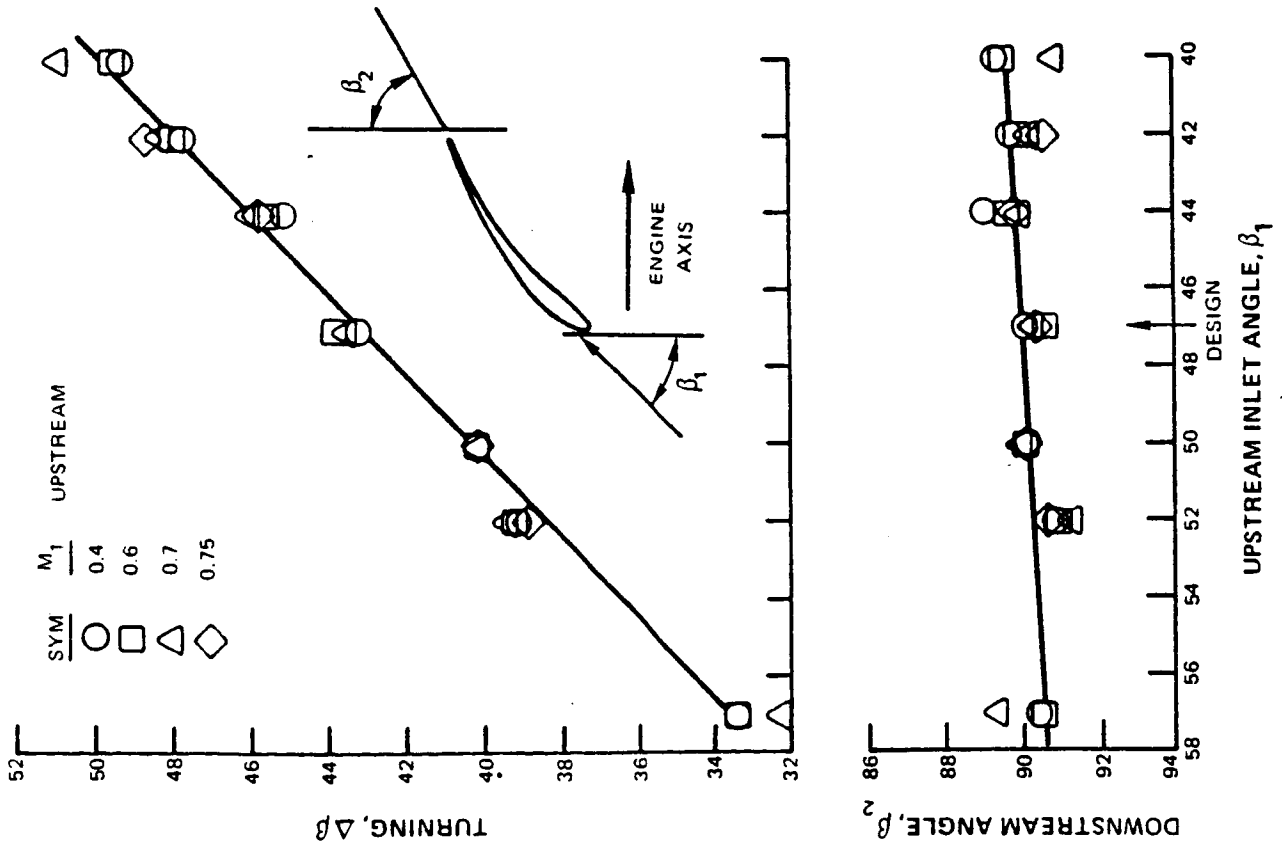


Figure 4.2.4-34 Turbine Exit Guide Vane Cascade Performance Test Results Under a Navy-Sponsored Program (Contract N00019-77-C-0546)

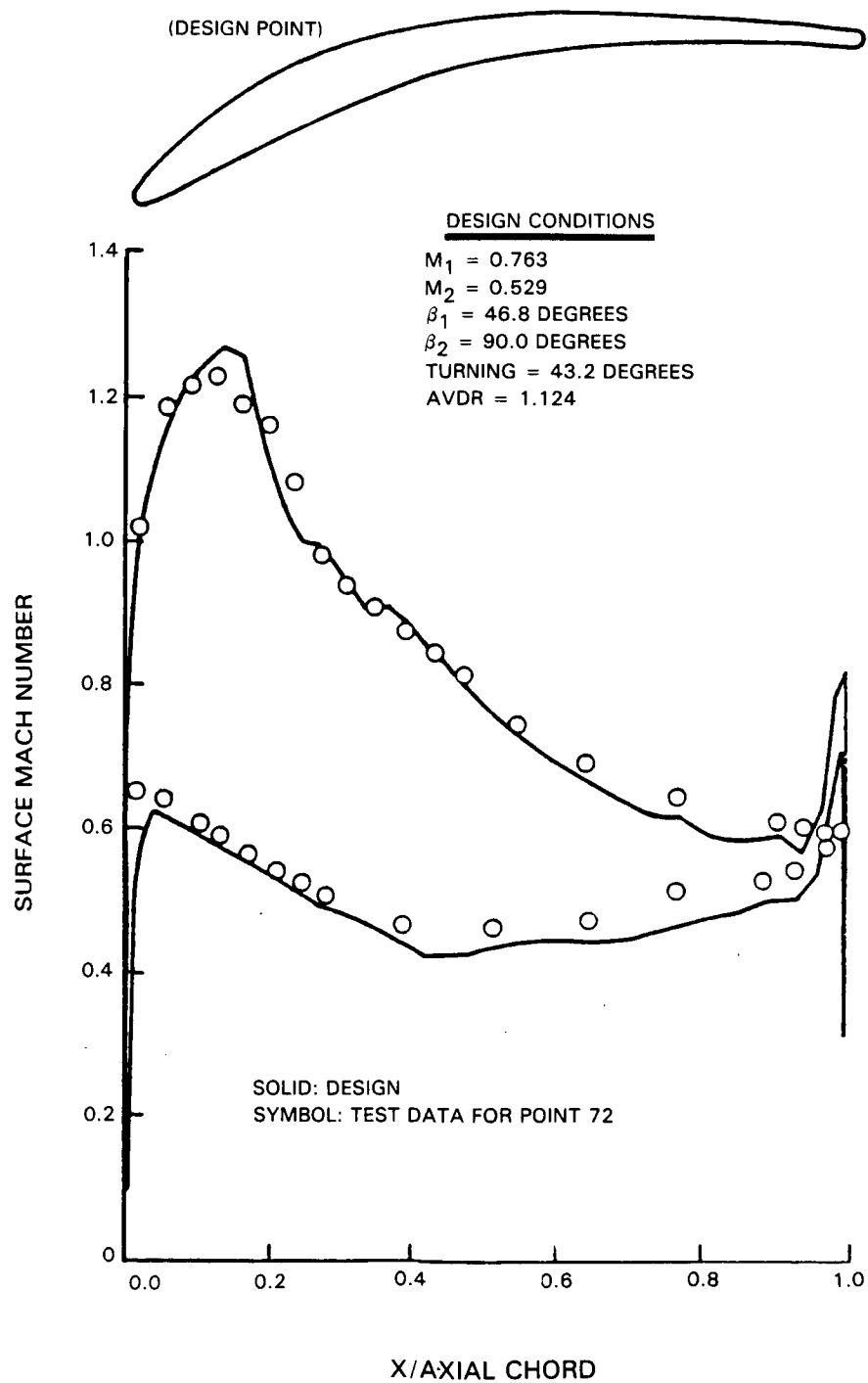


Figure 4.2.4-35 Turbine Exit Guide Vane Cascade Performance Test Results Under a Navy-Sponsored Program (Contract N00019-77-C-0546)

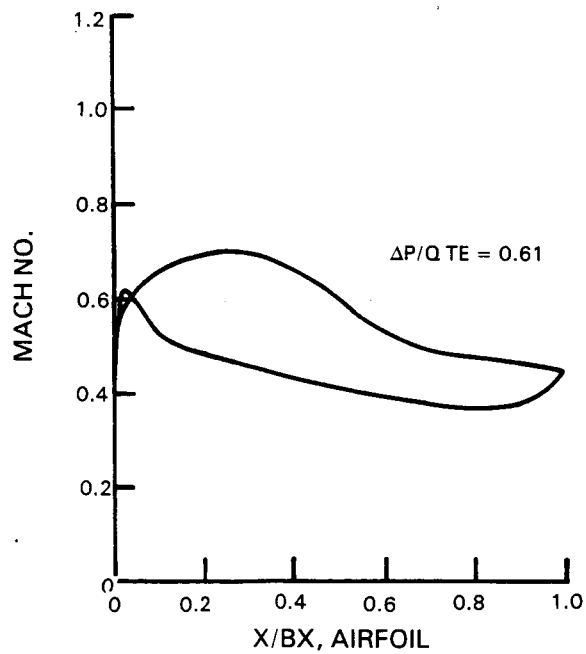
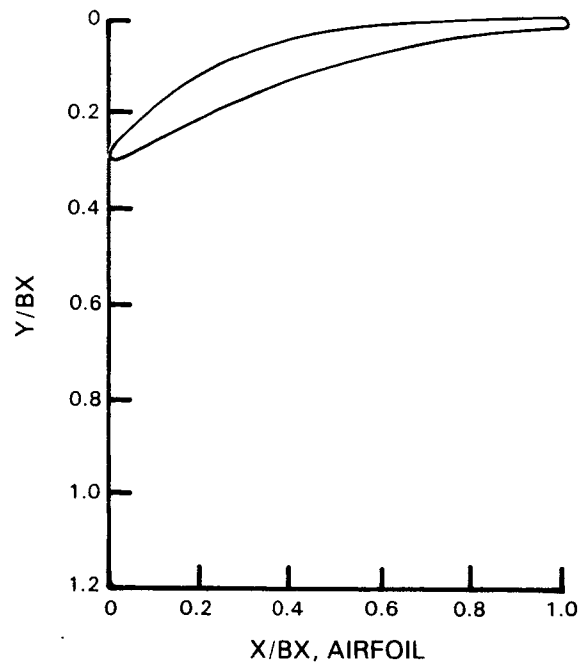


Figure 4.2.4-36 Turbine Exit Guide Vane Root Section Aerodynamic Definition and Pressure Distribution

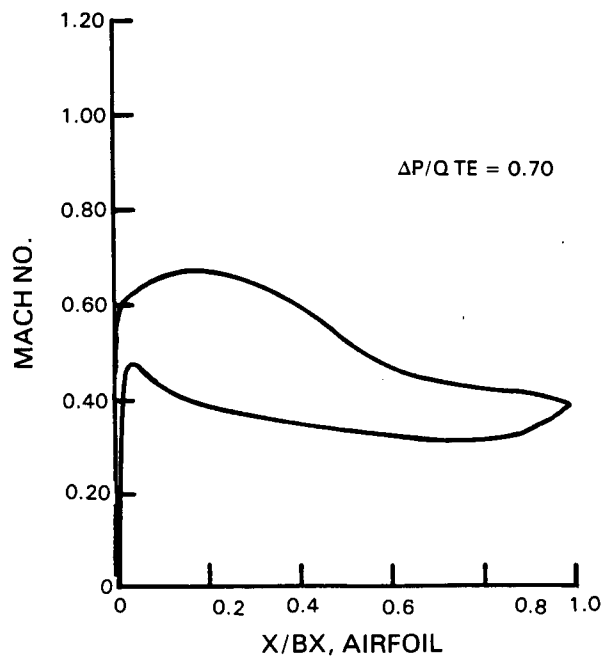
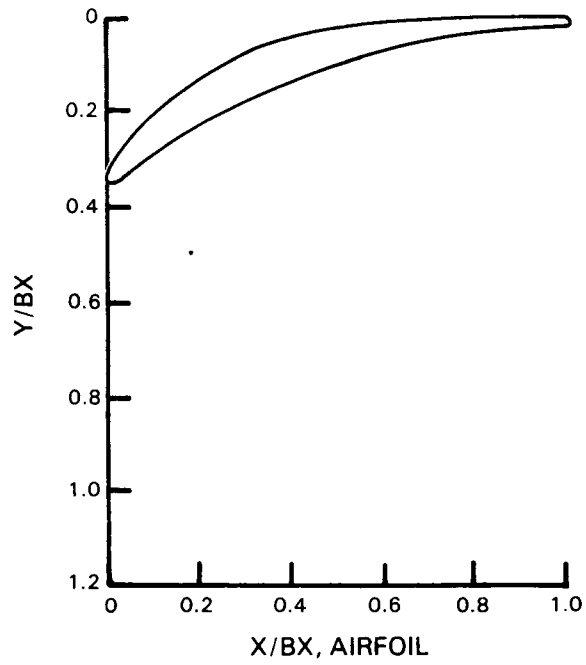


Figure 4.2.4-37 Turbine Exit Guide Vane One-Quarter Section Aerodynamic Definition and Pressure Distribution

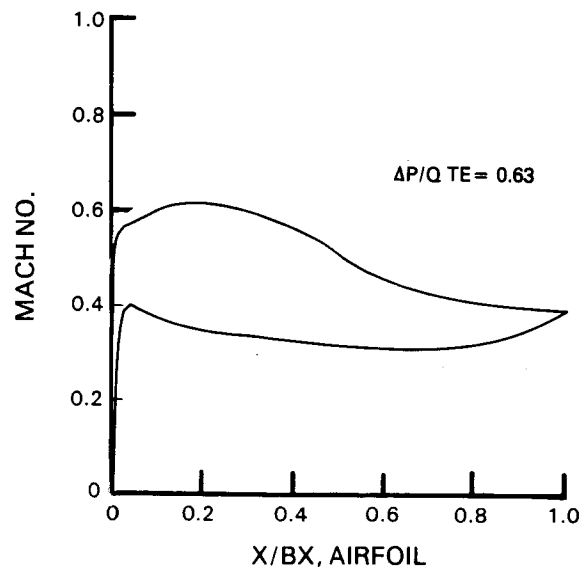
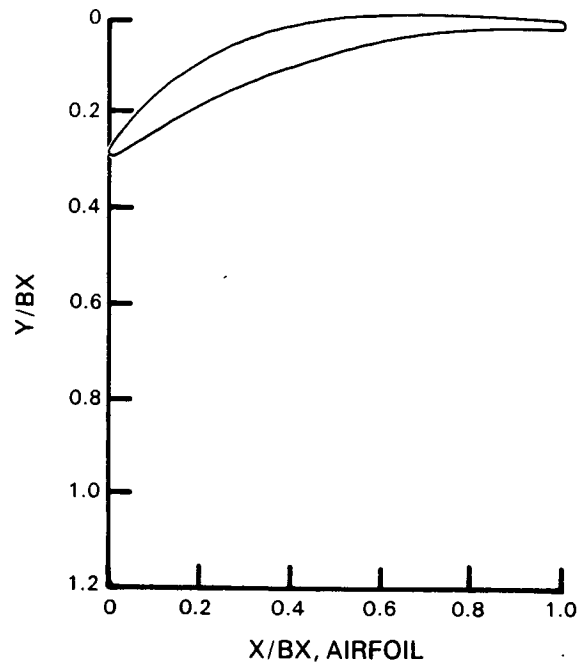


Figure 4.2.4-38 Turbine Exit Guide Vane Mean Section Aerodynamic Definition and Pressure Distribution

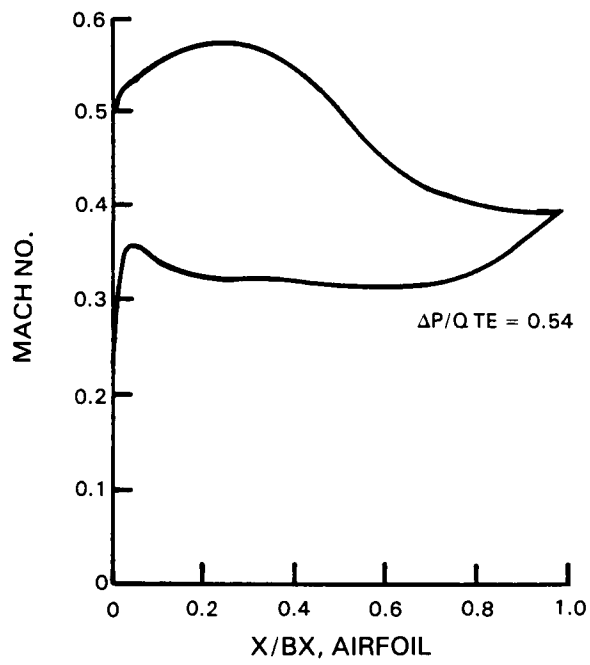
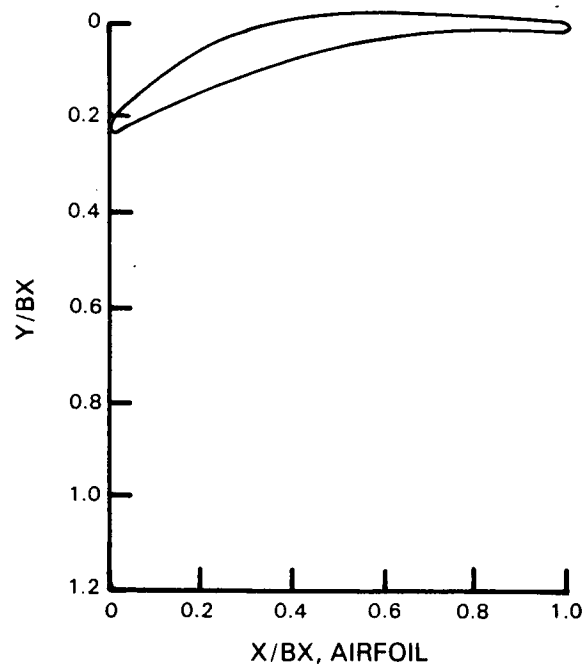


Figure 4.2.4-39 Turbine Exit Guide Vane Three-Quarter Section Aerodynamic Definition and Pressure Distribution

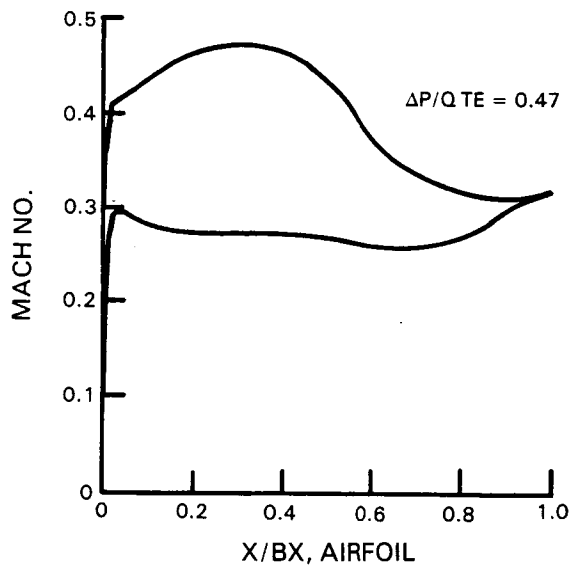
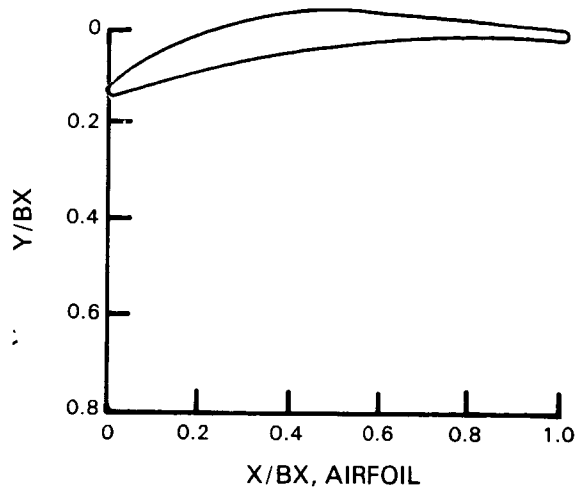


Figure 4.2.4-40 Turbine Exit Guide Vane Tip Section Aerodynamic Definition and Pressure Distribution

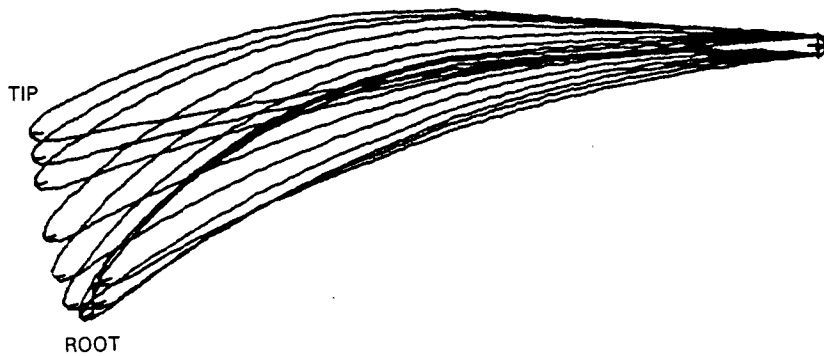


Figure 4.2.4-41 Turbine Exit Guide Vane Stacking Arrangement

4.3 SUPPORTING TECHNOLOGY PROGRAMS

4.3.1 Introduction

Three supporting technology programs were conducted during the design process to assess critical aspects of the turbine intermediate case and low-pressure turbine designs. Results acquired from these efforts provided technical guidance and insight to ensure a viable aerodynamic design. A Transition Duct Model Test Program was completed to verify duct performance. Also, a Low-Pressure Turbine Subsonic Cascade Technology Program demonstrated that the loss and incidence range of the low camber second-stage vane are reasonable as well as verifying the benefits of an aft-loaded pressure distribution. The Low-Pressure Turbine Boundary Layer Program corroborated that an aft-loaded pressure distribution was reasonable for low-loss airfoils.

The significant results from these programs are summarized in the following sections. Complete documentation of results is contained in the following NASA technical reports: Energy Efficient Engine Transition Duct Model Test Program (pending publication), Energy Efficient Engine Low-Pressure Turbine Boundary Layer Program (CR-165338) and Energy Efficient Engine Low-Pressure Turbine Subsonic Cascade Technology Program (CR-165592).

4.3.2 Transition Duct Model Test Program

This technology program was structured to verify the aerodynamic design of the turbine intermediate case. The effort consisted of a two phase test, using a model of the intermediate case, which included the fairing and low-pressure turbine inlet guide vane.

In the first phase, the intermediate case, designed on a preliminary basis for a 182,376 N (41,000 lb) thrust engine, was evaluated. At design flow conditions, the total pressure loss for the flight propulsion system transition duct design was 0.7 percent $\Delta P_T/P_T$, which was consistent with the goal. The pressure loss increased to 1.3 percent $\Delta P_T/P_T$ at off-design swirl conditions up to 5 degrees. Also, the pressure coefficient along the outer duct wall indicated that the desired diffusion was attained across the strut. Strut airfoil pressure distribution data verified that the design conditions were achieved with no flow separation.

Inlet, strut exit and low-pressure turbine inlet guide vane exit air angle data were in good agreement with the design prediction. With a 5 degree off-design inlet swirl angle, the struts returned the unturned flow to within one degree of the design point swirl.

In the second phase of the program, several modifications were made to the test model to reflect the intermediate case design for the integrated core/low spool. The changes consisted of: (1) an increased area ratio from 1.50 to 1.57, (2) a reduction in the number of structural support struts from 14 to 11, (3) tangential canting of the strut, and (4) revising the fairing from a 65 circular arc series nonworking airfoil to a 400 series working airfoil with a flow turning capability of 5 degrees.

In Figures 4.3.2-1 through 3, mass-averaged air angle spanwise data from the design and off-design test are compared to the design prediction. Data are presented for the rig inlet, strut exit and turbine inlet guide vane exit, respectively. Rig inlet data in Figure 4.3.2-1 show that the measured off-design swirl was approximately 6.7 degrees less than the measured design point inlet swirl. This impact on the exit swirl angle is shown in Figure 4.3.2-2, in which the measured strut exit swirl is approximately 2.8 degrees less than that represented by design point data.

Figure 4.3.2-3 indicates that the measured inlet guide vane exit swirl at the rig off-design inlet conditions was within 0.75 degree of design point data. This suggests that the high-pressure turbine off-design operation will have little effect on the angle of the flow entering the low-pressure turbine first-stage rotor.

Profiles of outer and inner wall loadings are presented in Figure 4.3.2-4 and 5, respectively. Data trends are compared to the design predictions, and results show a reduction in diffusion through the strut because of the change in inlet angle. The flow then accelerates through the low-pressure turbine inlet guide vane. These loading results indicate that the flow is separation free.

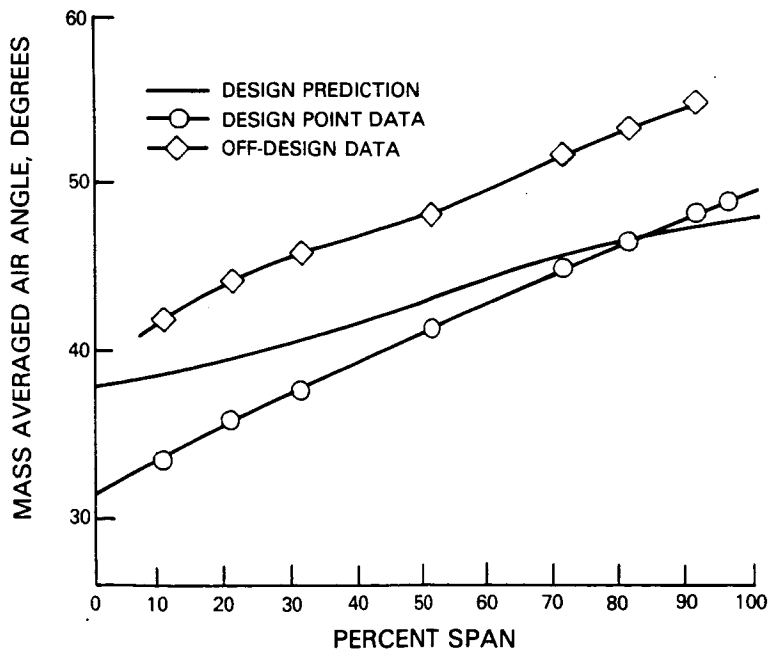


Figure 4.3.2-1 Rig Inlet Mass-Averaged Air Angle Spanwise Data

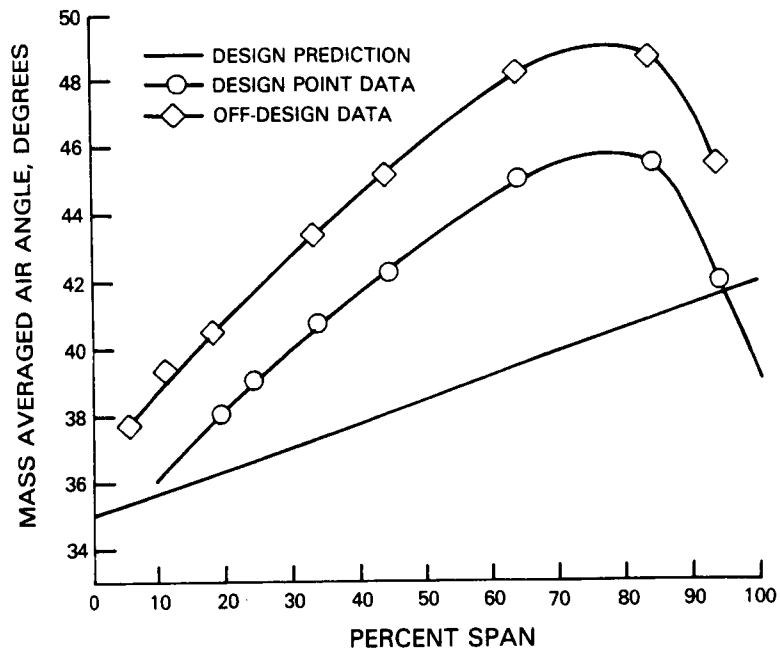


Figure 4.3.2-2 Strut Exit Mass-Averaged Air Angle Spanwise Data

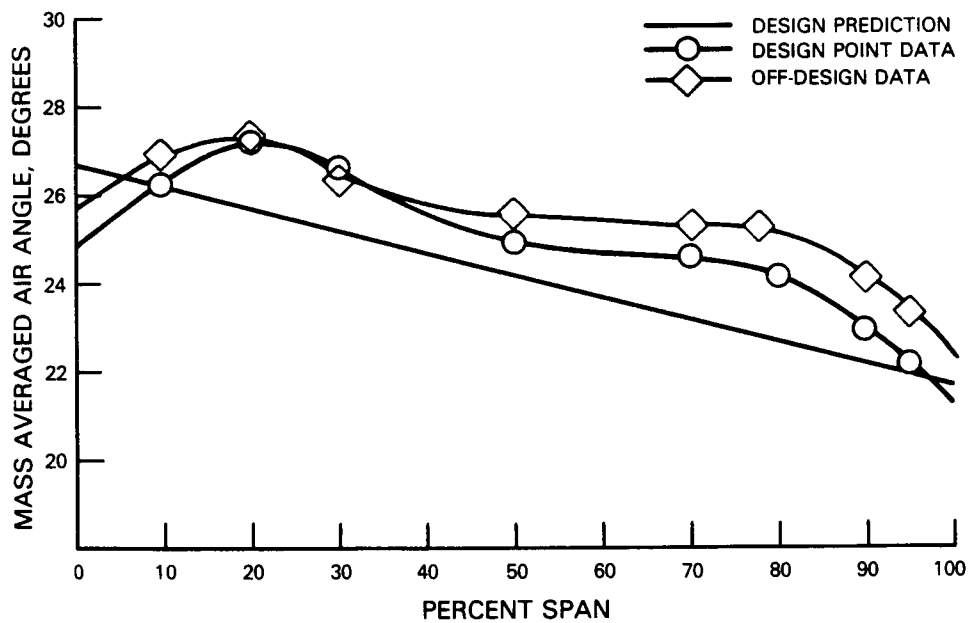


Figure 4.3.2-3 Low-Pressure Turbine Inlet Guide Vane Exit Mass-Averaged Air Angle Spanwise Data

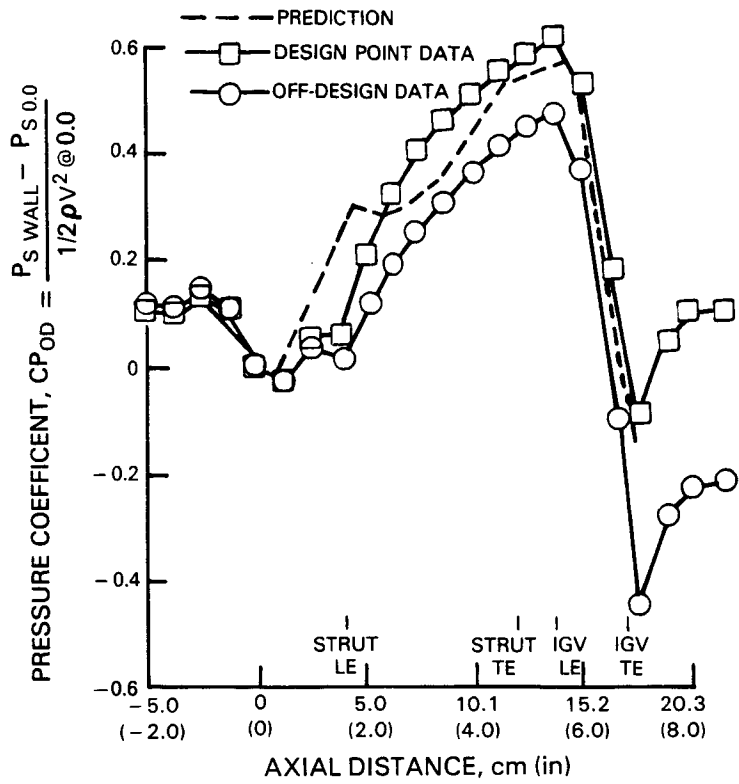


Figure 4.3.2-4 Outer Wall Loading Profile

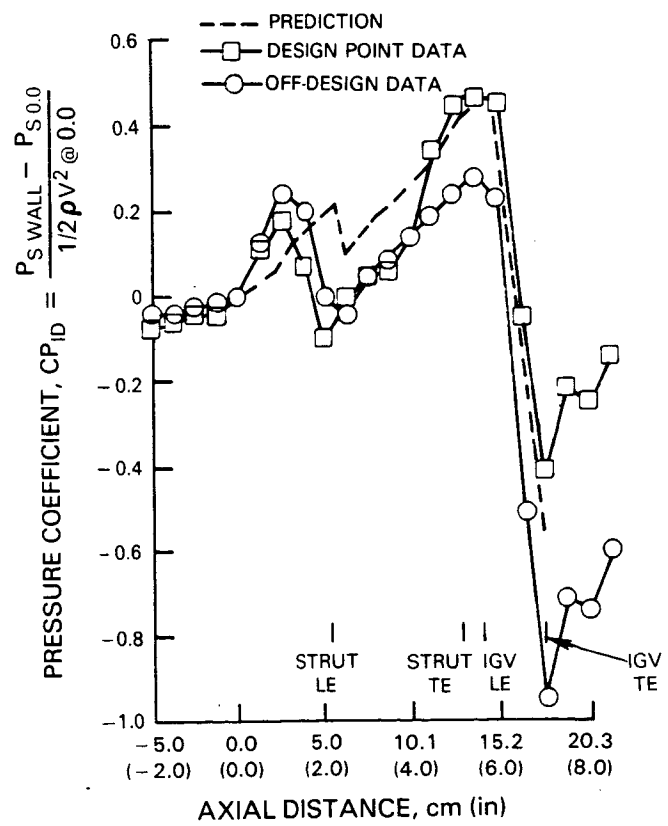


Figure 4.3.2-5 Inner Wall Loading Profile

4.3.3 Low-Pressure Turbine Subsonic Cascade Technology Program

The use of counterrotating turbines and the requirement for highly loaded, "low loss" airfoils results in airfoil geometries that are a substantial departure from conventional designs. The objective of the Subsonic Cascade Technology Program was to investigate the performance characteristics of a low camber inlet guide vane and to evaluate the fore and aft loading type loadings used to optimize the low-pressure turbine vane and blade aerodynamic definitions. This was accomplished through three airfoil cascade tests conducted at varying pressure ratios and inlet incidence angles.

To assess the performance of the low camber inlet guide vane, pressure loss data were generated for both design and off-design conditions in the first test series. Secondary loss data were acquired at the design incidence angle, and were found to be in good agreement with the Pratt & Whitney Aircraft cascade correlation. The secondary losses were 0.56 percent of the inlet total pressure and the prediction was 0.59 percent of the inlet total pressure. Profile losses, measured as a function of incidence angle, were found to be in good agreement with the Pratt & Whitney Aircraft boundary layer prediction method, as shown in Figure 4.3.3-1.

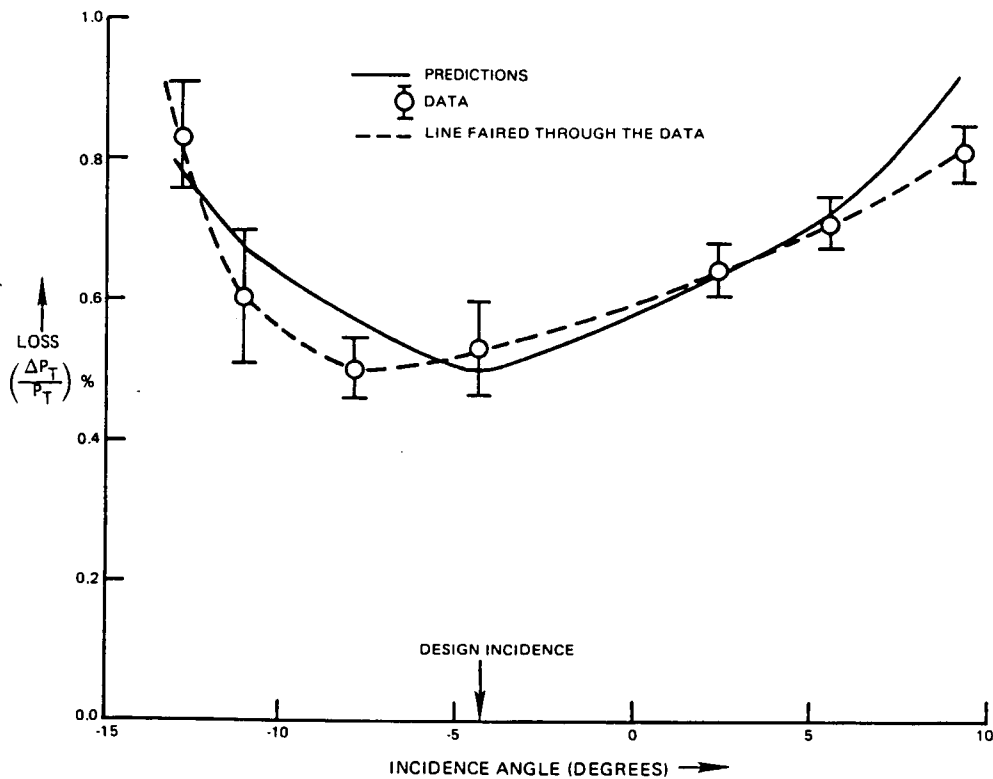


Figure 4.3.3-1 Loss Versus Incidence for the Low Camber Vane

The results presented in Figure 4.3.3-1 show that losses increase more rapidly for the negative incidence side of the loss bucket compared to the positive side. Consequently, the shape of the low camber airfoil loss bucket is different from that of a typical turbine airfoil. The measured off-design incidence performance at a constant exit Mach number showed the vane section to have a negative incidence range of 12.4 degrees and a positive incidence range of 7 degrees, as defined by the point where the loss level is 50 percent above the design loss point. Results showed that an improved incidence range could be achieved by revising the vane incidence angle from -5 to -3 degrees.

In the second part of the program, tests were completed with two airfoil cascades to evaluate the aerodynamic performance difference between an airfoil that accelerated the flow on the suction surface near the gaging point (aft loaded) and an airfoil that accelerated the flow more rapidly in the forward region of the suction surface (squared-off).

Most of the airfoil profile losses are generated on the suction surface because the average velocity on this surface is high. Furthermore, the flow on this surface of the airfoil accelerates from the leading edge to some high value and then diffuses to the trailing edge velocity. Two factors affect the suction side loss, the nature of the boundary layer, i.e. laminar, transitional, or turbulent in the accelerating portion of flow and the maintenance of attached flow in the diffusion region. The latter is characterized by the diffusion parameter $\Delta P/Q$, the ratio of exit static pressure minus static pressure at the maximum velocity point to the maximum dynamic head.

For a given Zweifel load coefficient, aft-loaded airfoils generally have a higher diffusion parameter, maximum Mach number and thickness to chord ratio than the "squared-off" airfoil. In addition, the squared-off concept offers a potential for lower weight. Figure 4.3.3-2 shows profiles and pressure distributions of two airfoils that have the same load coefficient and exit Mach number.

Test results are compared to theoretical predictions in Figure 4.3.3-3. As shown, the performance of the aft-loaded airfoil is better than or equal to the alternate configuration over the range of incidence angles tested. Similar results were obtained with variations in Mach number (Figure 4.3.3-4). Theoretical predictions were found to be in good agreement with measured data over the entire range of Mach number and incidence angles. Secondary loss measurements showed that the aft-loaded airfoil generated approximately 11 percent lower losses than the squared-off airfoil at the design incidence and Mach number conditions.

In a third series of tests, three airfoil sections, representing the mean section of the fourth-stage blade, were evaluated to determine surface static pressure distribution and profile loss characteristics for a range of inlet gas angles and Mach numbers. One airfoil section with an aft-loaded pressure distribution was used as a baseline. The other two, which had a squared-off type pressure distribution and different airfoil thickness distributions, were compared to the baseline. One squared-off airfoil was distinguished as a heavy-weight configuration because of its thick sections, and was designed with the same leading and trailing edge wedge angles as the aft-loaded airfoil. The other configuration, referred to as a lightweight airfoil, had almost the same static pressure distribution as the heavyweight airfoil. However, it was designed for low inlet and exit wedge angles to enable a thin foil geometry.

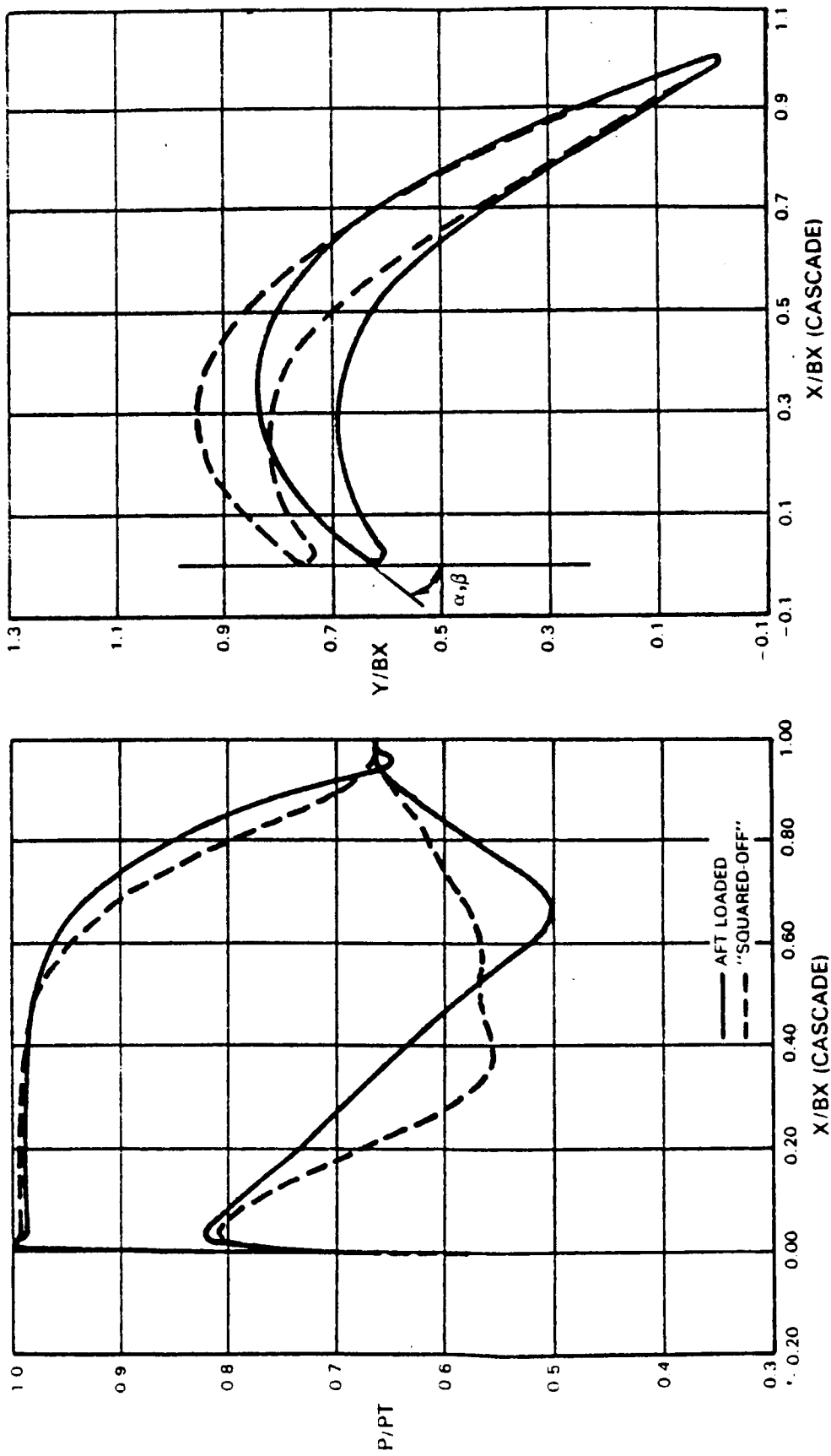


Figure 4.3.3-2 Aft-Loaded Transonic Versus Squared-Off Subsonic Airfoil Profiles and Pressure Distributions

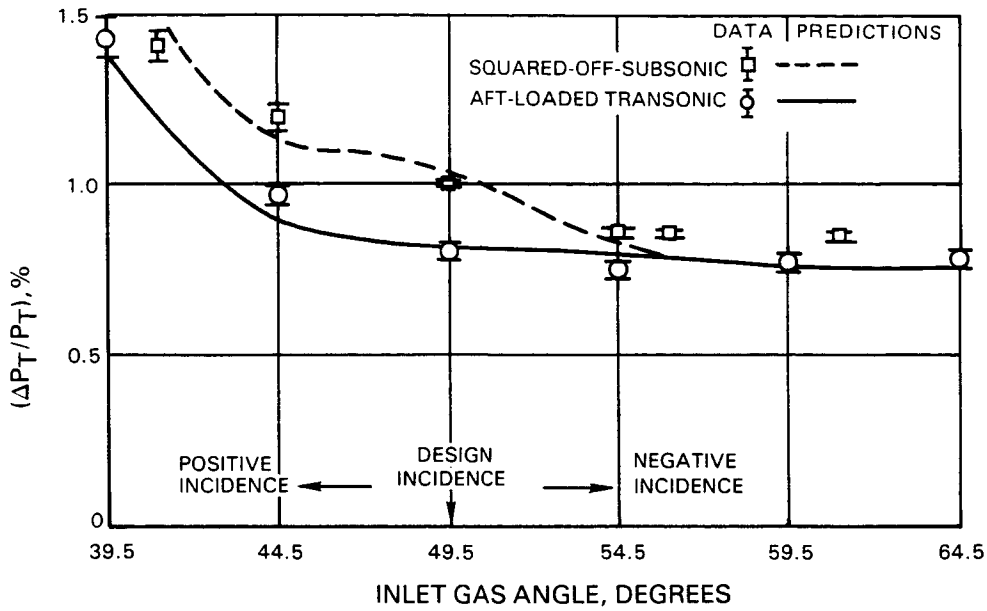


Figure 4.3.3-3 Aft-Loaded Transonic Versus Squared-Off Subsonic Airfoils Predicted Versus Measured Profile Loss Data

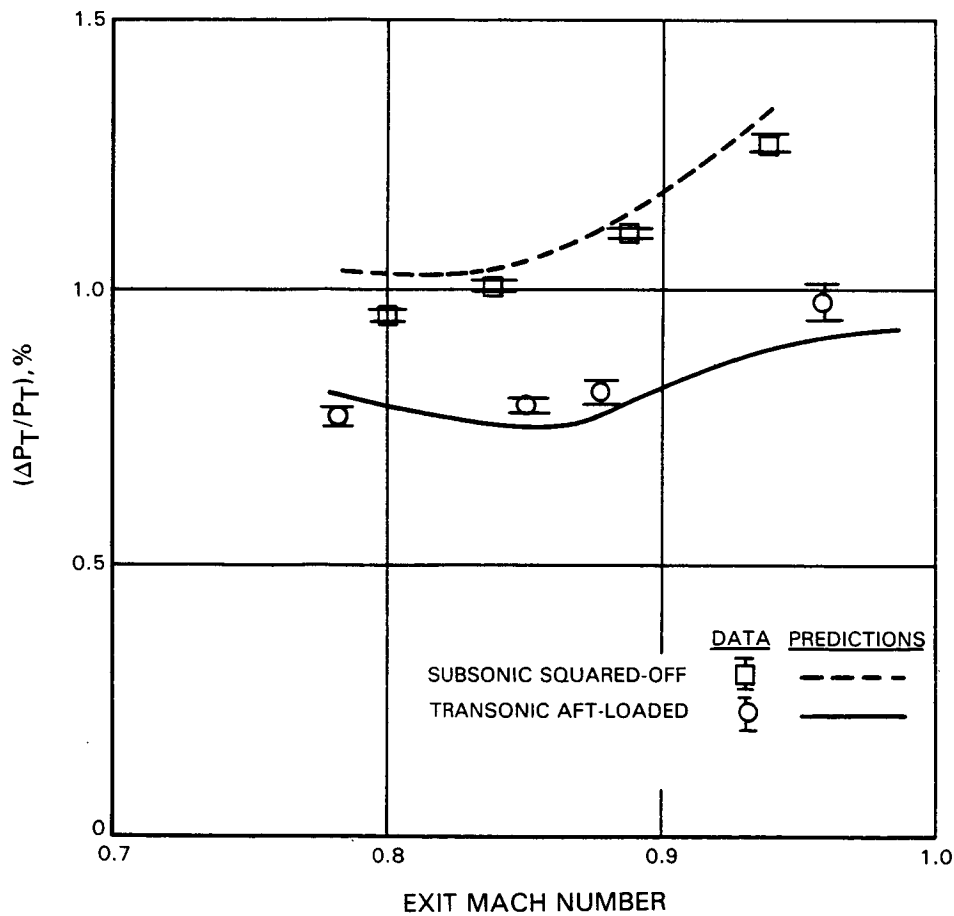


Figure 4.3.3-4 Aft-Loaded Transonic Versus Squared-Off Subsonic Airfoils Predicted Versus Mass-Averaged, Mixed-Out, Mid-Span Losses.

In general, surface static pressure distributions and profile losses were in good agreement with Pratt & Whitney Aircraft prediction methods over the entire range of Mach numbers and inlet gas angles. Cascade results showed the aft-loaded airfoil produced lower profile losses than the other designs. Performance trends from data and theoretical predictions are presented in Figures 4.3.3-5 and 4.3.3-6. Compared to the aft-loaded airfoil at the design point, the heavyweight and lightweight airfoils had 34 and 21.3 percent higher profile losses, respectively. The data indicate that the profile loss for the aft loaded airfoil is lower than either the heavyweight or lightweight airfoil for positive incidence, whereas all airfoil sections show almost equal losses for negative incidence.

A measurement of secondary loss was also obtained for the aft-loaded and lightweight airfoils at three separate incidence angles. The aft-loaded airfoil demonstrated lower secondary losses for the entire range of inlet gas angles and Mach numbers.

In summary, the cascade program verified that the loss and incidence range of the low camber inlet guide vane was reasonable. Also, the benefits of an aft-loaded pressure distribution for low loss airfoils were verified.

4.3.4 Low-Pressure Turbine Boundary Layer Program

The Low-Pressure Turbine Boundary Layer Program was aimed at investigating the probability of further improving turbine efficiency by reducing airfoil profile losses. The pressure distributions of aft-loaded and squared-off airfoils were assessed in terms of losses resulting from boundary layer development on the airfoil suction surface. Velocity distributions were simulated on flat plates in a low speed, high aspect ratio wind tunnel designed specifically for these investigations. Measurements of boundary layer mean velocity and turbulence intensity were acquired for an inlet turbulence level of 2.4 percent and an exit Reynolds number of 8×10^5 . Flush-mounted hot film probes were used to identify boundary layer transition regimes that were found to be located in the adverse pressure gradient regions for both test simulations.

Mean Velocity Profiles

A total of twenty mean velocity profiles was measured, ten for each of the two pressure distributions. Nine of the profiles were located in the laminar flow region, four in the transitional flow region, and the remaining seven in the fully turbulent flow region. A comparison of mean velocity profile data in the transitional and turbulent regimes with well established semi-empirical formulations is as follows.

All turbulent boundary layer data have a universal region where Equation 1 is valid.

$$U^+ = \frac{1}{k} \ln y^+ + B \quad (\text{Eq. 1})$$

The fully turbulent boundary layer mean velocity profile data from the two configurations are presented in Figure 4.3.4-1, using the dimensionless parameters of Equation 1.

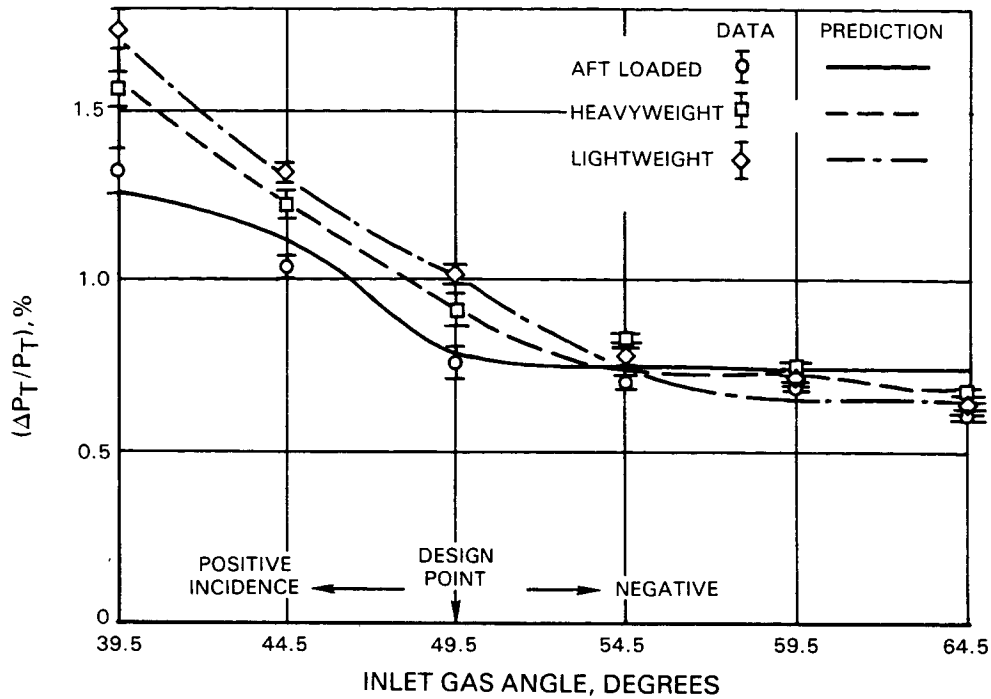


Figure 4.3.3-5 Aft-Loaded, Heavyweight, Lightweight -- Predicted Versus Profile Loss Over Range of Incidence, Fixed Exit Mach Number (0.72)

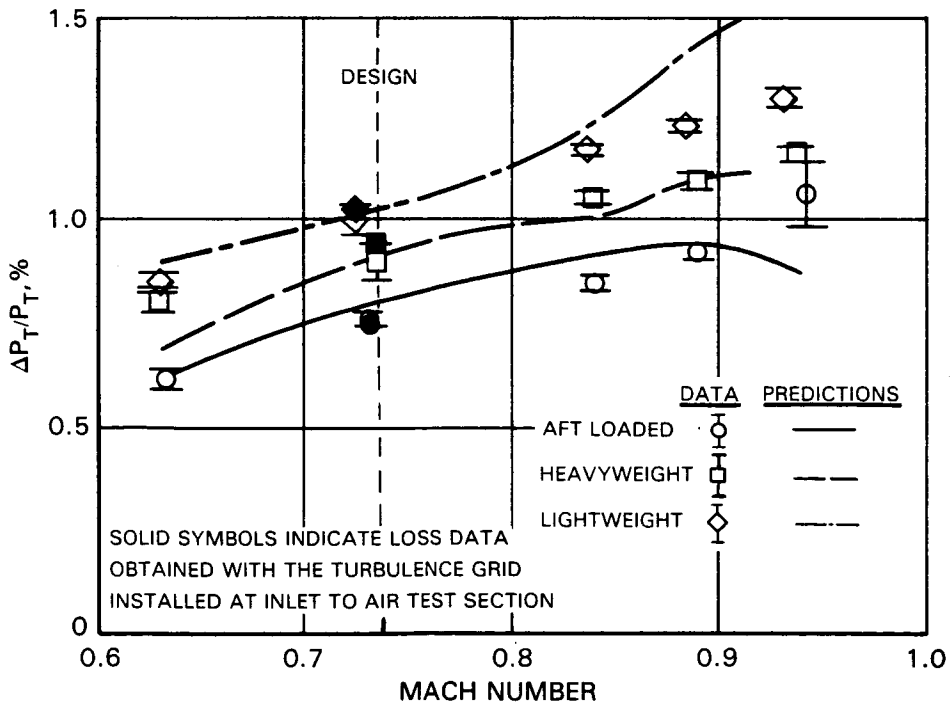


Figure 4.3.3-6 Aft-Loaded, Heavyweight, Lightweight -- Predicted Versus Measured Mass-Averaged Mid-Span Profile Loss at Design Point Incidence, Variable Exit Mach Numbers

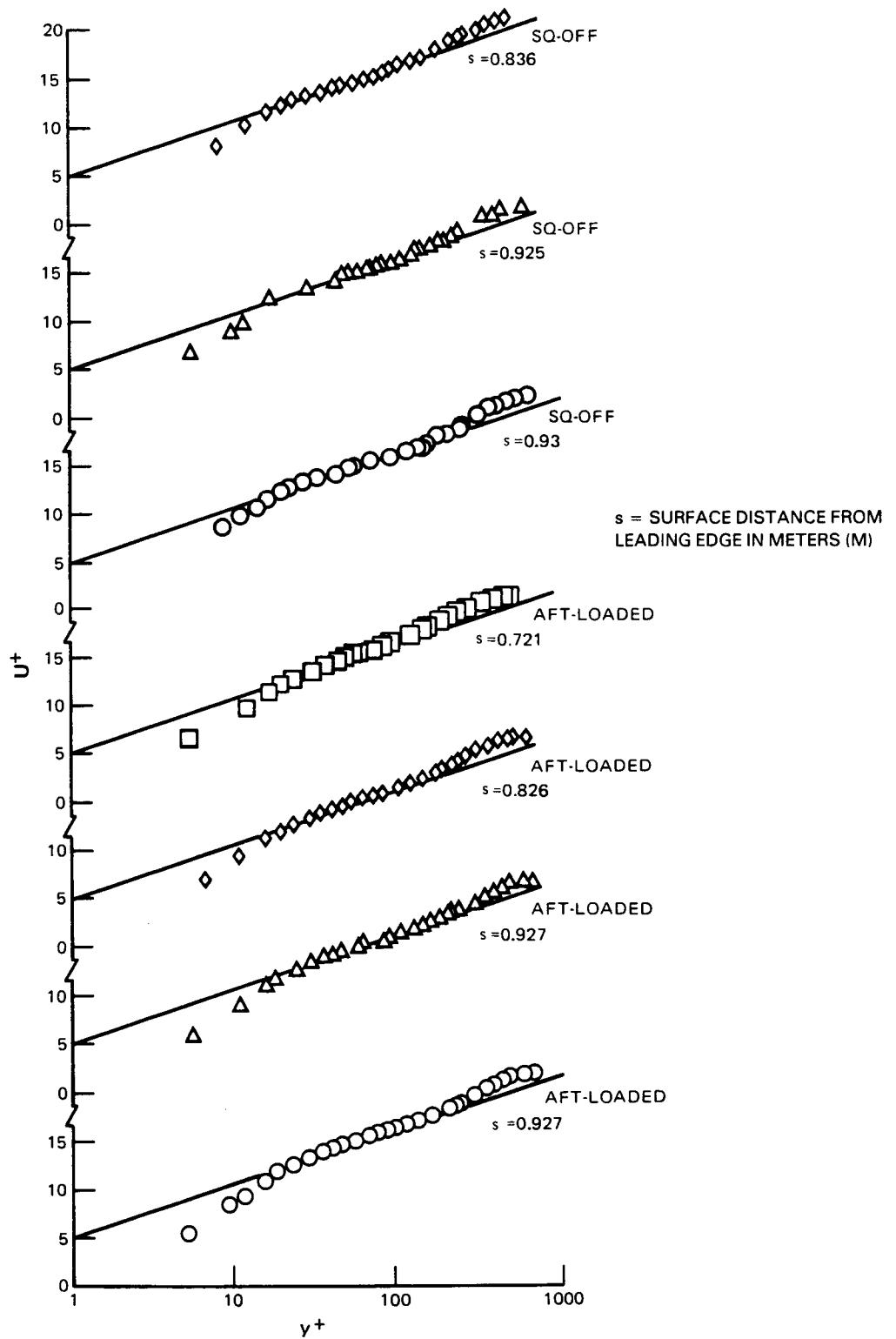


Figure 4.3.4-1 Turbulent Boundary Layer Velocity Profiles Using Dimensionless Parameters

Squared-Off Pressure Distribution

Experimental data for the integral parameters of boundary layer momentum loss thickness Reynolds number ($Re\theta$), shape factor (H) and skin friction (C_f), from the squared-off design are shown in Figure 4.3.4-2, along with analytically predicted values. In general, the predictions are in good agreement with test data. Figure 4.3.4-3 shows detailed mean velocity profile data compared to the predictions. The predictions are in good agreement with laminar and turbulent velocity profiles, but in somewhat poor agreement with transitional profile data.

Aft-loaded Pressure Distribution

A comparison of test data and predictions for the aft-loaded test is presented in Figure 4.3.4-4. The agreement is good for the accelerating part of the flow, but some flow separation in the diffusing part is indicated. The calculations were repeated and the boundary layer was artificially made transitional at a distance of two boundary layer thicknesses upstream of the expected separation point to obtain theoretical predictions. Although it is difficult to ascertain whether the boundary layer actually separated at the location that was predicted, the calculated separation point was slightly upstream of the transition region identified by the hot film probes. If separation occurred, however, it did not influence the behavior of the intermittency factor in the transitional region. Velocity profile data and predictions are presented in Figure 4.3.4-5. Again, measured and predicted profiles are in good agreement for the laminar and turbulent regions.

Profile Loss Assessment

Relative magnitudes of profile losses associated with aft-loaded and squared-off pressure distributions can be achieved by a direct comparison of the integral parameters obtained from test data. Distribution of the three integral parameters, boundary layer momentum thickness (θ), shape factor (H) and skin friction (C_f), is shown in Figure 4.3.4-6.

Momentum Loss Thickness Results indicated that the momentum loss thickness for the aft-loaded airfoil section was 8 percent larger than for the squared-off section, as shown in Figure 4.3.4-6(a). If the exit velocity for the two airfoil simulations was identical, a squared-off airfoil of the same design as the aft-loaded foil would have an 8 percent lower loss on the suction side. However, the exit velocity for the squared-off airfoil was about 4 percent higher than than the aft-loaded airfoil. This implies that the loss ($U_\infty^2 \theta$) for the two tests would be almost identical.

Shape Factor The shape factor associated with the aft-loaded test increased at a location before the transition region, thereby indicating a possibility of separation before transition. The distribution of boundary layer shape factor is shown in Figure 4.3.4-6(b). The distributions of each design are similar in the laminar ($H = 2.3$) and the turbulent ($H = 1.4$) regions.

Skin Friction The distribution of laminar and turbulent skin friction showed similar behavior. The aft-loaded skin friction rate of decrease with stream distance was high, indicating that laminar separation may have occurred.

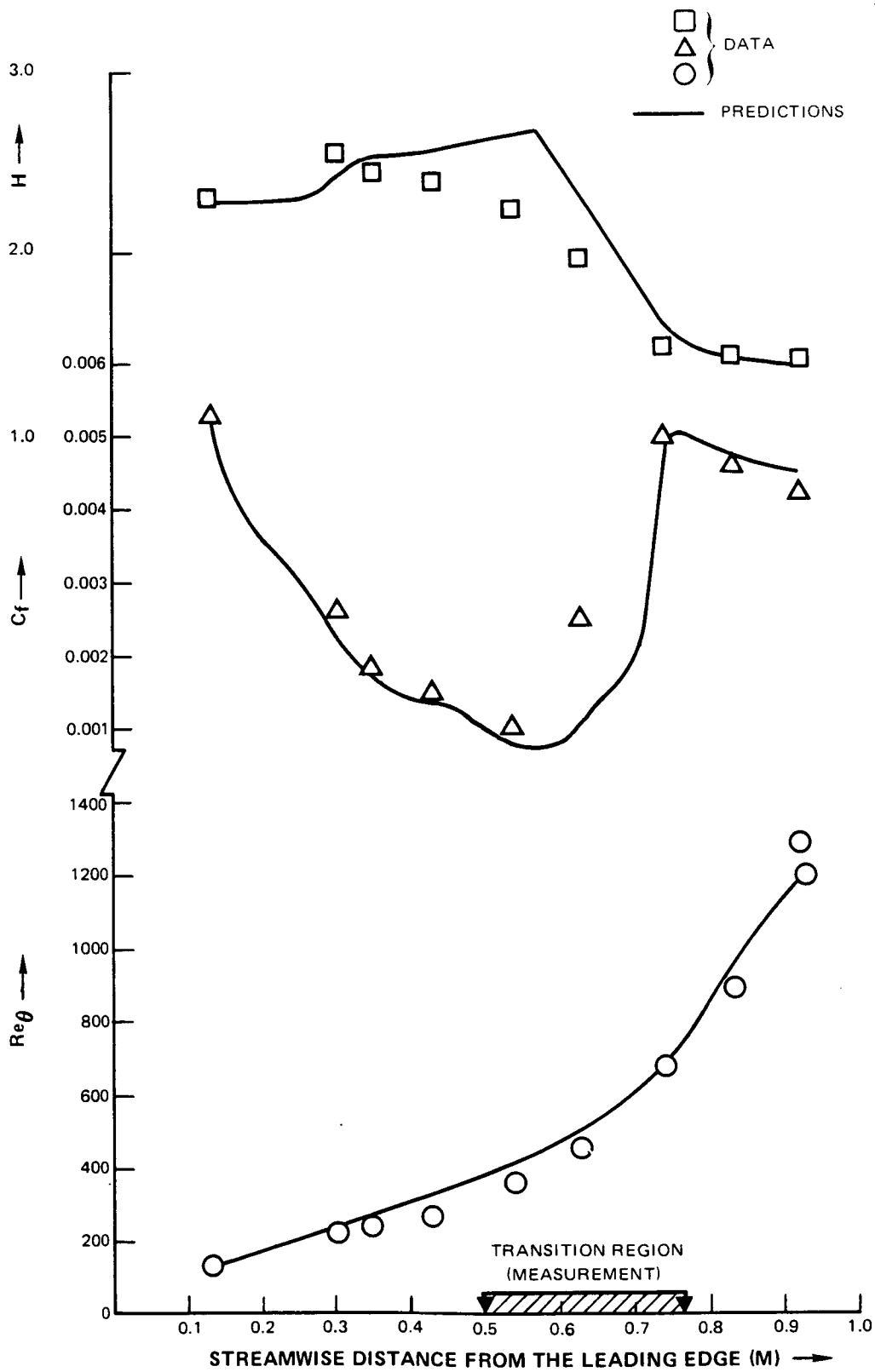


Figure 4.3.4-2 Comparison of Measured Integral Parameters for the Squared-Off Test Section With Theoretical Predictions

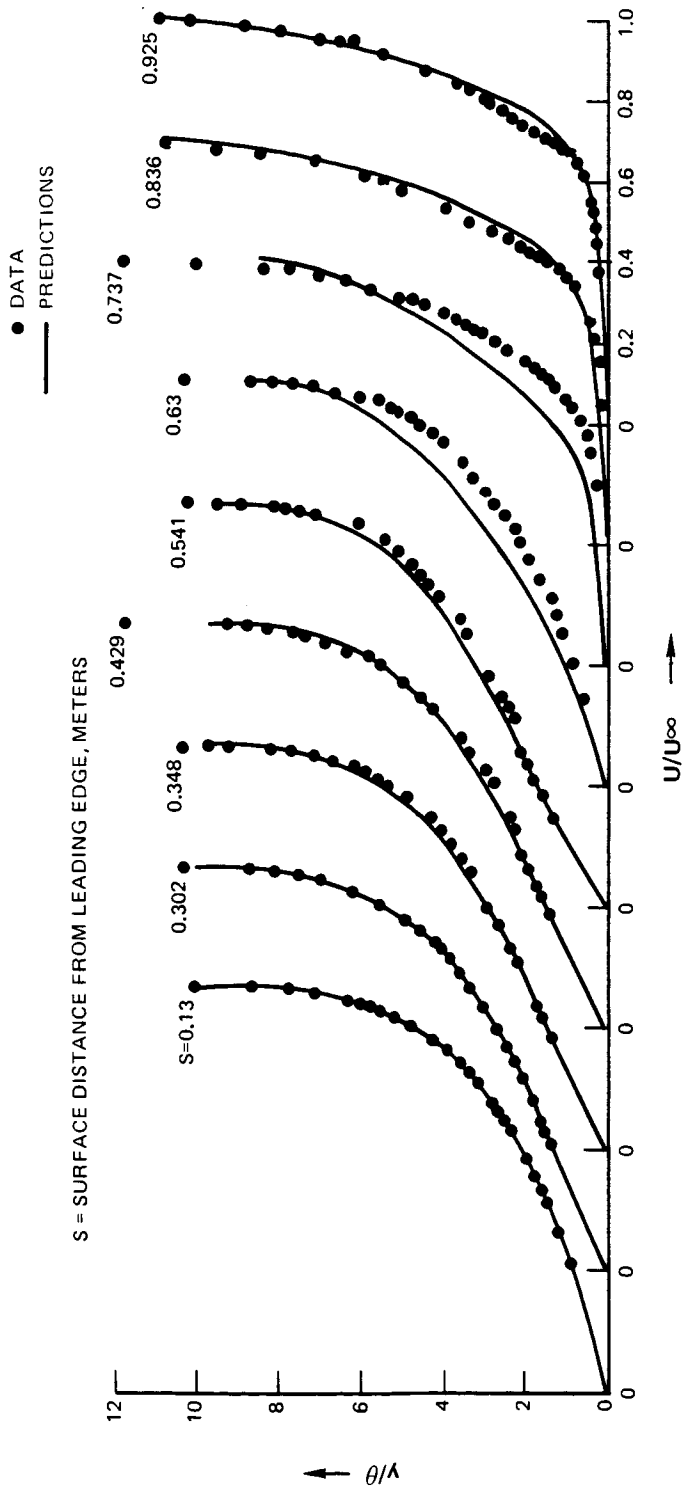


Figure 4.3.4-3 Comparison of Measured Mean Velocity Profile data (Squared-Off) With Theoretical Predictions

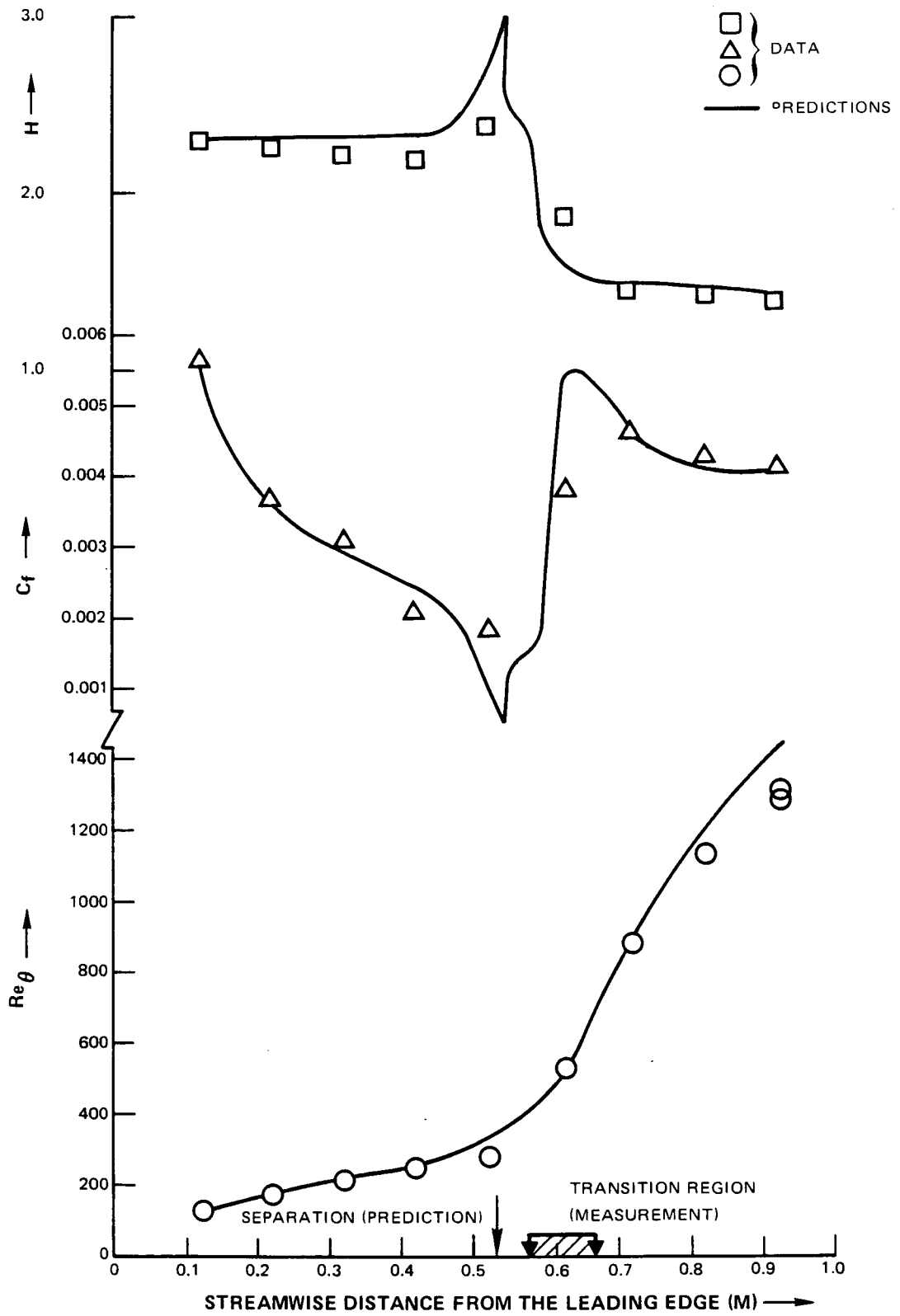


Figure 4.3.4-4 Comparison of Measured Integral Parameters for the Aft-Loaded Test Section With Theoretical Predictions

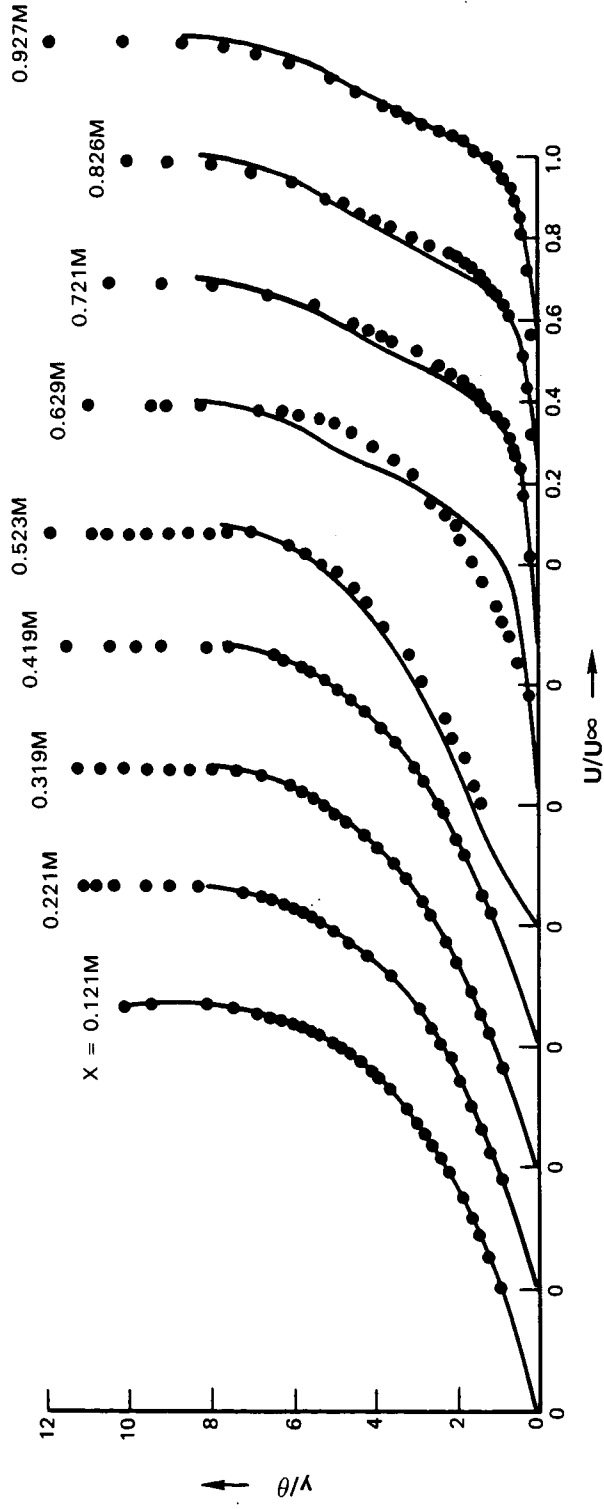


Figure 4.3.4-5 Comparison of Measured Mean Velocity Profile data (Aft-Loaded) with Theoretical Predictions

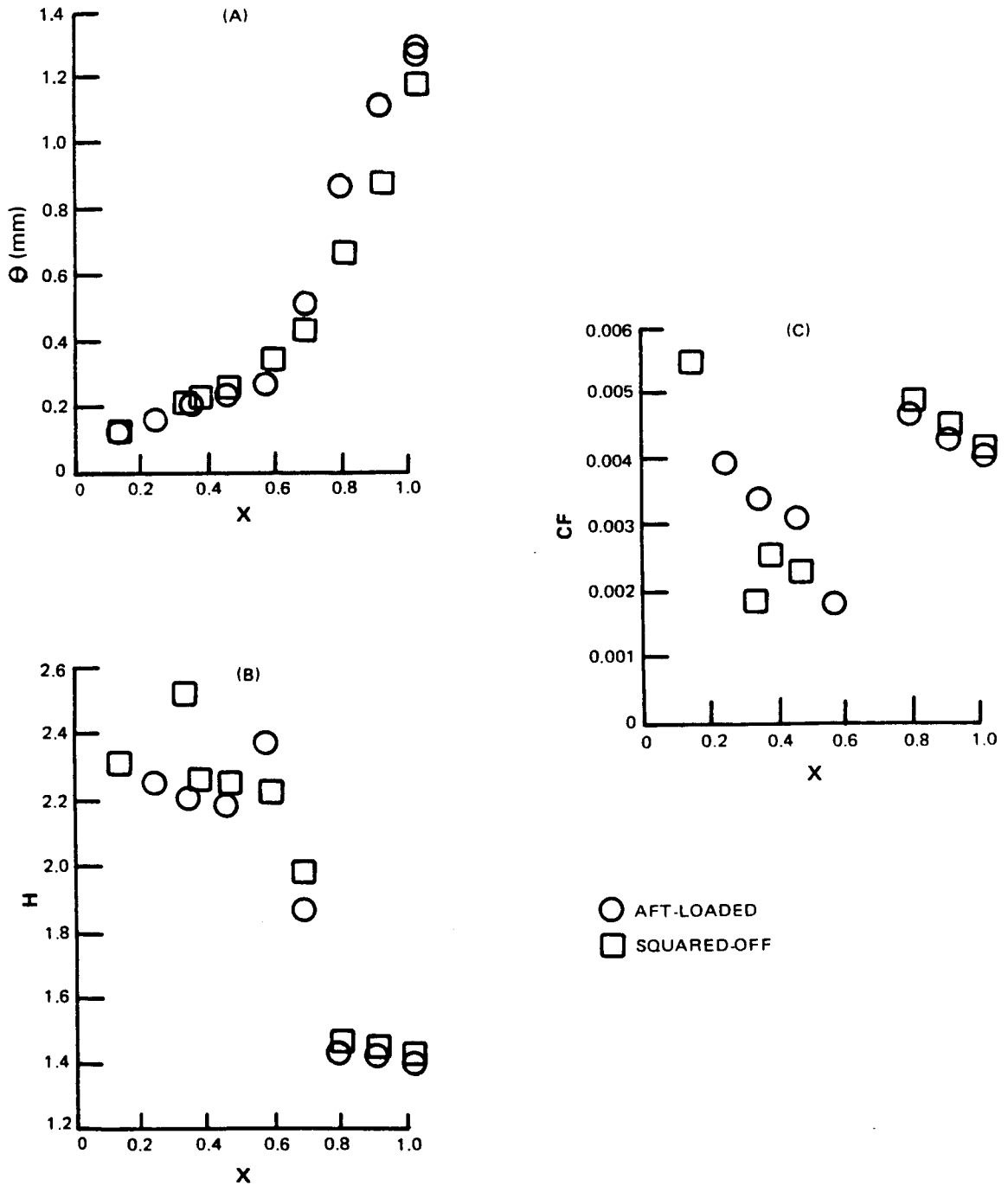


Figure 4.3.4-6 Distribution of Boundary Layer Momentum Loss Thickness (θ), Shape Factor (H), and Skin Friction (C_f)

Boundary Layer Turbulence Intensity Profiles

Boundary layer turbulence intensity profiles for the turbulent, transitional and laminar flow regions are described in the following paragraphs.

Turbulent Region Turbulent intensity profiles were obtained from the three components of turbulence (u^2 , v^2 and w^2) measured at the exit plane of the two airfoil designs. Test data are in good agreement with the flat plate data, as indicated in Figure 4.3.4-7. Relative magnitudes of the streamwise (u^2) and normal (v^2) components are shown for the squared-off configuration in Figure 4.3.4-8. The streamwise and normal components contain about 50 and 20 percent, respectively, of the total turbulence intensity. These results are consistent with the Pratt & Whitney Aircraft prediction system.

Transitional Region Relative magnitudes of turbulence intensity components for the transitional region of the squared-off design are shown in Figure 4.3.4-9. Data show that the streamwise and normal components contain approximately 80 and 10 percent, respectively, of the total turbulence intensity. This means that the turbulence in transitional boundary layers is more non-isotropic than in fully turbulent boundary layers.

Laminar Region Systematic growth of the streamwise component of turbulence intensity was observed in the laminar region of both airfoil designs. Dimensionless turbulent intensity (u^+) data in the laminar boundary region for both airfoil designs were presented as functions of y^+ in Figure 4.3.4-10. The data suggest two important features. First, turbulence intensity profiles in the laminar region had a maximum value at approximately $y^+ = 25$. Second, maximum turbulence intensity (u^+ at $y^+ = 25$) increased in the downstream direction as the onset of transition was approached.

Subsonic Cascade Test Results Versus Boundary Layer Test Results

Results from the boundary layer tests indicate that the Reynolds number based on momentum loss thickness for the two simulated airfoils was about the same at the exit plane. This suggests that the suction surfaces of the two airfoils generate about the same losses. However, loss data acquired from the Subsonic Cascade Program indicate that the heavyweight airfoil generates about 17 percent higher losses than the aft-loaded airfoil. This apparent paradox can be explained by examining the pressure distributions on the suction surfaces of the two airfoils and the simulated pressure distributions.

The Boundary Layer Program did not simulate the entire airfoil suction surface, omitting the leading edge region. It is in this region of the airfoil that the potential flow analysis indicates a difference between the two airfoils with the squared off pressure distribution predicting a larger velocity defect. This may be the explanation for the relative loss difference measured in the cascade. This theory tends to be supported by the off-design data which show that the loss difference between the two airfoils decreases as they operate at higher inlet angles, as previously indicated by Figure 4.3.3-4. At the higher negative incidence, the leading edge velocity distributions become nearly identical.

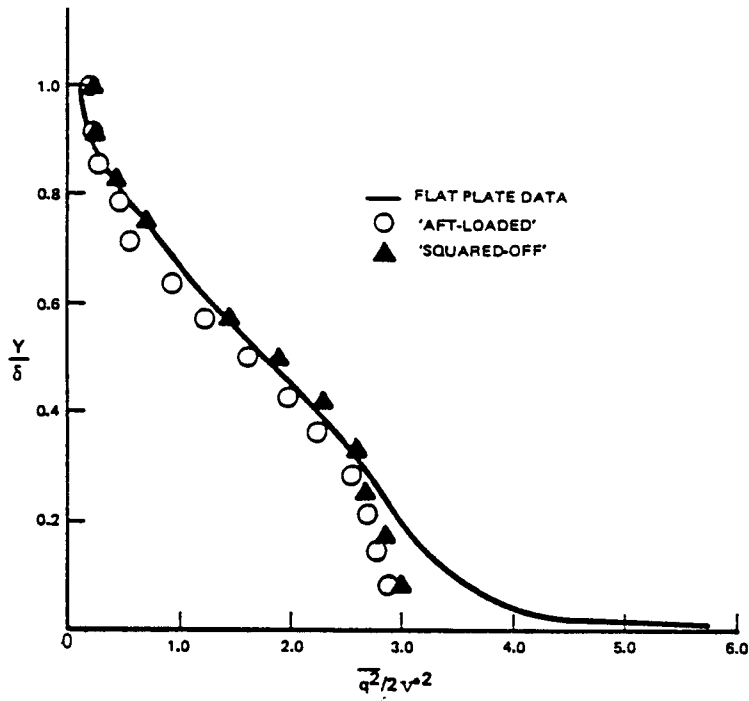


Figure 4.3.4-7 Comparison of Measured Total Turbulence Intensity Profiles with Flat Plate Data

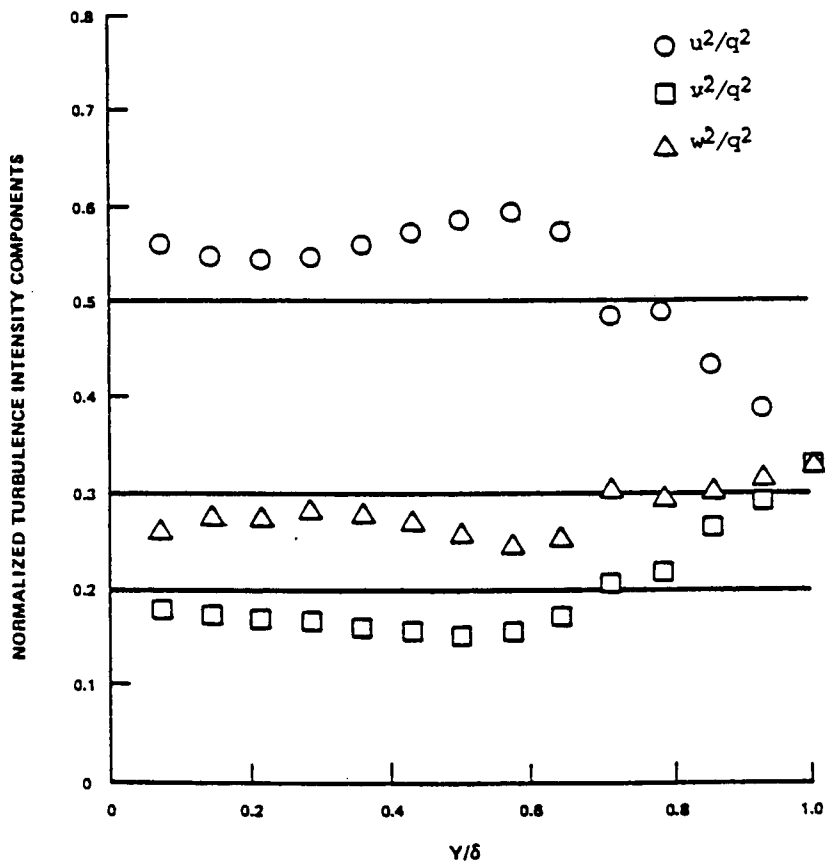


Figure 4.3.4-8 Distribution of Normalized Turbulence Intensity Components in the Fully Turbulent Region of the Squared-Off Test Configuration

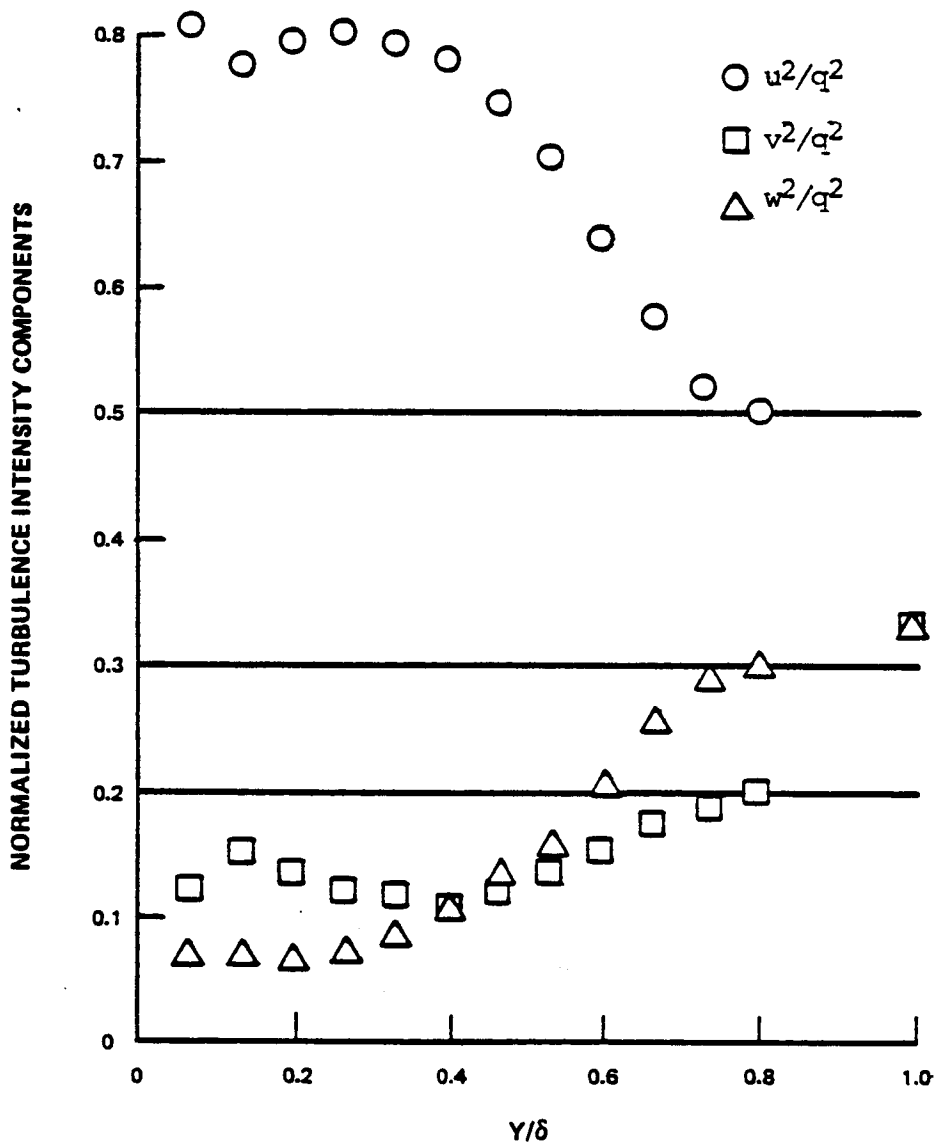


Figure 4.3.4-9 Distribution of Normalized Turbulence Intensity Components in the Transitional Region of the Squared-Off Test Configuration

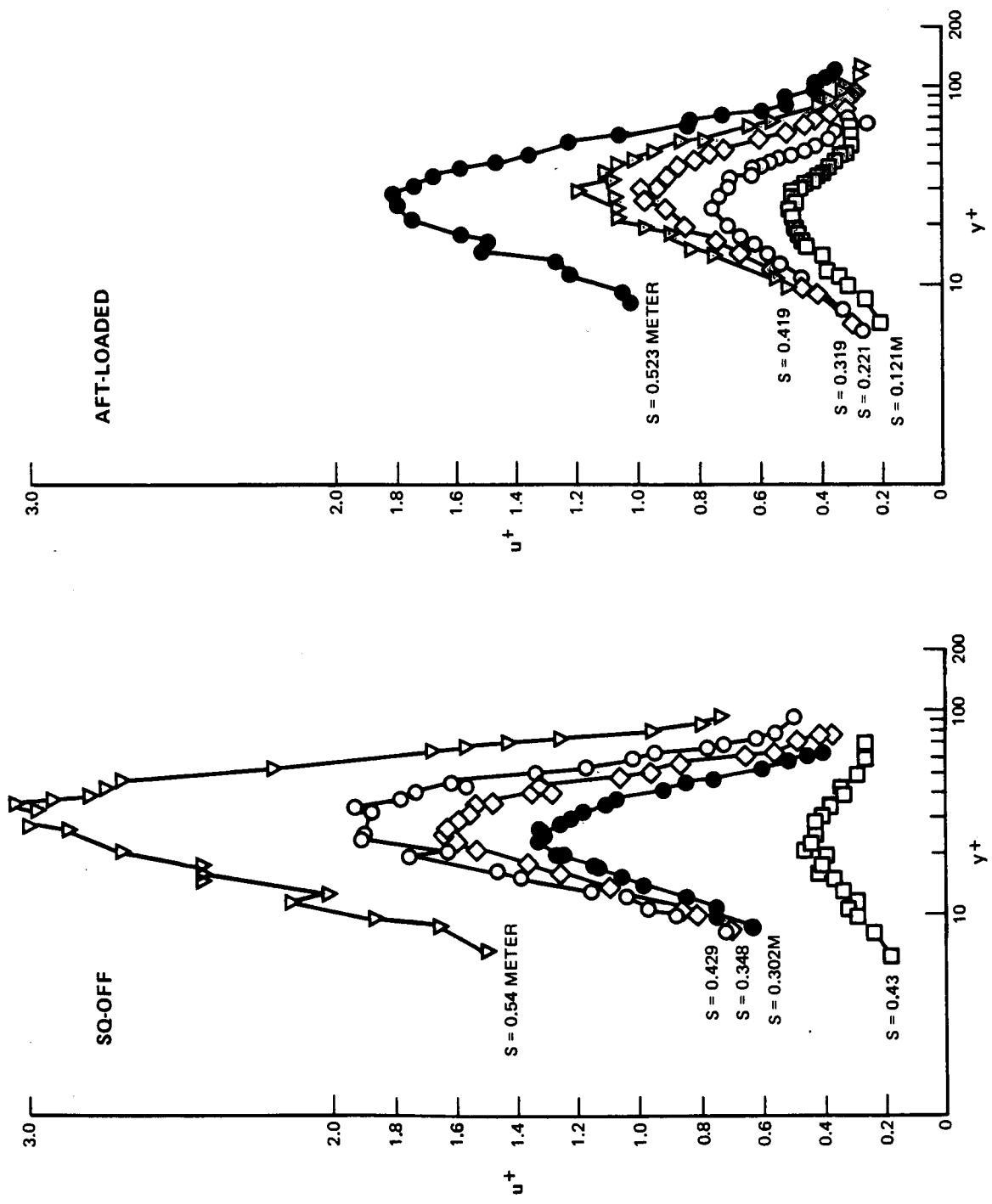


Figure 4.3.4-10 Growth of Turbulence Intensity in the Laminar Region of Each Boundary Layer

From the above discussion, it could be concluded that when the leading edge velocity defect is accounted for, the cascade test and large scale boundary test results are consistent. Further studies directed towards understanding the influence of airfoil leading edge velocity profile on the performance of turbine cascades are required before some definite conclusions can be formulated with respect to its application in turbine designs.

In summary, the results of the Low-Pressure Turbine Boundary Layer Program corroborated that an aft-loaded pressure distribution was reasonable for low-loss airfoils in the low-pressure turbine of the Energy Efficient Engine.

4.4 PERFORMANCE STATUS AND ADJUSTMENT

The performance history of the low-pressure turbine component, intermediate case, and exit guide vane can be summarized in three categories:

1. Goal efficiency established early in the program.
2. Efficiency predictions made prior to completion of the mechanical design.
3. Efficiency prediction update made after completion of the mechanical design.

The efficiencies in the first two categories for the low-pressure turbine were made with assumed blade tip and air seal clearances, while that in the third category reflects the clearances resulting from design analysis.

The goal efficiencies established early in the program and presented at the Low-Pressure Turbine Preliminary Design Review are as shown in Table 4.5-I.

When work progressed to the point where aerodynamic studies were nearly complete but the mechanical design was still in process, a review of predicted performance showed that component efficiency had the potential to exceed the goal in Table 4.5-I. The improvement was attributed to the aerodynamics of the airfoil contours. The updated performance levels are summarized in Table 4.5-II.

On completion of the mechanical design the performance was again updated. The mechanical design that resulted had an impact on performance because of final blade tip clearances. Rotor deflection studies showed that the goal 0.050 cm (0.020 in) blade tip clearances would not be sufficient for aircraft maneuvers. In addition, it was found that greater thermal closure of the active clearance control system (reduced blade tip clearance) was possible with eighth stage high-pressure compressor bleed air than with originally selected tenth stage air. Since considerable integrated core/low spool external part design work had been completed with the tenth stage system, it was retained for the integrated core/low spool design. To take advantage of the improved efficiency with reduced tip clearance, the flight propulsion system adopted the eighth stage high-pressure compressor bleed air system, partially off-setting the efficiency penalty resulting from increased tip clearance required for maneuver deflections.

TABLE 4.5-I
GOAL PERFORMANCE FOR LOW-PRESSURE TURBINE
(Intermediate Case and Exit Guide Vane at Aerodynamic Design Point)

	Flight Propulsion System	Integrated Core/ Low Spool
Low-Pressure Turbine Component Base Efficiency, %	89.0	89.0
Energy Efficient Engine Changes		
Improved Aerodynamics	+1.0	+0.5
Increased Velocity Ratio	+0.3	+0.3
Reduced Leakage	+1.2	+1.0
Integrated Core/Low Spool Effects		
Off-Design Operation		- 0.2
Part Quality		- 0.2
Increased Clearances and Leakage		- 0.3
Low-Pressure Turbine Total, %	91.5	90.1
Intermediate Case Pressure Loss, $\Delta P_T/P_T$, %	0.7	1.5
Exit Guide Vane Pressure Loss, $\Delta P_T/P_T$, %	0.9	0.9

Assumptions:

- (1) 0.051 cm (0.020 in) clearance for interstage air seals
- (2) 0.051 cm (0.020 in) clearance for outer blade tip air seals
- (3) 0.152 cm (0.060 in) clearance on flow guides
- (4) No loss included for gaspath instrumentation

TABLE 4.5-II
LOW-PRESSURE TURBINE EFFICIENCY UPDATE
(At Aerodynamic Design Point -- Prior to Completion of Mechanical Design)

	Flight Propulsion System	Integrated Core/ Low Spool
Low-Pressure Turbine Component Base Efficiency, %	89.0	89.0
Energy Efficient Engine Changes		
Improved Aerodynamics	+1.3	+1.3
Increased Velocity Ratio	+0.3	+0.3
Reduced Clearance and Leakage	+0.7	+0.7
Flow Guides	+0.5	+0.2
Integrated Core/Low Spool Effects		
Off-Design Operation		-0.1
Part Quality		-0.1
Increased Clearances and Leakage		-0.3
Low-Pressure Turbine Total, %	91.8	91.0
Intermediate Case Pressure Loss, $\Delta P_T/P_T$, %	0.7	1.5
Exit Guide Vane Pressure Loss, $\Delta P_T/P_T$, %	0.9	0.9

Assumptions:

- (1) 0.051 cm (0.020 in) clearance for interstage air seals
- (2) 0.051 cm (0.020 in) clearance for outer blade tip air seals
- (3) 0.152 cm (0.060 in) clearance on flow guides
- (4) No loss included for gaspath instrumentation

The resulting status efficiencies are 91.3 and 90.3 percent for the flight propulsion system and integrated core/low spool, respectively, as shown in Table 4.5-III. Reasons for the lower integrated core/low spool efficiency are presented below.

- o Leakage levels in the integrated core/low spool are expected to be greater than design values for the flight propulsion system because the quality of experimental hardware is not as likely to be as high as that specified for the flight hardware.
- o Clearance levels for the integrated core/low spool are expected to be greater for the same reason, plus the fact that the integrated core/low spool utilizes tenth stage high-pressure compressor bleed air for active clearance control, which is less effective than the eighth stage air used in the flight propulsion system. Eighth stage high-pressure compressor bleed air was chosen for the flight propulsion system because of a 0.19 percent efficiency advantage and 0.28 percent thrust specific fuel consumption advantage. Tenth stage compressor bleed air was selected for the integrated core/low spool to avoid design expense and additional hardware costs associated with external plumbing to the eighth stage.
- o Experimental hardware is not expected to achieve design-point operating conditions without more testing than is currently planned for the integrated core/low spool.

The flight propulsion system status efficiency of 91.3 percent falls short of the 91.5 percent goal because maneuver deflections produce higher than expected design blade tip clearances, particularly in the rear stages of the turbine. The resultant clearance gaps were sufficiently large so that closure to goal clearance levels could not be achieved with the active clearance control system at cruise conditions even by utilizing an optimized eighth stage high-pressure compressor bleed schedule. If the goal clearance of 0.050 cm (0.020 in) could be maintained, the calculated efficiency is 91.8 percent, as indicated in Table 4.5-II.

Reducing the impact of maneuver deflections would require basic changes in the rotor support system which translates into a major redesign effort. It was decided that this would not be prudent, since the status efficiency is so near the goal.

TABLE 4.5-III
 DETAIL DESIGN REPORT STATUS PERFORMANCE
 (At Aerodynamic Design Point -- After Completion of Mechanical Design)

	<u>Flight Propulsion System</u>	<u>Integrated Core/ Low Spool</u>
Low-Pressure Turbine Component	91.8	91.0
Mechanical Effects		
Reduction due to Tip Clearance		
Increase 0.051 to 0.086 cm (0.020 to 0.033 in)	-0.4	-0.4
Speed and Thermal Effect:		
with Eighth Stage Air	-0.1	
with Tenth Stage Air		-0.3
Low-Pressure Turbine		
Detailed Design Report Status, %	91.3	90.3
Intermediate Case Pressure		
Loss, $\Delta P_T/P_T$, %	0.7	1.5
Exit Guide Vane Pressure		
Loss, $\Delta P_T/P_T$, %	0.9	0.9

Assumptions:

- (1) Interstage seal clearances as shown on page 139
- (2) Outer blade tip seal clearances as shown on page 138
- (3) 0.152 cm (0.060 in) clearance on flow guides
- (4) No loss included for gaspath instrumentation

SECTION 5.0
TURBINE THERMAL-MECHANICAL DESIGN

5.1 MECHANICAL DESIGN OBJECTIVES AND GOALS

The primary objective of the mechanical design effort was to provide an intermediate case and low-pressure turbine configuration with acceptable life that would meet or exceed the component aerodynamic and performance goals. A secondary objective was to achieve this with the lightest possible structure at the lowest possible cost.

The mechanical definition of the low-pressure turbine component evolved through an iterative process based on the results of the aerodynamic analyses and various supporting technology programs. Where necessary, the turbine design for the flight propulsion system was modified to meet specific requirements associated with the integrated core/low spool. Life requirements for the major subassemblies are summarized in Table 5.1-I.

TABLE 5.1-I
LIFE REQUIREMENTS FOR MAJOR TURBINE SUBASSEMBLIES

<u>Subassembly</u>	<u>Required Life</u>	<u>Remarks</u>
Turbine Intermediate Case:		
Strut Fairings	15,000 hours ⁽¹⁾ / 3,300 missions	Oxidation life is limiting failure mode.
Case/Strut Frame	30,000 hours ⁽¹⁾ / 20,000 missions	Structural limitation is the radial load capacity required to prevent catastrophic failure in the event of fourth stage turbine blade failure.
Rotor:		
Hub, disk, shaft	30,000 hours/ 20,000 missions ⁽²⁾	
Blades	15,000 hours ⁽¹⁾ / 3,300 missions	
Vane and Case:		
Case	30,000 hours/ 20,000 missions	
Vaness	15,000 hours ⁽¹⁾ / 3300 missions	
Turbine Exhaust Case	30,000 hours ⁽¹⁾ / 20,000 missions	Materials and configuration set by plug tuning design requirements.

Notes:

(1) 50 hot hours for integrated core/low spool

(2) Greater than 10³ cycles for integrated core/low spool

5.2 TURBINE MECHANICAL CONFIGURATION

The mechanical configuration of the low-pressure turbine component is illustrated in Figure 5.2-1. The major subassemblies of this system are: (1) the turbine intermediate case; and (2) rotor, shaft, vanes and cases, and turbine exit guide vane. These and the active clearance control system are described in more detail in the following sections of this report. Significant design features and advanced technology concepts that enhance performance, performance retention, and durability are described where appropriate.

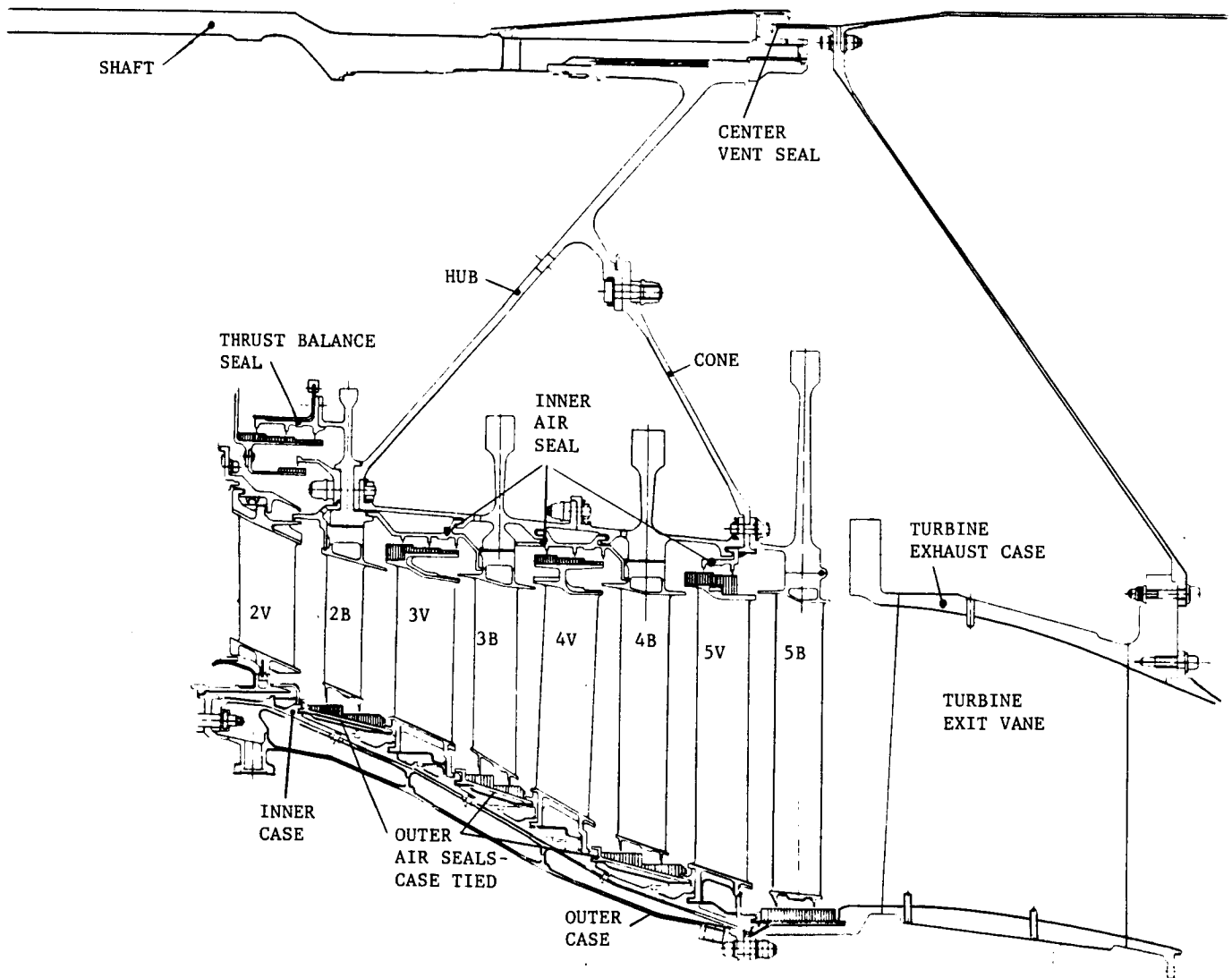


Figure 5.2-1 Low-Pressure Turbine Component Mechanical Configuration

5.2.1 Turbine Rotor Assembly

The short, stiff, high-speed rotor of the Energy Efficient Engine is straddle-mounted by locating its front bearing in the compressor intermediate case and its aft bearing in the turbine intermediate case forward of the low-pressure turbine. This eliminates the overhung high turbine configuration of other engine designs that can create large radial rotor deflections during flight maneuvers. Centralizing the rotor mass between and near the support structure causes the cases and rotors to deflect in a more similar fashion under normally encountered flight loads.

The low-speed rotor design takes advantage of this concept with a three-bearing support. The two front bearings, located at the fan intermediate case, provide moment restraint for the overhung fan/low-pressure assembly to minimize maneuver deflections. The low-pressure turbine rotor is cantilevered off a rear bearing that is axially positioned near the plane of the front stage of the low-pressure turbine to minimize rotor tip deflection where clearances have a more significant effect on efficiency than with the longer rear stages. An analysis of rotor system critical speed is discussed in Section 5.2.4 of this report.

The rotor assembly for the low-pressure turbine is illustrated in Figure 5.2.1-1. Its primary elements are the blades, winged disks and nonintegral hubs, a four-lip thrust balance seal, separate knife-edge seals for the inner cavities, and the shaft. Design details pertaining to these components are discussed in the following sections.

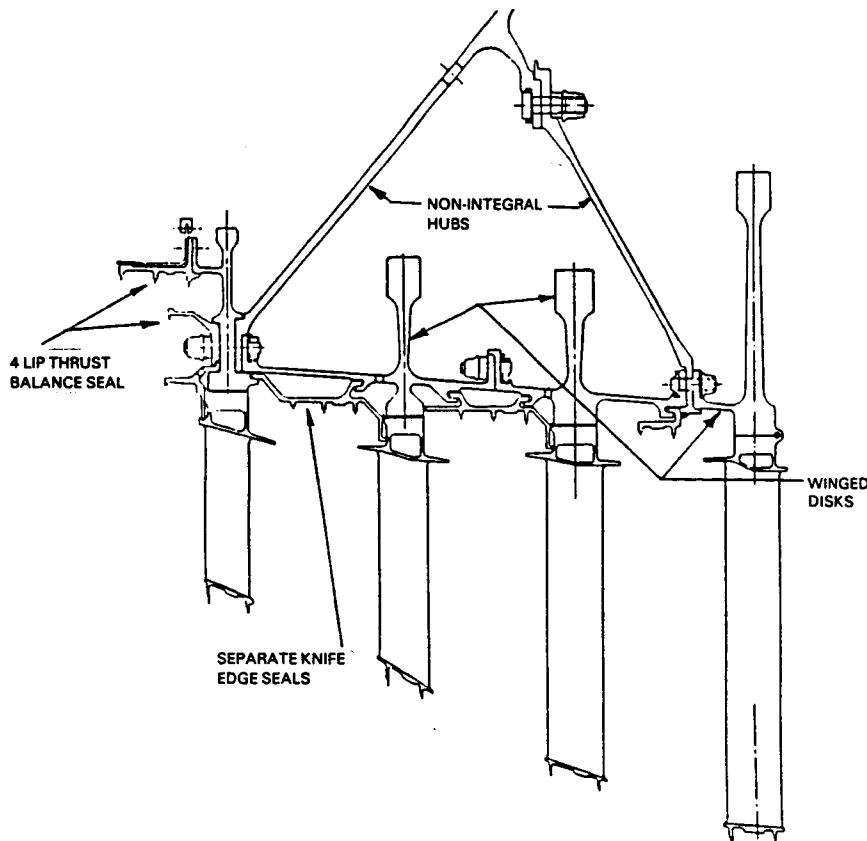


Figure 5.2.1-1 Energy Efficient Engine Low-Pressure Turbine Rotor Assembly

5.2.1.1 Blades

5.2.1.1.1 Mechanical Design Features

The major criterion guiding the mechanical design of the turbine blades was the elimination of the requirement for blade cooling, which eliminated the need for complex internal cooling flow passages and permitted fabrication of the blades from solid castings. Since the low-pressure turbine inlet temperature of 1161K (2090°R) is appreciably higher than current gas-turbine engines, this approach requires the use of high-strength, high-temperature capability materials and coatings on the front stages to provide the desired life.

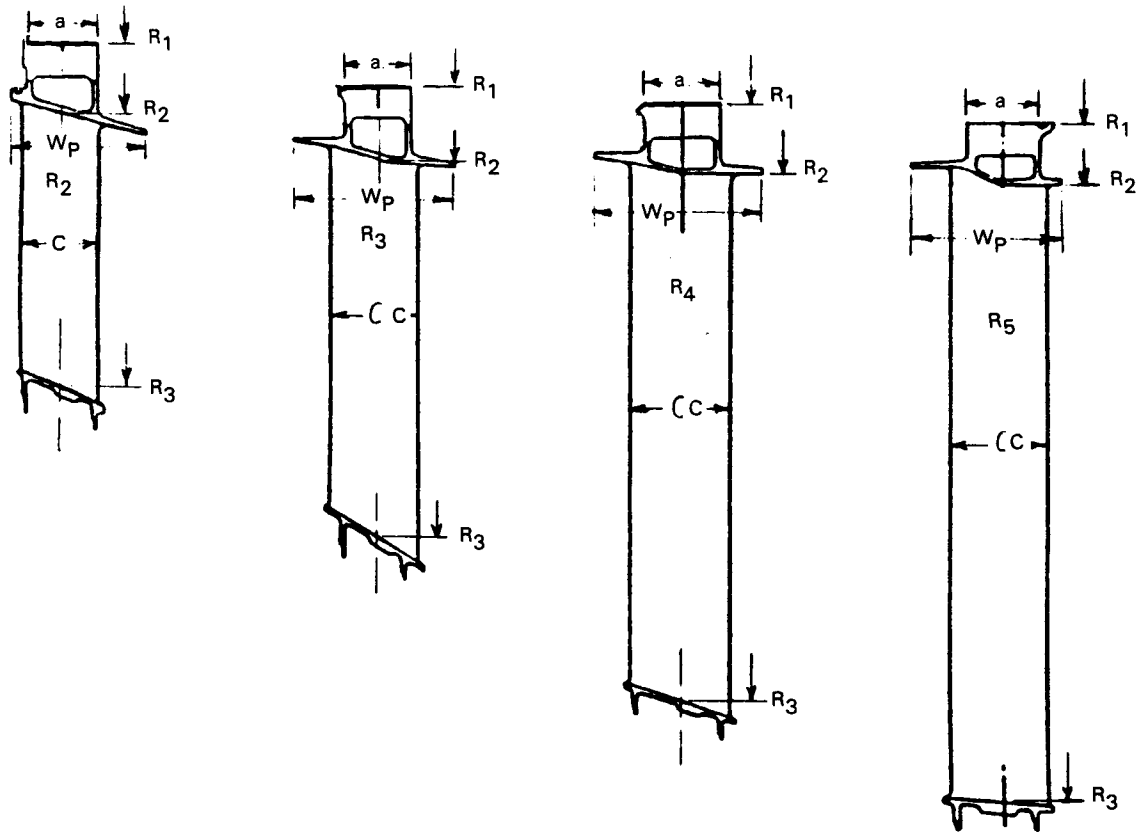
The general characteristics of the turbine blades are illustrated in Figure 5.2.1-2. Airfoil geometry was determined by aerodynamic analysis and is described in Section 4.3.2.2.2 of this report.

The total number of blades is 438. The second stage blade is cast of PWA 1447 (MAR-M-247) and coated with PWA 270 (vapor deposition NiCoCrAl_y) for the flight propulsion system in order to meet its life requirements. A conventional overlay coating, PWA 73, (diffused aluminide) is adequate to meet life requirements of the integrated core/low spool. For both the integrated core/low spool and flight propulsion system the third and fourth stage blades are cast of PWA 655 (Inconel 713) material. The third stage blade in the flight propulsion system requires a PWA 73 coating, but this coating is not necessary for this stage in the integrated core/low spool. The fifth stage blade in the integrated core/low spool is also cast of this material. However, the fifth stage blade in the flight propulsion system is fabricated from titanium-aluminum alloy because of its lower weight property.

Fourth and fifth stage blade platforms incorporate leading edge and trailing edge flow guides to reduce rim cavity flow ingestion and improve efficiency. Blade platform weight is minimized by providing cast, conical, constant thickness surfaces at the flowpath and cast pockets at the underside. Thickness of the pocket and walls was set to minimize leakage through the attachment. To balance out gas bending moments at the blade root, all blades incorporate a slight amount of built-in tilt.

Details of the blade-to-disk attachment are shown in Figure 5.2.1-3. To save time and minimize program cost, an existing two-tooth broach design was utilized. The selected design provided the lightest weight while still meeting design requirements. This broach was utilized on all four stages and no attempt was made to optimize the attachment. A conventional blade retention tang is used on the second, third, and fourth stages, while the fifth stage has a shear lock arrangement. The shear lock arrangement was chosen in order to reduce a fifth stage disk stress concentration factor and improve disk rim low-cycle fatigue life. This shear lock is the same configuration used in the seventh and eighth stage blades of the Energy Efficient Engine high-pressure compressor.

Tip shrouds are included on the blades to enhance aerodynamic efficiency and control blade vibration. Details of these shrouds are shown in Figure 5.2.1-4. Pretwist and bearing surface angles were set to achieve the required tightness, while maintaining low bearing stresses in order to prevent excessive wear on the bearing surfaces. Forward and aft surface angles were set to maintain curling stress within limits.



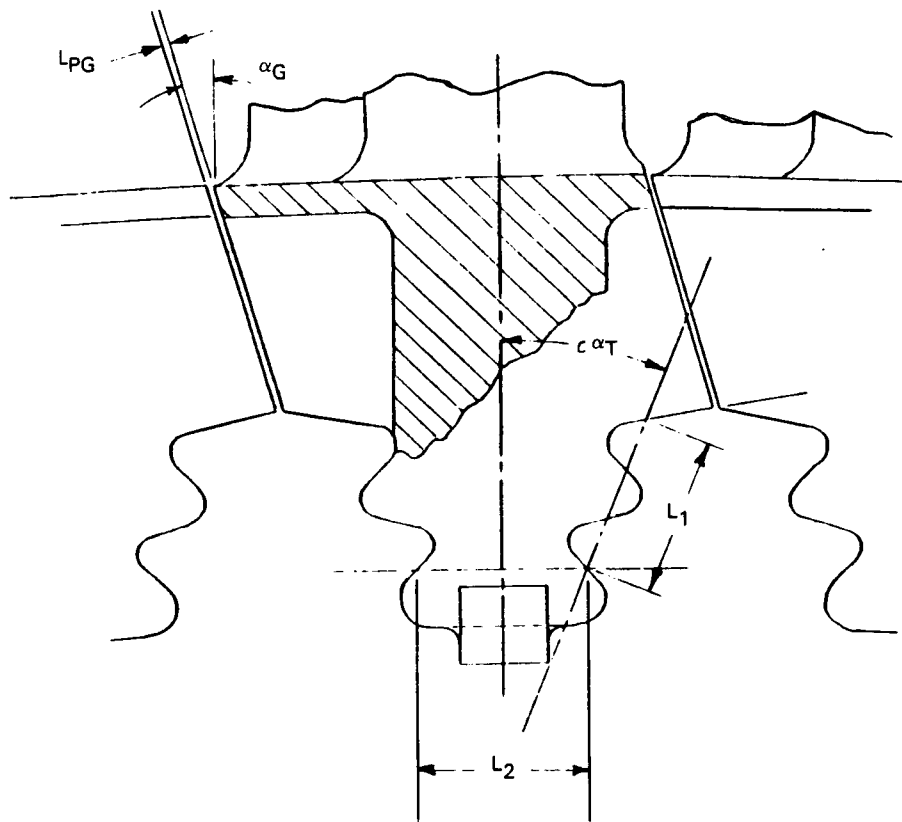
	<u>STAGE</u>			
	2nd	3rd	4th	5th
NO. OF BLADES	120	96	100	122
BLADE MATERIAL	PWA 1447	PWA 655	PWA 655	PWA 655 ⁽³⁾
COATING MATERIAL	PWA 270 ⁽¹⁾	PWA 73 ⁽²⁾	NOT REQ'D	NOT REQ'D
ATTACHMENT AXIAL LENGTH, (a), cm (in)	2.41 (0.95)	2.28 (0.90)	2.54 (1.00)	2.41 (0.95)
AVERAGE AIRFOIL CHORD, (C), cm (in)	2.66 (1.05)	3.07 (1.21)	3.37 (1.33)	3.42 (1.35)
R ₁ , cm (in)	40.1 (15.8)	41.6 (16.4)	42.1 (16.6)	42.6 (16.8)
R ₂ , cm (in)	42.4 (16.7)	44.1 (17.4)	44.4 (17.5)	44.7 (17.6)
R ₃ , cm (in)	51.5 (20.3)	56.6 (22.3)	61.9 (24.4)	65.2 (25.7)
PLATFORM AXIAL WIDTH, W _p INCLUDING FLOW GUIDE, cm (in)	4.77 (1.88)	5.61 (2.21)	5.91 (2.33)	5.46 (2.15)

(1) COATING REQUIRED FOR FLIGHT PROPULSION SYSTEM. INTEGRATED CORE/LOW SPOOL WILL USE PWA 73

(2) NOT REQUIRED FOR INTEGRATED CORE/LOW SPOOL

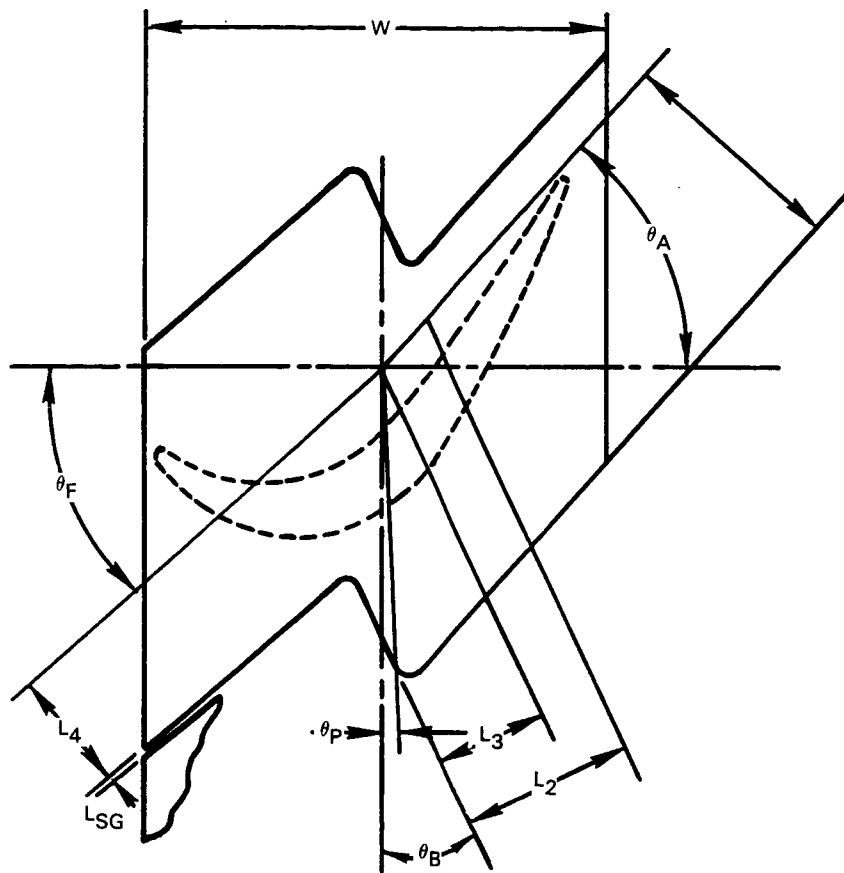
(3) MERL 101 (Ti-Al) IS BEING CONSIDERED FOR THE FLIGHT PROPULSION SYSTEM

Figure 5.2.1-2 Low-Pressure Turbine Blade General Characteristics



	STAGE			
	2nd	3rd	4th	5th
BROACH ANGLE	11°	7°30'	15°	0
PLATFORM GAP ANGLE, α_G	14°45'	25°	15°	27°15'
PLATFORM GAP, L_{PG} cm (in)	0.030 (0.012)	0.030 (0.012)	0.025 (0.010)	0.030 (0.012)
TAPER ANGLE, α_T	22°	22°	22°	22°
RESTAGGER CAPACITY	$\pm 4^\circ 30'$	$\pm 3^\circ$	$\pm 3^\circ$	$\pm 3^\circ$
L_1 cm (in)	0.78 (0.31)	0.78 (0.31)	0.78 (0.31)	0.78 (0.31)
L_2 , cm (in)	0.81 (0.32)	0.81 (0.32)	0.81 (0.32)	0.81 (0.32)

Figure 5.2.1-3 Blade-to-Disk Attachment Design Details



	<u>STAGE</u>			
	2nd	3rd	4th	5th
PRETWIST ANGLE, θ_P	0°45'	1°	1°15'	2°30'
BEARING SURFACE ANGLE, θ_B	25°	20°	30°	35°
FORWARD, SURFACE ANGLE, θ_F	42°	37°30'	33°	35°
AFT SURFACE ANGLE, θ_A	47°30'	46°30'	42°	35°
AXIAL WIDTH, (W) cm (in)	3.04 (1.20)	3.35 (1.32)	3.73 (1.47)	3.68 (1.45)
L_1 ~ cm (in)	1.44 (0.57)	2.00 (0.79)	1.93 (0.76)	1.85 (0.73)
L_2 ~ cm (in)	1.14 (0.45)	1.27 (0.50)	1.95 (0.77)	1.93 (0.76)
L_3 ~ cm (in)	0.73 (0.29)	0.81 (0.32)	1.14 (0.45)	1.11 (0.44)
L_4 ~ cm (in)	0.83 (0.33)	1.44 (0.57)	1.47 (0.58)	1.21 (0.48)
THRUST AIR, L_{SG} ~ cm (in)	0.38 (0.015)	0.030 (0.012)	0.038 (0.015)	0.030 0.012

Figure 5.2.1-4 Tip Shroud Design Details

5.2.1.1.2 Structural Analysis

Structural analysis of the blades involved an analysis of blade vibration and flutter characteristics, attachment stresses, tip shroud stresses, and blade airfoil durability.

Stage Vibration and Flutter Analysis

Individual rotor stage frequencies were selected to avoid engine orders known from experience to produce high stresses. These are the second and third orders for all stages, the eleventh (twenty-second order) excited by the upstream struts for the first two stages and the thirtieth order excited by the exit struts for the last stage.

For the second stage rotor, 11E and 22E resonances were of concern because of the proximity of the 11 upstream intermediate case struts. Figure 5.2.1-5 shows that for the 11E first mode, a frequency margin of 9.8 percent at the maximum rotor speed is predicted. For 22E first mode, a margin of -10.7 percent at the minimum cruise speed is calculated. All critical second mode resonances occur well outside of the operating range.

The third stage design has a -38 percent 22E and a -16 percent 11E first mode frequency margin at the minimum cruise speed, with the 22E resonance occurring away from the idle range. The 3E first mode frequency margin is 14 percent and the 22E second mode frequency is also 14 percent at the maximum rotor speed (Figure 5.2.1-6).

Critical resonances for stage four were limited to the low orders. The final design resulted in margins of 52 percent 2E and 18 percent 3E for the first mode at the maximum rotor speed (Figure 5.2.1-7). Avoidance of the 11E and 22E resonances was not required.

The fifth stage blade design in the integrated core/low spool incorporates a nickel-base alloy and has a 9 percent first mode 3E resonance margin at maximum rotor speed. The 30E first and second mode resonances are predicted to occur at 1400 and 1760 revolutions/minute, respectively. These were considered acceptable for the integrated core/low spool (Figure 5.2.1-8).

Titanium alloy blades are being considered for the flight propulsion system to reduce weight. Vibration analysis with this material indicated that the fifth stage has an ample first mode frequency margin above the second and third engine orders at maximum rotor speed. The thirtieth order resonance with the downstream struts will be well below minimum cruise speed for the first and second modes. Testing with strain gages will be required to demonstrate that stresses are low enough for flight engine safety. The resonance diagram is shown in Figure 5.2.1-9.

Figure 5.2.1-10 presents the results of a flutter analysis on the four low-pressure turbine rotors. The Energy Efficient Engine designs are compared to previous Pratt & Whitney Aircraft designs in terms of aerodynamic damping and tip exit reduced velocity parameters. The results of this analysis indicate that all four rotors operate well above the unstable limit and are therefore not expected to encounter flutter problems.

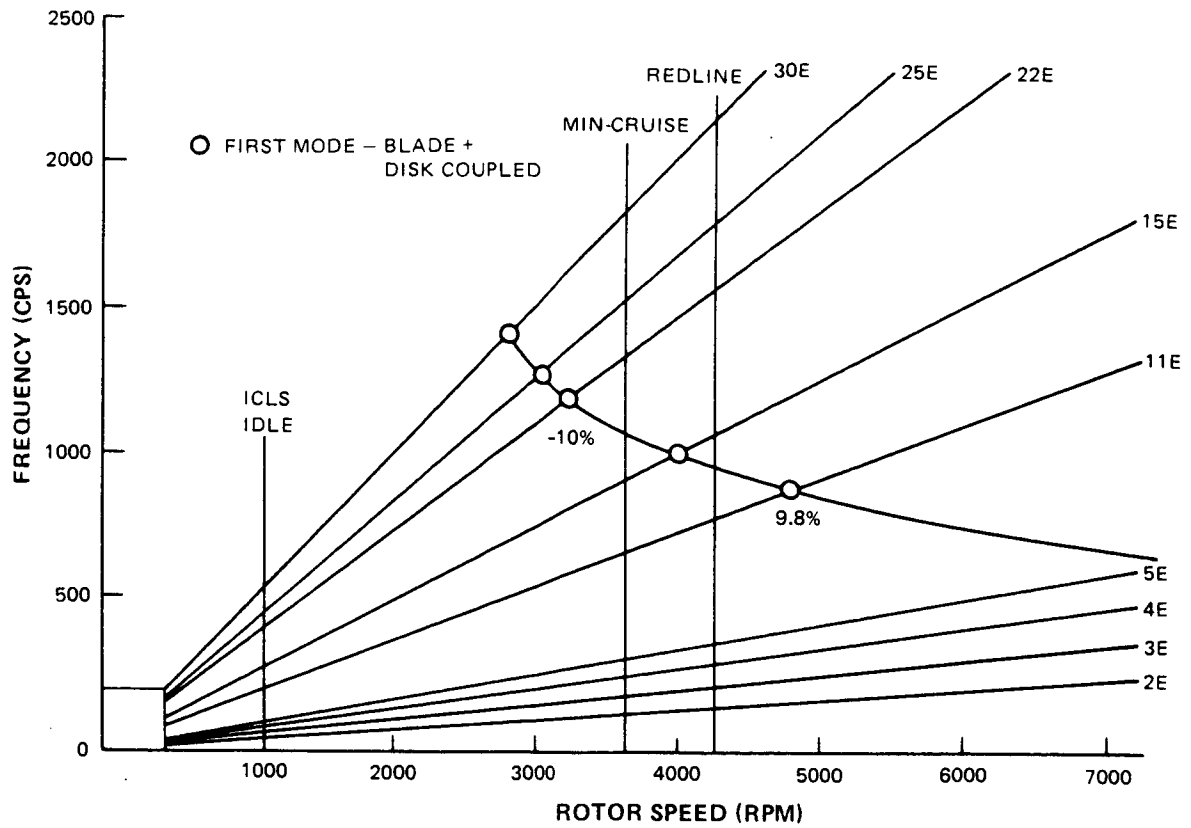


Figure 5.2.1-5 Low-Pressure Turbine Second Stage Rotor Resonance Diagram

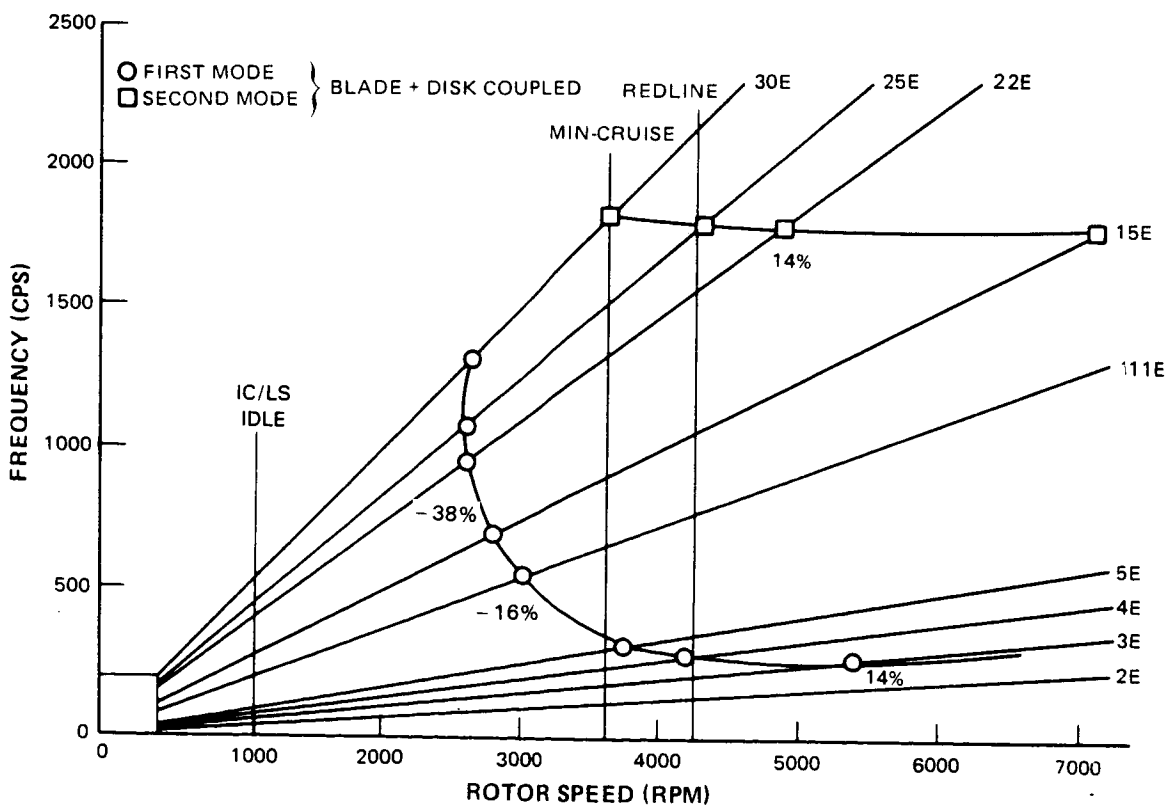


Figure 5.2.1-6 Low-Pressure Turbine Third Stage Rotor Resonance Diagram

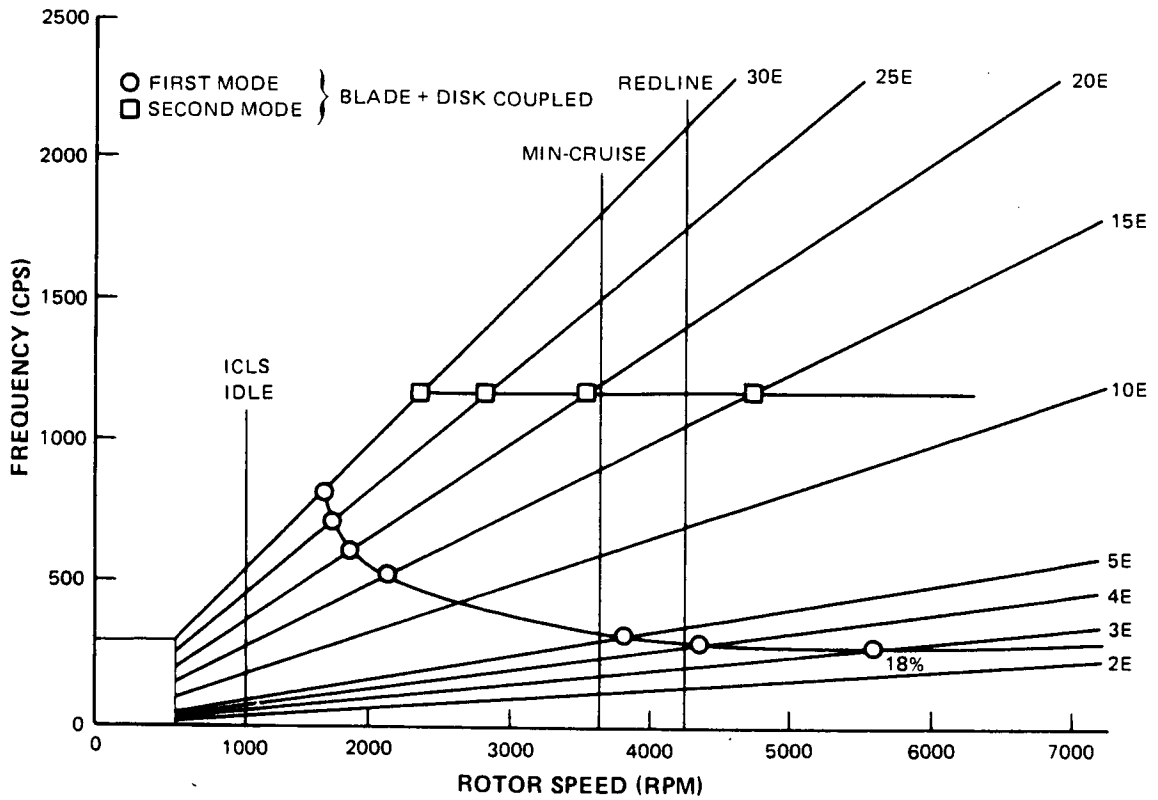


Figure 5.2.1-7 Low-Pressure Turbine Fourth Stage Rotor Resonance Diagram

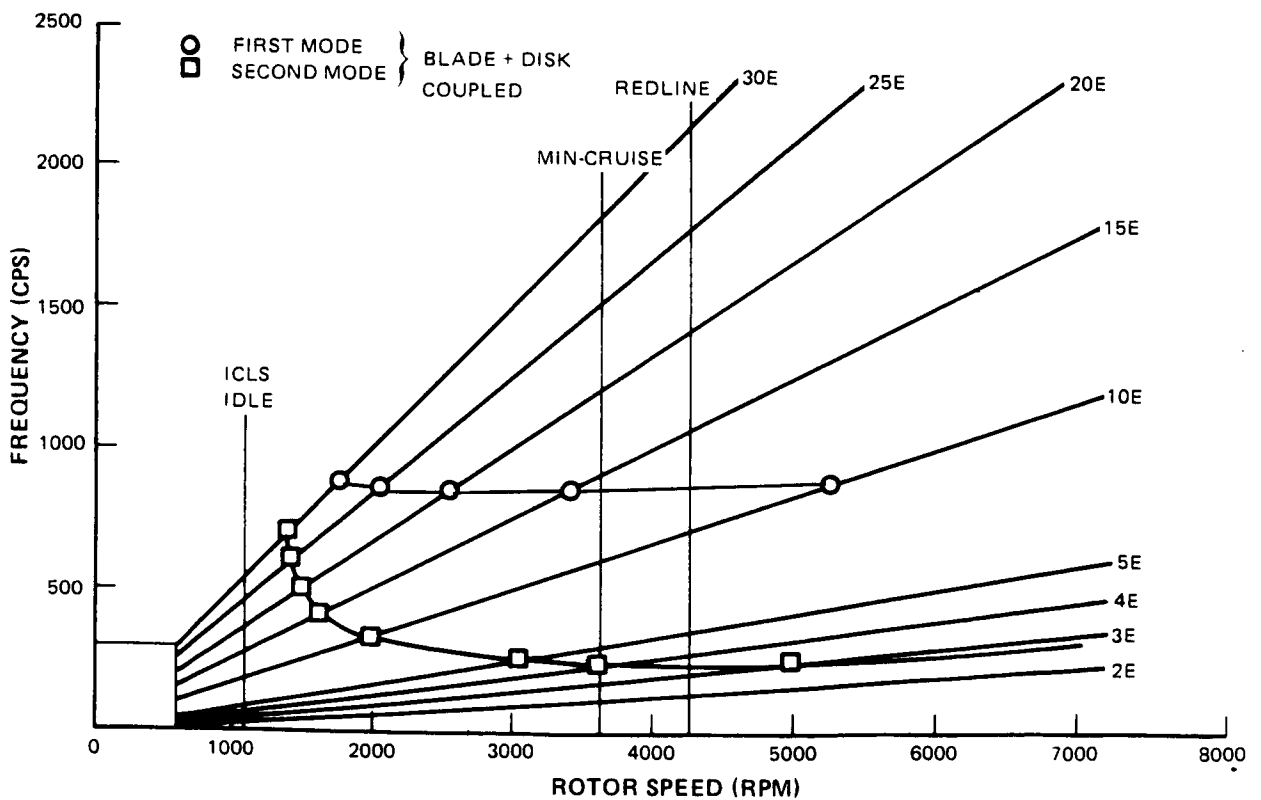


Figure 5.2.1-8 Low-Pressure Turbine Fifth Stage Rotor Resonance Diagram

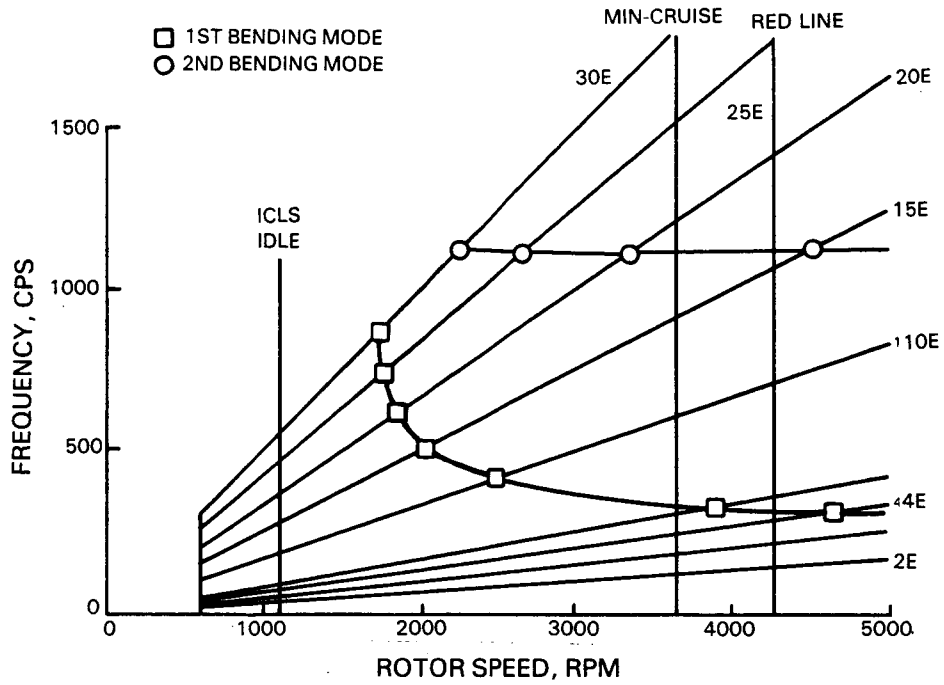


Figure 5.2.1-9 Low-Pressure Turbine Fifth Stage Rotor Resonance Diagram Titanium-Aluminum Alloy Blade

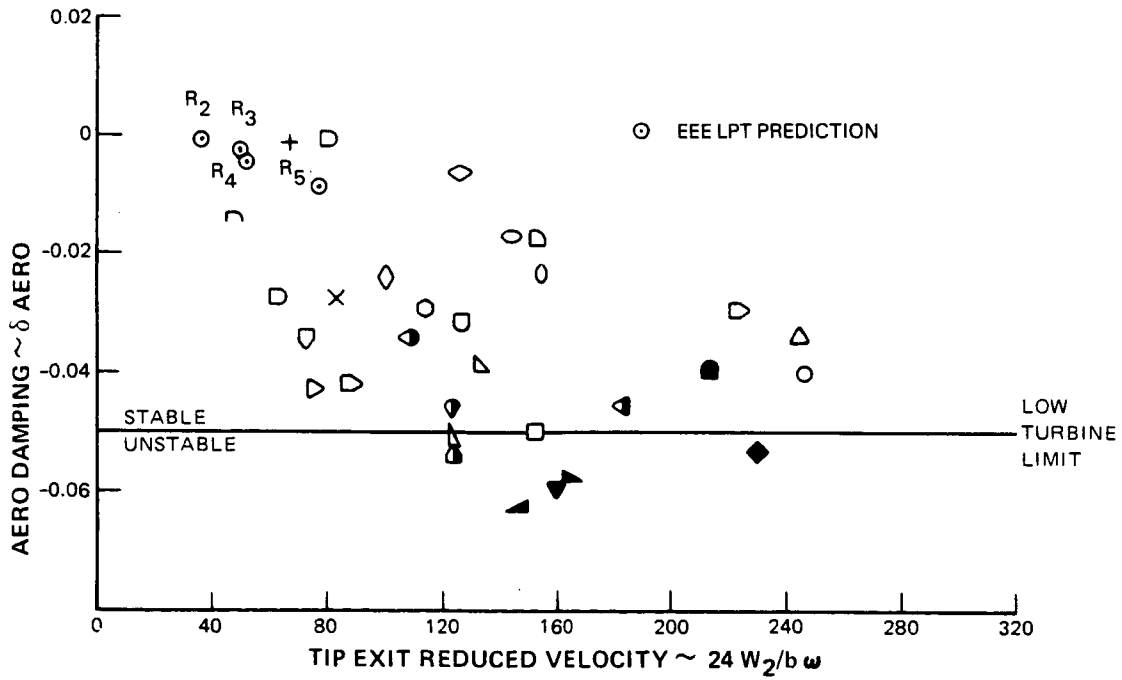


Figure 5.2.1-10 Shrouded Turbine Blade Flutter Analysis

Attachment Stress Analysis

Blade attachment stresses were calculated with consideration given to axial gas loads, airfoil and shroud residual moments, blade centrifugal pulls, and platform offset moments. Table 5.2.1-I summarizes the results of these analyses and indicates that the attachments for all stages have adequate stress margin. The margins shown represent the maximum stress levels.

TABLE 5.2.1-I
BLADE ATTACHMENT STRESS SUMMARY
(Margins in Percent)

	<u>Second Blade</u>	<u>Third Blade</u>	<u>Fourth Blade</u>	<u>Fifth Blade</u>
Blade Material	PWA 1447	PWA 655	PWA 655	PWA 655(*)
Neck Tension	173	247	167	188
Tooth Shear	130	51	38	27
Tooth Bending	349	232	197	172
Tooth Bearing	108	48	16	29

NOTE (*): A Ti-Al alloy (MERL 101) is being considered for the blade in the flight propulsion system. This would have even higher margins than those shown for PWA 655.

Tip Shroud Stress Analysis

Bearing stresses and curling stresses were analyzed for the tip shrouds. Results of this analyses indicated that adequate stress margins were achieved for all stages. These results are summarized in Table 5.2.1-II.

TABLE 5.2.1-II
TIP SHROUD STRESS SUMMARY
(Margins in Percent)

	<u>Second Blade</u>	<u>Third Blade</u>	<u>Fourth Blade</u>	<u>Fifth Blade</u>
Bearing Stress	15	24	3	8
Curling Stress	27	54	98	39

Blade Airfoil Durability Analysis

Blade airfoil durability objectives were to provide 15,000 hours of service life (or 3300 flight missions) in the flight propulsion system and 50 hours of hot life (28°C (84°F) day at sea level takeoff power) in the integrated core/low spool. The durability design analysis consisted of first defining metal temperatures and stresses at the design condition and then evaluating expected life relative to the durability objectives. Materials and coatings utilized in this analysis are listed in Figure 5.2.1-2.

Gas temperature profiles and resultant spanwise calculated stresses for the blade airfoils are shown in Figures 5.2.1-11 through 5.2.1-14. Blade stresses were calculated using average profile temperatures. Airfoil creep strength margins were calculated using the relationship:

$$\% \text{ Margin} = \frac{(\text{Allowed Stress} - \text{Actual Stress})}{\text{Allowed Stress}} \times 100$$

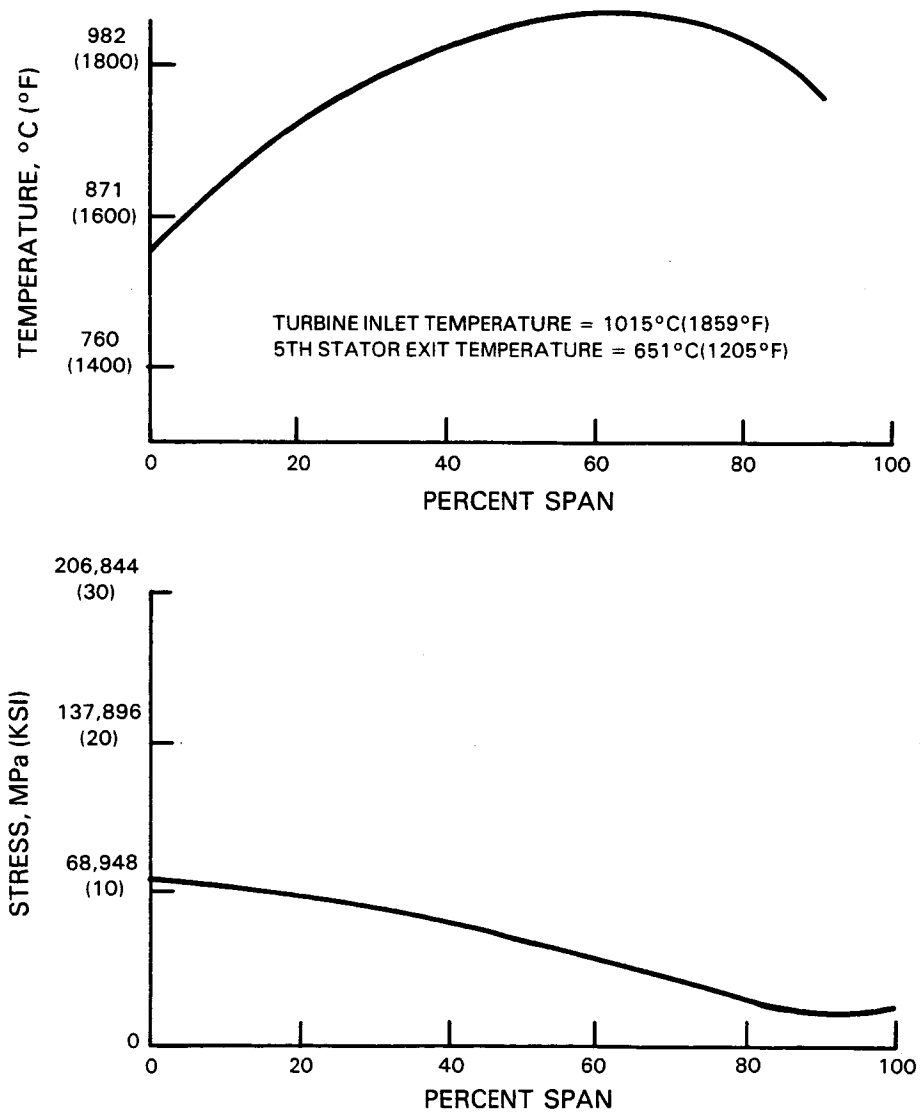


Figure 5.2.1-11 Second Stage Blade Durability Design Conditions and Calculated Stress (Blade Material: PWA 1447, Coating: PWA 73)

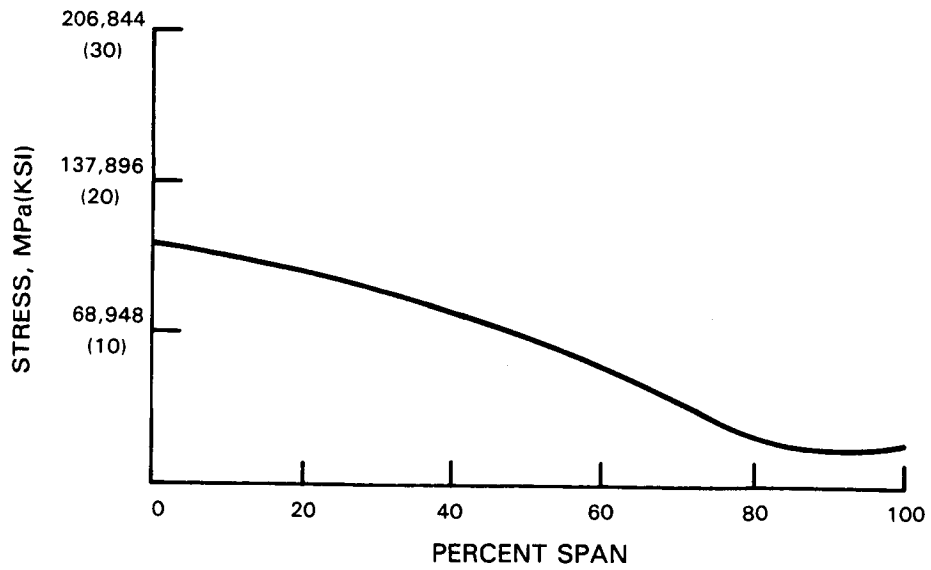
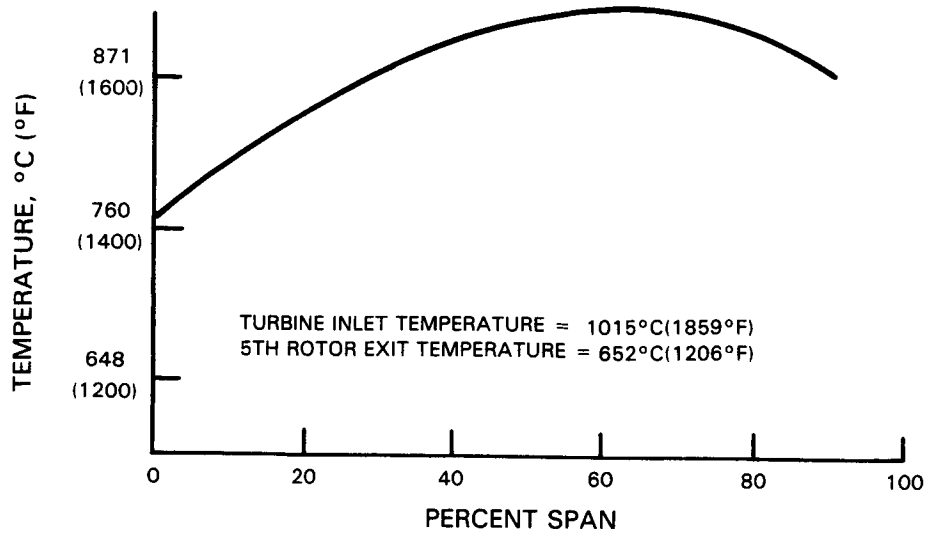


Figure 5.2.1-12 Third Stage Blade Durability Design Conditions and Calculated Stress (Blade Material: PWA 655; No Coating)

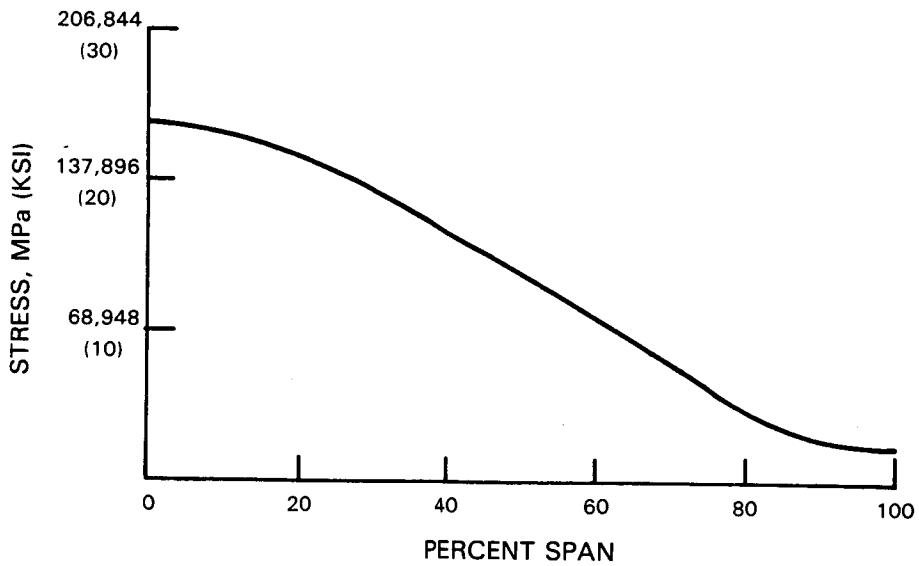
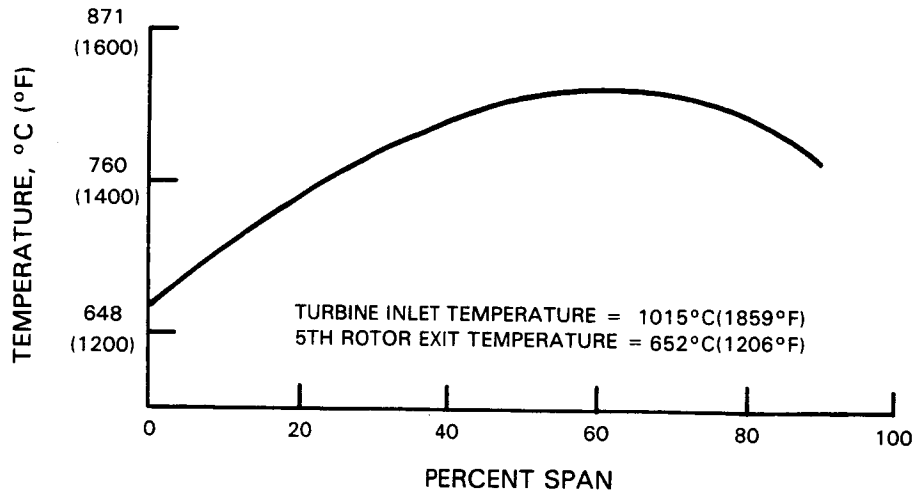


Figure 5.2.1-13 Fourth Stage Blade Durability Design Conditions and Calculated Stress (Blade Material: PWA 655, No Coating)

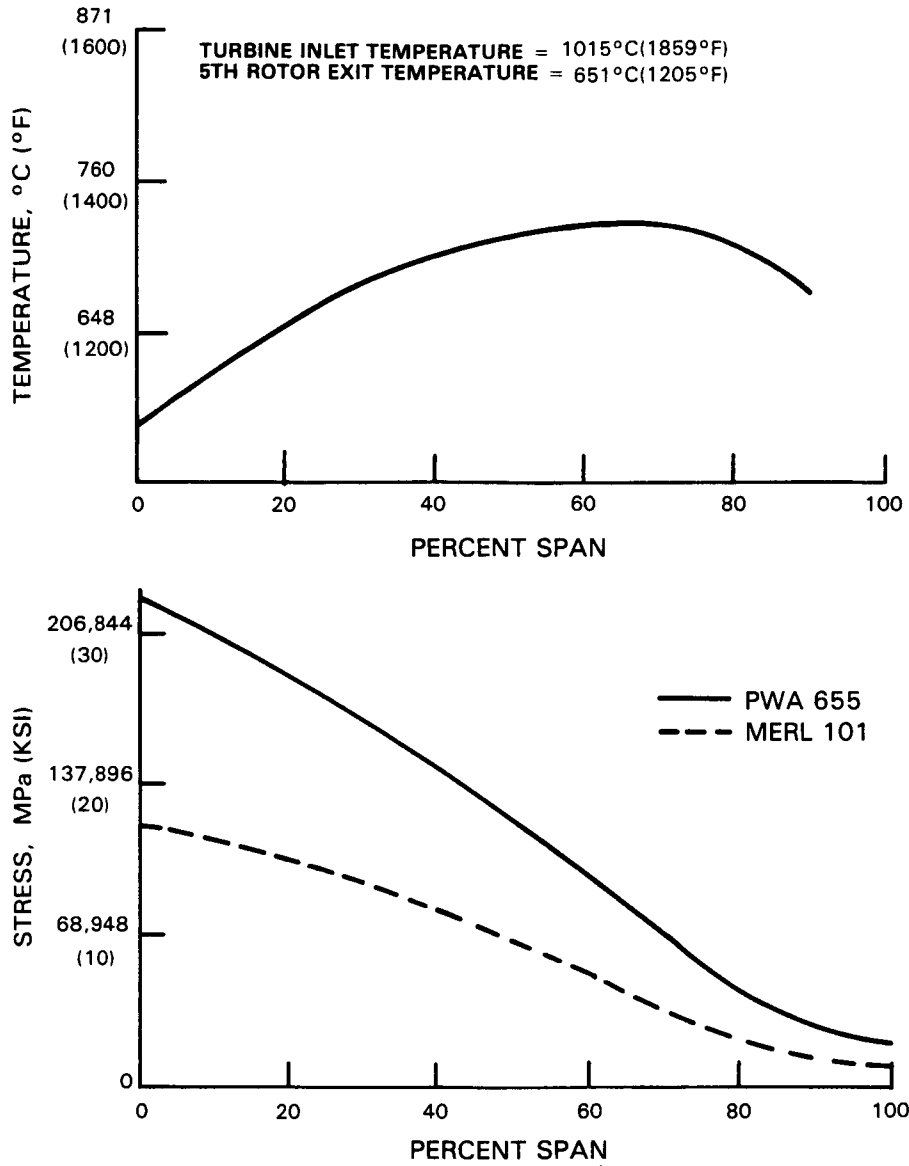


Figure 5.2.1-14 Fifth Stage Blade Durability Design Conditions and Calculated Stress (Blade Material: PWA 655, No Coating)

where allowed stresses were based on the desired life and 1.0 percent material creep properties.

The resultant airfoil creep strength margins are summarized in Table 5.2.1-III for both the flight propulsion system and the integrated core/low spool. All airfoils were determined to have adequate creep strength.

TABLE 5.2.1-III
BLADE AIRFOIL CREEP STRENGTH MARGINS
(Margins in Percent at Limiting Span)

	<u>Flight Propulsion System</u>	<u>Integrated Core/ Low Spool</u>
Second Blade	14	62
Third Blade	21	52
Fourth Blade	50	66
Fifth Blade	33	75

Since the second and third-stage blades operate in a high temperature environment, a transient thermal strain analysis was conducted to determine thermal fatigue life. Engine operating conditions in a typical flight cycle were utilized in the analysis. These included startup and idle, acceleration to takeoff power, takeoff, climb, cruise power, deceleration to flight idle, approach power, and thrust reverse. Two strain cycles are experienced during each typical flight. The resultant strain histories for the second and third blades are shown in Figures 5.2.1-15 and -16. As indicated, the maximum strain ranges (i.e., strain cycle amplitudes) for these two airfoils were equal to or less than 0.24 percent.

Airfoil lives were subsequently calculated and are presented in Table 5.2.1-IV. Life-limiting conditions of concern were cracking and metal surface oxidation. As noted in this table, life for both the flight propulsion system and the integrated core/low spool exceeded the goals. Oxidation was the only concern for the integrated core/low spool because the integrated core/low spool low-pressure turbine will not accumulate enough running time to initiate cracks.

TABLE 5.2.1-IV
SUMMARY OF PREDICTED BLADE LIVES

	<u>Flight Propulsion System</u>		<u>Integrated Core/ Low Spool</u>
	<u>Cracking (hrs)</u>	<u>Oxidation (hrs)</u>	<u>Oxidation (hrs)</u>
Second Blades	20,000	20,000	100
Third Blades	20,000	20,000	100
Fourth & Fifth Blades	(a)	(a)	(a)

Note:

(a) Not Life Limiting

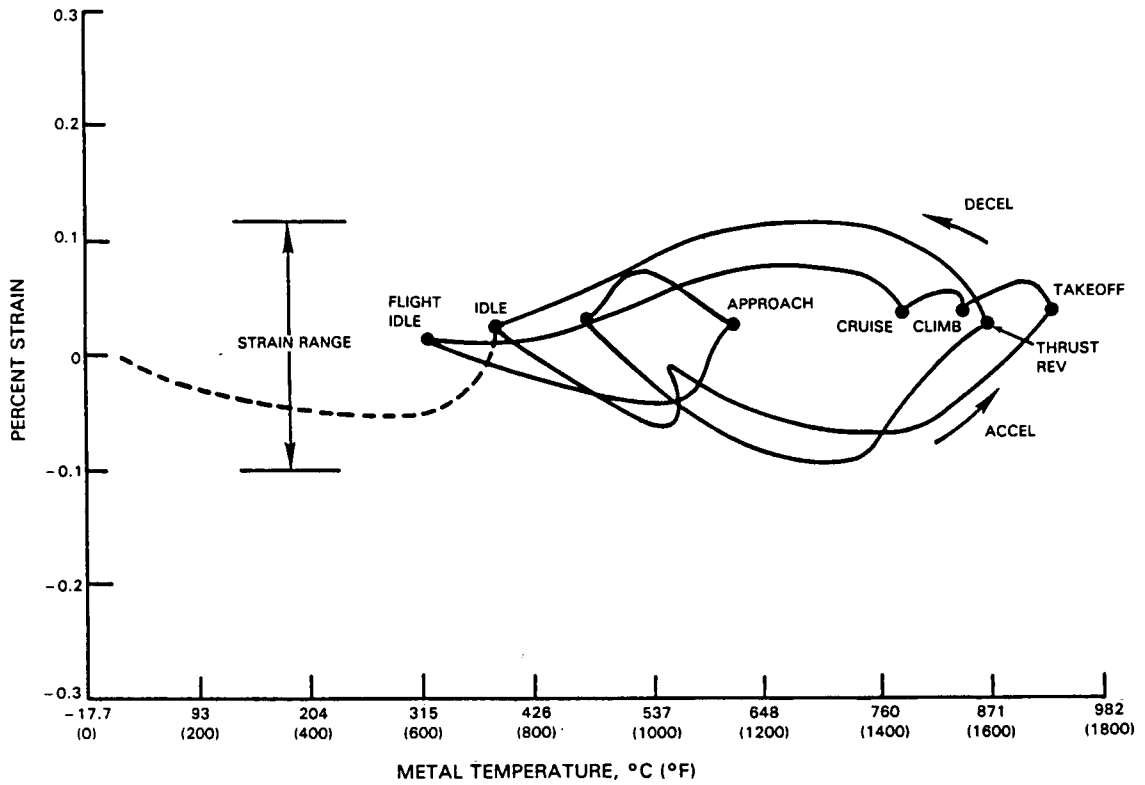


Figure 5.2.1-15 Energy Efficient Engine Second Blade Transient Strains (Flight Propulsion System)

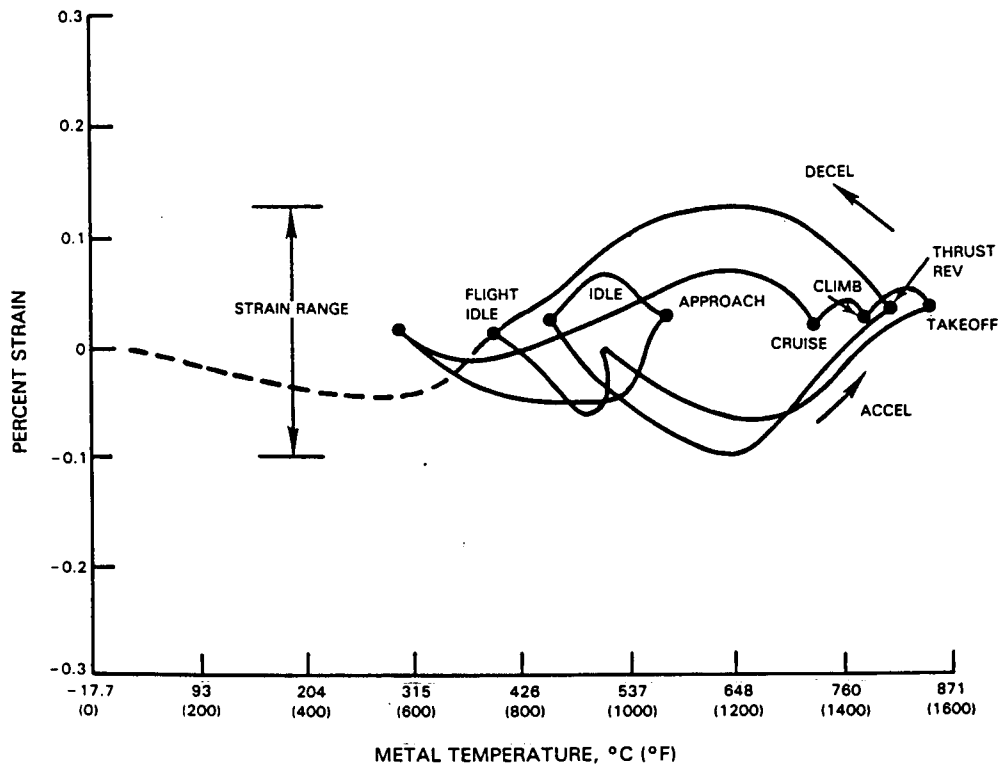


Figure 5.2.1-16 Energy Efficient Engine Third Blade Transient Strains (Flight Propulsion System)

5.2.1.2 Disk and Hub Assembly

5.2.1.2.1 Mechanical Design Features

The low-pressure turbine disk and hub assembly shown in Figure 5.2.1-17 incorporates an "A-frame" construction technique, designed to provide the stiffness required to control deflections caused by maneuver loads. The second and fifth disks are bolted to the legs of the "A-frame", and the third and fourth stage winged disks are bolted to the second and fifth stages to form the base of the "A-frame". Separate knife-edge inner air seals also shield the base of the "A-frame" from hot gaspath air and, in the third and fourth stages, provide cooling air passages to the disk attachments. (Cooling air from inside the drum is directed to the disk rim front and passes through the blade root gaps to cool the disk rim and blade roots.)

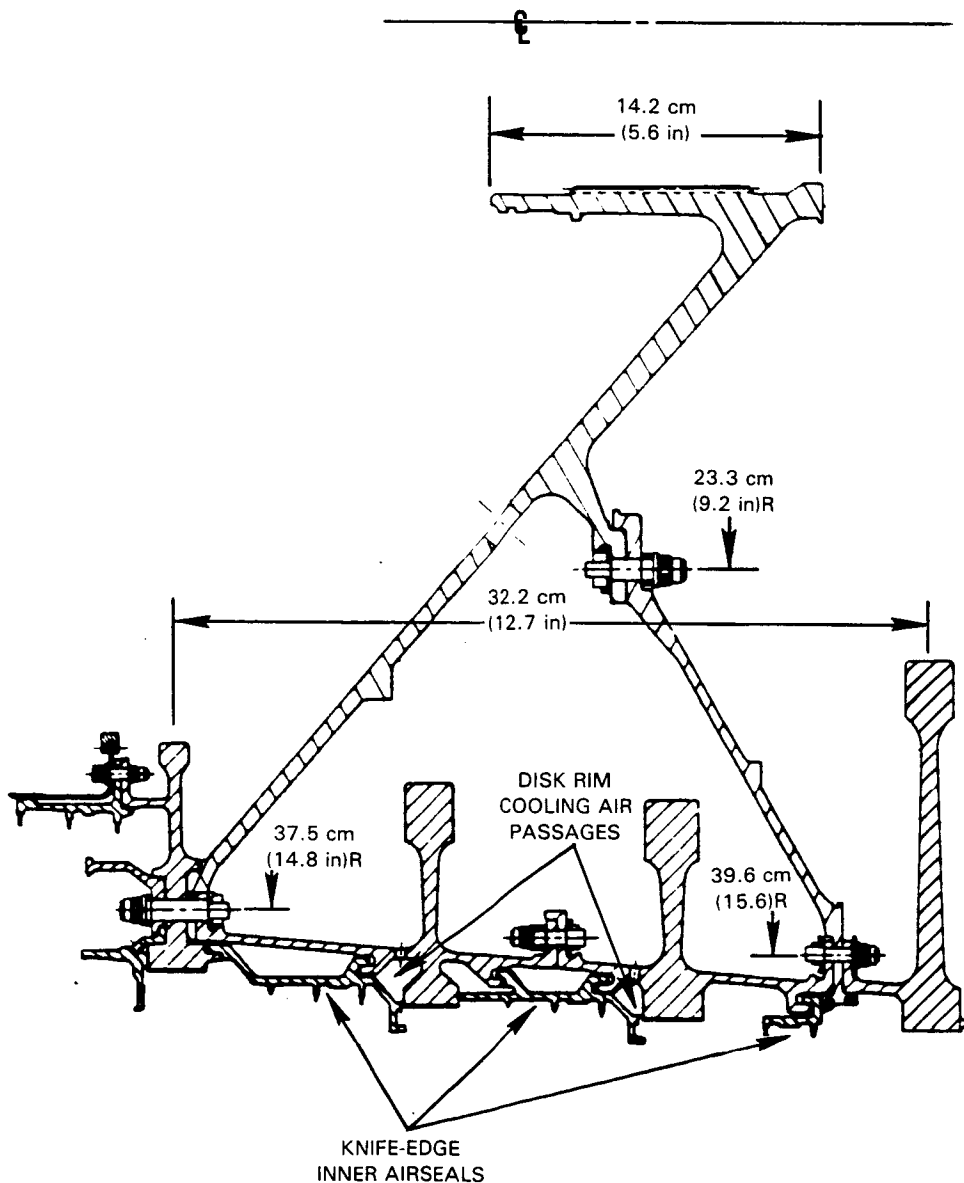


Figure 5.2.1-17 Low-Pressure Turbine Disk and Hub Assembly

For both the flight propulsion system and integrated core/low spool, the hub and inner airseal materials were selected on the basis of availability, cost, and structural/radial clearance requirements. Hubs are made from PWA 1003 (Incoloy 901). Inner air seals are made of PWA 1099 (modified Inconel 100 or MERL 76) to match the disk material, which is also PWA 1099.

Existing tierod bolts are used for the integrated core/low spool. Spacers are utilized to accommodate the existing bolt lengths. The number of bolts employed was established to satisfy the blade loss design criteria, except for the bolted joint between the fourth and fifth stage disks. Here, the number of bolts was doubled to improve flange sealing.

5.2.1.2.2 Structural Analysis

Structural analysis of the hub assembly was conducted using the results of the transient thermal analysis described in Section 5.2.5 of this report. Rotor metal temperatures used in the analysis are shown in Figure 5.2.1-18. They were calculated based on sea level takeoff hot day conditions. The resultant stresses, summarized in Figure 5.2.1-19, were calculated based on this temperature distribution and an assumed 60-second acceleration to takeoff power. Stress concentration factors for the disk rim locations were established by performing a finite element analysis on the fifth stage and correcting those values for the remaining stages. This was permissible because the same attachment geometry existed for all stages. All stresses were within allowable margins.

A subsequent life analysis indicated that all areas exceeded 100,000 cycles with the exception of those noted in Figure 5.2.1-20, which just meet flight propulsion system requirement of 20,000 cycles in the areas noted. Margin could be added here by a slight "tuning" of the design. Disk burst margins, creep life, and average tangential rim stresses are summarized in Table 5.2.1-V. All stresses and lives are adequate to meet integrated core/low spool requirements.

TABLE 5.2.1-V
DISK STRUCTURAL SUMMARY

	<u>Rotor 2</u>	<u>Rotor 3</u>	<u>Rotor 4</u>	<u>Rotor 5</u>
Burst Margin	1.66	1.43	1.36	1.48
Creep Life, hrs.	10 ⁴	10 ⁴	10 ⁴	10 ⁴
Avg. Tangential Stress, MPa (ksi)	434,372 (63)	584,679 (84.8)	652,248 (94.6)	549,515 (79.7)

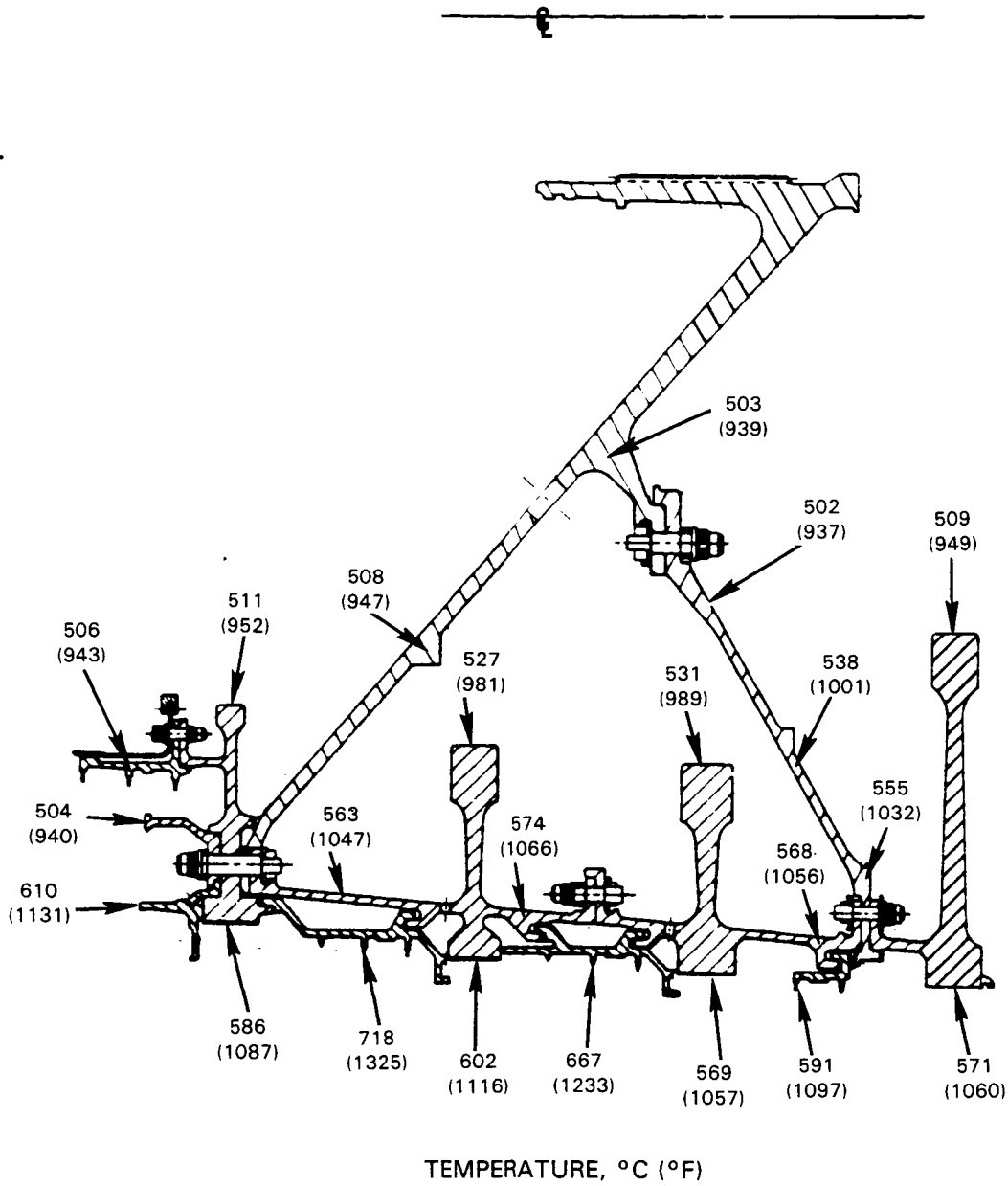


Figure 5.2.1-18 Rotor Metal Temperature Distribution Used in Stress and Life Analysis

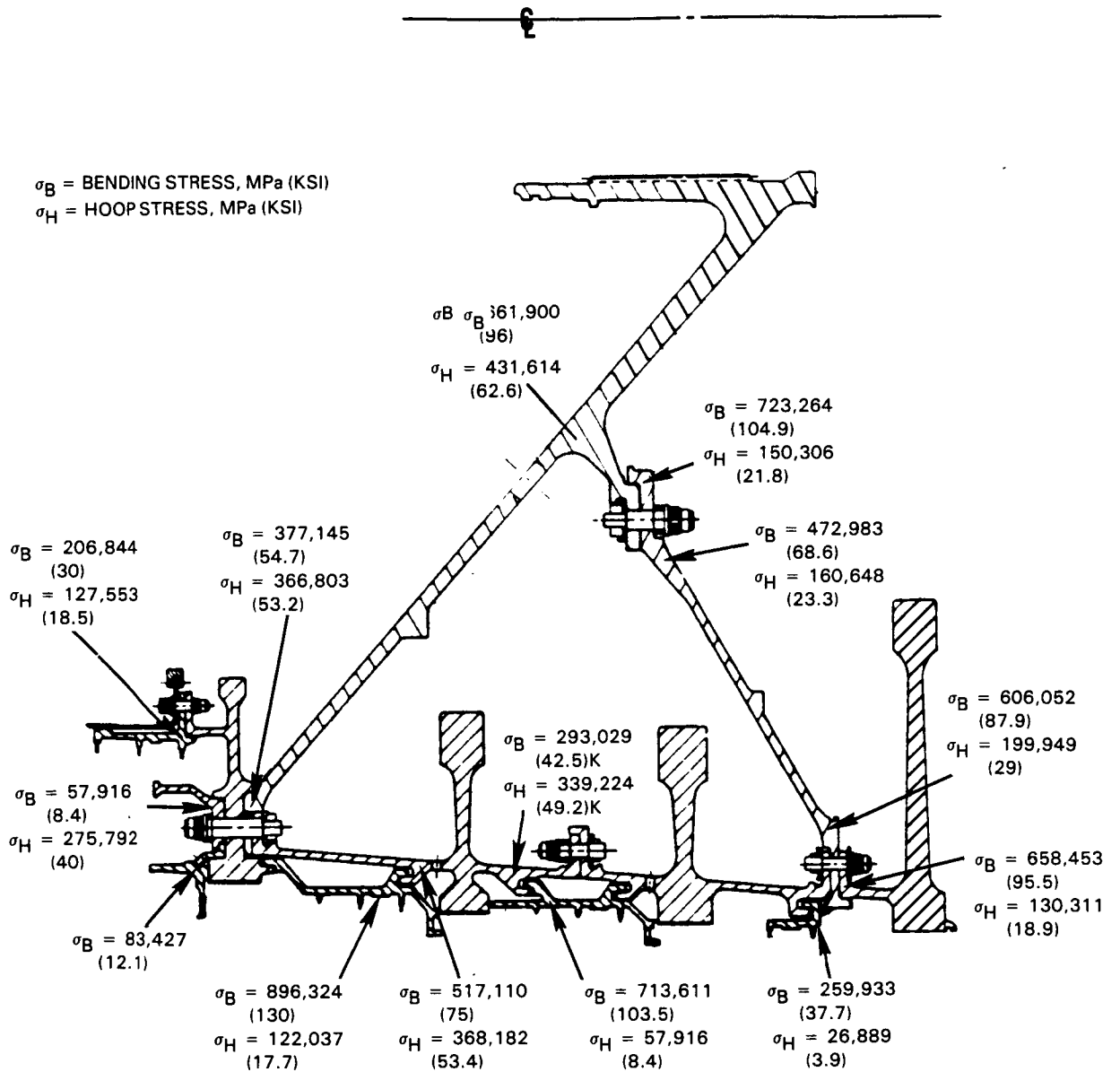


Figure 5.2.1-19 Rotor Stress Summary

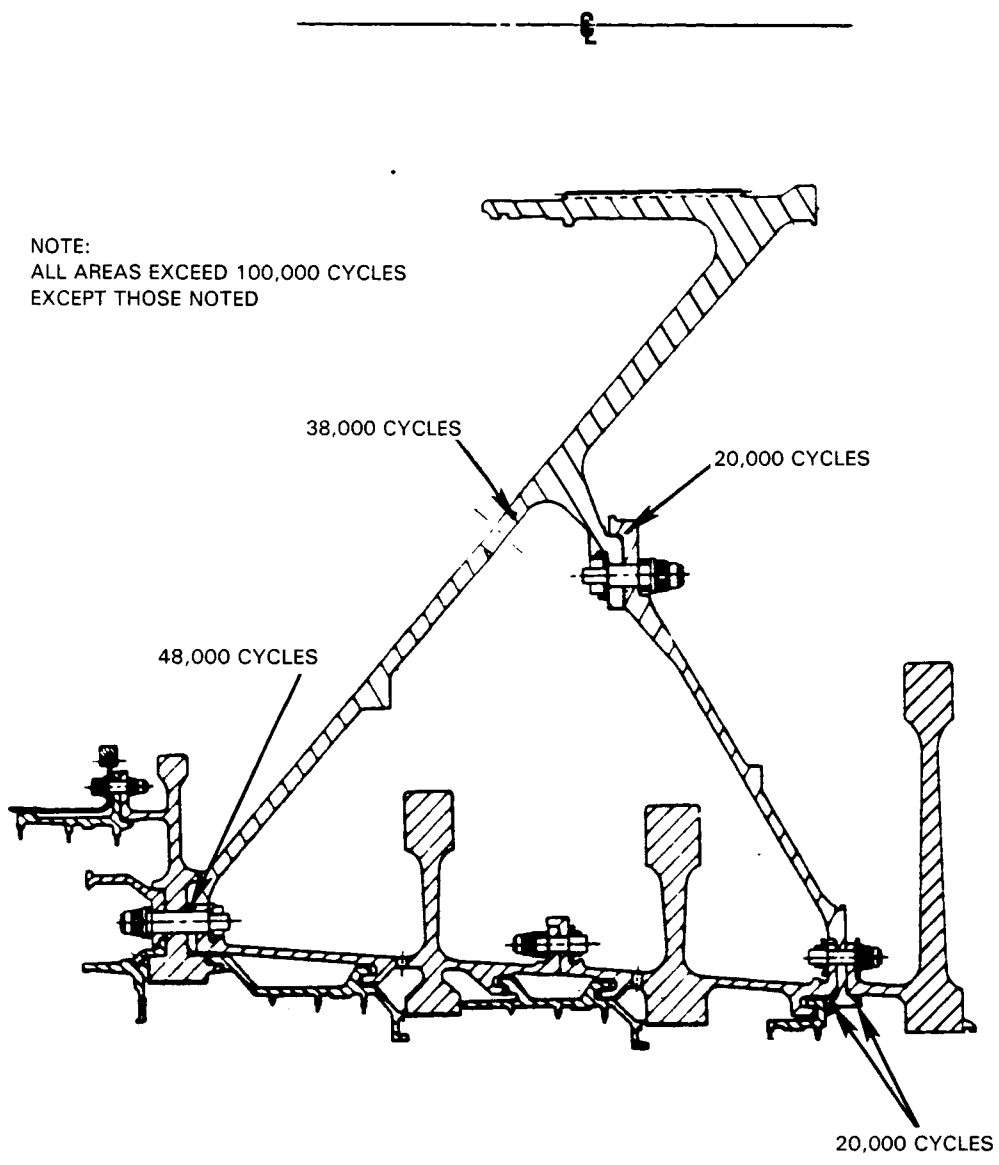


Figure 5.2.1-20 Rotor Low Cycle Fatigue Life Summary

5.2.1.3 Thrust Balance Seal Assembly

5.2.1.3.1 Mechanical Design Features

The configuration selected for the second stage thrust balance airseal is shown in Figure 5.2.1-21. It features a single knife-edge outer seal and a three knife-edge inner seal. Resonance and coincidence analyses indicated the need for a damper on the three knife-edge inner seal. Interlocking segmented sideplates on the front of the second disk protect the disk rim from hot gas-path air. The material for the rotating seals is PWA 1003 and PWA 655 for the sideplates.

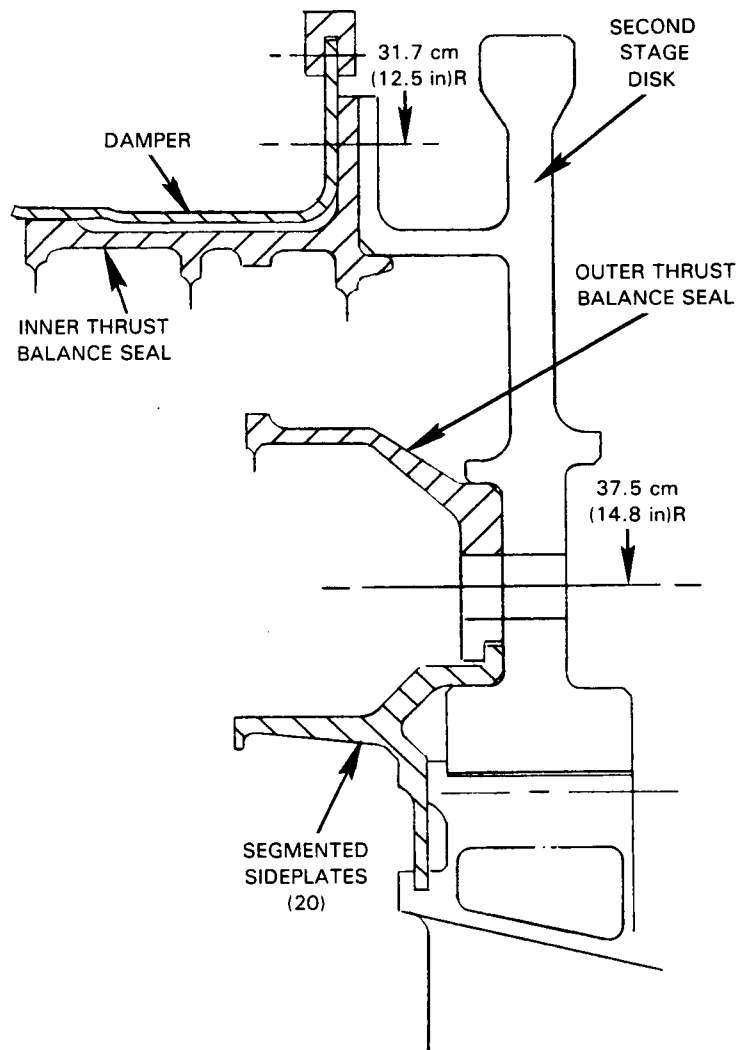


Figure 5.2.1-21 Low-Pressure Turbine Thrust Balance Seal Assembly

5.2.1.3.2 Structural Analysis

Stress analysis of the thrust balance seal was included as part of the rotor hub stress analysis, and results are shown in Figure 5.2.1-19. Stresses shown in the figure are well within allowables. In addition to stress analysis, a vibration analysis was conducted to ensure that no resonance or coincidence problems existed within the operating range (1103 to 3902 rpm). Resonance margins were 23 percent for the stator and 100 percent for the rotor. These results indicated that both the inner and outer rotating seals were free of resonance. However, a damper, as shown in Figure 5.2.1-21, was required on the inner seal to avoid coincidence with the static seal lands.

5.2.1.4 Inner Cavity Knife-Edge Seals

5.2.1.4.1 Mechanical Design Features

The interstage inner cavity knife-edge seals are shown in Figure 5.2.1-22. As mentioned in Section 5.2.1.2.1, the seals between stages two-three and three-four are multifunctional. They not only provide gaspath sealing between stages, but shield the disk flanges from hot gaspath air and provide a passage for cooling air to the disk rim and airfoil attachments, as shown in the figure. All of the inner air seal knife-edge axial stations were established to run axially over the seal lands at sea level takeoff and aerodynamic design point steady state conditions. Two of the three knife edges for the second-third and third-fourth stage seals and one of the two fourth-fifth stage knife edges will run over the seal lands during flight propulsion system engine transient conditions. (Seal clearance control is discussed in more detail in Section 5.2.3.6 of this report.) Seal material is PWA 1099 for thermal compatibility with the disk material.

5.2.1.4.2 Structural Analysis

Stress analysis of the inner cavity knife-edge seals was included as part of the rotor hub stress analysis and results are shown in Figure 5.2.1-19. The stresses shown in the figure are well within allowables. Vibration analysis of these seals indicated that resonance margins were 85 percent for the second-third stage seal, 74 percent for the third-fourth stage seal, and greater than 100 percent for the fourth-fifth stage seal. All were free of coincidence problems.

5.2.1.5 Rotor Shaft Assembly

5.2.1.5.1 Mechanical Design Features

The low rotor shaft assembly is illustrated in Figure 5.2.1-23. The low rotor shaft connects the fan and low-pressure compressor to the low-pressure turbine. It is supported at the front end by the Nos. 1 and 2 bearings and at the rear by the No. 5 bearing. The front end of the shaft connects to the fan and low-pressure compressor stub shaft through a spline. The low-pressure turbine rotor is mounted on the rear of the shaft and is cantilevered off the No. 5 bearing, which is damped to desensitize the case to rotor vibration. A center vent seal is located at the aft end of the shaft. In the No. 5 bearing compartment area, oil drain holes are provided to remove any oil that may accumulate in the low shaft inner diameter.

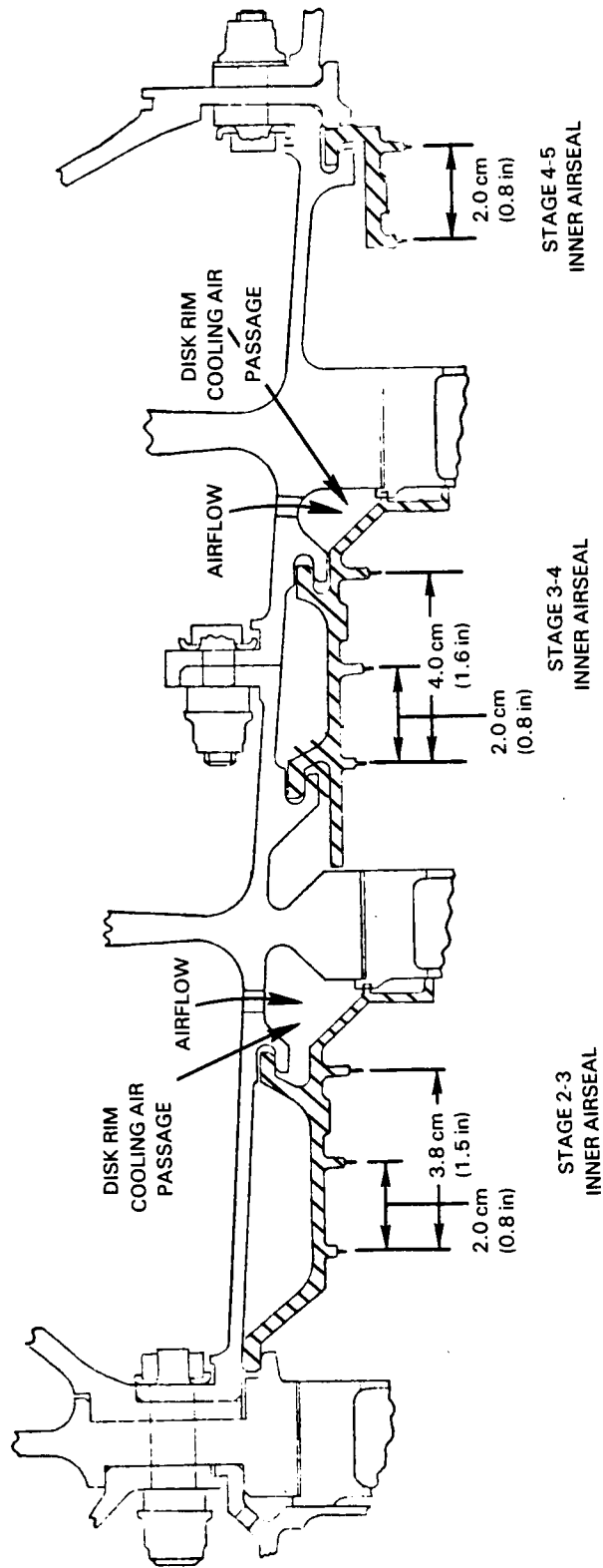


Figure 5.2.1-22 Low-Pressure Turbine Interstage Inner Cavity Knife-Edge Seals

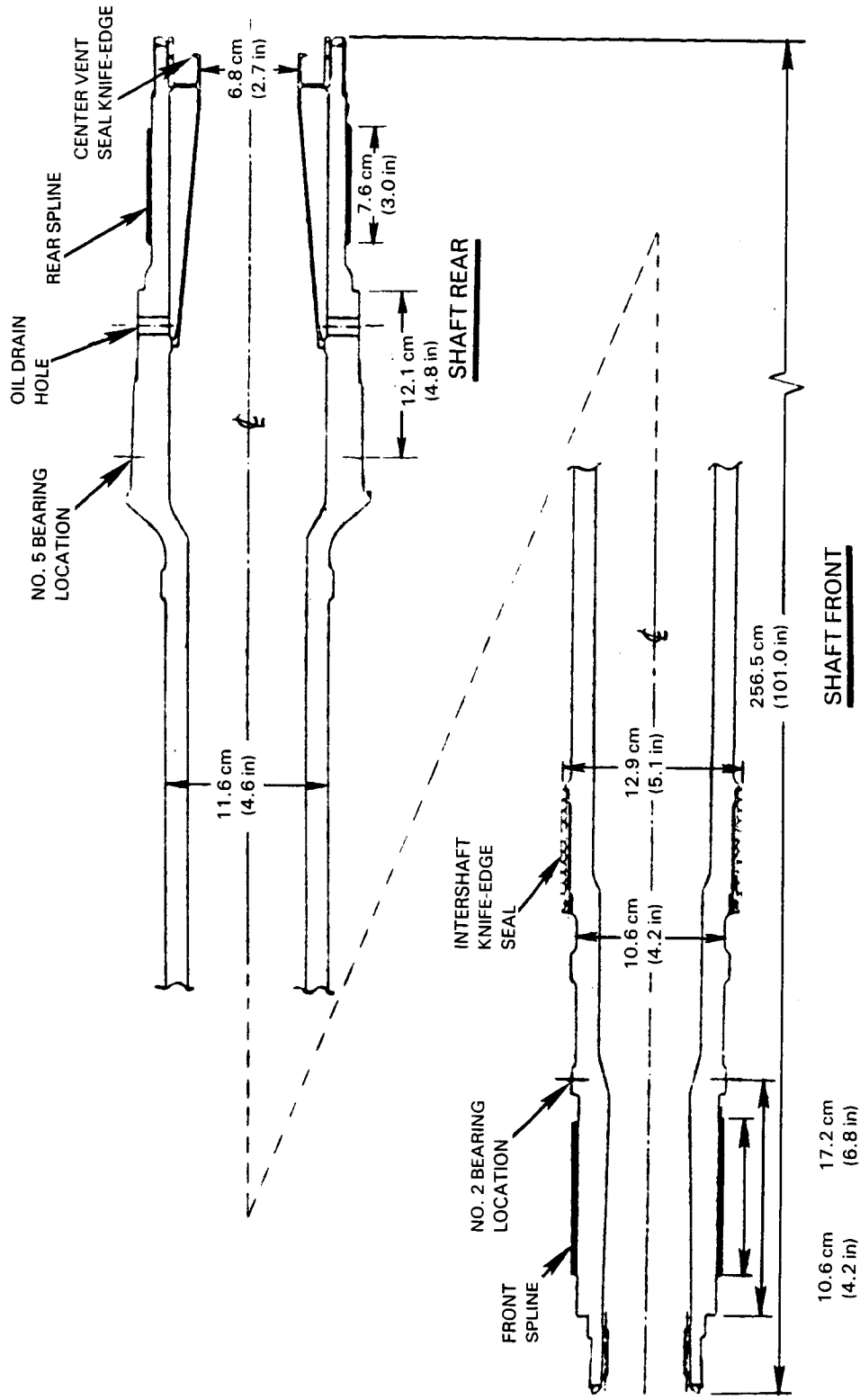


Figure 5.2.1-23 Low Rotor Shaft Assembly

The shaft is sized to satisfy stress requirements under the combined loadings of gyroscopic limit maneuver loads, maximum design torque, and shaft thrust. Adequate intershaft clearance has been provided to prevent intershaft contact under limit load conditions. The relative radial deflection has been predicted to be 0.317 cm (0.125 in) under a one radian/second gyro, plus 3 g's, plus 3 radians/second acceleration. With the design "zero-load" radial clearance of 0.825 cm (0.325 in), this results in a minimum running clearance under load of 0.508 cm (0.2 in). The maximum deflection occurs approximately 64.7 cm (25.5 in) forward of the No. 5 bearing location.

The intershaft seal is a constant diameter seal designed to eliminate the potential for a self-destructive rub mechanism occurring. Seal geometry permits an axial translation of 0.330 cm (0.130 in) between knife edges and seal land during engine transient excursions. The aft center vent seal inner diameter was sized by the flow area required for the No. 1 bearing compartment deoiler.

Seal geometry was established by allowing 1.651 cm (0.65 in) rearward and 1.016 cm (0.40 in) forward translation of the rotating hardware relative to the static structure in order to satisfy intermesh criteria and engine transient excursions. Shaft material for the flight propulsion system is PWA 733 (low alloy steel). To save cost for the integrated core/low spool, AMS 6304 has been selected.

5.2.1.5.2 Structural Analysis

Structural analysis of the shaft was conducted using sea level takeoff hot day conditions. All notched locations on the shaft were evaluated for high cycle fatigue life and bearing stresses were evaluated at the front and rear spline locations. In addition, shaft ovalization, flutter and low cycle fatigue life were assessed.

Figure 5.2.1-24 summarizes the temperatures and calculated maximum stresses at critical stress locations on the shaft front. All stresses are within allowable limits. A water quench heat treat of the front of the shaft at the spine area is required to develop the high tensile and fatigue properties needed for adequate vibratory shear stress margin.

Low cycle fatigue lives in all locations exceeded the flight propulsion system goal of 20,000 cycles, with the exception of the front spline, which had a life of 1300 cycles. This deficiency can be resolved by increasing the pitch diameter by 0.381 cm (0.15 in), increasing the root fillet radius, and crowning the spline to better distribute the loads. The intershaft seal has adequate burst margin and no vibration analysis of this seal was required.

Temperatures and calculated stresses at critical stress locations on the shaft rear are summarized in Figure 5.2.1-25. All stresses are within allowables and low cycle fatigue lives at all locations exceed the design goal of 20,000 cycles. The center vent seal has adequate burst margin and vibration analysis established its resonance margin at greater than 100 percent and its coincidence margin at 45 percent.

High cycle fatigue lives and ovalization flutter are well within allowables for the shaft design.

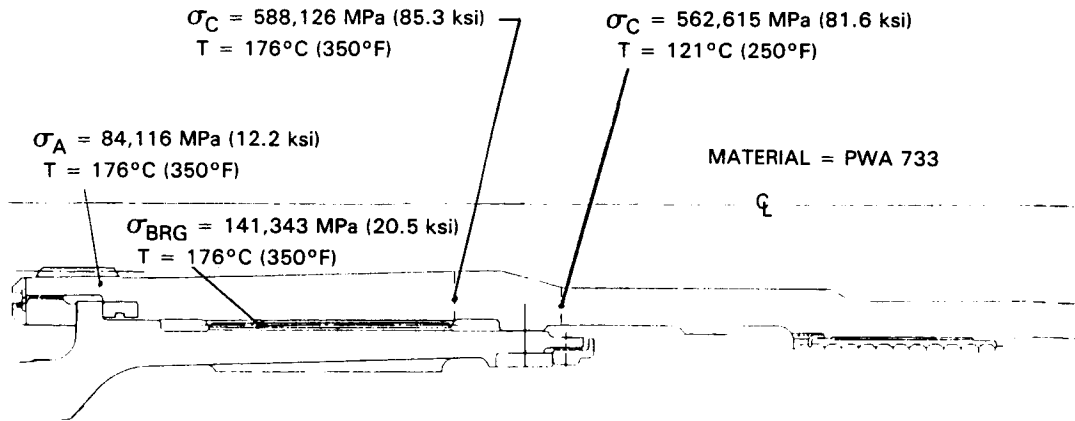


Figure 5.2.1-24 Low Rotor Shaft Front Temperature and Stress Summary

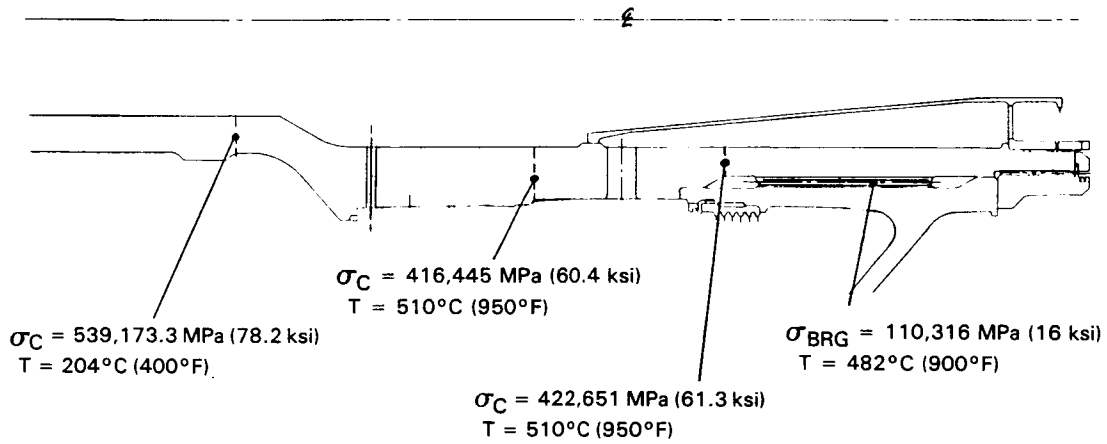


Figure 5.2.1-25 Low Rotor Shaft Rear Temperature and Stress Summary

5.2.2 Turbine Vane and Case Assembly

The low-pressure turbine vane and case design is based on a requirement for tight clearance control and uncooled vane airfoils; both aimed at achieving a high level of component efficiency. In addition, the case structure must be adequate for blade containment. Major elements of this assembly, illustrated in Figure 5.2.2-1, are the vanes, the inner and outer cases, and the turbine exhaust case/exit guide vane. Design details pertaining to these components are discussed in the following sections.

5.2.2.1 Vanes

5.2.2.1.1 Mechanical Design Features

The major criterion for the mechanical design of the vanes was the same as that for the blades -- elimination of the requirement for cooling. As with the blades, advanced high-strength, high-temperature capability materials and coatings are required to provide the desired life.

The general characteristics of the turbine vanes are illustrated in Figure 5.2.2-2. Airfoil geometry was determined by aerodynamic analysis and is described in Section 4.3.2.2.2 of this report.

There are 318 vanes in the four low-pressure turbine stages. To achieve flight propulsion system life goals without the use of air cooling, the second vane (inlet guide vane) is cast in single crystal SC 2000 (advanced high nickel alloy single crystal) with a PWA 286 (advanced NiCoCrAl_y vapor deposition) coating and the third vane is cast in PWA 1447 with a PWA 73 coating. Life requirements for the integrated core/low spool second vane can be met with cast single crystal PWA 1480 and PWA 73 coating. Third vane life requirements for the integrated core/low spool can be met with cast PWA 1455 and PWA 73 coating. Fourth and fifth stage vanes for both applications are cast PWA 655. Coatings are not required for these airfoils.

All vane airfoils are stacked on a radial line passing through the center of gravity at the root section and incorporate a slight amount of tangential tilt to balance out root bending stresses. All have elliptical leading edges to enhance aerodynamic performance. The inner diameter platforms of stages three, four, and five incorporate flow guides for compatibility with the adjacent blades. The inner airseals on stages three, four, and five incorporate 0.158 cm (0.0625 in) cell honeycomb made from 0.005 cm (0.002 in) thick Hastelloy X foil and are brazed to the vane inner diameter seal lands.

The third, fourth, and fifth stage vanes are supported in the conventional manner, cantilevered from the vane case and attached with vane feet and case hooks as illustrated in Figure 5.2.2-3. The rear vane feet for stages three and four are notched to reduce surface contact with the case and minimize conductive heat flow into the case structure. The second vane support structure is illustrated in Figure 5.2.2-4. The outer diameter support, made of AMS 5707 Waspaloy, is a simple hook arrangement that permits the vane to move radially, but restrains axial motion. The inner diameter support made of AMS 5666 incorporates a double hook arrangement, in conjunction with an anti-rotation pin, to provide the required axial, radial, and torque restraint. The inner support is bolted to the turbine intermediate case inner torque box.

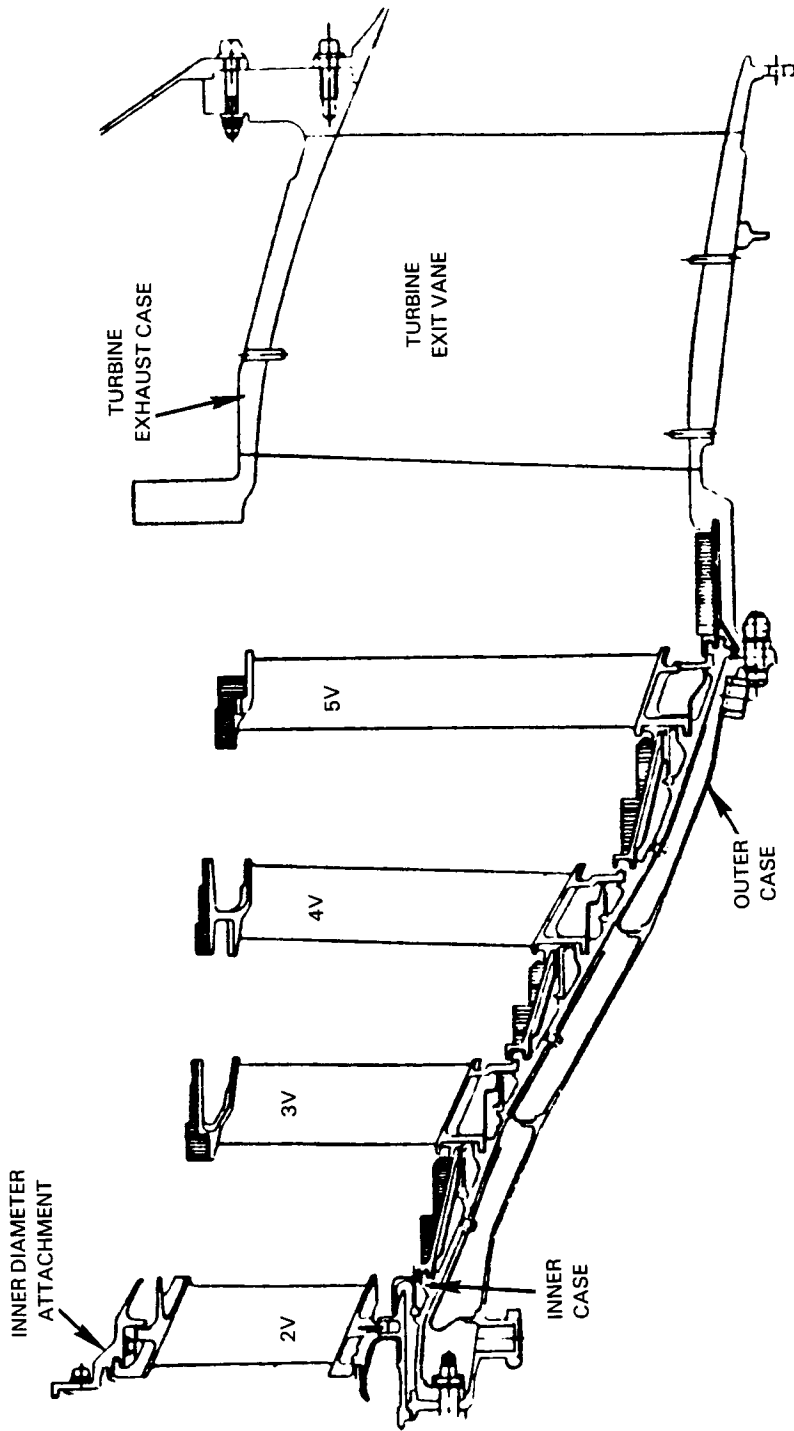
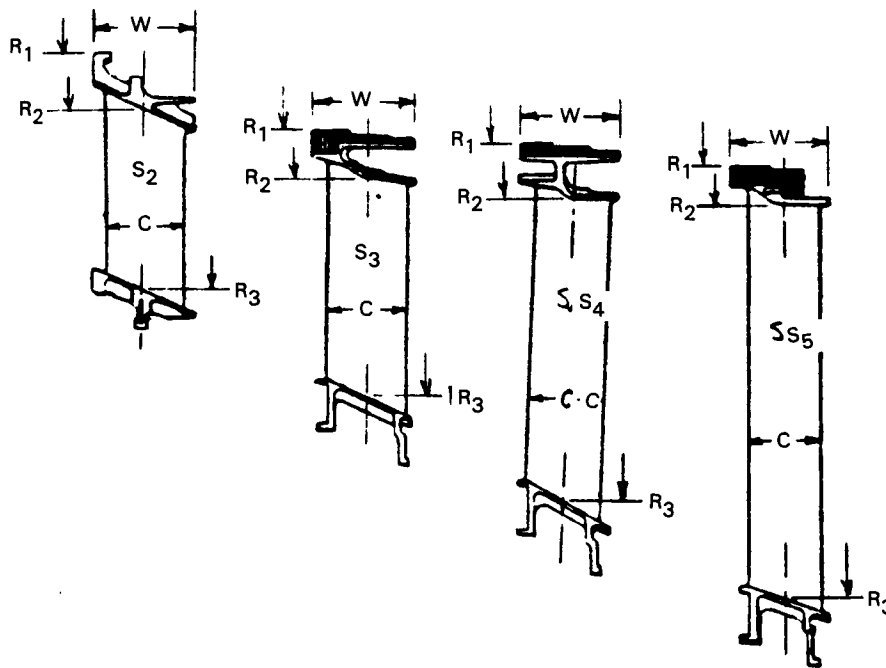


Figure 5.2.2-1 Low-Pressure Turbine Vane and Case Assembly



	<u>STAGE</u>			
	2nd	3rd	4th	5th
NO. OF VANES	54	72	84	108
VANE MATERIAL	SC2000 ⁽¹⁾	PWA 1447 ⁽²⁾	PWA 655	PWA 655
COATING MATERIAL	PWA 286 ⁽³⁾	PWA 73	NOT REQ'D	NOT REQ'D
WIDTH (W), cm (in)	4.97 (1.96)	5.18 (2.04)	4.87 (1.92)	5.02 (1.98)
AVERAGE AIRFOIL CHORD, (C), cm (in)	3.96 (1.56)	4.08 (1.61)	3.73 (1.47)	3.68 (1.45)
R ₁ , cm (in)	37.5 (14.8)	41.4 (16.3)	41.9 (16.5)	42.9 (16.9)
R ₂ , cm (in)	40.3 (15.9)	43.6 (17.2)	44.4 (17.5)	44.7 (17.6)
R ₃ , cm (in)	49.0 (19.3)	54.1 (21.3)	59.4 (23.4)	64.0 (25.2)

(1) INTEGRATED CORE/LOW SPOOL WILL USE PWA 1480

(2) INTEGRATED CORE/LOW SPOOL WILL USE PWA 1455

(3) INTEGRATED CORE/LOW SPOOL WILL USE PWA 73

Figure 5.2.2-2 Low-Pressure Turbine Vane General Characteristics

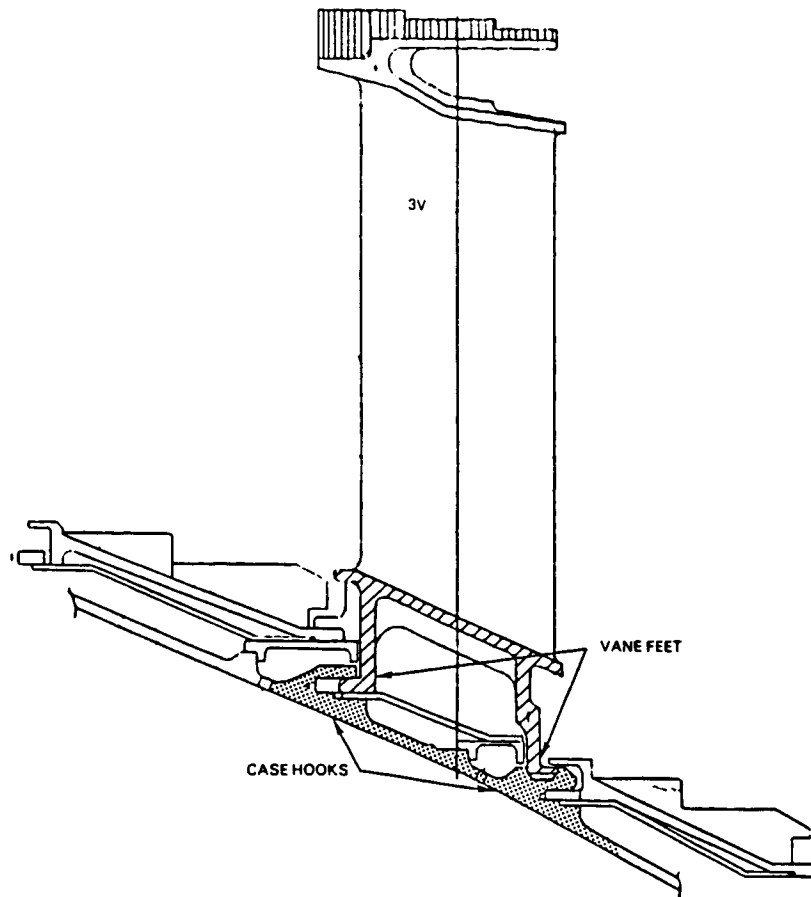


Figure 5.2.2-3 Attachment Scheme Utilized for Third, Fourth, and Fifth Stage Vanes

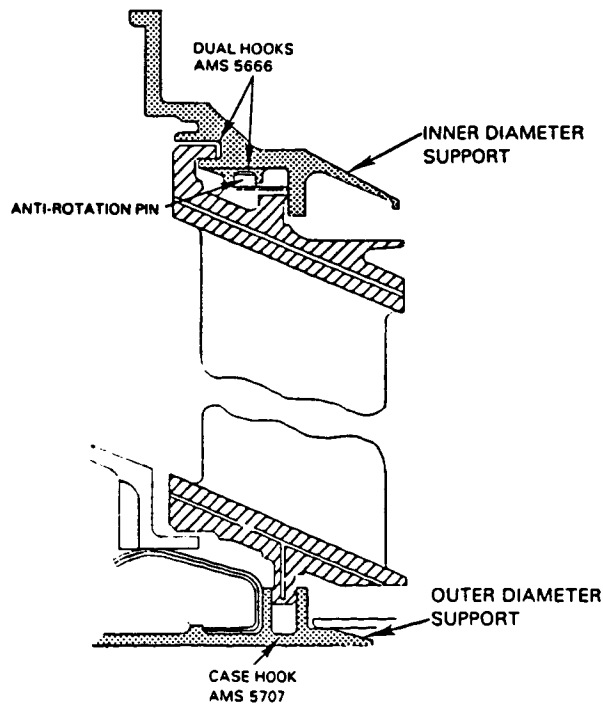


Figure 5.2.2-4 Second Vane Support Structure

This configuration provides for proper mating of the turbine flowpath with that of the turbine intermediate case strut fairings and minimizes steps in the flowpath during engine operation. The second vane support structure permits the vane to tilt slightly fore and aft under thermal and gas loads. To minimize attachment leakage caused by this tilt action, chordal sealing surfaces are machined on the vane and attachment mating surfaces at the locations shown in Figure 5.2.2-5. The fourth stage vane incorporates a slight amount of rearward tilt to satisfy a blade meshing criteria in the event of a shaft failure.

Individual semi-machined vanes are Transient Liquid Phase (TLP[®]) bonded together into clusters for improved strength and reduced leakage. Second stage vane cluster size (Figure 5.2.2-6) is limited to two vanes. This is the maximum cluster size that will permit straight chordal seal faces to be cut in the radial space available. Each second stage vane cluster incorporates one anti-rotation pin. As shown in Figure 5.2.2-7, the third through fifth stage vanes are TLP[®] bonded in clusters of three. Each vane in the cluster incorporates an anti-rotation pin.

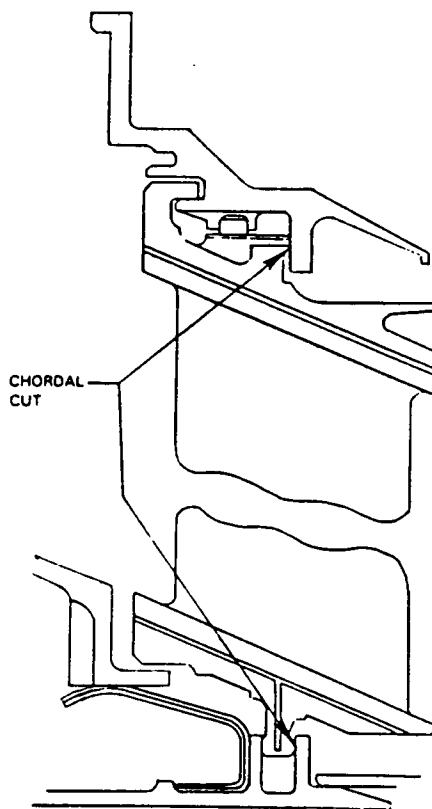


Figure 5.2.2-5 Location of Second Vane Chordal Cuts Employed for Attachment Leakage Control

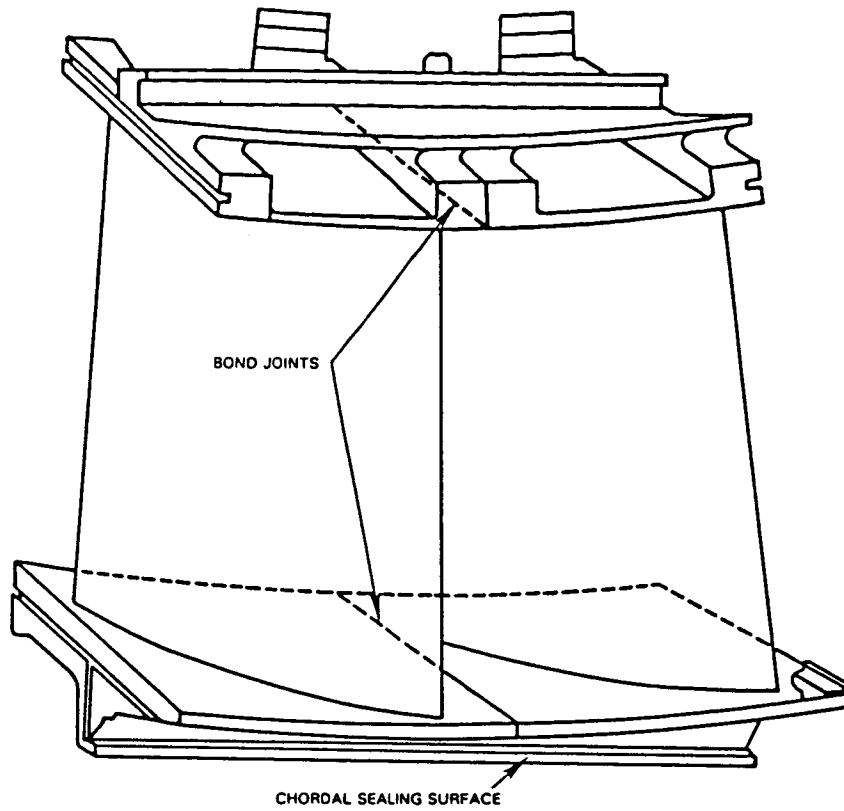


Figure 5.2.2-6 Low-Pressure Turbine Second Stage Vane Cluster

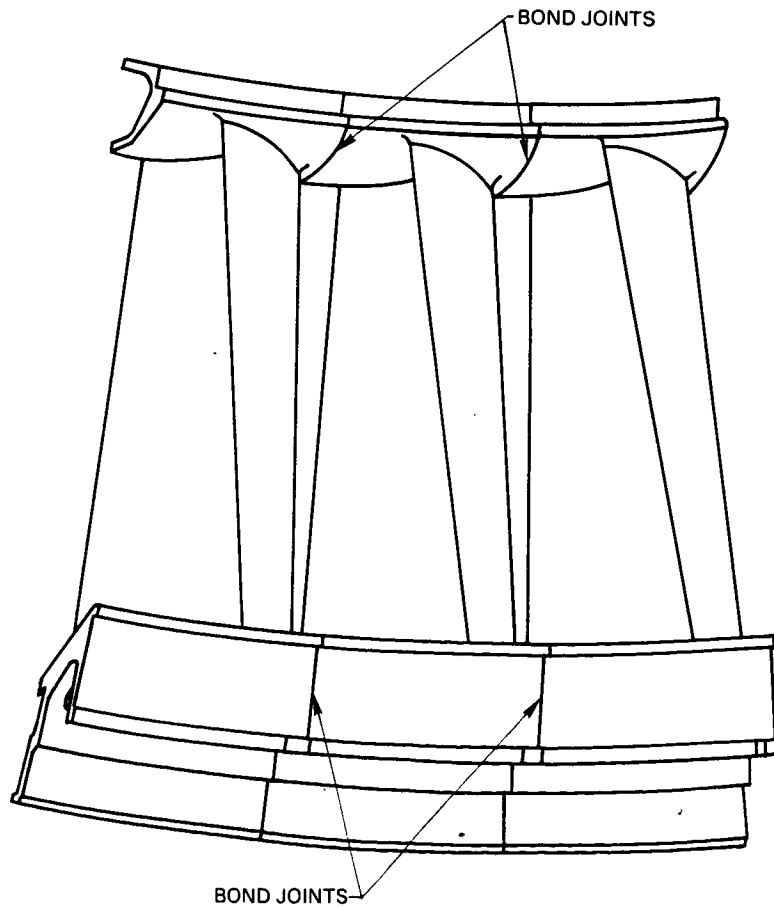


Figure 5.2.2-7 Typical Third, Fourth, and Fifth Stage Vane Cluster

5.2.2.1.2 Structural Analysis

Structural analysis of the vanes comprised analysis of stresses in the vane airfoils, vane hooks, and anti-rotating pins, plus an assessment of vane airfoil durability.

Vane Stress Analysis

A vane stress analysis was conducted assuming sea level takeoff operating conditions. Hot streak temperatures were considered where appropriate. Limits were based on one percent creep and 0.2 percent yield strength for 50 hours (anticipated integrated core/low spool running time). Calculated stresses are listed in Table 5.2.2-I. All are well within allowables with the highest being a combined stress of 226,149 MPa (32.8 ksi) at the second vane inner diameter hook and a bending stress of 226,838 MPa (32.9 ksi) at the third stage anti-rotation pins.

TABLE 5.2.2-I
AIRFOIL STRESS SUMMARY
(Stresses in MPa (ksi) and Temperatures °C (°F))

	<u>2nd Stage</u>	<u>3rd Stage</u>	<u>4th Stage</u>	<u>5th Stage</u>
<u>Airfoil:</u>				
Bending Stress	20,684 (3.0)	29,647 (4.3)	62,742 (9.1)	60,674 (8.8)
Hot Streak Temperature	1176 (2150)	1048 (1920)	915 (1680)	787 (1450)
<u>Vane Hook:</u>				
Bending Stress	- - - -	108,248 (15.7)	200,638 (29.1)	153,064 (22.2)
Max. Combined Stress	226,149 (32.8)	- - - -	- - - -	- - - -
Temperature	- - - -	732 (1351)	677 (1251)	671 (1240)
Hot Streak Temperature	940 (1725)	- - - -	- - - -	- - - -
<u>Anti-Rotation Pins:</u>				
Shear Stress	15,858 (2.3)	70,326 (10.2)	61,363 (8.9)	43,437 (6.3)
Bending Stress	19994 (2.9)	226,838 (32.9)	197,191 (28.6)	146,169 (21.2)
Temperature	- - - -	623 (1154)	597 (1107)	615 (1140)
Hot Streak Temperature	1,037 (1900)	- - - -	- - - -	- - - -

Vane Airfoil Durability Analysis

Durability analysis of the vanes was conducted in a manner similar to that of the blades described earlier. Life objectives for the vanes were identical to those for the blades. Materials and coatings utilized in the vane durability analysis are listed in Figure 5.2.2-2.

Gas temperature profiles and resultant spanwise calculated stresses for the clustered vane airfoils are shown in Figures 5.2.2-8 through 5.2.2-11. Since the vanes are stationary, the worst case is when a vane is exposed to a hot streak. Consequently, full hot streak temperatures were used in the calculations.

The resultant airfoil creep strength margins are summarized in Table 5.2.2-II for both the flight propulsion system and the integrated core/low spool. All airfoils were determined to have adequate creep strength.

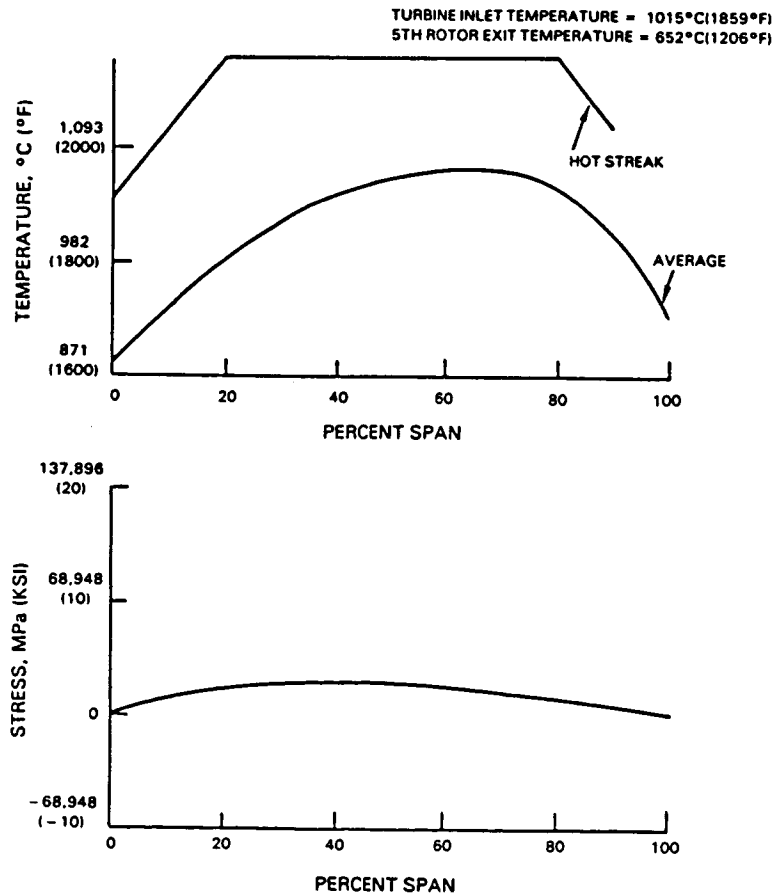


Figure 5.2.2-8 Second Stage Vane Durability Design Conditions and Calculated Stress (Vane Material: PWA 1480, Coating: PWA 73)

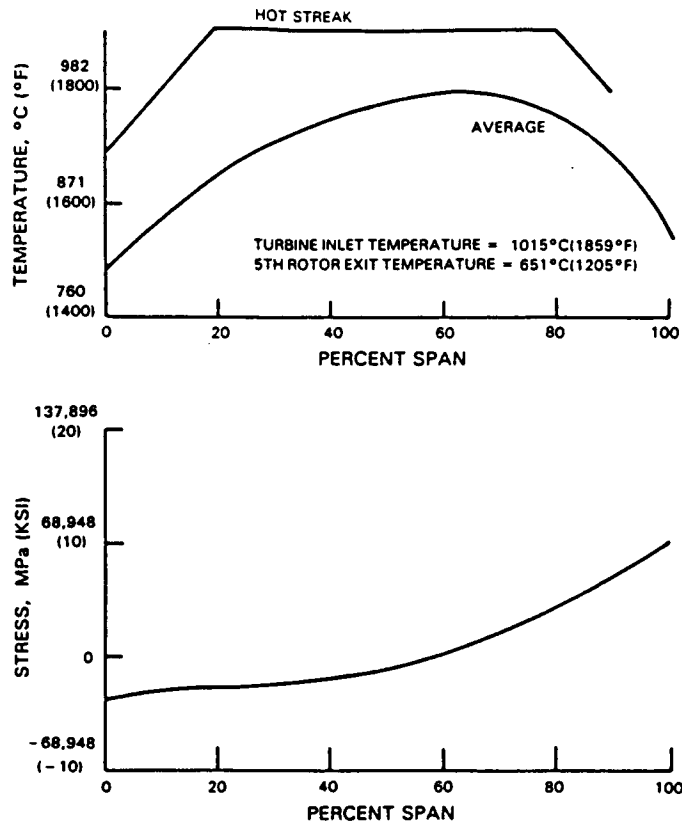


Figure 5.2.2-9 Third Stage Vane Durability Design Conditions and Calculated Stress (Vane Material: PWA 1455, No Coating)

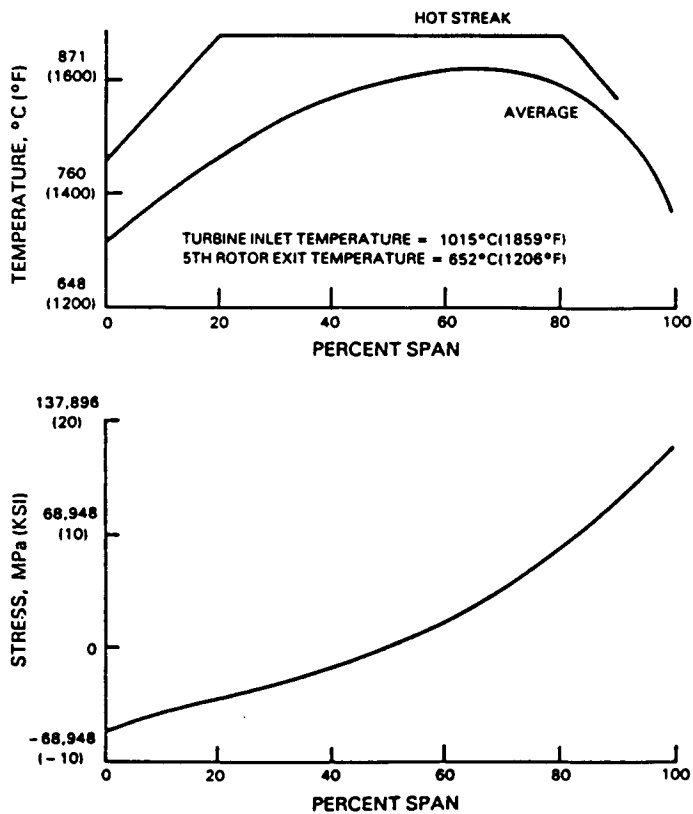


Figure 5.2.2-10 Fourth Stage Vane Durability Design Conditions and Calculated Stress (Vane Material: PWA 655, No Coating)

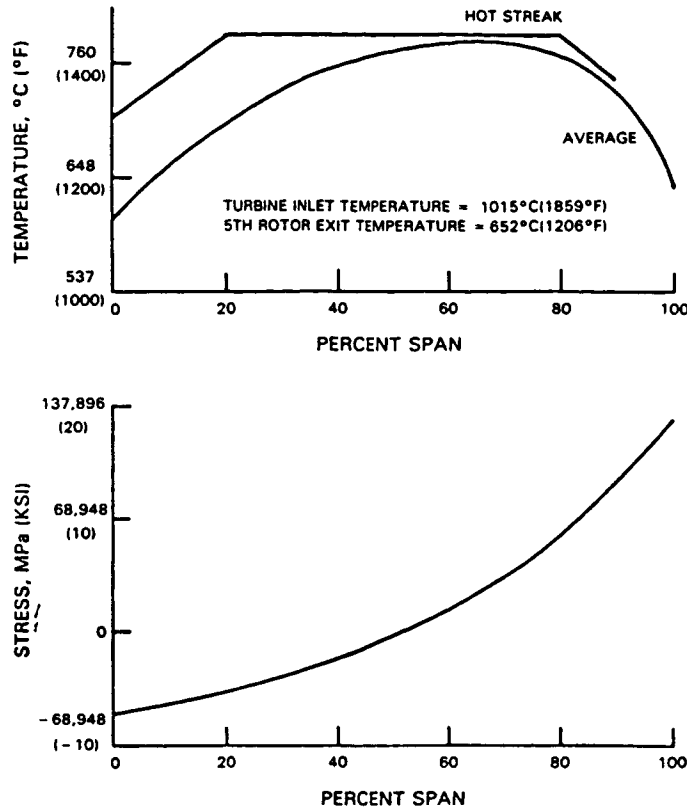


Figure 5.2.2-11 Fifth Stage Vane Durability Design Conditions and Calculated Stress (Vane Material: PWA 655, No Coating)

TABLE 5.2.2-II
VANE AIRFOIL CREEP STRENGTH MARGINS
(Margins in Percent at Limiting Span)

	<u>Flight Propulsion System</u>	<u>Integrated Core/ Low Spool</u>
Second Vane	28	45
Third Vane	34	55
Fourth Vane	44	59
Fifth Vane	75	82

Since the second and third vanes operate in a high temperature environment, a transient thermal strain analysis was conducted to determine their thermal fatigue life. Engine operating conditions were the same as those used in the blade durability analysis described earlier. The resultant strain histories for the two airfoils are shown in Figures 5.2.2-12 and 5.2.2-13. As indicated, the maximum strain range for the second vane was 0.51 percent and for the third vane was 0.49 percent. Strain range for fourth vane was 0.42 percent. The fifth vane is not life limited as a result of transient strain. The strain range for the vanes was higher than for the blades because of the effects of clustering the vanes.

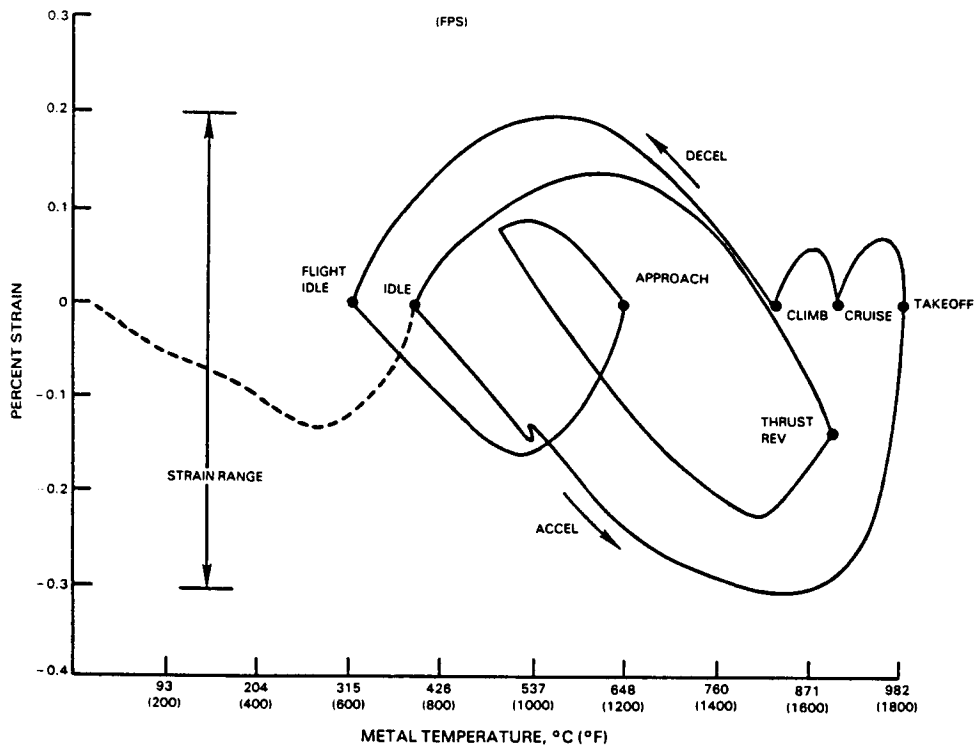


Figure 5.2.2-12 Energy Efficient Engine Second Vane Transient Strains

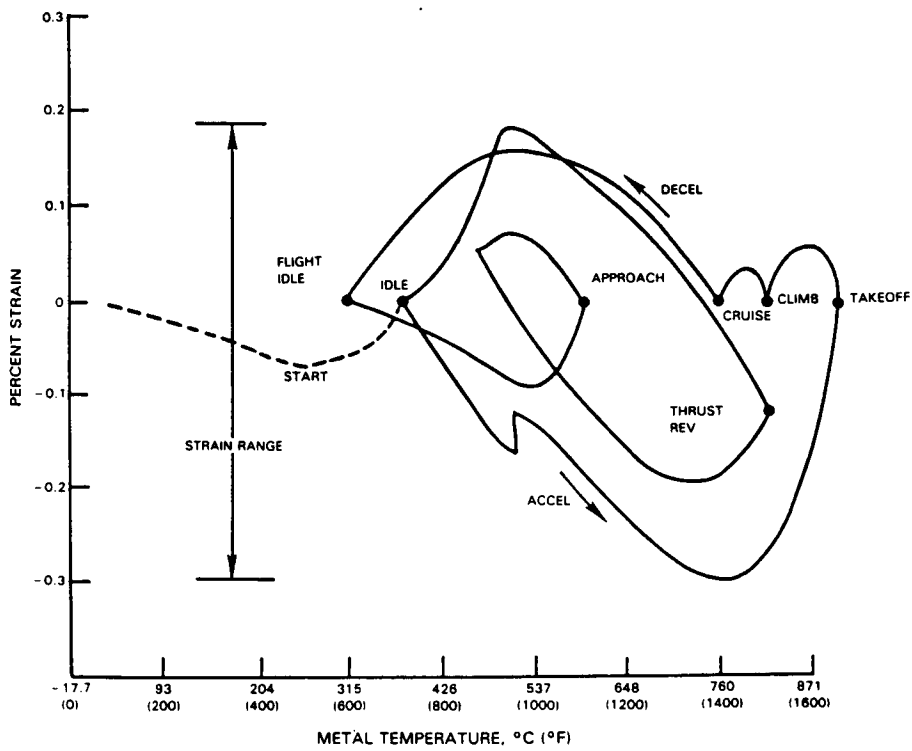


Figure 5.2.2-13 Energy Efficient Engine Third Vane Transient Strains

Airfoil lives were calculated and are presented in Table 5.2.2-III. Life-limiting conditions of concern were cracking and metal surface oxidation. As noted, life goals for the integrated core/low spool were exceeded for all vanes. Goals for the flight propulsion system were met or exceeded for all vanes, with the exception of the second vane whose life was limited to 9300 hours with a single coating. Analysis indicated that one recoating of this vane would extend the life beyond 15,000 hours.

TABLE 5.2.2-III
SUMMARY OF PREDICTED VANE LIVES

	<u>Flight Propulsion System</u>		<u>Integrated Core/ Low Spool</u>
	<u>Cracking (hrs)</u>	<u>Oxidation (hrs)</u>	<u>Oxidation (hrs)</u>
Second Vanes	20,000	9,300 (1)	100
Third Vanes	20,000	15,000	100
Fourth Vanes	20,000	20,000	100
Fifth Vanes	(2)	(2)	(2)

Notes: (1) Life 15,000 hrs. with one recoating.
(2) Not life limiting.

5.2.2.2 Vane Cases

5.2.2.2.1 Mechanical Design Features

The basic design objectives for the low-pressure turbine case were to: (1) provide blade containment, (2) support the vanes, (3) provide active clearance control, and (4) meet life requirements.

The case design evolved from preliminary design studies that compared bolted vane support and hooked vane support designs (both with external active clearance control) with a hooked vane support design incorporating a double wall and internal active clearance control. The latter design approach was selected as being the lightest, least expensive, and best for active clearance control.

The concept was refined in the detail design process and the resultant design is shown in Figure 5.2.2-14. The main feature of this design is the double wall, with the space between the walls serving as a passage for cooling air. This cooling air provides a dual service in that active clearance control air is also used for cooling the vane feet and case hooks via drilled holes that meter the air into the cooling passage manifolds. This system of metering makes cooling flow control independent of part-to-part tolerances. The active clearance control baffle-to-case gap can be tailored for each stage and cooling air supply temperature adjusted, through the use of mixing valves, to achieve optimum case thermal response characteristics. (Active clearance control is discussed in more detail in Section 5.2.2.4 of this report.)

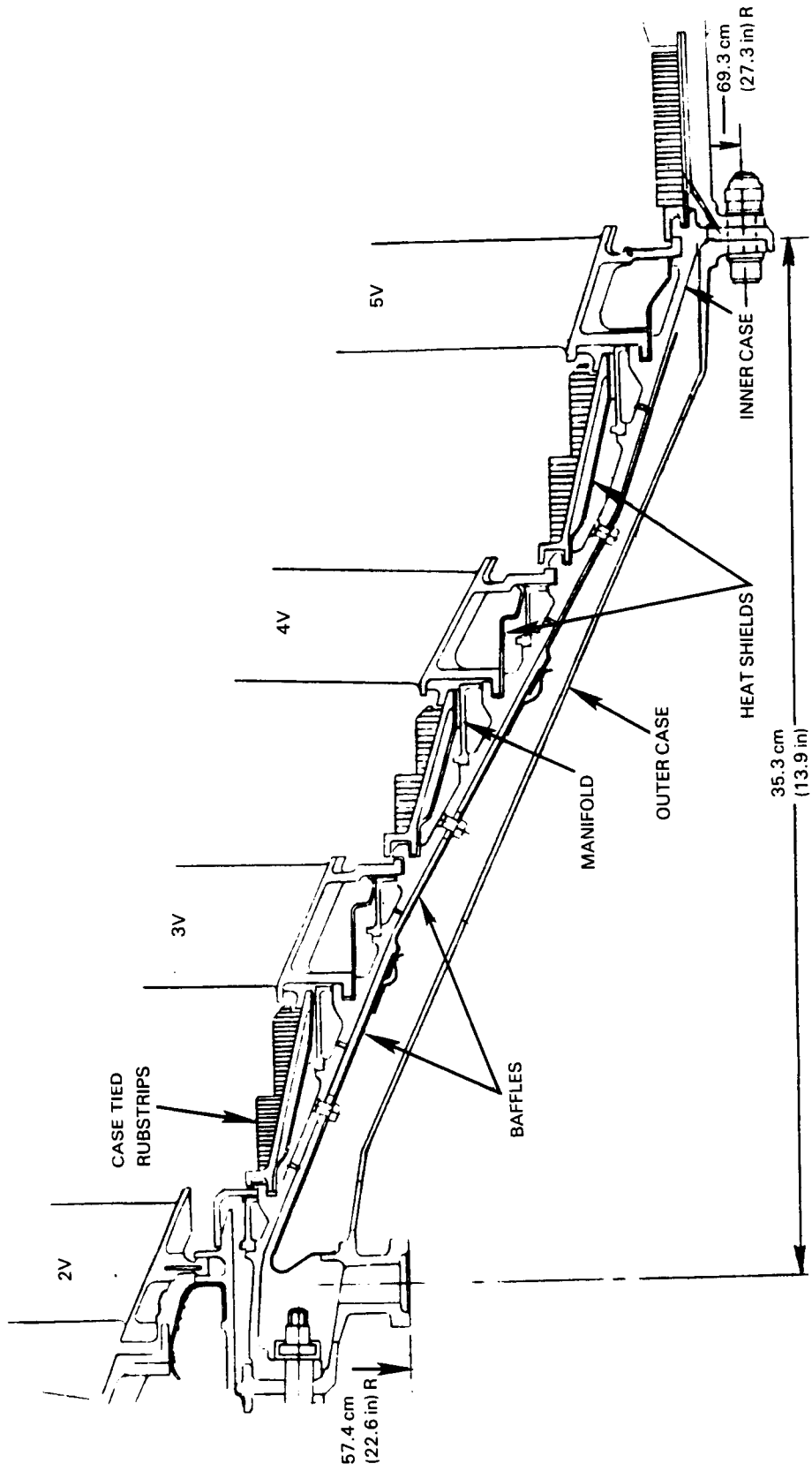


Figure 5.2.2-14 Low-Pressure Turbine Case Assembly

Details of a typical case-tied outer airseal are shown in Figure 5.2.2-15. Airseals are fabricated from forged rings by electron beam cutting. The honeycomb rubstrip is fabricated from Hastelloy X, has a 0.157 cm (0.062 in) cell size with a 0.005 cm (0.002 in) foil thickness and is nickel brazed to the outer airseal. Anti-torque pins serve to position the outer airseals so as to cover the gaps between vane clusters. The heatshields are also fabricated from Hastelloy X in segments of eight per stage. Heatshields under the vanes are assembled with an axial pinch for vibration damping. Those under the outer airseals incorporate standoffs formed into the sheetmetal to minimize heat transfer from the outer airseals and heatshields to the cooling manifold.

Materials selected for the case, baffles, and cooling manifolds are summarized in Figure 5.2.2-16. Inconel 718 was selected for the turbine inner case because of its inherent strength at elevated temperatures. The outer case material, A 286 was chosen for its higher thermal expansion characteristics to minimize thermal growth differences between the two cases, since the outer case is always cooler than the inner case. The internal cooling air manifolds were to be initially fabricated from Inconel 718 for all six locations but stress analysis dictated a change to Waspaloy for the three manifolds adjacent to the front feet of the vanes. The forward set of baffle panels absorb the axial seal load from the outer case and are made from Inconel 718. The rear two sets of baffle panels are not load-carrying and are made from stainless steel. All the panels incorporate circumferential sheet metal seals between panels to minimize leakage.

5.2.2.2.2 Structural Analysis

Structural analysis of the case comprised an evaluation of blade containment and low cycle fatigue life. In the containment analysis, no credit was taken for any containment capability in the segmented outer airseals, sheet metal heatshields, and active clearance control intercase flow guides. The inner and outer cases were assumed to provide total blade containment. The thickness variation required was provided only in the inner structural case so that the outer case thickness was maintained constant. The resultant wall thickness distribution required to provide adequate containment capability is shown in Table 5.2.2-IV.

TABLE 5.2.2-IV
CASE THICKNESS REQUIREMENTS
FOR BLADE CONTAINMENT

<u>Blade Stage</u>	<u>Inner Case Thickness, cm (in)</u>	<u>Outer Case Thickness, cm (in)</u>
Second	0.203 (0.080)	0.114 (0.045)
Third	0.266 (0.105)	0.114 (0.045)
Fourth	0.393 (0.155)	0.114 (0.045)
Fifth	0.558 (0.220)	---

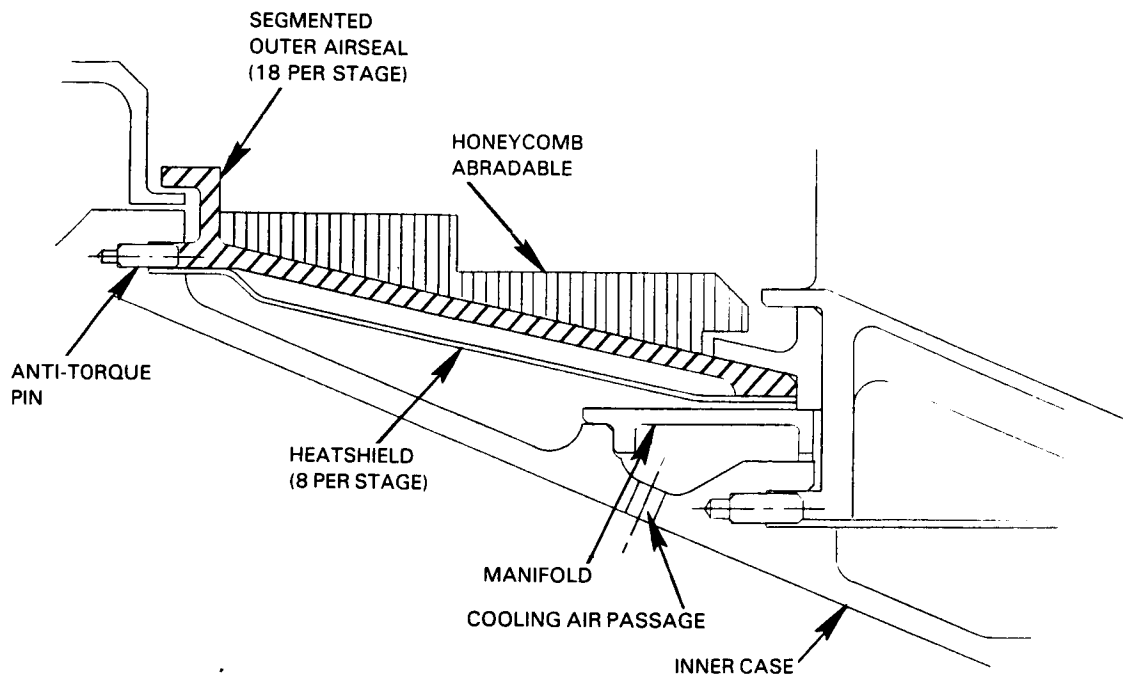


Figure 5.2.2-15 Typical Outer Airseal Configuration

Life analysis considered the combined effects of stresses resulting from case buckling loads and stresses due to thermal transients. The four types of loading that contribute to low-pressure turbine case buckling and used in the analysis are external pressure, bending, axial compression, and shear. Also, a 6-g limit maneuver load for the flight propulsion system was included in the analysis.

Thermal stresses were calculated based on the transient thermal strain analysis used for the blade and vane durability analyses. Sea level takeoff hot day conditions were assumed. The case temperature distribution for these conditions is shown in Figure 5.2.2-17. Buckling stresses (predominantly due to maneuver loads) were superimposed over those caused by thermal transients and the resultant stresses are summarized in Figure 5.2.2-18. Case life based on this distribution was determined to be in excess of the required 20,000 cycles for the flight propulsion system.

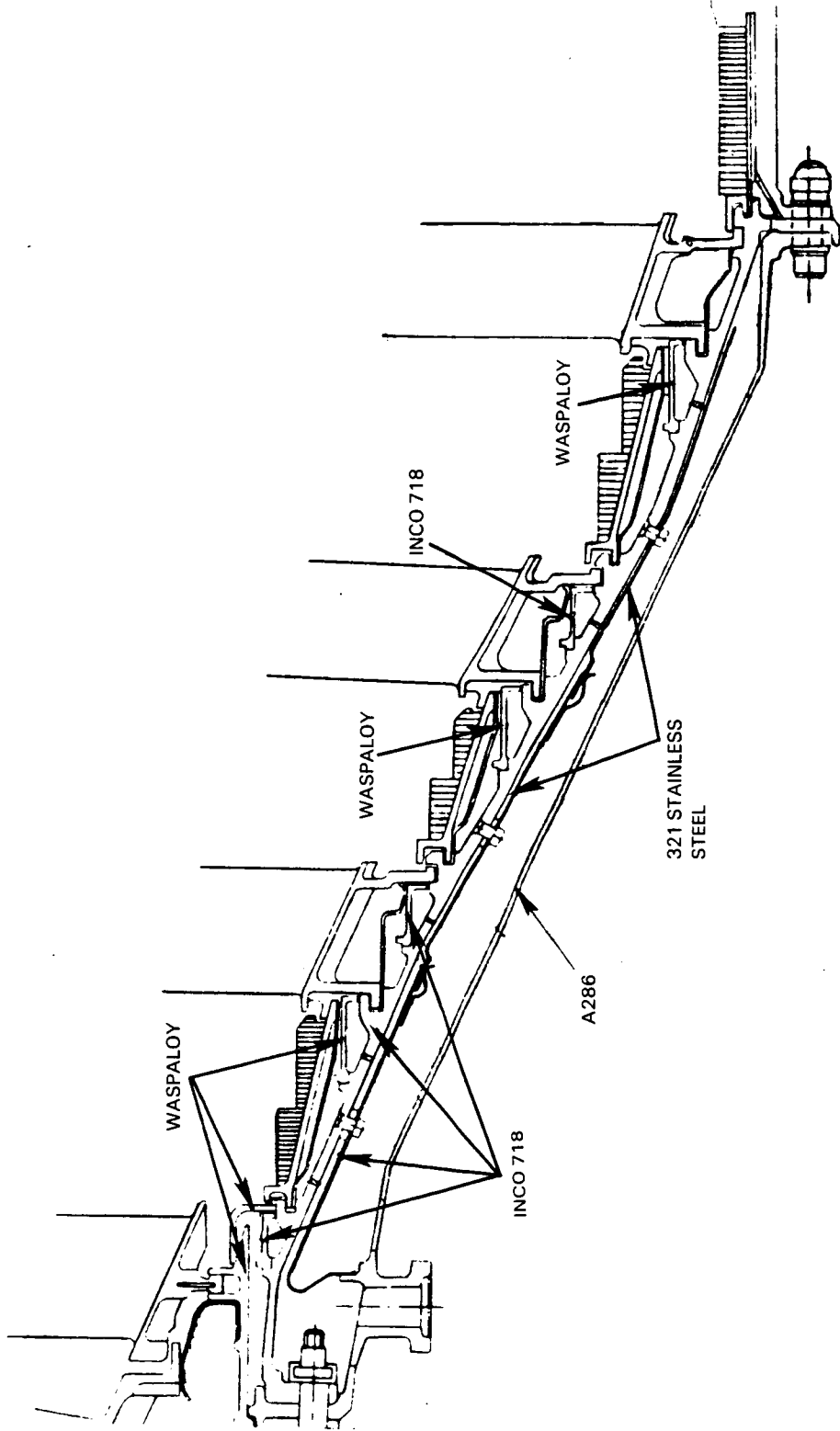


Figure 5.2.2-16 Low-Pressure Turbine Case, Baffle and Cooling Manifold
Materials Summary

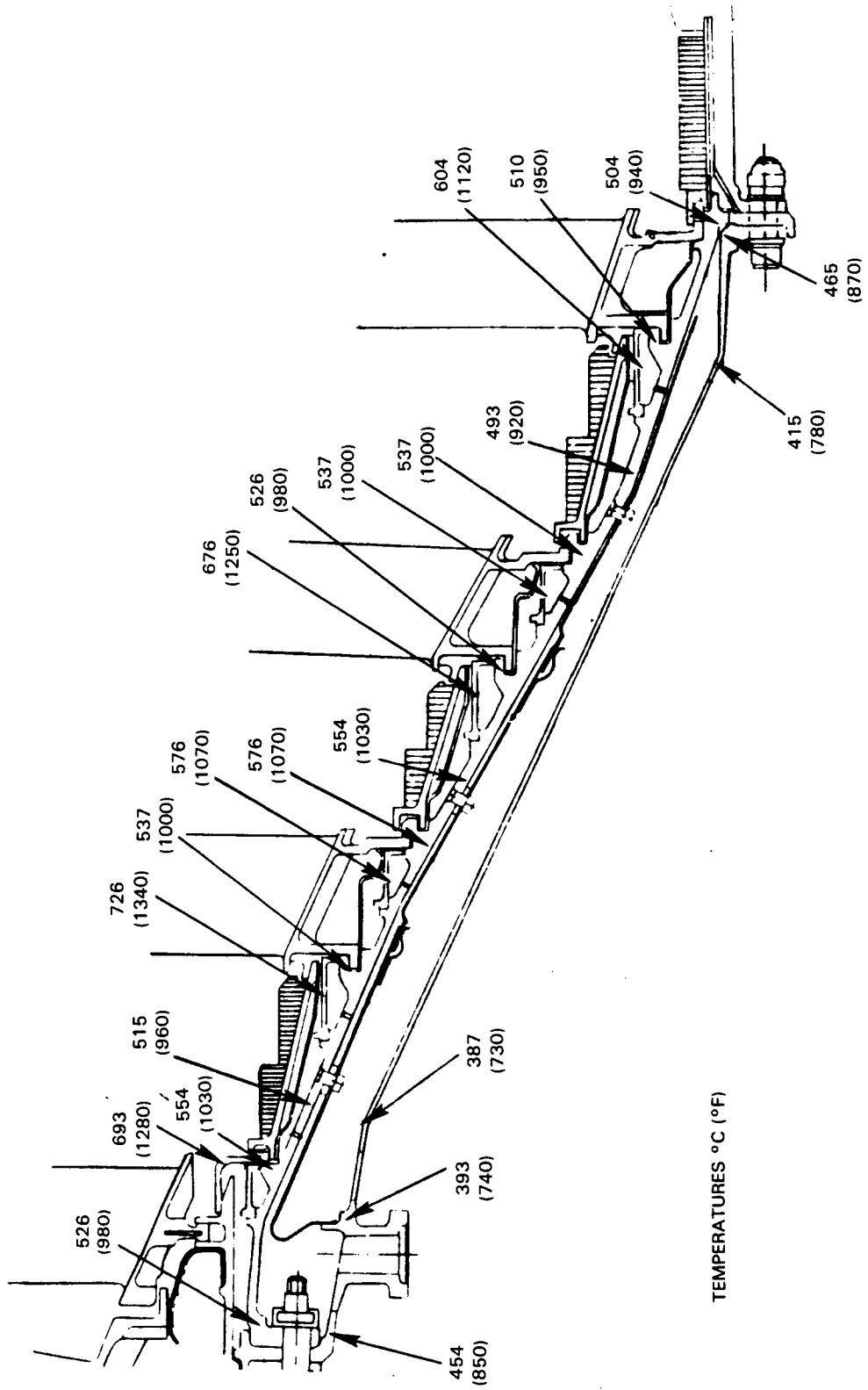


Figure 5.2.2-17 Low-Pressure Turbine Case Temperature Summary at Sea Level Takeoff Hot Day Conditions

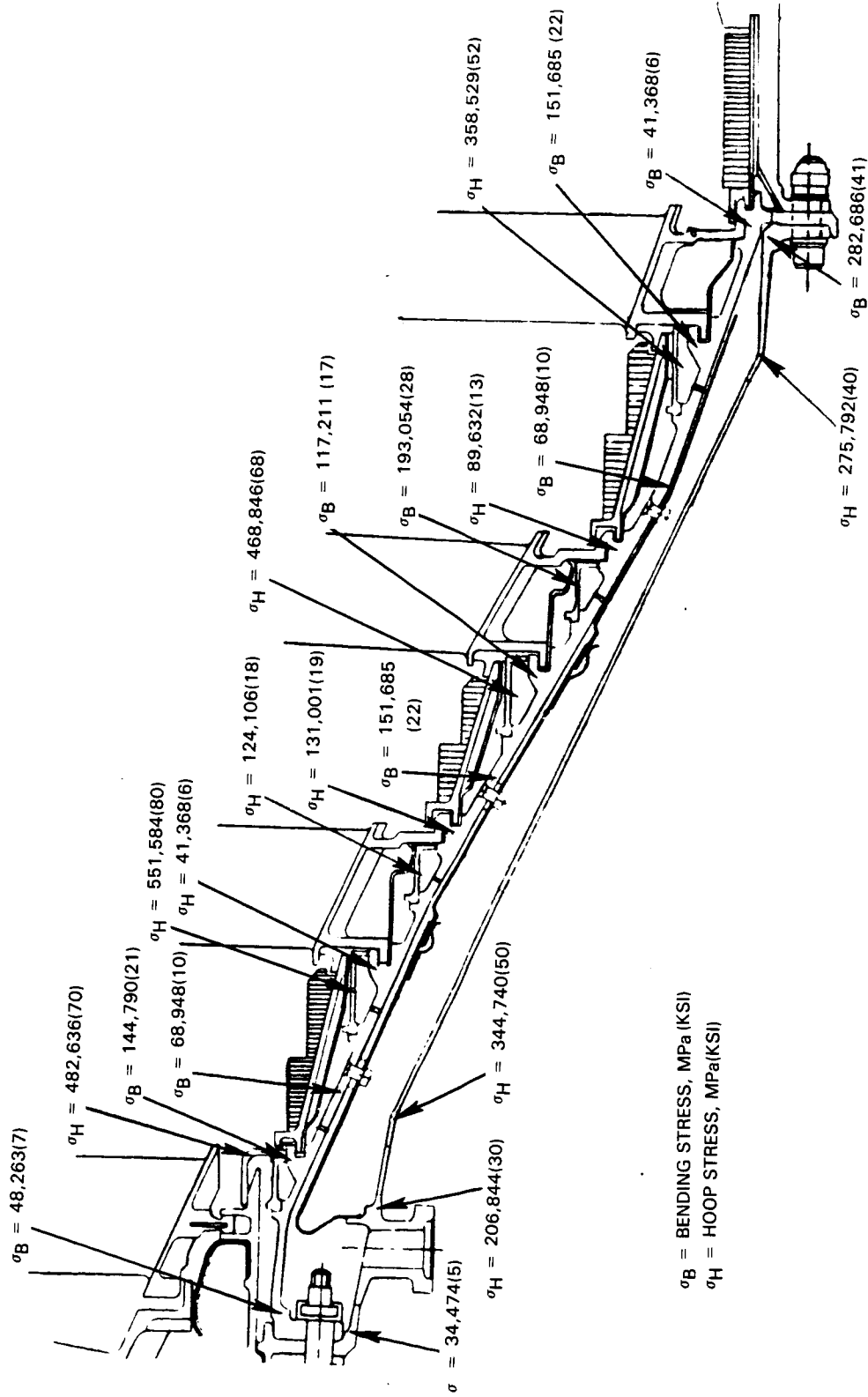


Figure 5.2.2-18 Low-Pressure Turbine Case Stress Summary

5.2.2.3 Turbine Exhaust Case

5.2.2.3.1 Mechanical Design Features

The turbine exhaust case includes a turbine exit guide vane to remove swirl from the low-pressure turbine exit flow. It is an integral ring-strut-ring, welded structure, with the 30 struts doubling as airfoils for the exit guide vanes. Design requirements for this structure were to meet design life and provide radial and trunion springrates in the ring-strut-ring structure that would tune exhaust plug pitch and vibratory modes outside the excitation frequency. The flight propulsion system preliminary design which meets these requirements is illustrated in Figure 5.2.2-19. It is a lightweight structure with hollow vanes/struts fabricated from sheet Ti-Al. The inner and outer rings are forged from the same material and welded to the struts. The inner ring supports the exhaust plug as shown. A flange at the rear of the outer ring provides support for the exhaust/mixer and serves as the engine-to-fan duct interface for cowl load sharing. The front outer support flange transfers axial loads from the turbine exhaust case forward to the low-pressure turbine case and provides containment for the fifth stage rotor blade.

In order to reduce cost for the integrated core/low spool, a simpler design was established that would provide the same structural and aerodynamic characteristics as the flight design, but was heavier and less costly. The design is illustrated in Figure 5.2.2-20. Here, the vanes/struts are solid castings of Greek ASCOLOY material. The inner and outer rings and flanges are forged from the same material. All are welded together into a single assembly.

5.2.2.3.2 Structural Analysis

The structural feasibility of the turbine exhaust case designs for the flight propulsion system and the integrated core/low spool is based on experience with similar structures fabricated from current, lower strength material and operate in more severe thermal environments. The maximum metal temperatures expected for the integrated core/low spool turbine exhaust case assembly are 526°C (980°F) for the inner case ring, 648°C (1200°F) for the vanes/struts, and 604°C (1120°F) for the outer duct case ring.

A three-dimensional NASTRAN analysis of the flight propulsion system ring-strut-ring structure was performed to determine trunion and radial springrates. These springrates were used to determine the vibratory resonances of the tailplug. The turbine exhaust case structure was resized as needed to tune the tailplug pitch and bounce vibratory modes out of the operating ranges. The predicted tailplug resonant frequencies are shown in Table 5.2.2-V. They meet or exceed the requirements for the modes indicated.

TABLE 5.2.2-V
PREDICTED TAILPLUG RESONANT FREQUENCIES

<u>Vibratory Mode</u>	<u>Resonant Frequency</u>
Pitch	4,800 rpm
Bounce	20,000 rpm

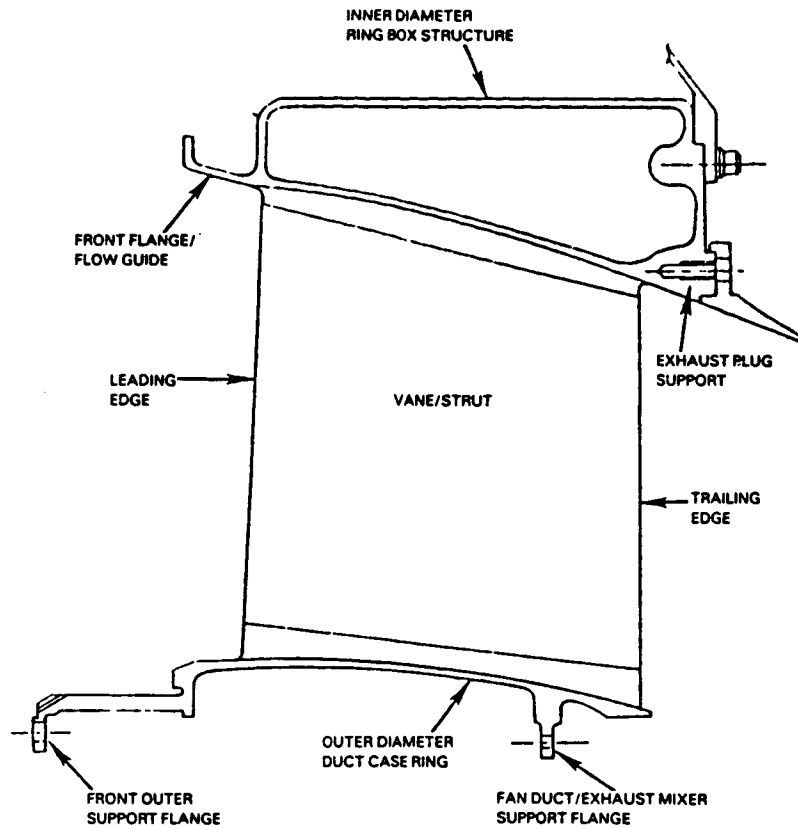


Figure 5.2.2-19 Flight Propulsion System Turbine Exhaust Case Assembly - Preliminary Design

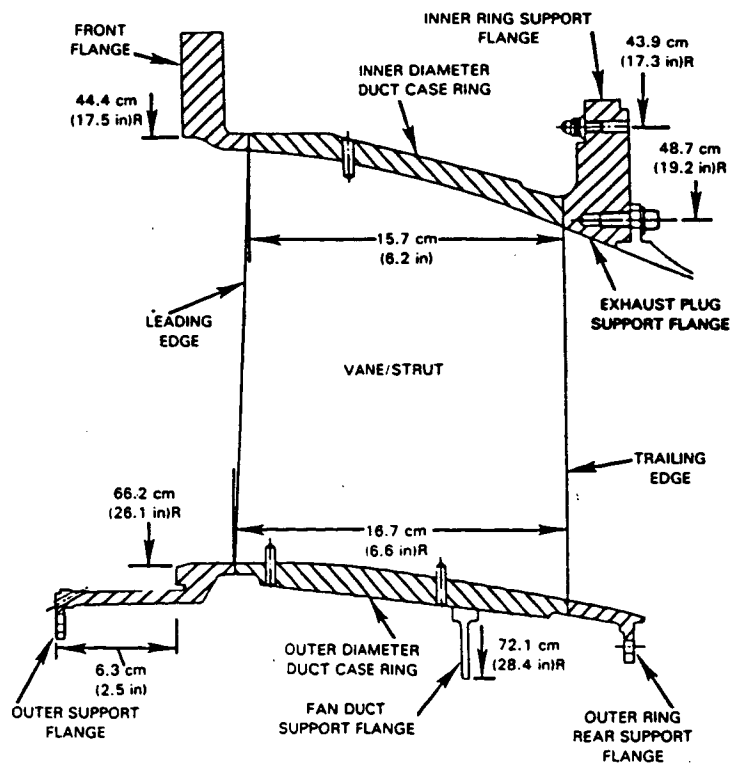


Figure 5.2.2-20 Integrated Core/Low Spool Turbine Exhaust Case Assembly

5.2.2.4 Low-Pressure Turbine Active Clearance Control System

5.2.2.4.1 Design Approach

To achieve high efficiency in the low-pressure turbine, it is desirable to maintain tight clearances at the blade tips and inner airseals throughout the engine operating envelope and especially at the design point. Causes for these clearances (or gaps) fall into two major categories: (1) those associated with the relative difference in radial growth between the rotor and case resulting from centrifugal forces and thermals; and (2) those associated with maneuver deflections, rotor whirl, case ovalization, tolerances, and eccentricities. The latter, which were included in the structural design criteria for the component, are essentially uncontrollable once the design has been fixed. Gaps caused by the former can be controlled, to a certain extent, by modulating case thermal expansion or contraction through the application of controlled temperature cooling air. It is the function of the active clearance control system to provide the case movement required to minimize clearances and avoid rotor-to-case "pinch", while maintaining case temperature within acceptable limits.

To minimize deterioration, a "no-rub" philosophy was adopted. In conjunction with this, a clearance goal of 0.050 cm (0.020 in) was established for the blade tips and inner airseal at the aerodynamic design point.

5.2.2.4.2 Mechanical Design Features

The major features of the low-pressure turbine case active clearance control system are shown in Figure 5.2.2-21. Cooling air is pumped to the turbine case, enters a manifold, and is directed aft between segmented sheet metal flow guides and the inner turbine case wall. These flow guides are attached to the inner case with rivets and spacers to provide a controlled gap dimension at each stage, tailored to maintain high thermal coefficients for optimum case response. Outer airseals are case-tied to ensure no relative motion between them and the case. A portion of the cooling flow is metered through holes in the inner turbine case wall to internal manifolds adjacent to the vane feet. This cooling air flows around the vane feet areas and reduces heat transfer from the vanes and outer airseals into the case.

Outer airseal radial growth for active clearance control is regulated through the use of a combination of tenth and fifteenth stage high-pressure compressor bleed air; maximum growth occurring through the use of all fifteenth stage air and minimum growth through the use of all tenth stage air. However, use of all fifteenth stage air at sea level takeoff power produces case hook temperatures beyond the capability of the Inconel 718 case material. Therefore, the active clearance control system proposed for the integrated core/low spool uses a combination of tenth and fifteenth stage high-pressure compressor bleed air. The pressure in the outer manifold of the case is 30 percent of the total pressure at the high-pressure compressor exit, and 0.1 percent of core engine airflow is used to cool each hook. Total active clearance control air in this case is 1.0 percent of core engine airflow.

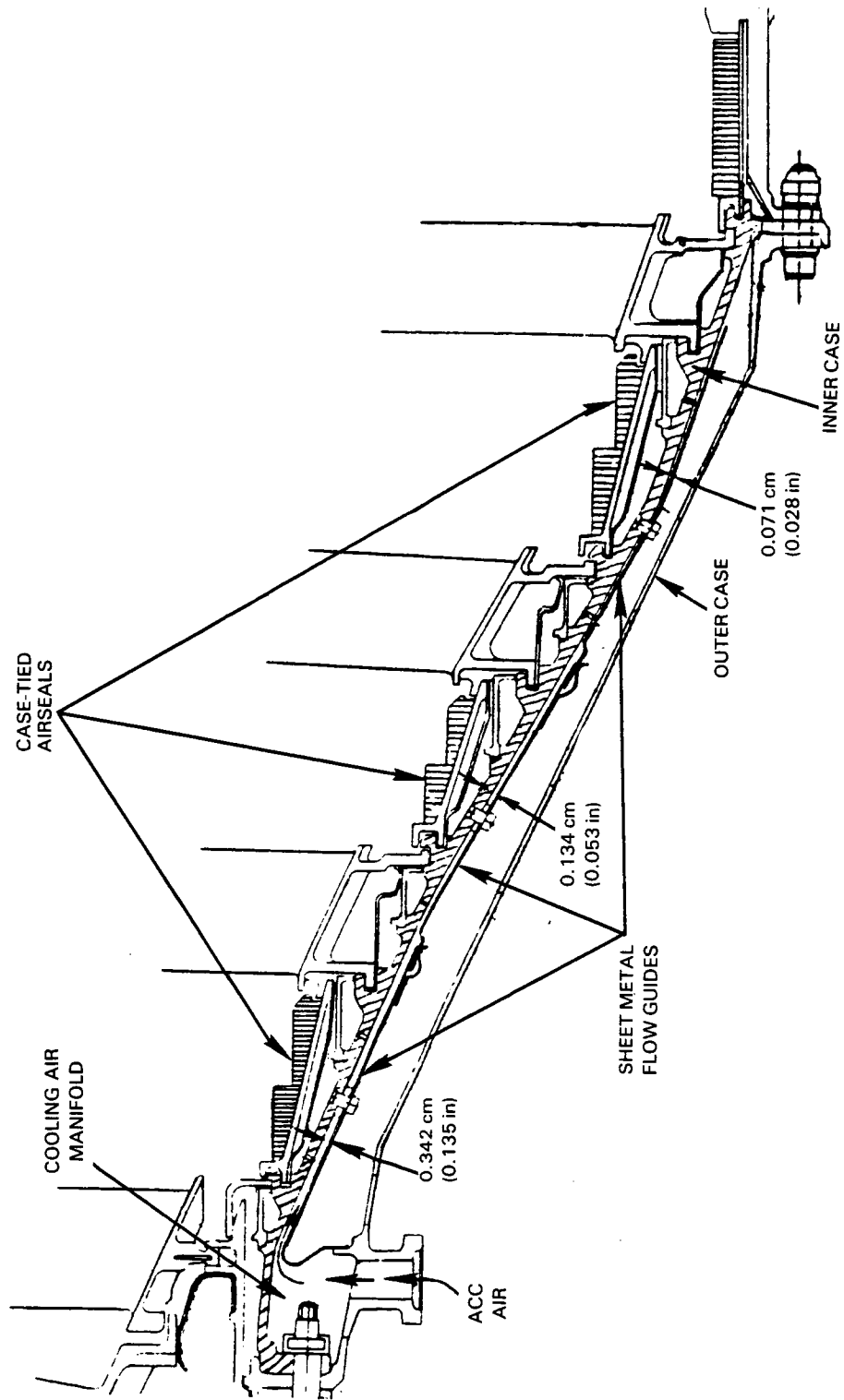


Figure 5.2.2-21 Low-Pressure Turbine Case Active Clearance Control Features

In contrast, the flight propulsion system uses a combination of eighth and fifteenth stage high-pressure compressor bleed air. Use of eighth stage air increases case closure capability over tenth stage air, but use of all eighth stage air reduces the supply pressure in the active clearance control manifold below the inlet guide vane gaspath static pressure. Therefore, cooling holes are not drilled in the second stage vane support hook area or the third vane front support hook area. Cooling passages in these areas are filled with insulation. In this case, pressure in the outer manifold of the case is 16 percent of the total pressure at the high-pressure exit and total active clearance control air is reduced to 0.8 percent of core engine airflow. The case design, as modified for the flight propulsion system, is illustrated in Figure 5.2.2-22.

5.2.2.4.3 Clearance Analysis

To establish the relative growth between the case and rotor as a result of rotor centrifugal forces, thermals, and pressure, shell analyses were conducted over the full range of engine operating conditions. The resultant radial growth of the case and rotor were plotted versus time and superimposed to establish "pinch" points. As shown in Figure 5.2.2-23, the "pinch" point occurred during a snap acceleration from idle to takeoff power. Clearance deviations associated with maneuver loads, rotor whirl, ovalization, tolerances, and eccentricities were assumed to occur at the pinch point to ensure a "no rub" condition. Combining the effects of these deviations with clearances determined from the rotor and case growth analyses resulted in clearances substantially in excess of the 0.050 cm (0.020 in) goal. Thermal matching with the active clearance control system yielded excellent clearance results at the aerodynamic design point and sea level takeoff conditions, but these were negated by large maneuver deflections.

In an effort to achieve clearances closer to the aerodynamic design point, a requirement was added that the blade tip knife edges be ground at assembly to $+ 0.005$ cm ($+ 0.002$ in) tolerance on the diameter. In addition, any tolerances that cause deviation from nominal would be allowed to rub in at the pinch point and in effect "custom machine" blade tips and seals to a line-on-line or nominal condition. While this alters the "no-rub" philosophy, the rubbing is not considered deterioration since the parts, in effect, are rubbed to nominal dimensions. Approximately 0.012 cm (0.005 in) tip clearance reduction is gained through the tip grind and rub in philosophy.

The cooling flow management scheme that resulted from these analyses is shown in Table 5.2.2-VI.

Eighth stage compressor bleed air was chosen for the flight propulsion system because of a 0.19 percent efficiency advantage and 0.28 percent thrust specific fuel consumption advantage. Tenth stage bleed air was selected for the integrated core/low spool to avoid design expense and additional hardware costs involved with external bleed plumbing to the eighth stage.

Blade tip and interstage airseal clearances resulting from these analyses for the integrated core/low spool are listed in Tables 5.2.2-VII and -VIII. Those for the flight propulsion system are listed in Tables 5.2.2-IX and -X.

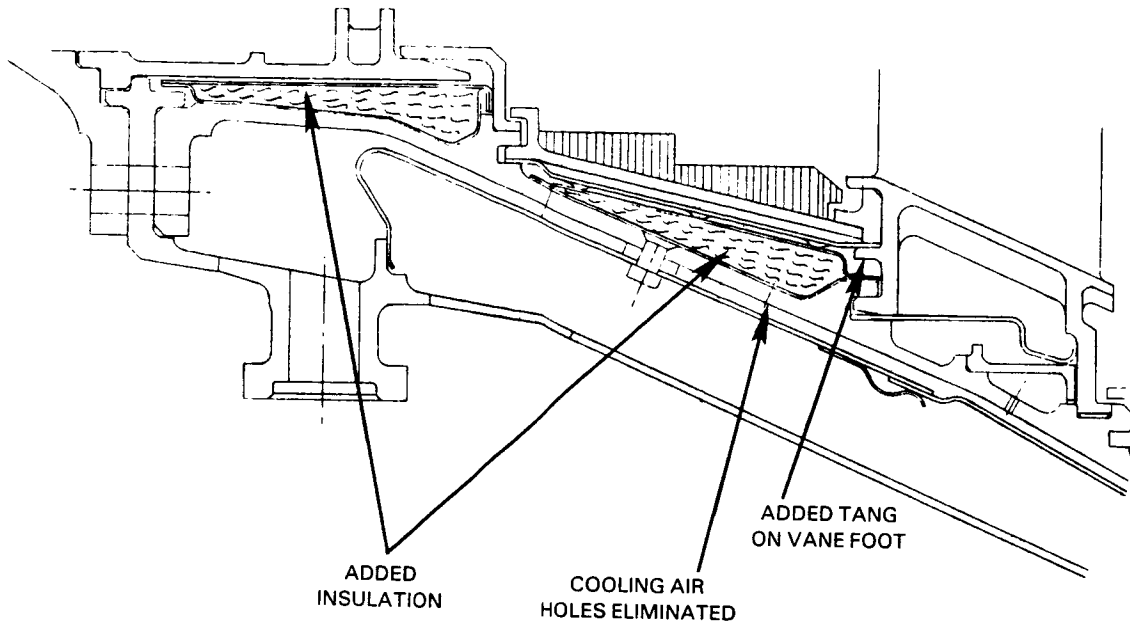


Figure 5.2.2-22 Low-Pressure Turbine Case Modifications for Flight Propulsion System Active Clearance Control System

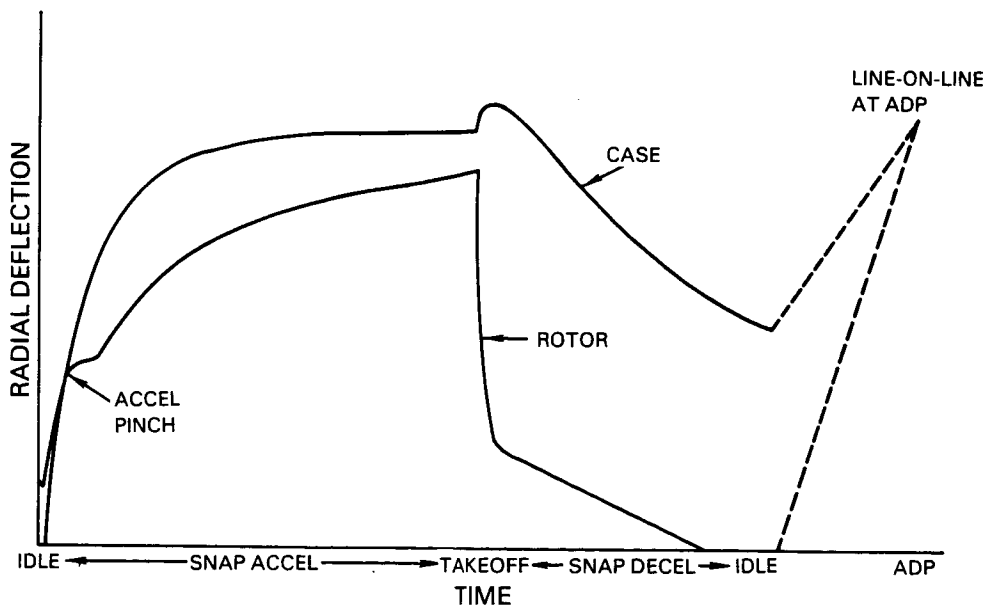


Figure 5.2.2-23 Typical Low-Pressure Turbine Rotor and Case Radial Growth Caused by Centrifugal Force, Thermals, and Pressure

TABLE 5.2.2-VI
ACTIVE CLEARANCE CONTROL SYSTEM
COOLING FLOW MANAGEMENT

<u>Power Setting</u>	<u>Integrated Core/Low Spool</u>	<u>Flight Propulsion System</u>
Idle	No cooling air	No cooling air
Accel-Sea Level Takeoff	Mixed 10th & 15th stage compressor bleed air	Mixed 8th & 15th stage compressor bleed air
Aerodynamic Design Point	All 10th stage compressor bleed air	All 8th stage compressor bleed air
Decel	No cooling air	No cooling air

TABLE 5.2.2-VII
ENERGY EFFICIENT ENGINE LOW-PRESSURE TURBINE
BLADE TIP CLEARANCE SUMMARY
(Clearances are in cm (in))

TENTH STAGE ACTIVE CLEARANCE CONTROL SYSTEM AIR

<u>Gap Component</u>	<u>Rotor 2</u>	<u>Rotor 3</u>	<u>Rotor 4</u>	<u>Rotor 5</u>
Concentricity (1/2 Max.)	0.015 (0.006)	0.015 (0.006)	0.017 (0.007)	0.017 (0.007)
Maneuvers	0.020 (0.008)	0.027 (0.011)	0.048 (0.019)	0.071 (0.028)
Whirl	0.010 (0.004)	0.012 (0.005)	0.015 (0.006)	0.015 (0.006)
Bearing Clearance	0.005 (0.002)	0.007 (0.003)	0.007 (0.003)	0.007 (0.003)
Ovalization & Cowl Loads	0.005 (0.002)	0.005 (0.002)	0.005 (0.002)	0.005 (0.002)
Total Mechanical	0.055 (0.022)	0.068 (0.027)	0.093 (0.037)	0.116 (0.046)
Speed & Thermals @ ADP	0.010 (0.004)	0.020 (0.008)	0.020 (0.008)	0.027 (0.011)
Speed & Thermals @ SLTO	0	0	0	0.033 (0.013)
ADP Clearance	0.066 (0.026)	0.088 (0.035)	0.114 (0.045)	0.144 (0.057)
SLTO Clearance	0.055 (0.022)	0.068 (0.027)	0.093 (0.037)	0.149 (0.059)

TABLE 5.2.2-VIII
ENERGY EFFICIENT ENGINE LOW-PRESSURE TURBINE
INTERSTAGE SEAL CLEARANCE SUMMARY
(Clearances are in cm (in))

TENTH STAGE ACTIVE CLEARANCE CONTROL SYSTEM AIR

<u>Gap Component</u>	<u>Rotor 2-3 Middle Tooth</u>	<u>Rotor 3-4 Middle Tooth</u>	<u>Rotor 4-5 Front Tooth</u>	<u>Outer Thrust Balance</u>	<u>Inner Thrust Balance</u>
Concentricity (1/2 Max.)	0.012 (0.005)	0.012 (0.005)	0.012 (0.005)	0.012 (0.005)	0.012 (0.005)
Maneuvers	0.022 (0.009)	0.038 (0.015)	0.058 (0.023)	0.022 (0.009)	0.022 (0.009)
Whirl	0.012 (0.005)	0.012 (0.005)	0.015 (0.006)	0.010 (0.004)	0.010 (0.004)
Bearing Clearance	0.007 (0.003)	0.007 (0.003)	0.007 (0.003)	0.005 (0.002)	0.005 (0.002)
Ovalization & Cowl Loads	0.005 (0.002)	0.005 (0.002)	0.005 (0.002)	0.005 (0.002)	0.005 (0.002)
Total Mechanical	0.060 (0.024)	0.076 (0.030)	0.099 (0.039)	0.055 (0.022)	0.055 (0.022)
Speed & Thermals @ ADP	0.045 (0.018)	0.040 (0.016)	0.038 (0.015)	0.007 (0.003)	0.002 (0.001)
Speed & Thermals @ SLTO	0	0	0.025 (0.010)	0	0
ADP Clearance	0.106 (0.042)	0.116 (0.046)	0.137 (0.054)	0.063 (0.025)	0.058 (0.023)
SLTO Clearance	0.060 (0.024)	0.076 (0.030)	0.124 (0.049)	0.055 (0.022)	0.055 (0.022)

TABLE 5.2.2-IX
ENERGY EFFICIENT ENGINE LOW-PRESSURE TURBINE
BLADE TIP CLEARANCE SUMMARY
(Clearances are in cm (in))

EIGHTH STAGE ACTIVE CLEARANCE CONTROL SYSTEM AIR

<u>Gap Component</u>	<u>Rotor 2</u>	<u>Rotor 3</u>	<u>Rotor 4</u>	<u>Rotor 5</u>
Concentricity (1/2 Max.)	0.015 (0.006)	0.015 (0.006)	0.017 (0.007)	0.017 (0.007)
Maneuvers	0.020 (0.008)	0.027 (0.011)	0.048 (0.019)	0.071 (0.028)
Whirl	0.010 (0.004)	0.012 (0.005)	0.015 (0.006)	0.015 (0.006)
Bearing Clearance	0.005 (0.002)	0.007 (0.003)	0.007 (0.003)	0.007 (0.003)
Ovalization & Cowl Loads	0.005 (0.002)	0.005 (0.002)	0.005 (0.002)	0.005 (0.002)
Total Mechanical	0.055 (0.022)	0.068 (0.027)	0.093 (0.037)	0.116 (0.046)
Speed & Thermals @ ADP	-	-	-	0.017 (0.007)
Speed & Thermals @ SLTO	0.068 (0.027)	0.063 (0.025)	0.066 (0.026)	0.055 (0.022)
ADP Clearance	0.055 (0.022)	0.068 (0.027)	0.093 (0.037)	0.134 (0.053)
SLTO Clearance	0.124 (0.049)	0.132 (0.052)	0.160 (0.063)	0.172 (0.068)

TABLE 5.2.2-X
ENERGY EFFICIENT ENGINE LOW-PRESSURE TURBINE
INTERSTAGE SEAL CLEARANCE SUMMARY
(Clearances are in cm (in))

EIGHTH STAGE ACTIVE CLEARANCE CONTROL SYSTEM AIR

Gap Component	Rotor 2-3 Middle Tooth	Rotor 3-4 Middle Tooth	Rotor 4-5 Front Tooth	Outer Thrust Balance	Inner Thrust Balance
Concentricity (1/2 Max.)	0.012 (0.005)	0.012 (0.005)	0.012 (0.005)	0.012 (0.005)	0.012 (0.005)
Maneuvers	0.022 (0.009)	0.038 (0.015)	0.058 (0.023)	0.022 (0.009)	0.022 (0.009)
Whirl	0.012 (0.005)	0.012 (0.005)	0.015 (0.006)	0.010 (0.004)	0.010 (0.004)
Bearing Clearance	0.007 (0.003)	0.007 (0.003)	0.007 (0.003)	0.005 (0.002)	0.005 (0.002)
Ovalization & Cowl Loads	0.005 (0.002)	0.005 (0.002)	0.005 (0.002)	0.005 (0.002)	0.005 (0.002)
Total Mechanical	0.060 (0.024)	0.076 (0.030)	0.099 (0.039)	0.055 (0.022)	0.055 (0.022)
Speed & Thermals @ ADP	0.068 (0.027)	0.007 (0.003)	0.033 (0.013)	0.007 (0.003)	0.002 (0.001)
Speed & Thermals @ SLTO	0.104 (0.041)	0.055 (0.022)	0.083 (0.033)	-	-
ADP Clearance	0.129 (0.051)	0.083 (0.033)	0.132 (0.052)	0.063 (0.025)	0.058 (0.023)
SLTO Clearance	0.165 (0.065)	0.132 (0.052)	0.182 (0.072)	0.055 (0.022)	0.055 (0.022)

5.2.3 Turbine Intermediate Case

5.2.3.1 Mechanical Designs Features

The turbine intermediate case provides for gaspath transition between the high-pressure turbine exit and the inlet of the low-pressure turbine. It also provides a frame for rotor supports and the rear engine mounts. A basic aerodynamic requirement is to duct gasflow between the turbines without separation and with minimal loss.

Figure 5.2.3-1 identifies the major design features of the turbine intermediate case assembly. The assembly comprises the high-pressure turbine outer case, the high-pressure turbine blade tip seal, eleven structural struts that traverse the gaspath and are shielded by aerodynamic fairings, an inner ring torque box that forms an interface between the structural struts and the rear bearing support structure, and second stage turbine vane inner support, and the front and rear secondary air seal lands. Engine mount and ground handling attachment lugs are located on the outer case between the pads where tiebolts and dowels secure the bearing support structure to the case. The strut and its associated support structure serve to maintain structural integrity of the bearing support frame in the event of a turbine failure, to minimize case ovalization caused by engine mount loads, and to provide a route for oil service lines to the No. 4-5 bearing compartment. Flight propulsion system design life goals are 15,000 hours/3300 missions for the fairing and 30,000 hours/20,000 missions for the structure. Integrated core/low spool life goal for all hardware are 50 hours of hot time and 1000 cycles. The aerodynamic pressure loss goal for the transition duct flowpath is 1.5 percent $\Delta P_T/P_T$.

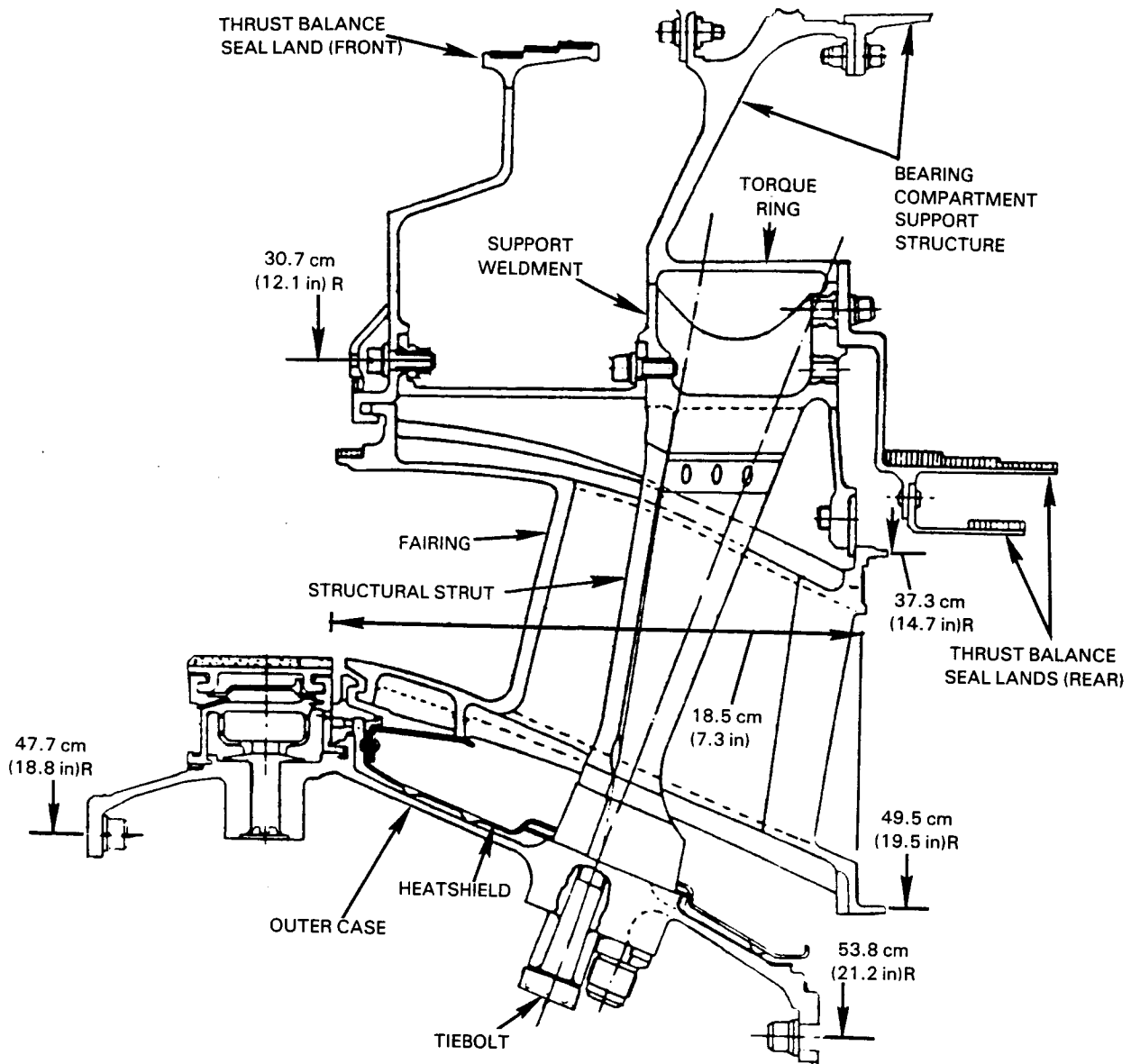


Figure 5.2.3-1 Turbine Intermediate Case

5.2.3.1.1 Structural Struts

The structural struts, as shown in Figure 5.2.3-2 are forged from Inconel 718 material and include drilled cooling air passages. The cooling hole exits in the integrated core/low spool strut are circular for ease of manufacturing while they are elliptical in the flight propulsion system for a lower stress concentration factor and thus greater life. Each strut is flame sprayed with an aluminum oxide insulation coating to reduce radiation heating from the fairings and local conductive heating from possible temporary contact with the fairing during high structural deflections. The struts are canted rearward from the outer case tiebolt connection to carry a rearward thrust balance load of approximately 111,205 N (25,000 lb), while reducing bending stresses to an acceptable level. Strut axial loads as well as the radial loads imposed on the bearing compartment from maneuver and imbalance are shown in Figure 5.2.3-3.

Each strut is electron beam welded to the torque ring at the inner diameter, as shown in Figure 5.2.3-4, and fastened to the outer case with a single, high-strength tiebolt. Externally removable dowels are installed on either side of each tiebolt to help the struts resist the tightening torque, absorb twisting moments at the end of the strut arising from blowoff and thermal loads, and prevent potential shear loads on the tiebolt at the strut-to-outer case joint surface. Minimum clearance between the strut and the strut fairing, due to relative motion between the two, was calculated to be 0.076 cm (0.03 in), as shown in Figure 5.2.3-2.

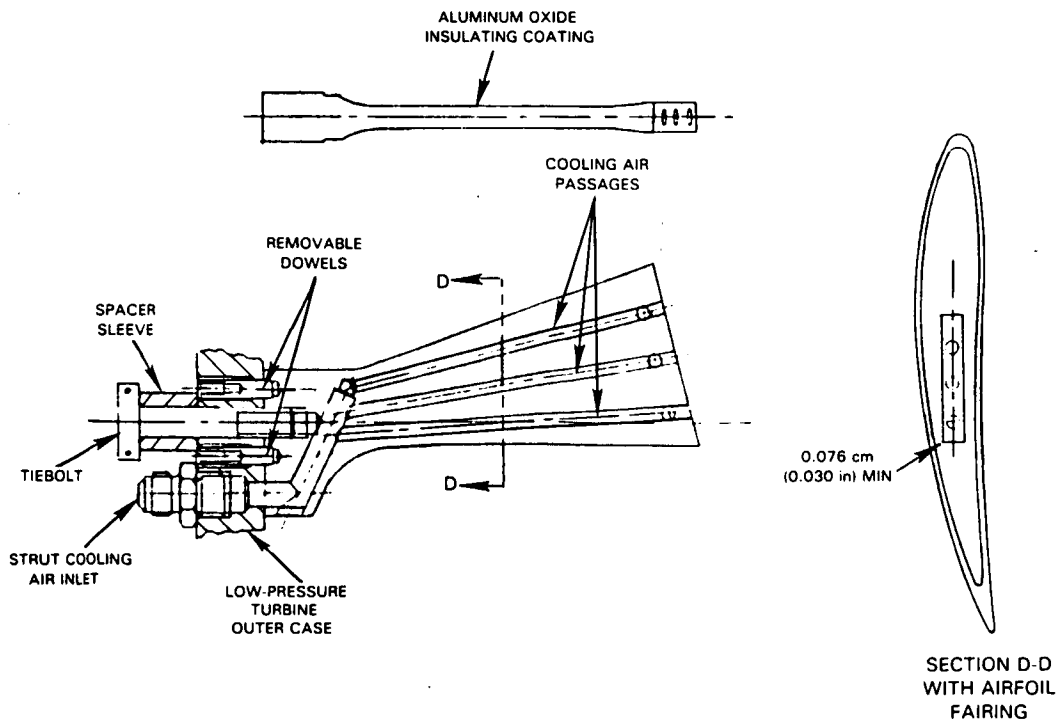


Figure 5.2.3-2 Turbine Intermediate Case Structural Strut Details

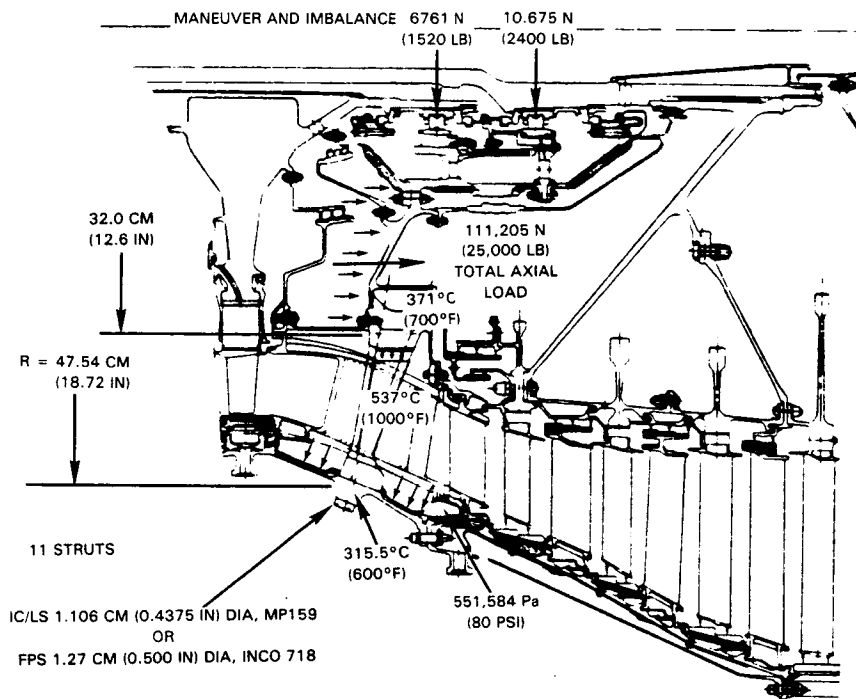


Figure 5.2.3-3 Bearing Compartment Axial and Radial Maneuver and Imbalance Loads

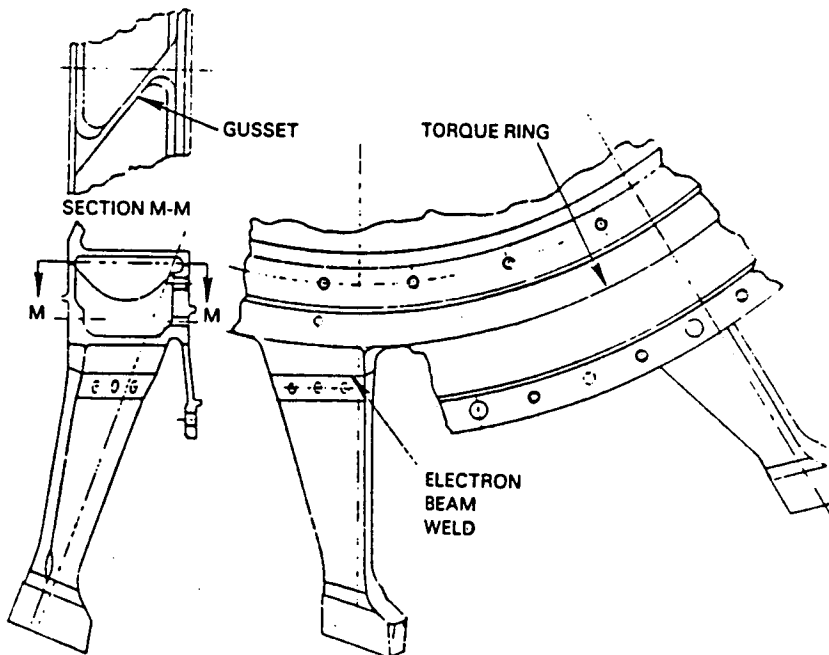


Figure 5.2.3-4 Structural Strut-to-Torque Ring Weldment

5.2.3.1.2 Strut Fairings

The strut fairings, illustrated in Figure 5.2.3-5, are cast in eleven circumferential segments that are sealed at the inner and outer platform gaps through the use of Haynes 188 cobalt alloy feather seals. To meet life requirements, SC 2000 single crystal alloy was selected for the flight propulsion system strut fairings and MAR-M-509 cobalt alloy for the integrated core/low spool. Segment edges are set at the angles of the gas flow streamlines at the inner and outer shrouds (platforms) to minimize boundary layer flow disturbances. Shroud edges are thickened to provide straight grooves for the feather seals. The inner shroud seals are retained axially by tabs at the front seal support and at the segment rear flange by a split ring. The outer shroud seals are trapped at the front end by a fairing support ring and at the rear by the second stage vane outer shroud. The fairing inner front shroud is supported by a hook arrangement on a flange which, in turn, is supported by the torque ring. This inner support arrangement reduces transient thermal variations in the radial gap between the high-pressure turbine disk rear sideplate seal lip and the front end inner shroud inner diameter. The fairing inner diameter rear shroud is supported through a hook arrangement with the second vane inner diameter support flange.

5.2.3.1.3 Outer Case and Outer Case Heatshield

The outer case for the flight propulsion system is a lightweight design that features a polygonal cross section at the strut connection plane with flat plates joined at the tiebolt bosses. This has been modified for the integrated core/low spool to a continuous ring section between tiebolts in order to reduce fabrication cost and time. These rings are machined from Inconel 718 forgings. The outer case incorporates a heatshield, shown in Figure 5.2.3-6, which channels hot discharge air from the high-pressure turbine blade tip seal along the case inner wall. This flow raises the case temperature and reduces strut thermal compression experienced during engine acceleration when radiation from the strut fairings results in strut temperatures appreciably hotter than outer case and torque ring temperatures.

The high-pressure turbine blade tip seal exhaust air flows out of the heatshield channel rear end into the cavity between the outer case and the outer shroud. Some of this flow leaks past the fairing segment edge seals, some through the flexible finger seals at the front and rear ends of the outer shroud, and some passes through the fairing segment airfoils into the inner cavity and its exit orifice holes. The heatshield is retained in position by bolts at each strut pad location, where flat heatshield inserts are in contact with the case. Six of these bolts, spaced at alternate pads, are inserted through bushings engaging holes both in the case pad and the heatshield to locate the heatshield more precisely. The Hastelloy S heatshield material is selected to provide a relatively constant gap between its outer diameter and the outer case inner diameter for the slow accelerations of the integrated core/low spool test program. The heatshield temperature is higher than that of the case, but its lower coefficient of expansion keeps its thermal growth closely matched to the outer case. For the flight engine, with fast accelerations the heatshield grows faster than the outer case, with the possibility of buckling. This problem can be eliminated by adding slip joints in the heatshield between each strut location to permit circumferential expansion.

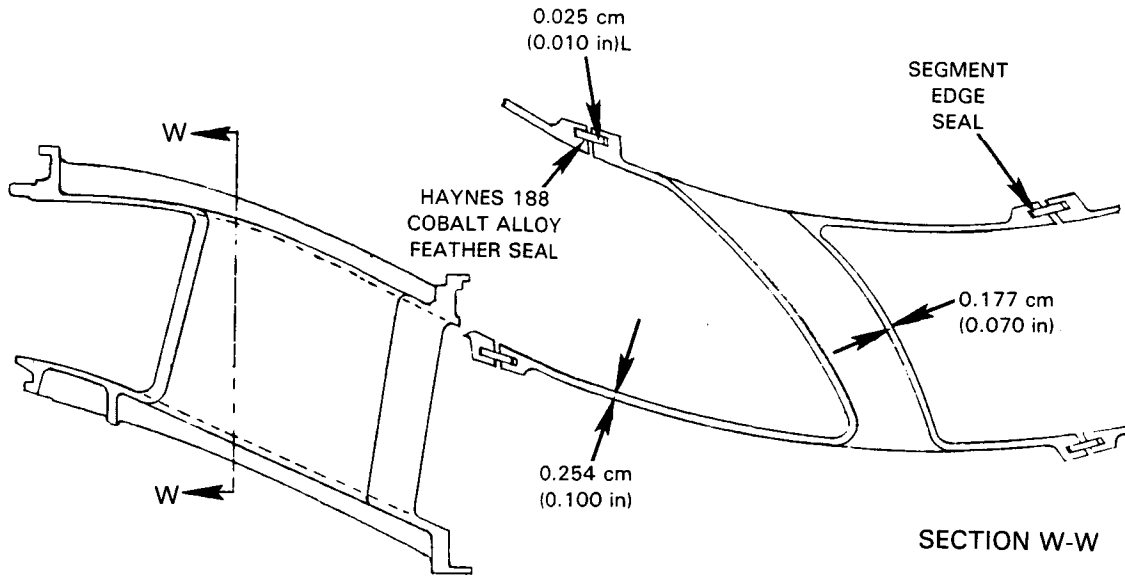


Figure 5.2.3-5 Turbine Intermediate Case Strut Fairing

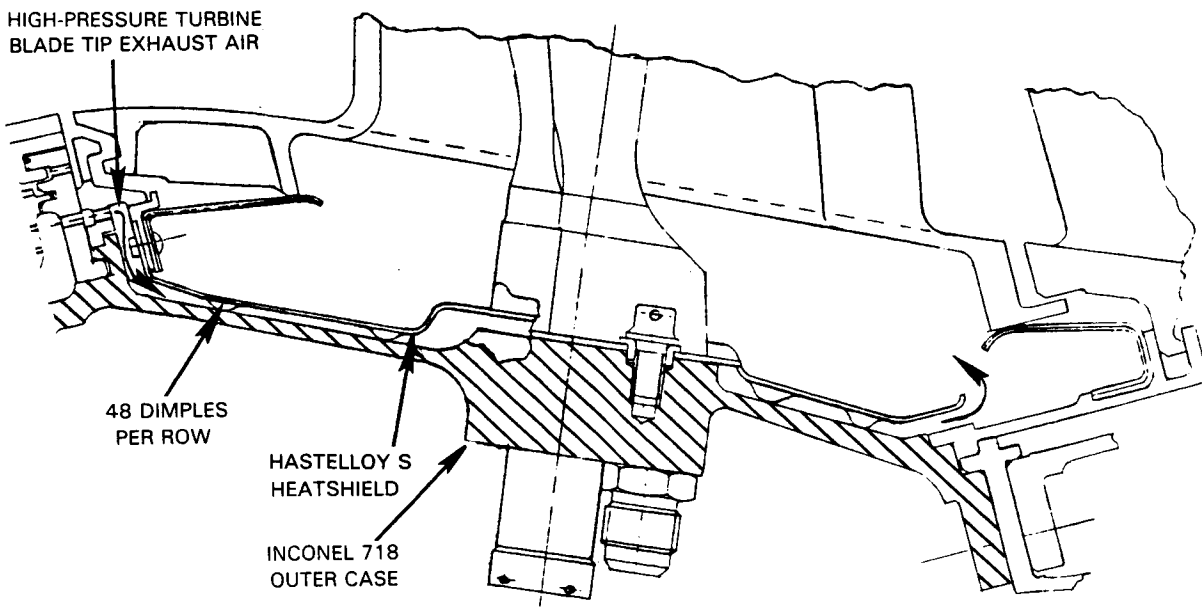


Figure 5.2.3-6 Turbine Intermediate Case Outer Case and Outer Case Heatshield Details

5.2.3.1.4 Engine Mount Lugs

The engine rear mount comprises three sets of double lugs that are located between struts on the upper half of the outer case as shown in Figure 5.2.3-7. For the integrated core/low spool, these lugs are designed only for test stand load conditions and are electron beam welded to the outer case to save cost. Flight propulsion system lugs would be integrally forged with adequate strength to meet the flight loads indicated in the figure. Single lugs for ground handling are also welded to the outer case, one in each bottom quadrant at the aft end of the case strut ring, leaving the forward location free for instrumentation bosses.

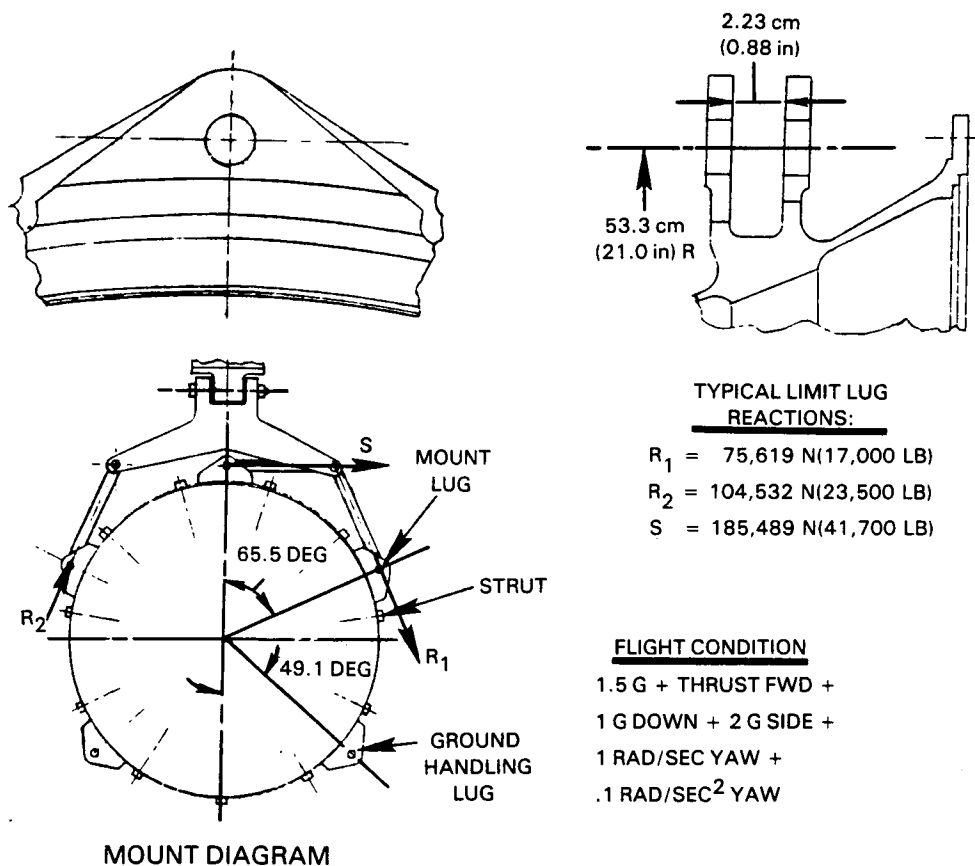


Figure 5.2.3-7 Engine Rear Mount Details

5.2.3.1.5 Oil Supply and Scavenge Lines

Oil supply and scavenge lines for the No. 4-5 bearing compartment are routed through the cavity formed between the structural strut and the strut fairing leading edge as shown in Figure 5.2.3-8. These lines are fully insulated to protect the oil flow from the high temperature environment within the strut fairing.

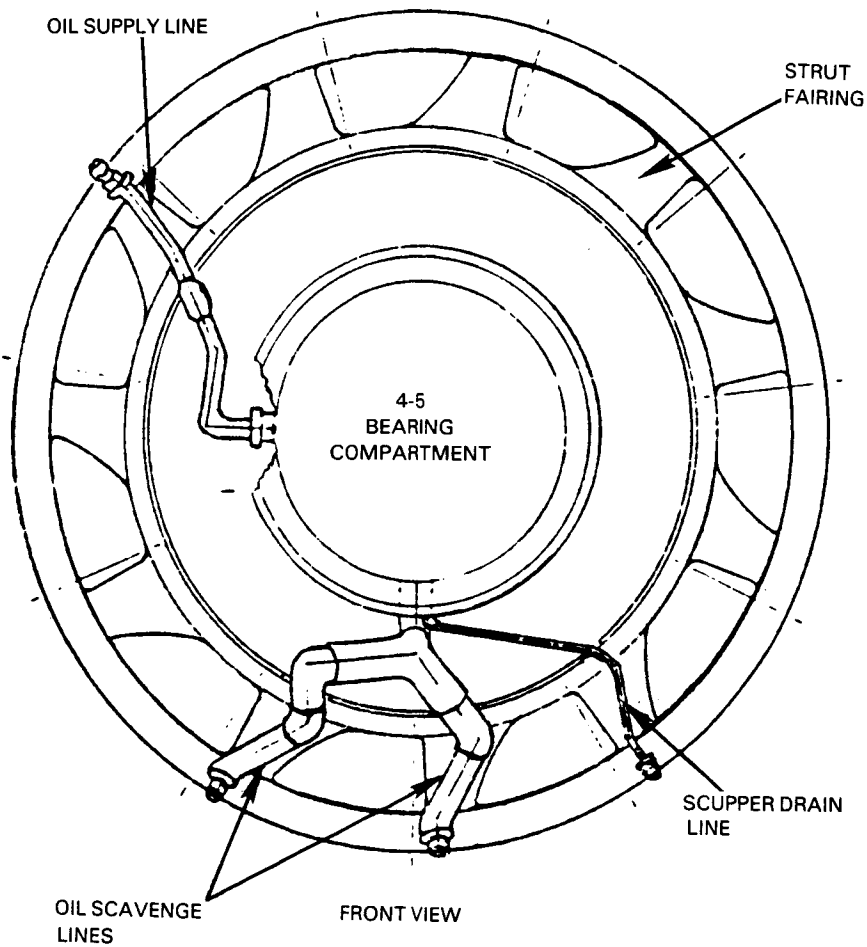


Figure 5.2.3-8 Routing for Nos. 4-5 Bearing Compartment Oil Supply, Scavenge and Drain Lines

5.2.3.1.6 Thrust Balance Seal Lands

The front and rear thrust balance seal lands are shown in Figure 5.2.3-9. The front seal land accommodates the three knife-edge seal bolted to the rear of the high-pressure turbine disk. It is bolted to a ring spacer which, in turn, is bolted to the front face of the inner torque ring. Support for the front inner diameter strut fairing segments is provided through a hook arrangement, shown in the figure. The rear seal accommodates the single knife-edge outer seal and three knife-edge inner seals that one bolts to the front face of the first stage low-pressure turbine disk. This land is bolted to the rear face of the inner torque ring. Material for both is AMS 5671. Rubstrip material bonded to the front seal land is PWA 24-3 fiber metal. Material for the rear seal rubstrip is AMS 5536 honeycomb.

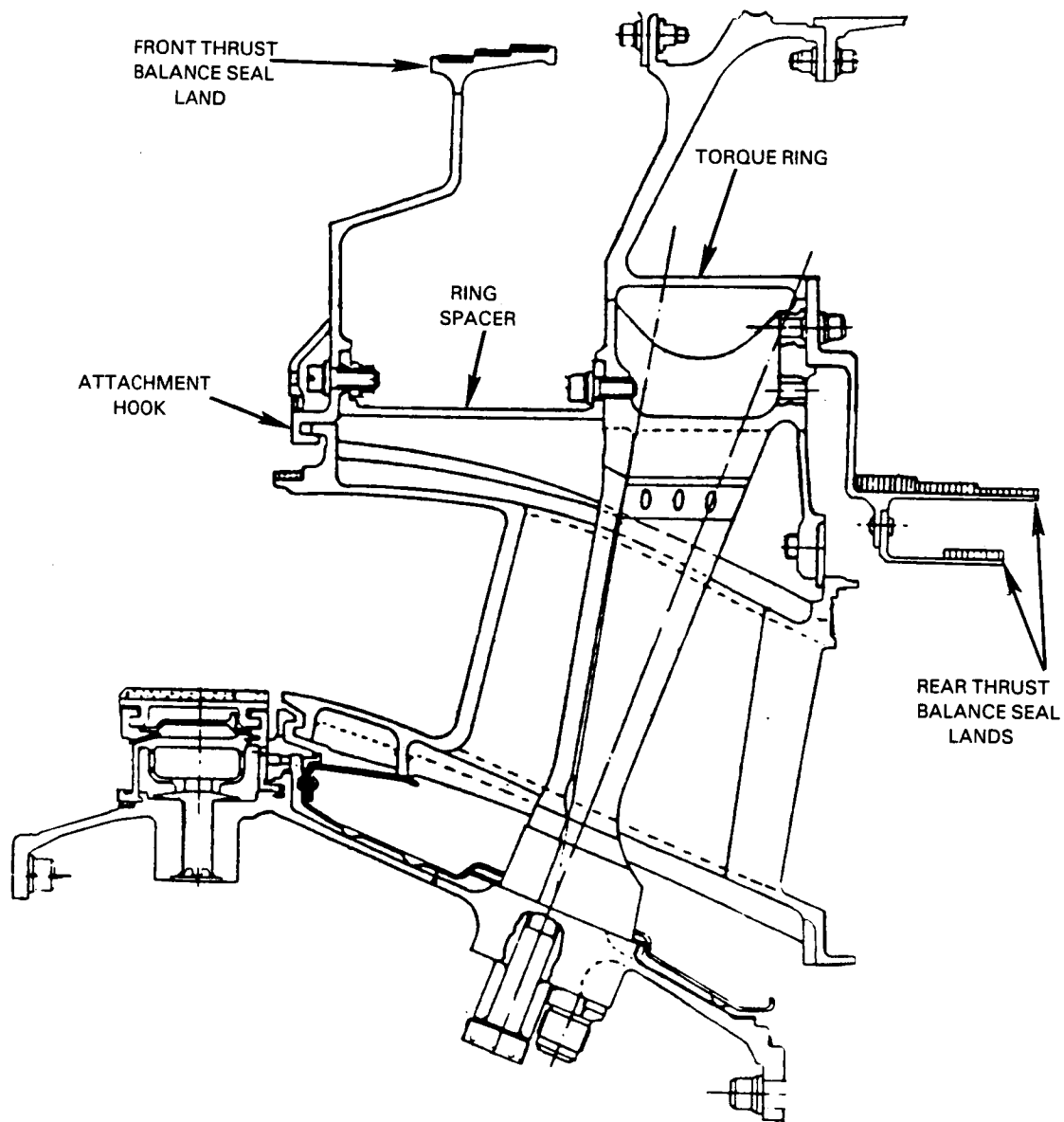


Figure 5.2.3-9 Turbine Intermediate Case Front and Rear Thrust Balance Seal Lands

5.2.3.2 Structural Analysis

Major concerns addressed in the structural analysis of the intermediate case included the high temperature environment 1010°C (1850°F) average and 1176°C (2150°F) maximum hot spot). This temperature environment can produce high thermal stresses resulting from temperature gradients between the structural struts and inner and outer cases. The differential pressure across the inner bearing support results in high axial thrust balance loads that can cause high bending stresses. Rotor imbalance and maneuver loads transmitted to the turbine intermediate case through the bearings and bearing support structure add to the stresses. Life requirements for the primary elements of the turbine intermediate case assembly are presented in Table 5.1-I. Structural analysis of the primary support structure included calculation of strut stresses and lives, and strut bolt loads. Durability of the strut fairing was analyzed in detail because of its exposure to a high-temperature environment.

5.2.3.2.1 Primary Support Structure Stress and Life Analysis

Because of the complex loading to which the turbine intermediate case is subjected and the complex geometry of the case itself (Figure 5.2.3-10) with both axial and tangential tilt in the structural struts, a three-dimensional analysis was required to determine load paths, loading and deflections in the various turbine intermediate case components. The structural deflections were required to determine the No. 4 and 5 bearing support spring rates and for

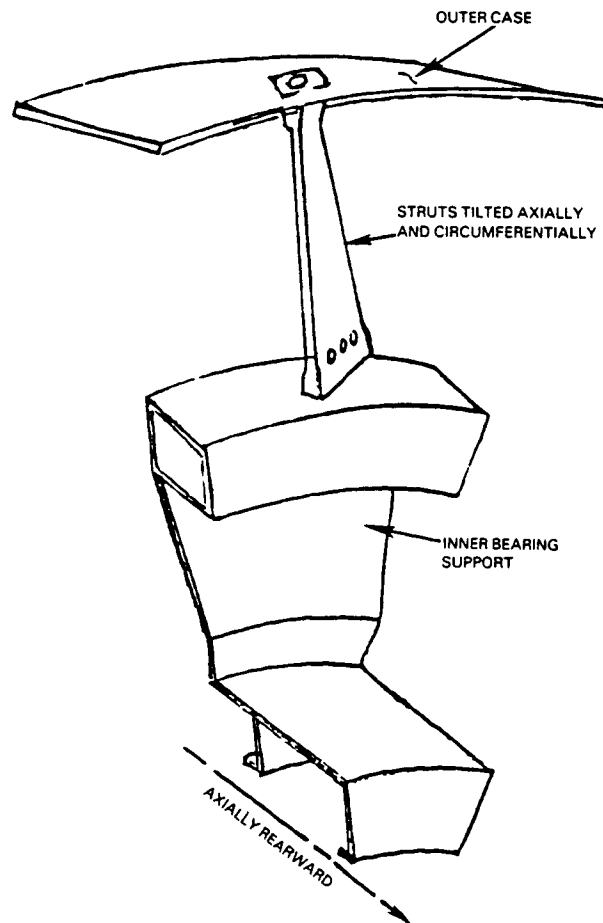


Figure 5.2.3-10 Turbine Intermediate Case Structure Illustrating Complex Geometry

calculating clearances between the strut and aerodynamic fairing. Two separate NASTRAN models were used. A full 360-degree model, shown in Figure 5.2.3-11, was used to analyze nonaxisymmetric loads. This model comprises 900 plate and bar elements. A cyclic symmetry model (modeling only a segment of the structure), shown in Figure 5.2.3-12, was used to analyze axisymmetric loads such as thermal loading.

Thermal and pressure loads were applied for acceleration, steady-state takeoff and deceleration conditions. The acceleration and deceleration time points chosen for analysis were those having maximum potential for ring-strut-ring thermal interference. The acceleration thermals produced the largest thermal loads.

Bearing support springrates were established for the No. 4 bearing (rear high rotor) and No. 5 bearing (rear low rotor) from the NASTRAN analysis and were used in the critical speed analyses discussed in Section 5.2.4 of this report. The springrates shown in Figure 5.2.3-13 for both the No. 4 and 5 bearing supports satisfied critical speed requirements.

Circumferential and axial deflections resulting from the NASTRAN analysis are summarized in Figures 5.2.3-14 and 5.2.3-15. The circumferential deflection of the structural strut was found from the NASTRAN analysis to be almost entirely due to the thermal gradient between the strut and the inner and outer cases.

Approximately 40 percent of the axial deflection resulted from the thermal gradient between the strut and the inner and outer cases, and 60 percent from the large axial pressure load. Deflection analysis of the structural strut and the aerodynamic fairing determined that the minimum operating clearance between the fairing and the strut was 0.076 cm (0.030 in) at a section near the strut outer diameter, as shown in Figure 5.2.3-16. This represents the worst possible dimensional tolerance stack-up and occurs during a snap acceleration. The minimum strut fairing clearance shown will actually be increased by fairing deflection due to gas loading. To provide an added margin of safety for the integrated core/low spool, the structural strut are coated with 0.025 cm (0.01 in) thick ceramic to eliminate any possibility of metal-to-metal contact between the fairing and the strut.

There was some initial concern that local distortions from the eleven structural struts would be "felt" by the case over the tips of the high-pressure turbine blades and thus adversely affect high-pressure turbine tip clearances. The NASTRAN models did not extend as far forward as the plane of the high-pressure turbine; the case was modeled only to a plane which is approximately 3.810 cm (1.5 in) aft of the plane of the high-pressure turbine. At the forward edge of the model, the maximum distortions were less than 0.005 cm (0.002 in) and occurred during a normal flight propulsion system maneuver. The distortions at the plane of the high-pressure turbine would be even less than 0.005 cm (0.002 in). It was judged that these distortions are reasonably small and that they would have minimal influence on high-pressure turbine tip clearances for the flight propulsion system. The integrated core/low spool is not subjected to maneuver loads and local distortions are even smaller than 0.005 cm (0.002 in).

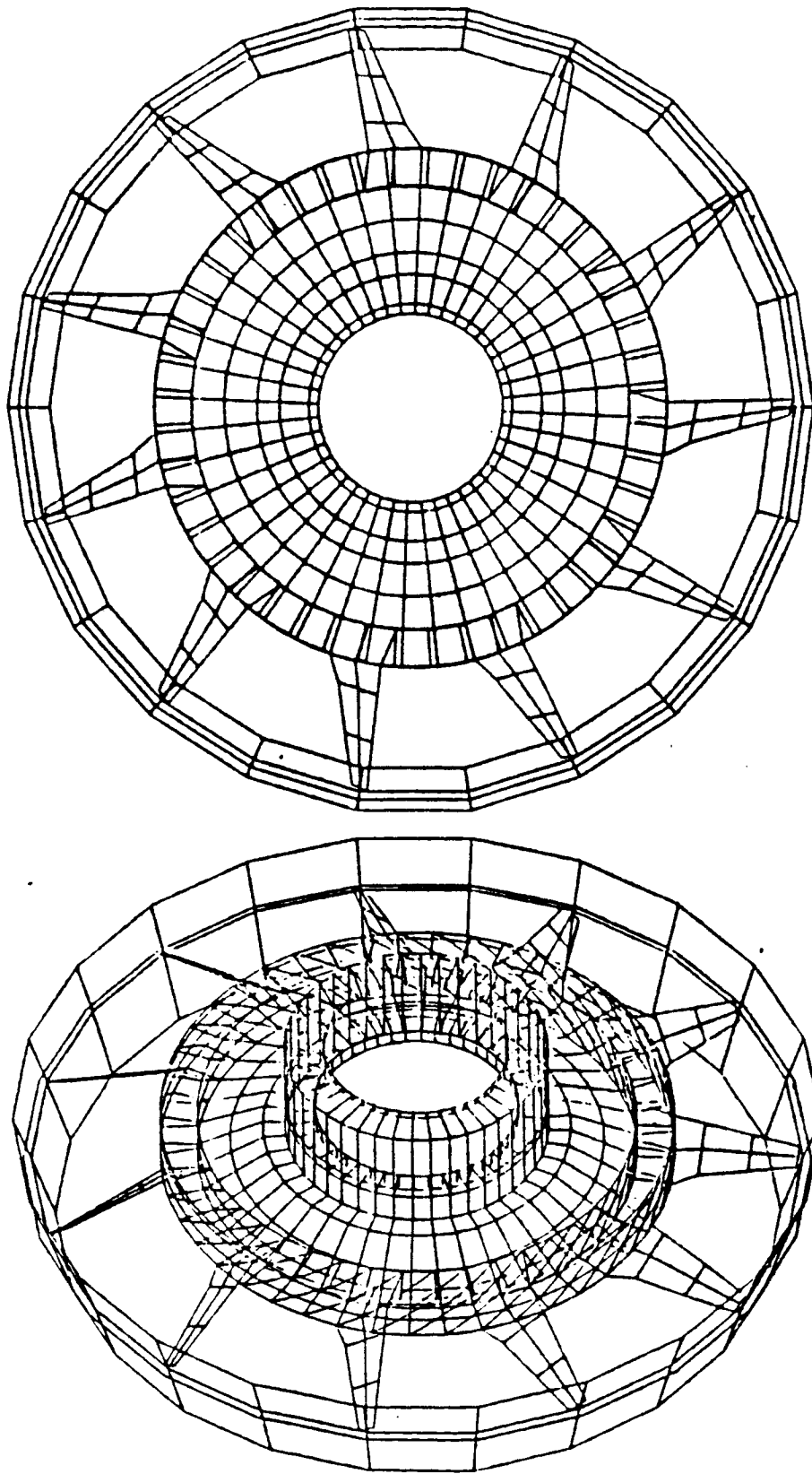


Figure 5.2.3-11 NASTRAN Model used to Analyze Nonaxisymmetric Structural Loads

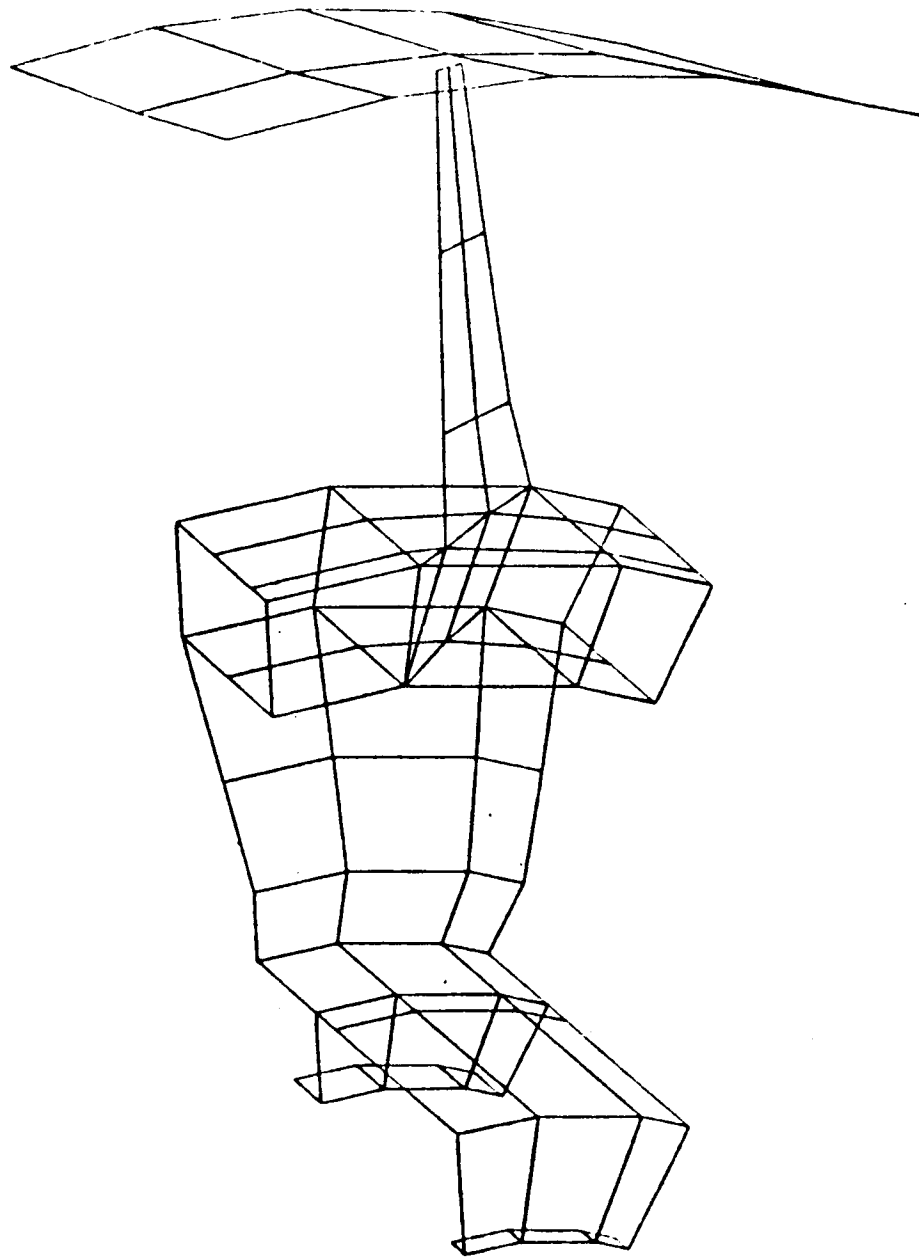


Figure 5.2.3-12 NASTRAN Model used to Analyze Axisymmetric Loads

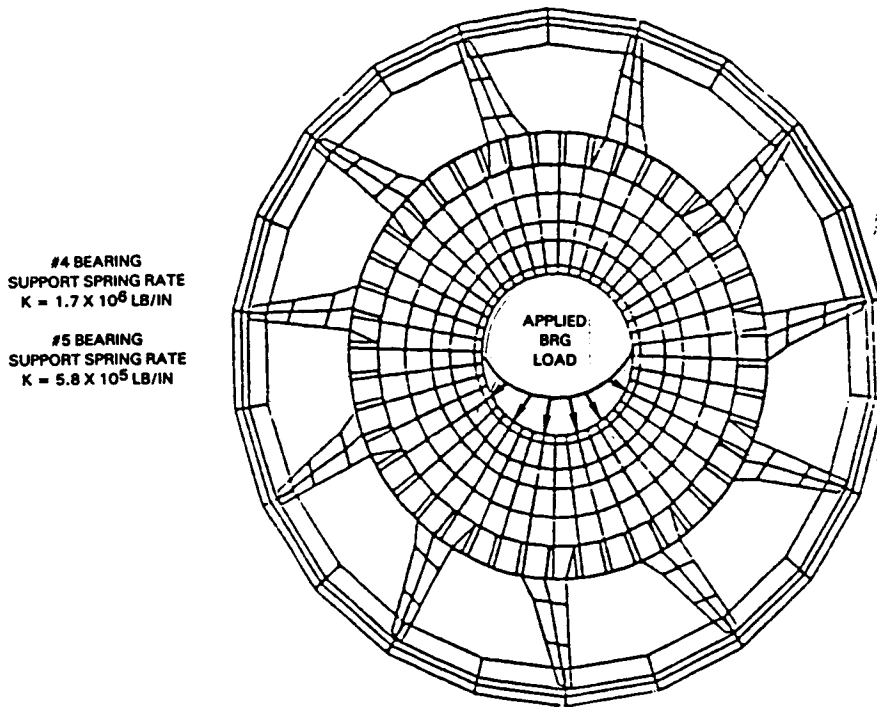


Figure 5.2.3-13 Bearing Load Diagram and Spring Rates Resulting from NASTRAN Analysis

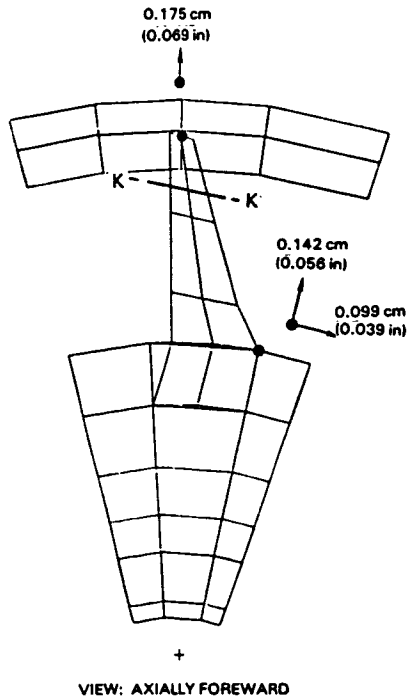


Figure 5.2.3-14 Radial and Circumferential Deflections Caused by Thermal Gradients Between Strut and Cases

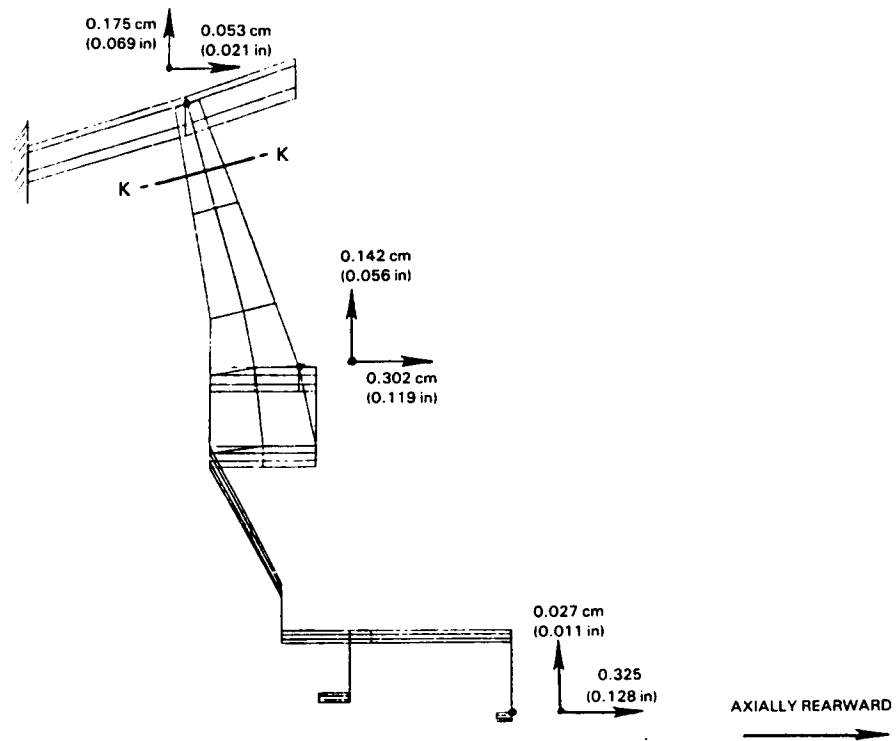


Figure 5.2.3-15 Axial Deflections Caused by Thermal Loads and Thrust Balance Pressure Loads

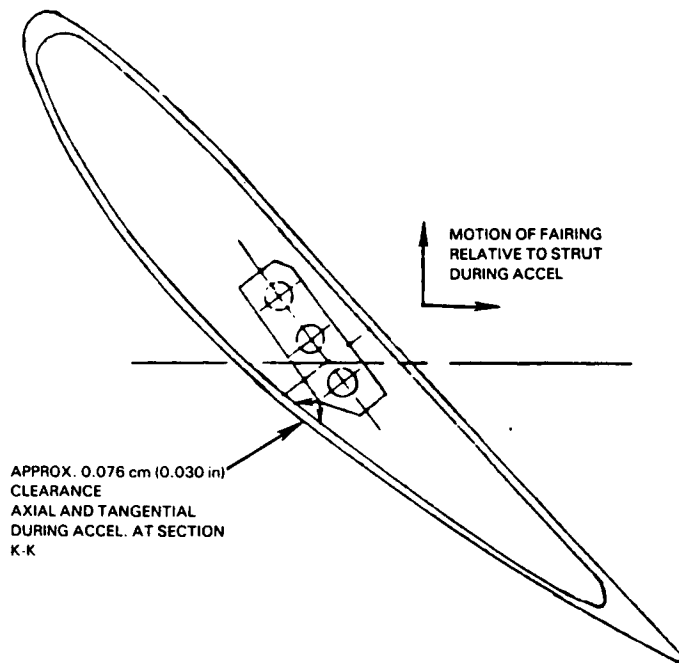


Figure 5.2.3-16 Location of Minimum Clearance Between Structural Strut and Aerodynamic Fairing

Loads in the structural strut, determined from the NASTRAN analysis, were used to determine stresses in the strut. These stresses, together with appropriate stress concentration factors, are summarized in Figure 5.2.3-17. Flight propulsion system structural strut lives at all strut sections are greater than 20,000 cycles and have greater than 30,000 hour capability to 0.1 percent creep. All integrated core/low spool strut lives were found to be greater than the design requirements of 1000 cycles or 50 hours at maximum temperature to 0.1 percent creep.

The struts for the flight propulsion system are bolted to the outer case with 1.2 cm (0.5 in) Inconel 718 bolts, whereas the integrated core/low spool uses 1.112 cm (0.438 in) MP 159 bolts because Inconel 718 bolts are not presently available. The stresses in these tiebolts are summarized in Table 5.2.3-I. The preloads shown were set at a level to prevent separation of the strut from the outer case during "worst-case" normal loads, which occur during engine acceleration.

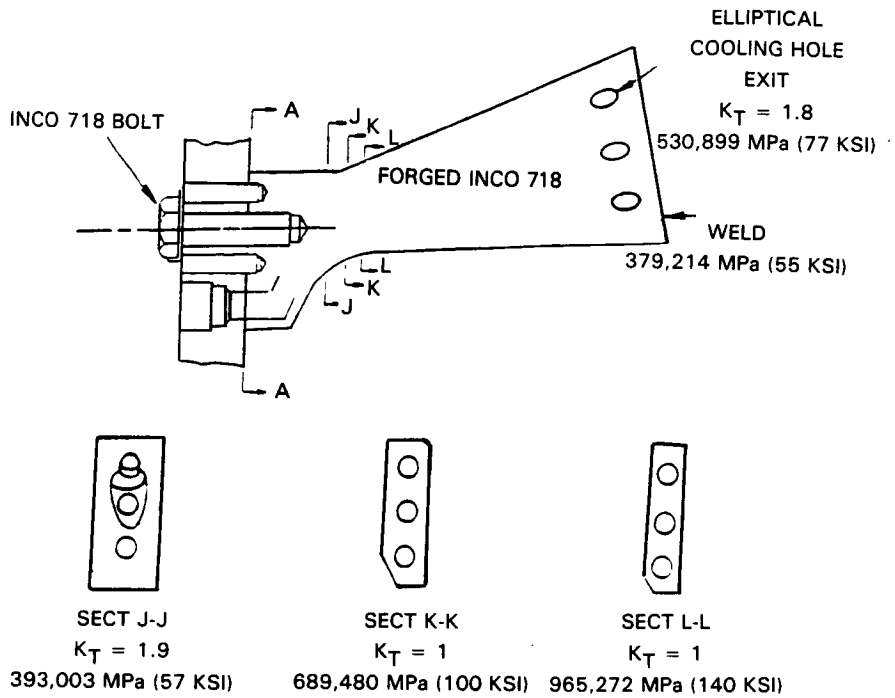
Low-pressure and high-pressure turbine blade loss analyses indicated that the structural strut and tiebolts could successfully resist the imbalance loads caused by the loss of either a high-pressure turbine blade or a fifth-stage low-pressure turbine blade.

5.2.3.2.2 Strut Fairing Durability Analysis

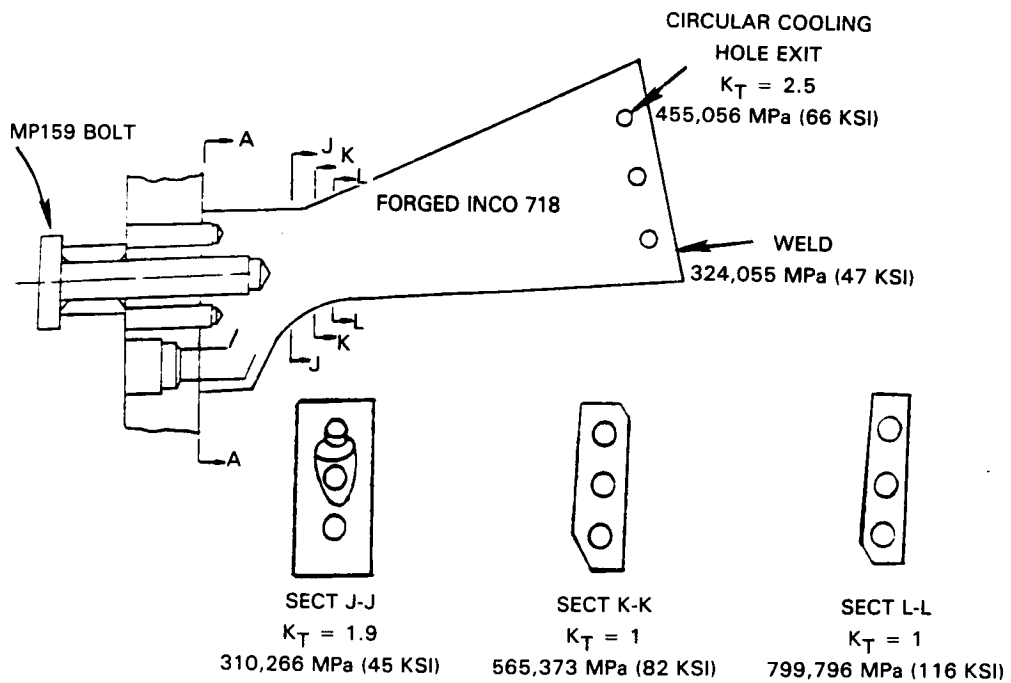
In the durability analysis, the strut fairing was considered in the analysis an airfoil and, therefore, low-pressure turbine airfoil criteria were used. Durability goals for the fairing are 15,000 hours service life (3300 flight missions) in the flight propulsion system and 50 hours of hot life at 28°C (84°F) day sea level takeoff conditions in the integrated core/low spool.

The analysis was conducted using a simplified NASTRAN model, where the fairing airfoil and platforms were assumed to be plate elements, as shown in Figure 5.2.3-18. The loads on the fairing considered in the analysis included: (1) those caused by the differential in pressure distribution between the gaspath and cooling air sides of the fairing, (2) those caused by differential radial growth between adjacent fairing segments, resulting from hot spot thermal loadings on one of the fairings, and (3) those caused by nonuniform temperature distributions on the fairing surface during transient engine operating conditions. The latter would be of concern only in the flight propulsion system, since transient operation is not planned for the integrated core/low spool.

Gaspath parameters assumed for the analysis are summarized in Table 5.2.3-II. The assumed temperature profiles for the integrated core/low spool and flight propulsion system are shown in Figure 5.2.3-19. These profiles reflect combustor exit "hot-spot" conditions as defined in the component preliminary design phase. Figure 5.2.3-20 summarizes the calculated maximum steady stresses for the flight propulsion system strut airfoil fairing. All stresses shown are primarily bending stresses, with the high stress locations predictably at the fillet areas; the inner diameter leading edge fillet (location 2) being highest. Maximum steady stresses calculated for the integrated core/low spool are shown in Figure 5.2.3-21. As with the flight propulsion system, the highest stress is at the inner diameter leading edge fillet. The material used for the integrated core/low spool strut fairing (PWA 647) is expected to undergo local creep deformation from these stresses at hot spot temperature conditions, but this will not be an inhibiting factor in the integrated core/low spool test program.



FLIGHT PROPULSION SYSTEM



INTEGRATED CORE/LOW SPOOL

Figure 5.2.3-17 Structural Strut Stress and Life Summary for Flight Propulsion System and Integrated Core/Low Spool

TABLE 5.2.3-I
STRUT BOLT STRESS SUMMARY

	<u>Flight Propulsion System Inconel 718 Bolt</u>	<u>Integrated Core/Low Spool MP 159 Bolt</u>
Cold Assembly		
Max Direct Tensile	903,218 MPa (131 ksi)	1,241,064 MPa (180 ksi)
Max Shear	592,952 MPa (86 ksi)	827,376 MPa (120 ksi)
Max Principal	1,027,325 MPa (149 ksi)	1,434,118 MPa (208 ksi)
Yield Strength	1,137,642 MPa (165 ksi)	1,654,752 MPa (240 ksi)
Ultimate Strength	1,378,960 MPa (200 ksi)	1,896,070 MPa (275 ksi)
Steady State		
Max Direct Tensile	772,217 MPa (112 ksi)	1,006,640 MPa (146 ksi)
Max Shear	503,320 MPa (73 ksi)	579,163 MPa (84 ksi)
Max Principal	882,534 MPa (128 ksi)	1,082,483 MPa (157 ksi)
Yield Strength	999,746 MPa (145 ksi)	1,378,960 MPa (200 ksi)
Ultimate Strength	1,275,538 MPa (185 ksi)	1,551,330 MPa (225 ksi)
Assembly Preload	6,667 kg (14,700 lbs)	5,896 kg (13,000 lbs)

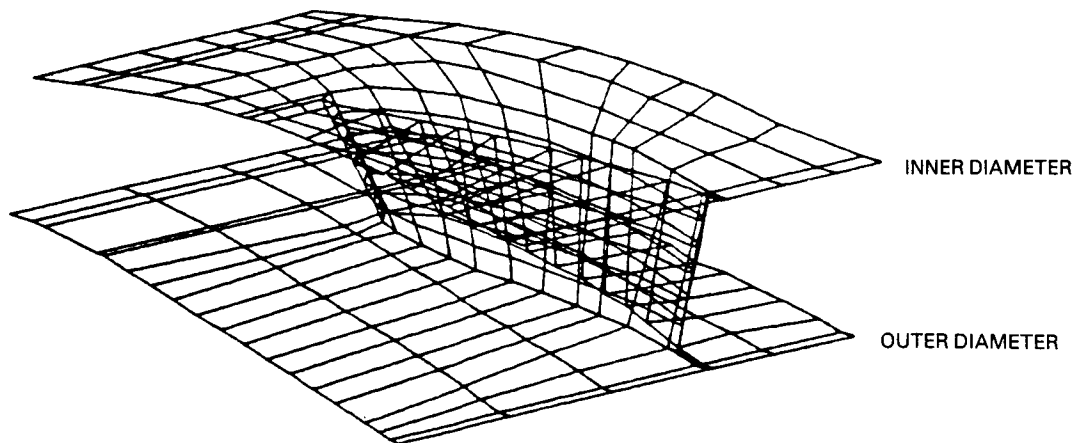


Figure 5.2.3-18 NASTRAN Model Utilized to Conduct Turbine Intermediate Case Strut Fairing Durability Analysis

TABLE 5.2.3-II
GAS ENVIRONMENT DEFINITION

	<u>Flight Propulsion System*</u>	<u>Integrated Core/Low Spool</u>
Combustor Exit		
Average Temperature, °C (°F)	1500 (2733)	1519 (2767)
Design Pattern Factor	0.42	0.42
Strut Fairing		
Average Temperature, °C (°F)	1004 (1840)	1015 (1859)
Design Pattern Factor	0.37	0.37
Hot Streak		
Temperature, °C (°F)	1162 (2125)	1181 (2158)

Note: *Includes Deterioration and Tolerances

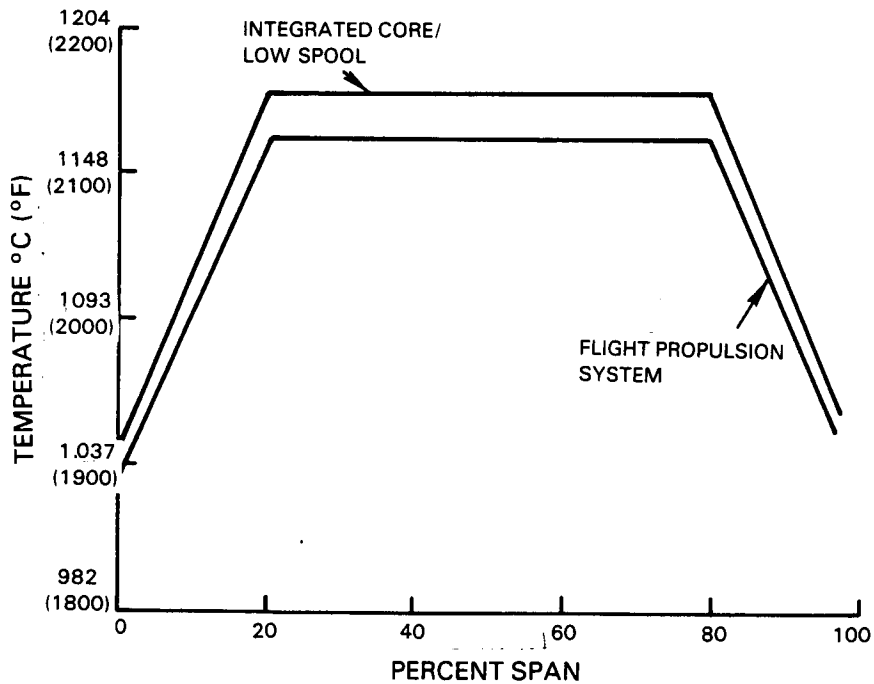


Figure 5.2.3-19 Hot-Spot Temperature Profiles Utilized in Strut Fairing Durability Analysis

LOCATION	CALCULATED STRESS (ELASTIC)		CREEP AT 15,000 HRS (NO RELAXATION)
	PRESSURE LOADS, MPa (ksi)	HOT SPOT, MPa (ksi)	
1. AIRFOIL	35,163 (5.1)	8,963 (1.3)	2%
2. ID FILLET	149,617 (21.7)	36,542 (5.3)	2.5%
3. ID FILLET	47,574 (6.9)	14,479 (2.1)	0.2%
4. OD FILLET	106,869 (15.5)	12,410 (1.8)	1%
5. ID PLATFORM	42,058 (6.1)	17,237 (2.5)	0.1%

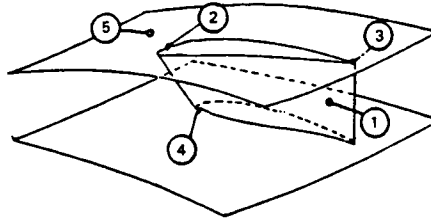


Figure 5.2.3-20 Flight Propulsion System Structural Analysis Summary

LOCATION	CALCULATED STRESS (ELASTIC)		COMMENTS
	PRESSURE LOADS, MPa (ksi)	HOT SPOT, MPa (ksi)	
1. AIRFOIL	36,542 (5.3)	8,963 (1.3)	- LOCAL DEFORMATION AT HOT SPOTS
2. ID FILLET	157,201 (22.8)	36,542 (5.3)	
3. ID FILLET	49,642 (7.2)	14,479 (2.1)	- MAX CREEP < 1.3%
4. OD FILLET	112,385 (16.3)	12,410 (1.8)	- LOCAL DEFORMATION AT HOT SPOTS
5. ID PLATFORM	44,126 (6.4)	17,237 (2.5)	- MAX. CREEP < 1.0%

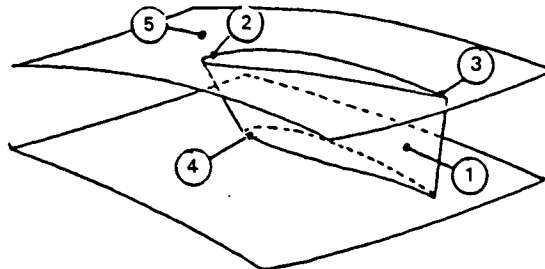


Figure 5.2.3-21 Integrated Core/Low Spool Structural Analysis Summary

The procedure used to calculate transient strains in the flight propulsion system strut fairing is illustrated in Figure 5.2.3.22. Here, the strain cycle for a typical snap acceleration-deceleration transient was calculated using a standard beam analysis. Results of this analysis were then adjusted to match strain results from the more sophisticated NASTRAN analysis. This matching was done at the most critical location (inner diameter leading-edge fillet) in order to obtain a conservative transient strain range estimate. The adjusted beam analysis procedure could then be utilized for the remainder of the analyses. The results of this analysis are summarized in Figure 5.2.3-23.

Predicted lives, based on these analyses, are summarized in Table 5.2.3-III, which indicates that durability goals can all be met with one recoating of the flight propulsion system fairing. Operation of the integrated core/low spool parts without a recoating does not present a failure risk, but as noted earlier, some local deformation can be expected in hot spot regions.

Sample stress and deflection contours for the strut fairing platform and air-foil sections, which were calculated as part of the NASTRAN analysis, are shown in Appendixes A and B.

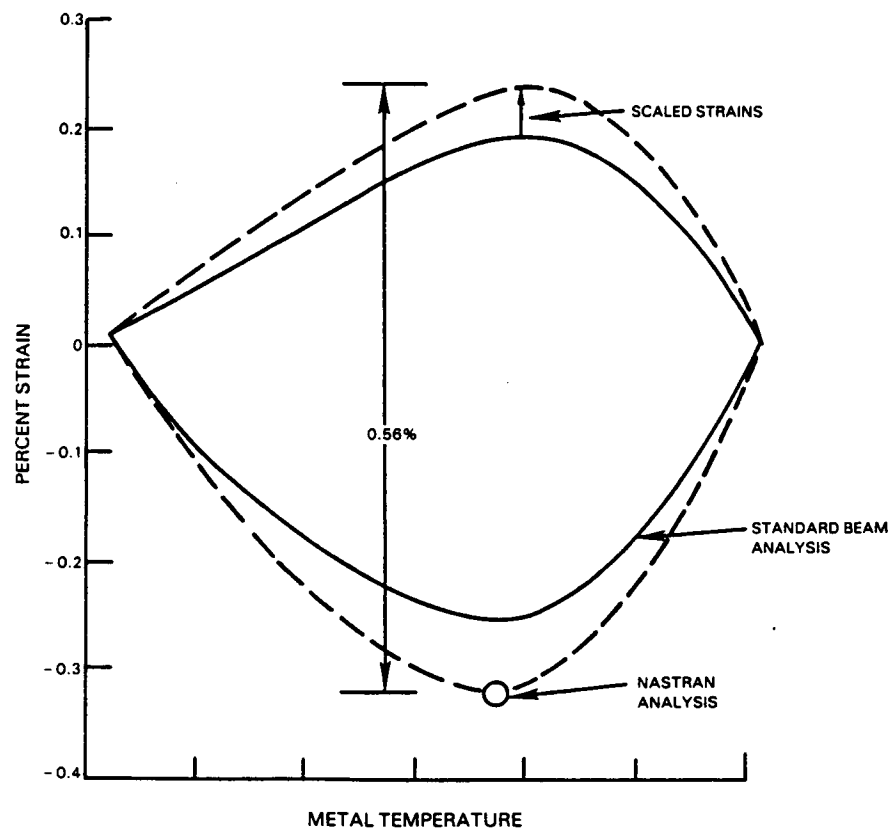


Figure 5.2.3-22 Illustration of Flight Propulsion System Strut Fairing Transient Strain Calculation Procedure

<u>LOCATION</u>	<u>STRAIN RANGE</u>
1. AIRFOIL	0.27%
2. ID FILLET	0.56%
3. OD FILLET	0.39%
4. ID PLATFORM	0.53%

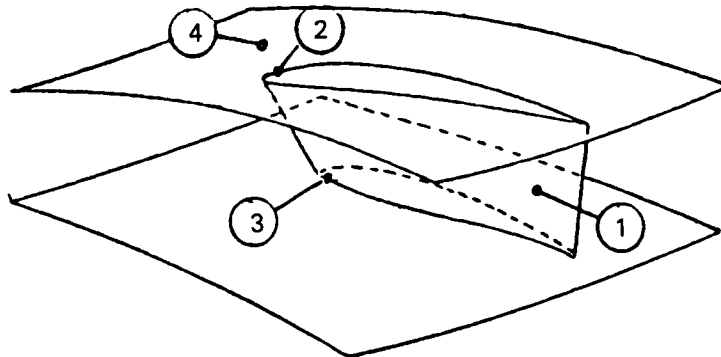


Figure 5.2.3-23 Summary of Flight Propulsion System Strut Fairing Transient Strains at Maximum Stress Locations

TABLE 5.2.3-III
PREDICTED LIVES

FLIGHT PROPULSION SYSTEM

Cracking	23,000 Hours (5100 Flights)
Coating Oxidation	9300 Hours (Life 15,000 hours with one recoating)

INTEGRATED CORE/LOW SPOOL

Coating Oxidation	90 hours
-------------------	----------

5.2.3.2.3 Thrust Balance Seal Vibration Analysis

Frequency response analysis of the front thrust balance seal assembly was conducted as part of the high-pressure turbine component design and analysis effort. Results of that analysis indicated that margins for resonance and coincidence met or exceeded commercial requirements and that operation would be flutter-free. Results for the rear thrust balance seal assembly are summarized in Section 5.2.1.3.2.

5.2.4 Low Rotor Critical Speed Analysis

The low-pressure rotor comprises the fan, low-pressure compressor, low-pressure turbine, and the shaft connecting these components. The rotor is supported by three bearings, as illustrated in Figure 5.2.4-1. The two front bearings, located at the fan intermediate case, provide moment restraint for the overhung fan/low-pressure compressor assembly to minimize maneuver deflections. The low-pressure turbine is cantilevered off a rear bearing, which is damped to control the low-pressure turbine mode. For analysis purposes, the entire engine rotor and case structure was modeled as a system of beams that simulated the high and low rotor, the core cases, and the inner and outer fan ducts. These were connected by a series of linear and torsional springs which duplicated the stiffness of the bearings and bearing support structures. In this way, the rotor-frame model, illustrated in Figure 5.2.4-2, was able to account for vibratory interaction between components. Critical speed design goals for the low rotor were to position the low strain energy fan and low-pressure turbine modes below minimum cruise speed, and the high strain energy shaft bending mode above redline speed to provide a mode-free running range.

During the component preliminary design effort, critical speed analysis indicated that the fan and low-pressure turbine modes were below minimum cruise speed and that both had low strain energy (less than 15 percent). The shaft bending mode, although indicating high strain energy, occurred well above maximum low rotor speed (67 percent margin). All low rotor bearings at this time were undamped. Results of this early analysis are summarized in Figure 5.2.4-3.

As the low rotor design evolved and components weights and structural spring-rates became better defined, strain energy in the low-pressure turbine mode increased, as shown in Figure 5.2.4-4. This raised a concern because of the sensitivity of this mode to rotor imbalance. A viscous oil-film damper was subsequently incorporated into the number 5 bearing design to control the low-pressure turbine mode response. Addition of this damper has the following effects, which are illustrated in Figure 5.2.4-5.

1. Shaft bending strain remained at its initial level, but the bending mode margin above maximum low rotor speed dropped from 67 percent to 25 percent -- still an acceptable margin.
2. Fan mode strain energy dropped to 7 percent, while fan mode speed increased.
3. Low-pressure turbine mode speed was reduced and strain energy was reduced to 14 percent.

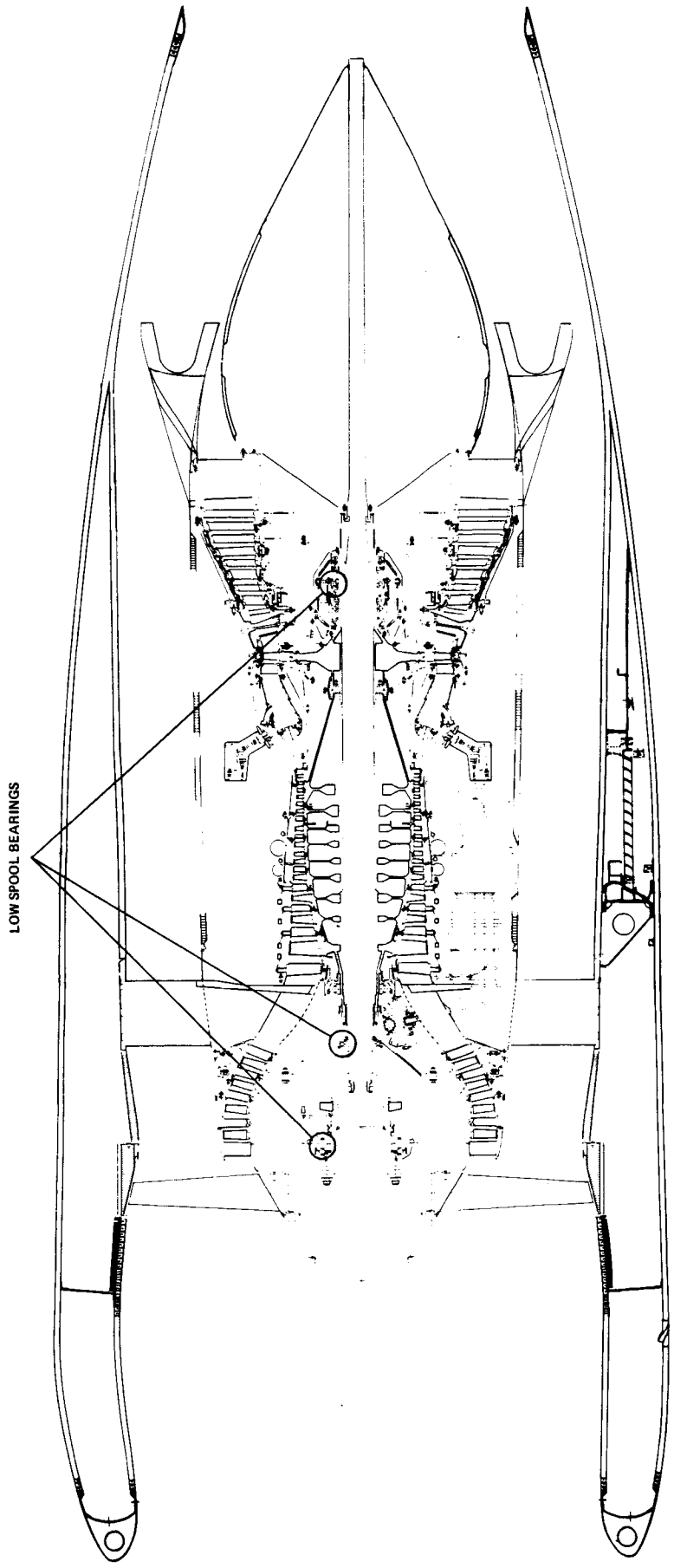


Figure 5.2.4-1 Low Rotor Bearing Locations

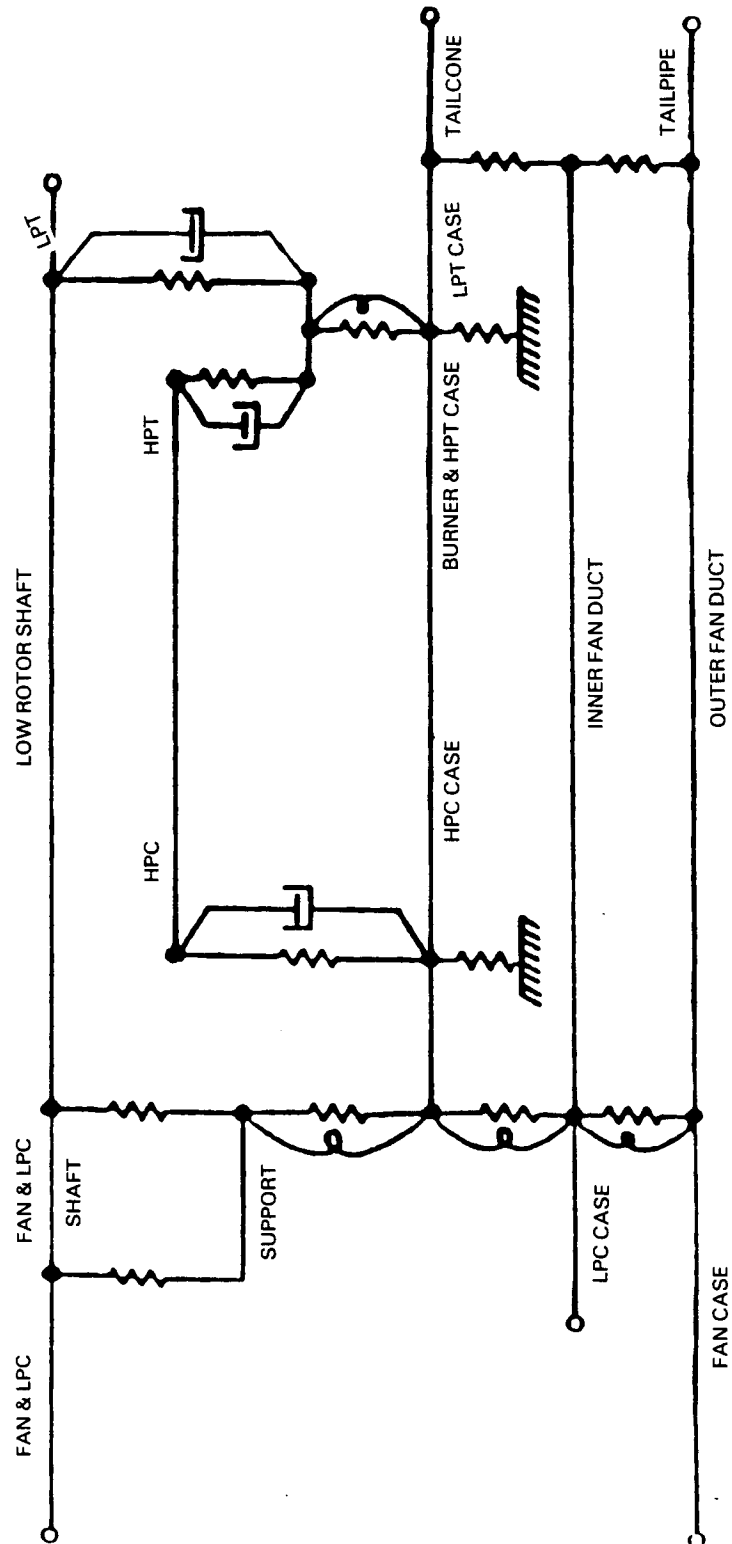


Figure 5.2.4-2 Rotor-Frame Model Used for Critical Speed Analysis

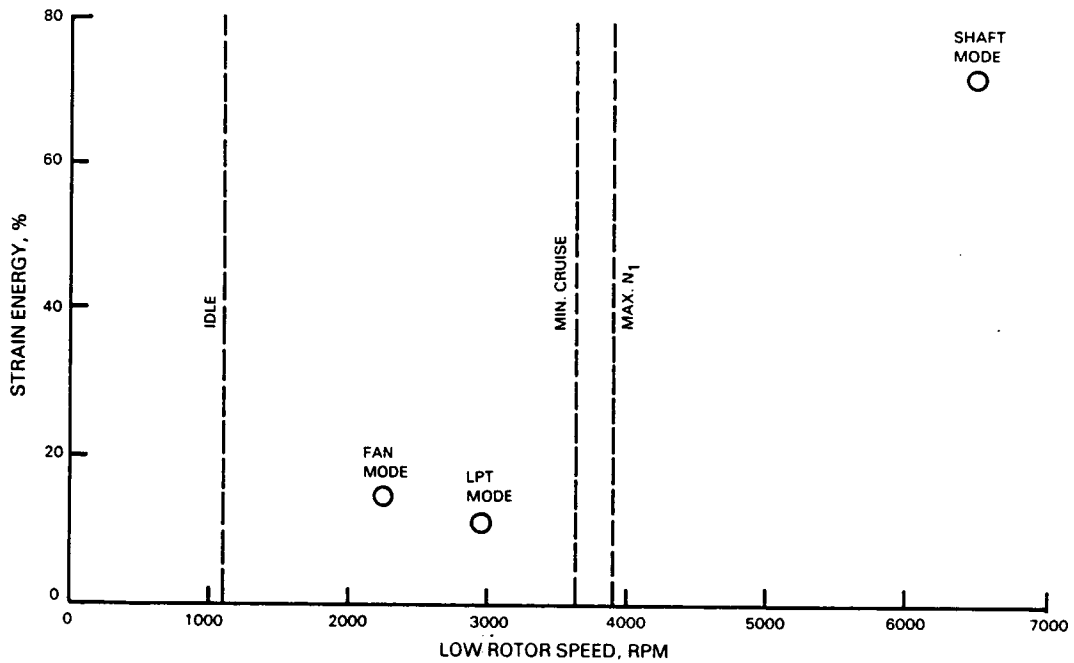


Figure 5.2.4-3 Strain Energy Results from Component Preliminary Design Critical Speed Analysis

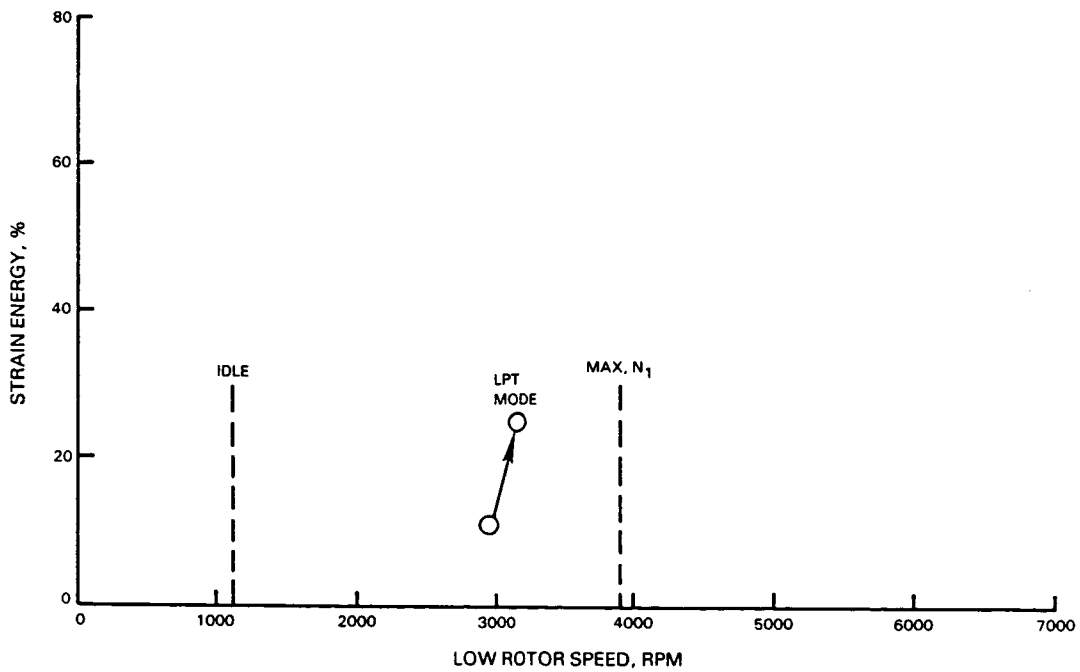


Figure 5.2.4-4 Increase in Low-Pressure Turbine Mode Strain Energy as Low Rotor Design Evolved

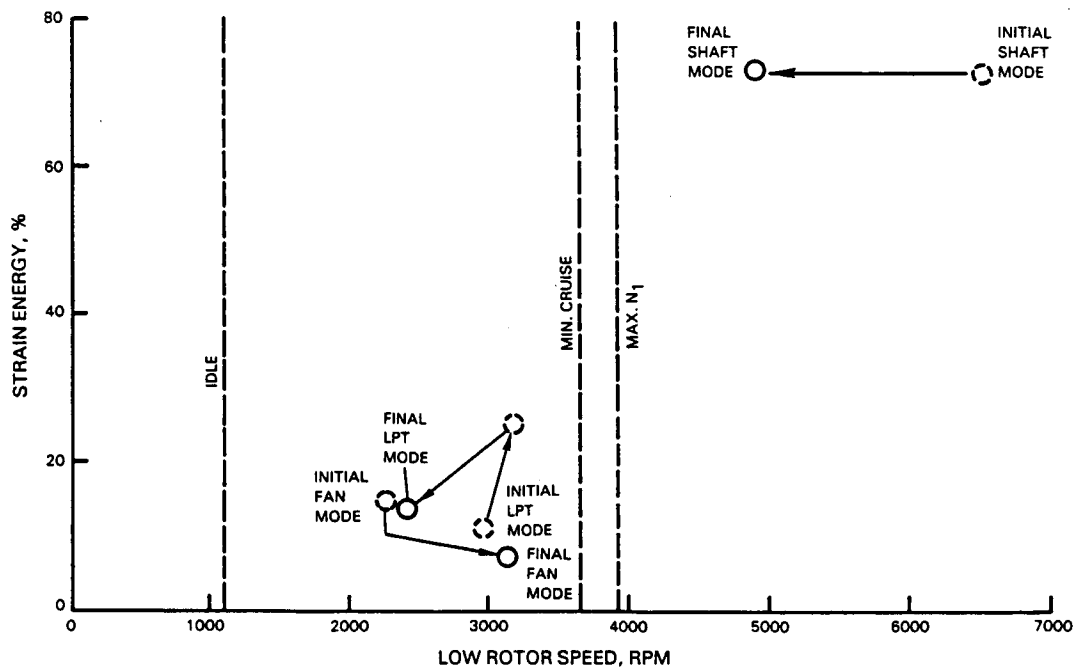


Figure 5.2.4-5 Effects on Fan, Low-Pressure Compressor and Shaft Mode Responses Due to the Addition of an Oil-Film Damper to the Number 5 Bearing

The effectiveness of this damper in controlling low-pressure turbine mode response is also shown in Figure 5.2.4-6, where the relative amplitude is based on an arbitrary amount of induced rotor imbalance.

Results of the critical speed analysis for the integrated core/low spool and flight propulsion system are summarized in Figure 5.2.4-7. No high strain energy modes are anticipated in the range of operating speeds. The fan and low-pressure turbine modes have low strain energy and occur below minimum cruise speed. The high strain energy shaft bending mode occurs above maximum low rotor speed with an acceptable margin. Resultant mode shapes for the integrated core/low spool are presented in Figures 5.2.4-8, -9 and -10.

5.2.5 Low-Pressure Turbine Secondary Flow System

5.2.5.1 System Description

The low-pressure turbine secondary flow system shown in Figure 5.2.5-1, is designed to provide maximum utilization of secondary airflow required for cooling and active clearance control. Major sources of low-pressure turbine cooling air are:

1. 1.07 percent of core engine airflow from high-pressure turbine disk bore cooling; (source: twelfth stage high-pressure compressor and fifteenth stage high-pressure compressor inner bleeds)
2. 0.22 percent of core engine airflow from high-pressure turbine active clearance control system; (source: tenth stage high-pressure compressor/fifteenth stage high-pressure compressor mixture)

3. 0.35 percent of core engine airflow from turbine intermediate case strut cooling; (source: tenth stage high-pressure compressor outer bleed)
4. 1.00 percent of core engine airflow from low-pressure turbine case cooling and active clearance control; (source: tenth stage high-pressure compressor mixture)

TOTAL = 2.64 percent airflow

The rotor, case and turbine intermediate case incorporate specific features to best utilize this cooling air. They are described in the following sections.

5.2.5.2 Low-Pressure Turbine Rotor

The major features of the rotor cooling air distribution system are:

- o A pressure-balanced system independent of rim seal clearances.
- o A-frame rotor construction that provides uniform cooling flow to the disk rims.
- o Individually metered cooling air to disk rims.
- o Rim shields to thermally isolate disk-blade attachments from rim cavities.
- o Flow guides to minimize hot gas ingestion and recirculation.

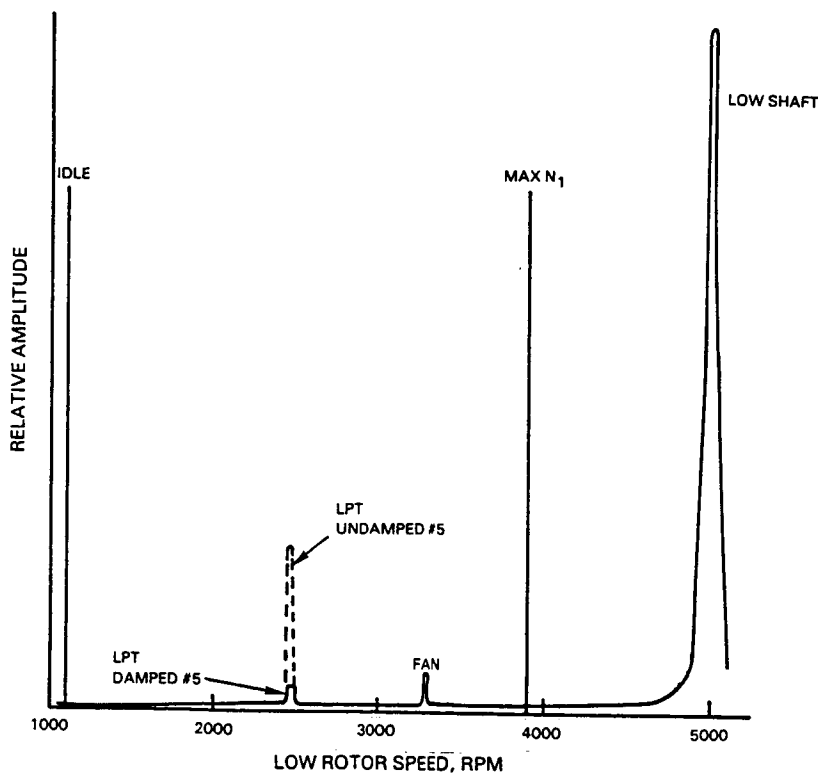


Figure 5.2.4-6 Illustration Showing Effectiveness of Damped Number 5 Bearing in Reducing Low-Pressure Turbine Mode Imbalance Response

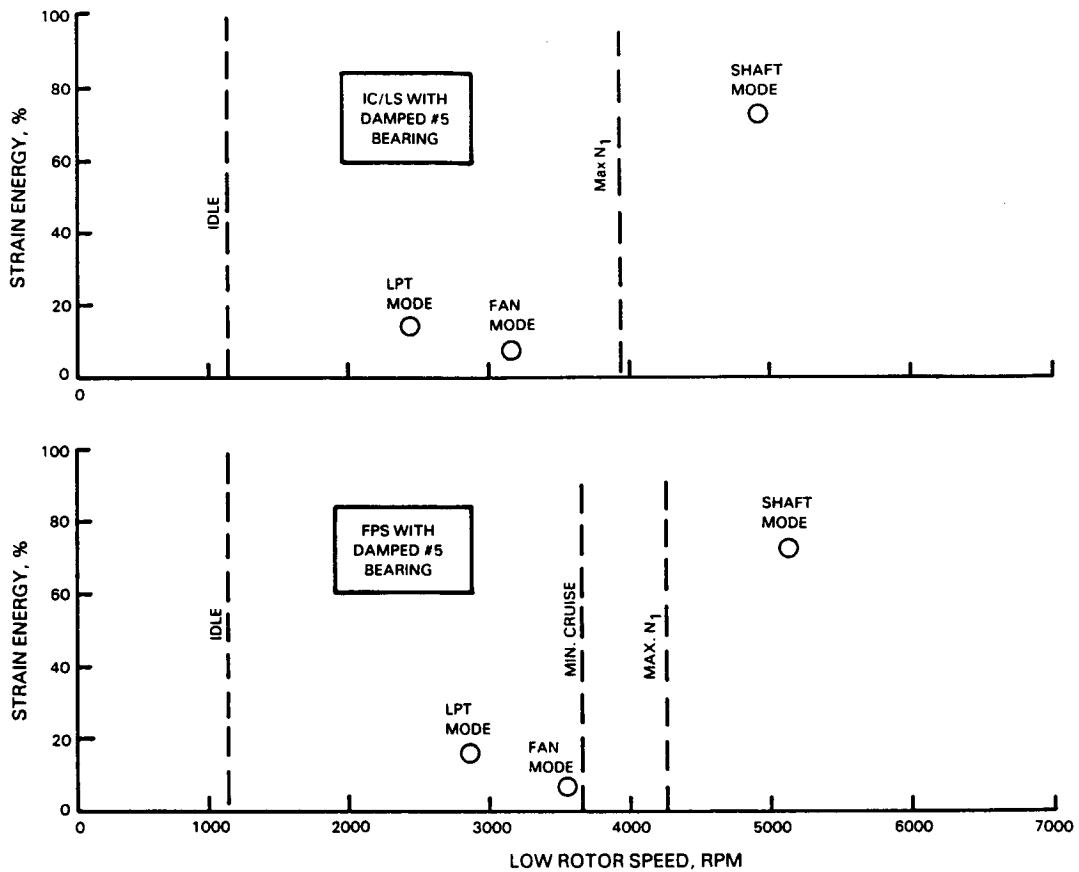


Figure 5.2.4-7 Summary of Critical Speed Analysis Results for Integrated Core/Low Spool and Flight Propulsion System

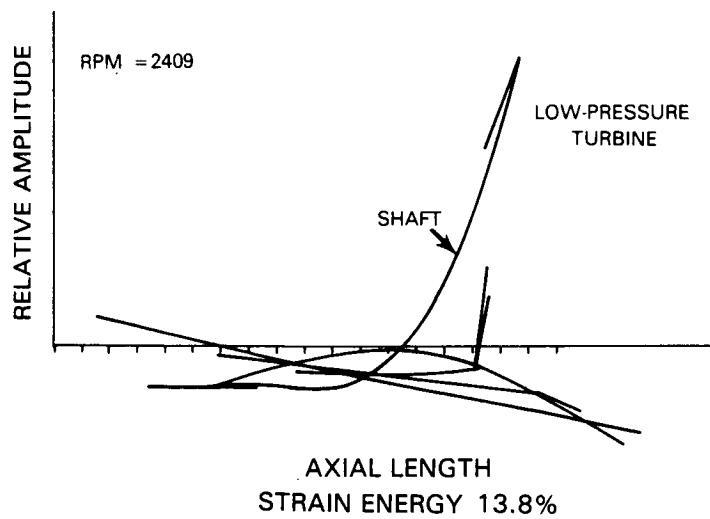


Figure 5.2.4-8 Mode Shape for Integrated Core/Low Spool Low-Pressure Turbine Mode -- Damped Number 5 Bearings

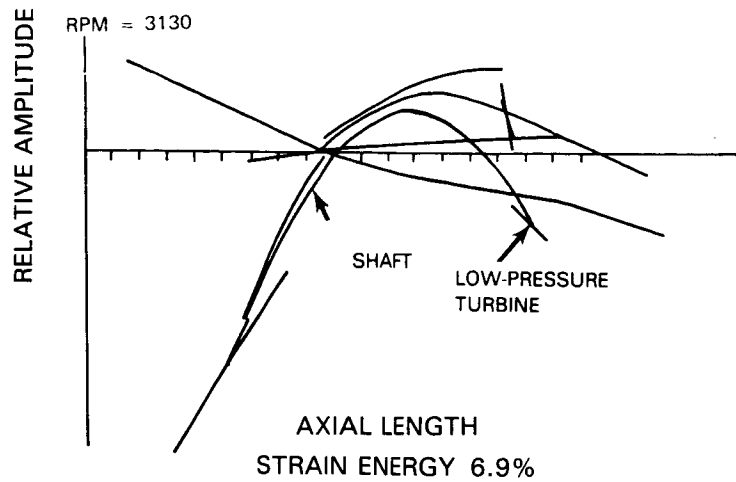


Figure 5.2.4-9 Mode Shape for Integrated Core/Low Spool Fan Mode -- Damped Number 5 Bearing

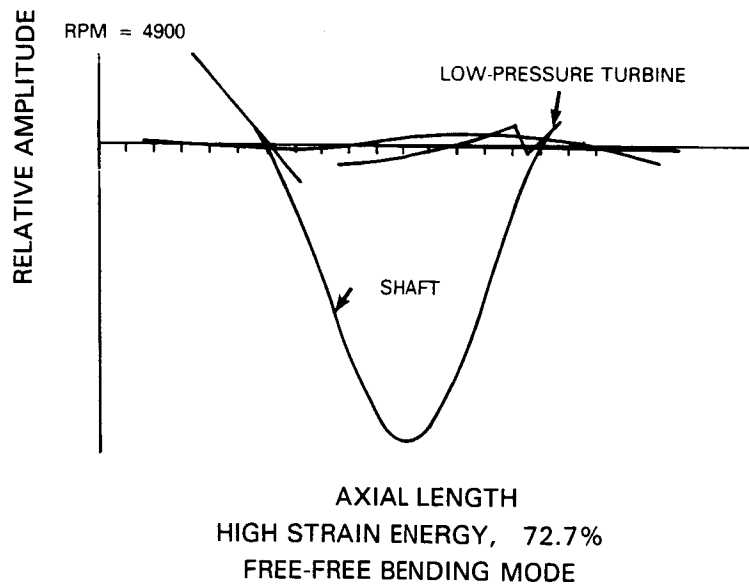


Figure 5.2.4-10 Mode Shape for Integrated Core/Low Spool Shaft Mode -- Damped Number 5 Bearing

The major elements of the pressure-balanced system are shown in Figure 5.2.5-2. Holes at the rear of the strut accurately meter 0.83 percent of core engine airflow for cooling flow into the cavity bounded by the strut, the rear thrust balance seal, and the second stage turbine disk rim. 0.44 percent of this air leaks past the thrust balance seal and is used to cool the low-pressure turbine bore. 0.26 percent of the remaining air passes through holes in the disk rim shield and serves to cool the blade attachment before being spent in the disk rim rear cavity, where it effectively reduces the temperature in the cavity to less than 732°C (1350°F). The disk rim shield protects the disk rim from gaspath temperatures and incorporates a "fishmouth" seal, which prevents hot gaspath ingestion back into the inner cavity. A small amount of flow (0.13 percent of core engine airflow) is permitted to leak past this seal to maintain the pressure between the gaspath and the inner cavity. One of the advantages of this system of flow control is that extremely well controlled rim seal clearances are not required.

A portion of the low-pressure turbine bore cooling airflow is introduced at the base of the A-frame and is metered to the third and fourth stage disk rims to cool the attachments, as shown in Figure 5.2.5-3. As the air flows radially outward toward the metering holes, a free-vortex flow field is established that efficiently maintains a positive pressure gradient across the metering holes. The split between the metered flows reflects the temperature exposure of the third and fourth stage turbine disks. As shown in the figure, spent attachment cooling air is exhausted into the downstream rim cavities and serves to reduce cavity temperatures.

For structural and life purposes, it was desirable to maintain the third and fourth stage disk 'wing' support structures at the lowest possible temperature. This was accomplished through the use of spent disk rim attachment cooling air, disk rim shields, and disk rim flow guides, as shown in Figure 5.2.5-4. The amount of hot gas ingested into the rim cavity is directly proportional to the amount of leakage past the inner airseal. Therefore, a three knife-edge, stepped seal was incorporated to minimize this leakage. Spent rim attachment cooling air from the upstream disk mixes with the ingested gas to effectively reduce its temperature. The knife-edge support structure functions as a temperature shield between the rim cavity and disk rim support structure.

Steady-state and transient thermal analyses of the rotor were conducted to verify the effectiveness of the cooling flow distribution system in controlling rotor structure temperature. A steady-state thermal analysis of the flight propulsion system rotor at sea level takeoff hot day +29°C (+84°F) engine operating conditions indicated a high degree of uniformity in disk and spacer temperatures as well as effective shielding of the rim cavities from gaspath temperatures. This can be seen in the finite element model results shown in Figure 5.2.5-5. Temperatures shown would be approximately +17°C (+30°F) higher for the integrated core/low spool.

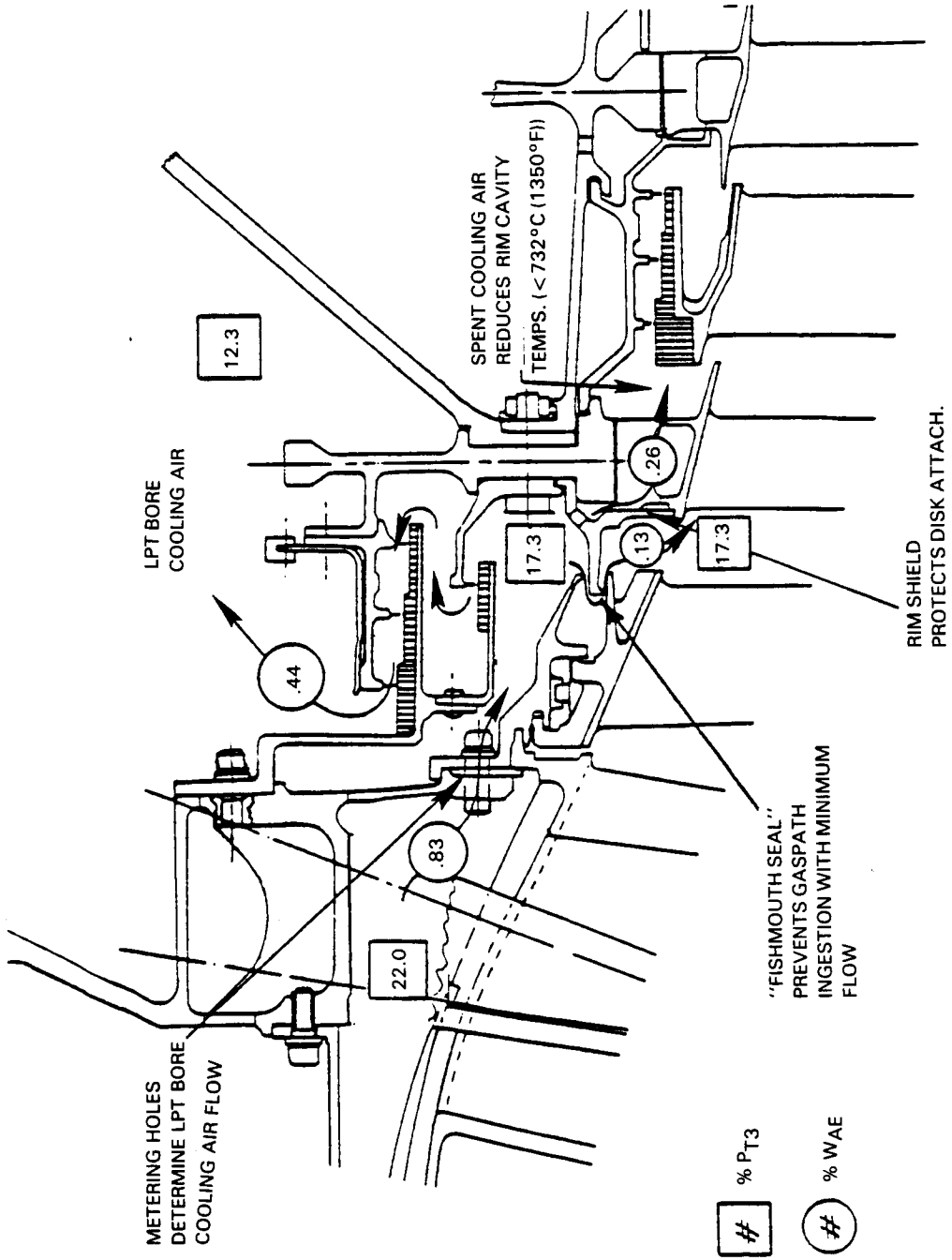


Figure 5.2.5-2 Pressure-Balanced Cooling Air Distribution System

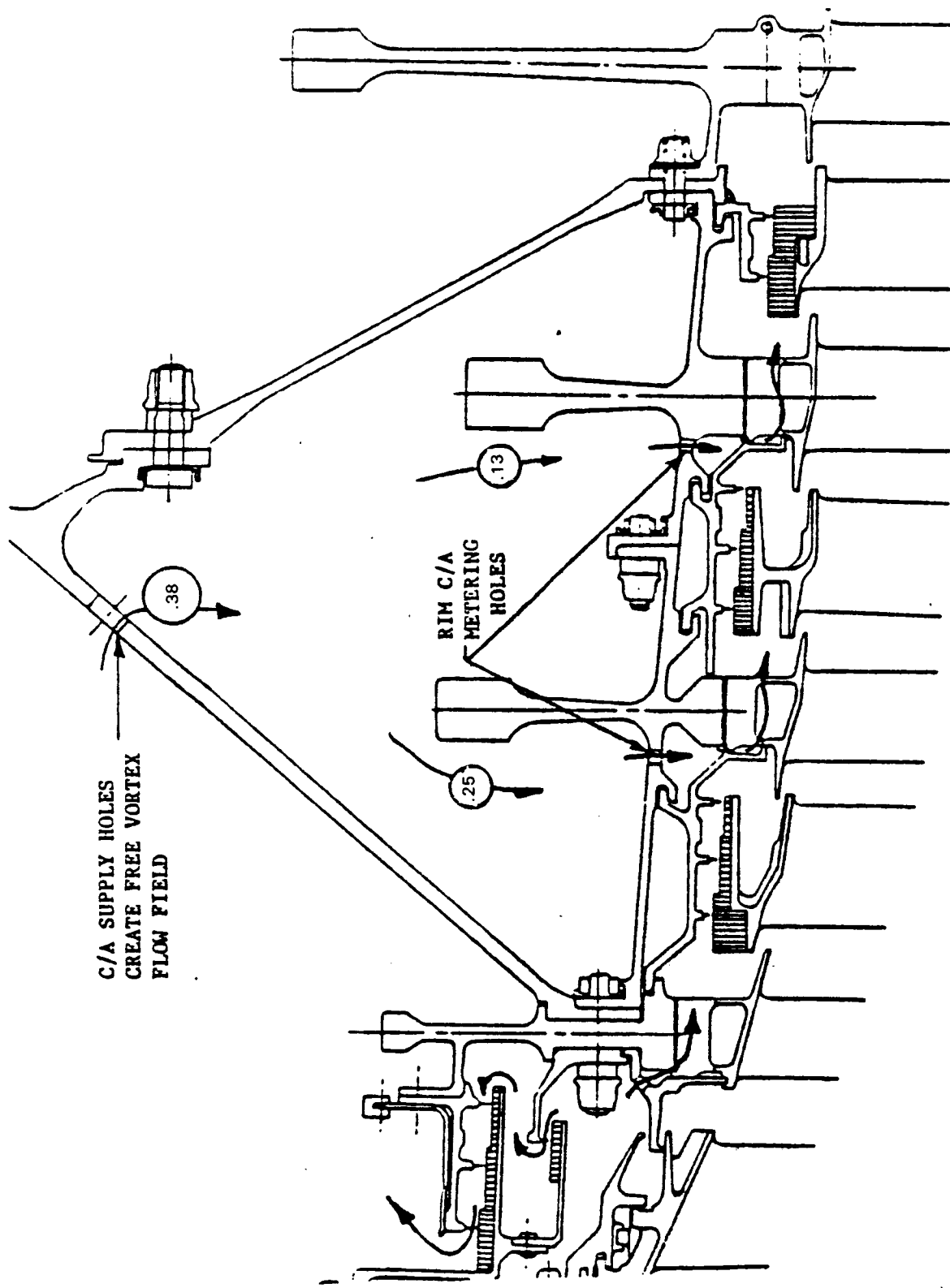


Figure 5.2.5-3 A-Frame Rotor Construction Showing Turbine Rim Cooling Air Flow Distribution

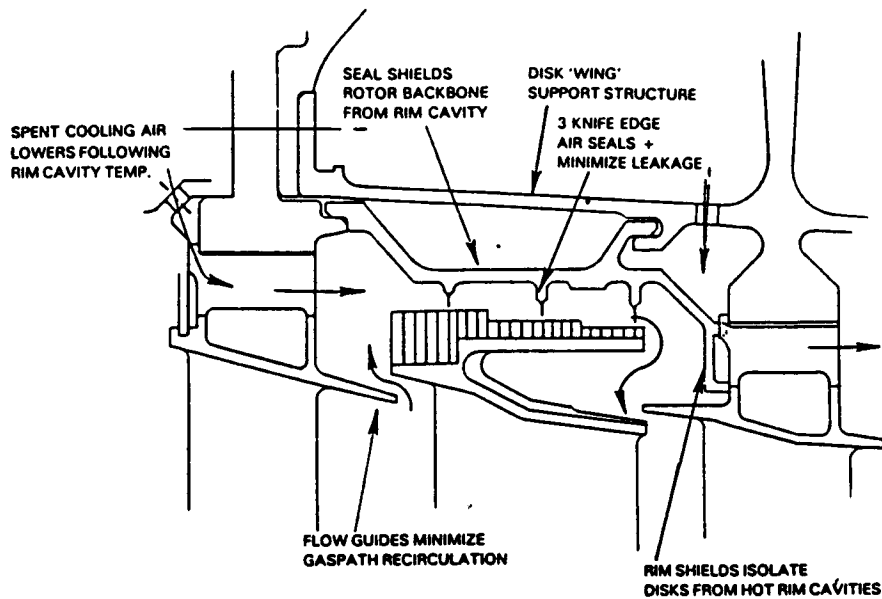


Figure 5.2.5-4 Disk Rim and 'Wing' Support Structure Cooling Scheme

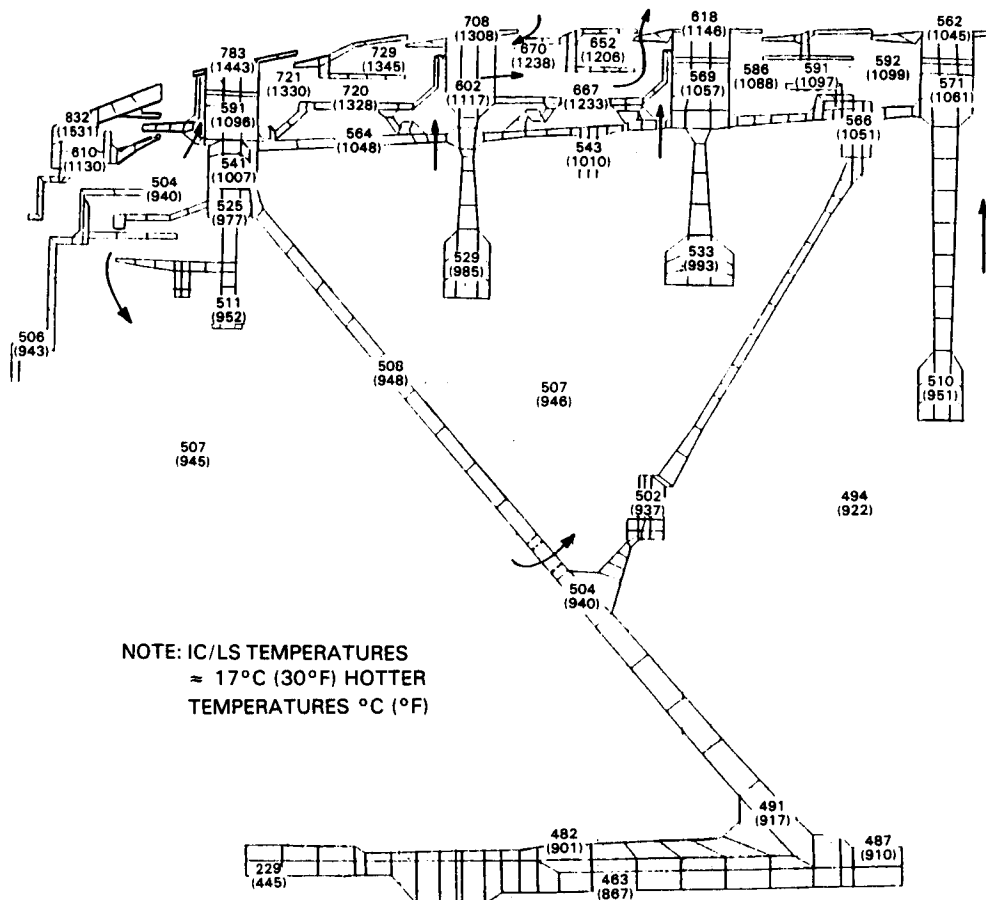


Figure 5.2.5-5 Rotor Finite Element Model Showing Temperature Distribution at Steady-State Sea Level Takeoff Hot Day Engine Operating Conditions

A transient thermal response analysis was conducted for the second and fourth stage disks to determine the thermal gradients imposed on the disk during severe power excursions (i.e., 6 seconds from steady state idle to steady state sea level takeoff power and then back to idle). The second stage disk was selected because it is exposed to the highest temperatures. The fourth stage disk was selected to assess the transient response of a disk within the A-frame. Results of this analysis are presented in the temperature-time histories shown in Figures 5.2.5-6 and -7, where the temperature gradients at the noted disk locations are represented by the slopes of the curves. Differences between curve shapes are an indication of the thermal "fight" going on at the noted disk locations with the exception of the snap deceleration region the curves exhibit similar characteristics. Even in this region, the thermal gradients were within design limits. The analysis, therefore, verified that the thermal gradients in the second and fourth stage disks were well within design limit. It also verified the benefits of the free vortex flow field generated by the A-frame in minimizing fourth stage disk thermal gradient.

5.2.5.3 Low-Pressure Turbine Case

Major features of the case cooling air distribution system are:

- o A combined cooling air and active clearance control system approach to minimize total flow requirements.
- o Thermal isolation of the structural case from the hot gaspath.
- o Cooling airflows metered through drilled holes - independent of part-to-part tolerances.
- o Circumferential staggering of vane and airseal segment gaps to ensure minimum leakage.
- o An active clearance control shield-to-case flow passage tailored to each stage for optimum thermal response.
- o Temperature modulation of active clearance control air to provide minimum blade tip clearance.

The primary function of the case cooling air distribution system, shown schematically in Figure 5.2.5-8, is to provide case temperature modulation for blade tip active clearance control. Adjustment to the blade tip clearances are accomplished by controlling the temperatures of the inner case hooks. A double wall case construction facilitates this inasmuch as the outer case functions as a cooling air manifold from which air is taken to cool the individual hooks. Referring to Figure 5.2.5-8, high-pressure bleed air enters the case manifold and is channeled through a passage created by the inner case and a segmented baffle. This air has a dual function. It first cools the inner case structure and is then fed through metering holes in the case to cool the individual case hooks, as shown in Figure 5.2.5-9. Through this metering technique, the cooling airflow distribution becomes independent of part-to-part tolerances.

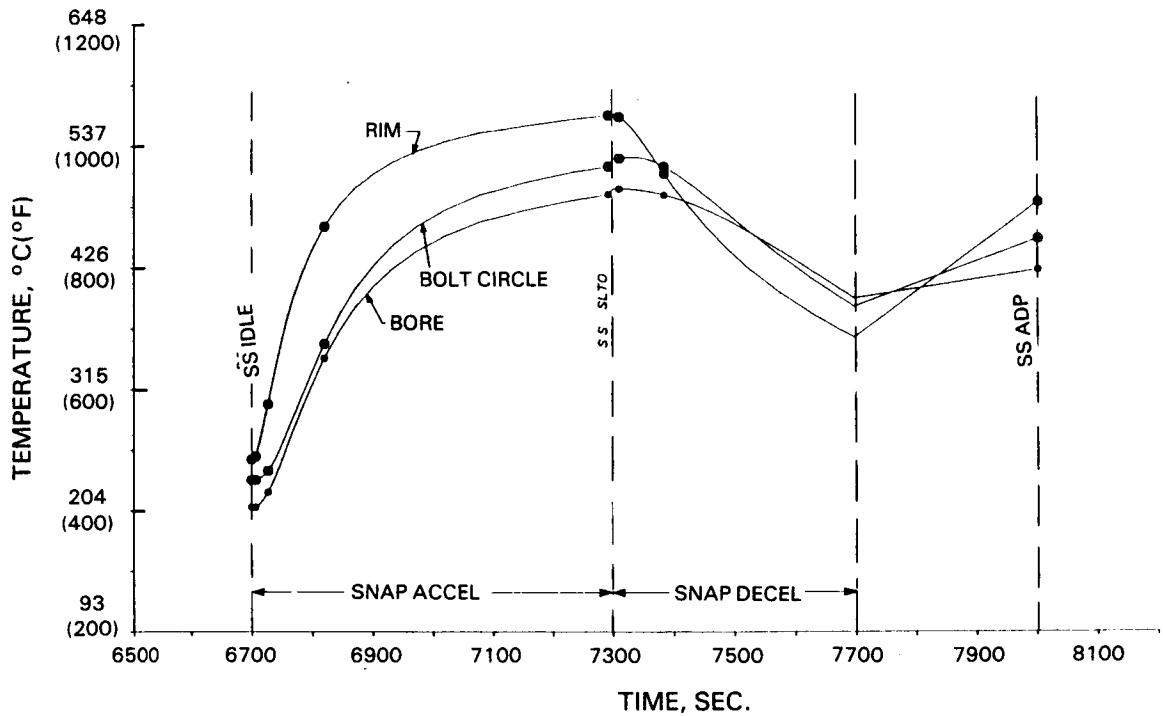


Figure 5.2.5-6 Temperature Versus Time History at Selected Second Stage Low-Pressure Turbine Disk Locations During Severe Engine Power Excursions

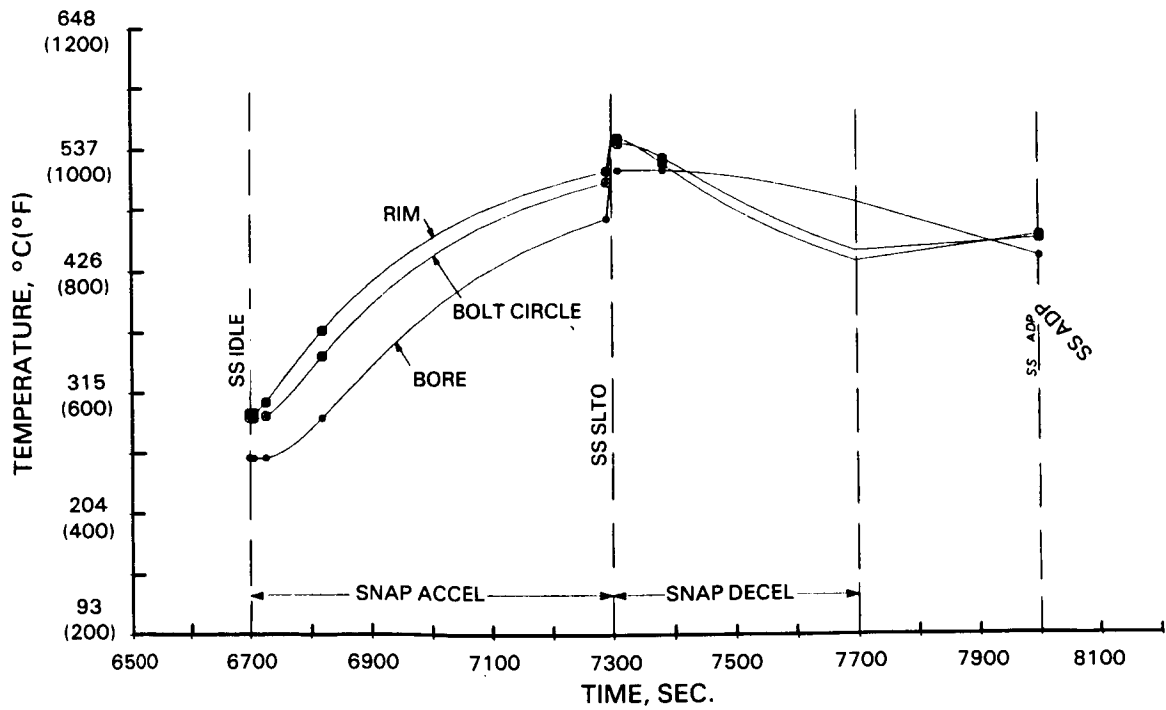


Figure 5.2.5-7 Temperature Versus Time History at Selected Fourth Stage Low-Pressure Turbine Disk Locations During Severe Engine Power Excursions

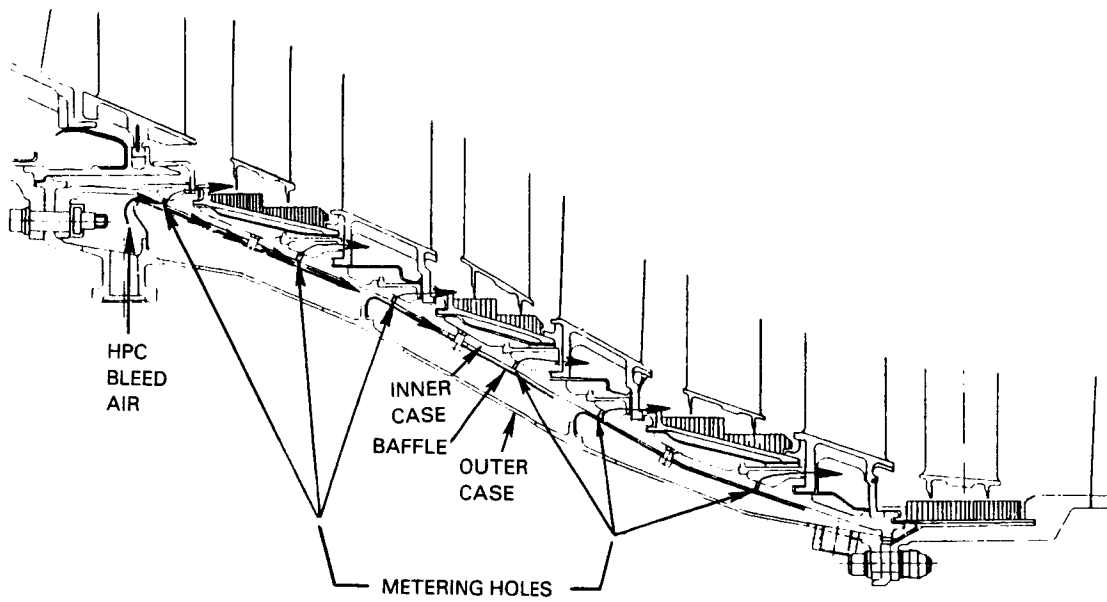


Figure 5.2.5-8 Low-Pressure Turbine Case Cooling Flow Distribution System

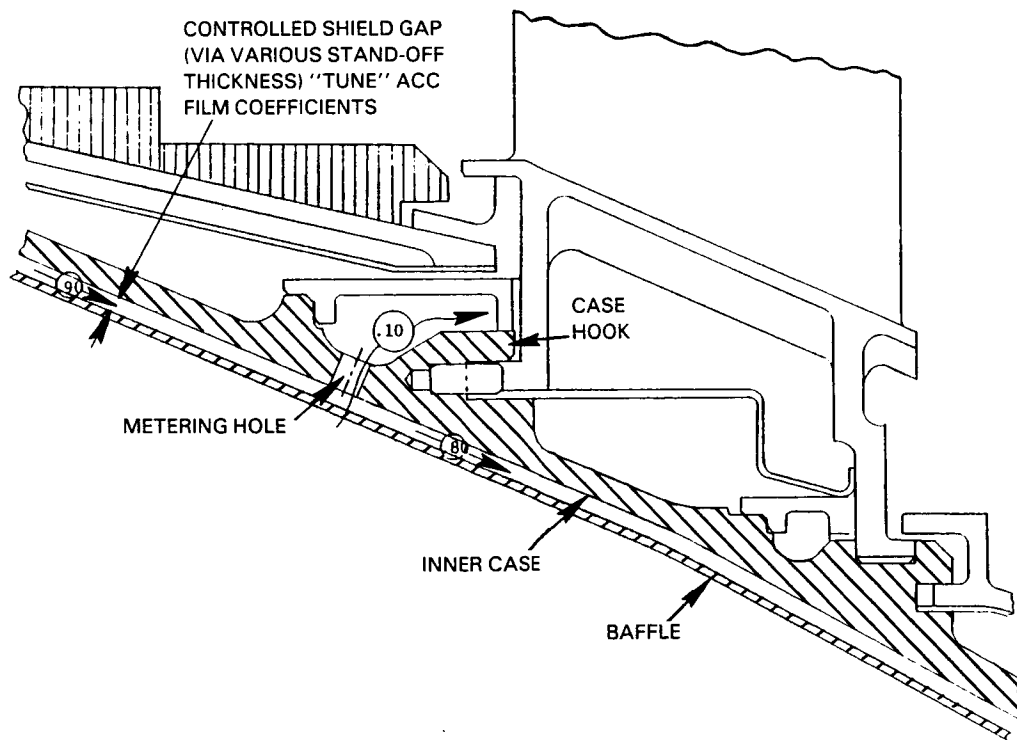


Figure 5.2.5-9 Details of Case Hook Cooling Configuration

Temperature variation in the inner case and case hooks is accomplished in two ways. First, by mixing bleed air from different stages in the high-pressure compressor and second, by controlling the flow gap between the inner case and baffle. For the integrated core/low spool, a mixture of tenth and fifteenth stage high-pressure compressor bleed air was found acceptable. For the flight propulsion system, a mixture of eighth stage and fifteenth stage air was selected, as discussed in Section 5.2.2.4 of this report. By adjusting the inner case-to-baffle gap, the cooling air film coefficient can be regulated to provide the optimum case temperature at each stage. The range of film coefficients available for this "tailoring" process is shown in Figure 5.2.5-10. The distribution of case cooling airflow for both the integrated core/low spool and the flight propulsion system is shown in Figure 5.2.5-11. The flight propulsion system uses less total cooling airflow than the integrated core/low spool because it has two less case hook metering holes. The reasons for this are described in Section 5.2.2.4 of this report. To maintain optimum control of the outer airseal radial position, the inner case and inner case hooks must be thermally isolated from gaspath temperatures as much as possible. This thermal isolation is accomplished by the use of the design features illustrated in Figure 5.2.5-12. First, the gaps between segments of the outer airseals and vane platforms are staggered so that the airseal segment gap does not line up with the adjacent vane platform gap. This effectively reduces a potential leak path from the gaspath to the case. Second, the case is further isolated from the gaspath wall through the use of heatshields at all outer airseal and vane platform locations indicated in the figure. These heatshields act as radiation barriers as well as diverters of any hot gaspath air that might leak into the cavities. Finally, the cooling air manifolds provided at each case hook location, while directing 0.10 percent of core engine flow for cooling flow through the case hooks and vane feet, act as an additional shield between the gaspath and the inner case structure.

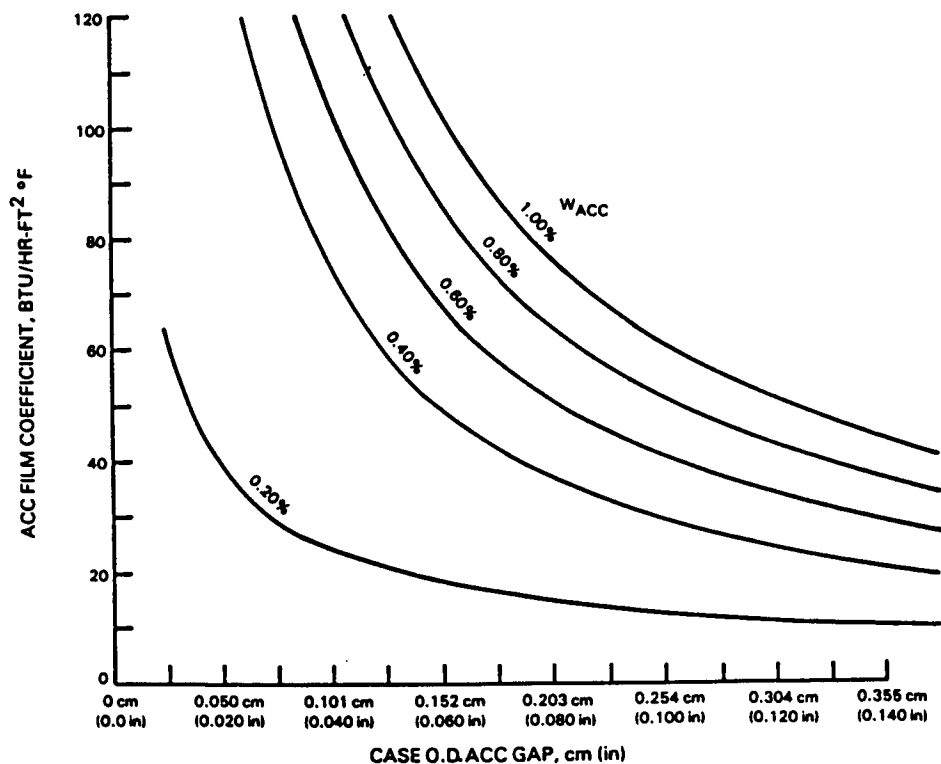


Figure 5.2.5-10 Cooling Flow Film Coefficient Variation as a Function of Inner Case-To-Baffle Gap Width

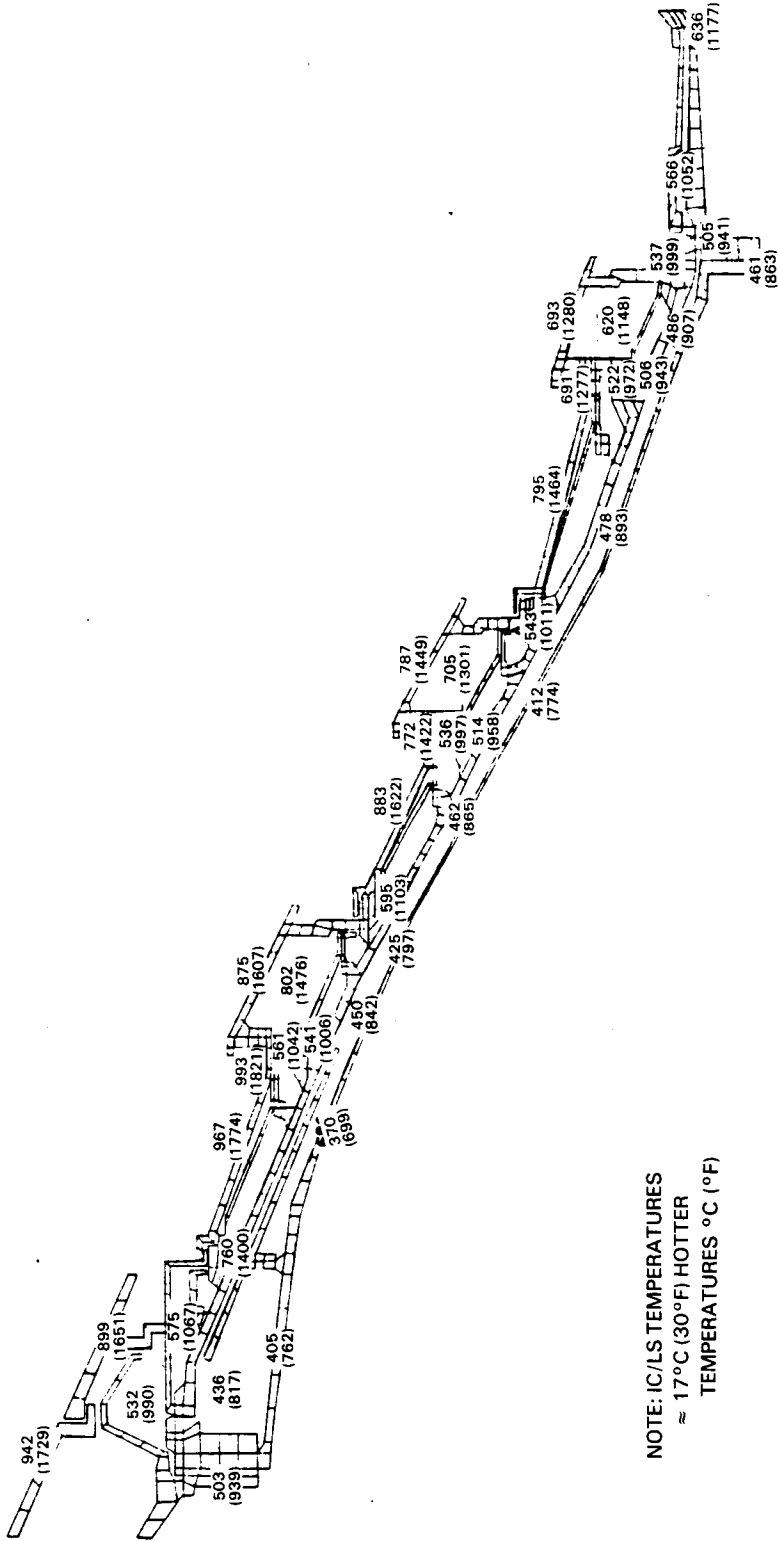
A steady-state thermal analysis of the flight propulsion system case at sea level takeoff operating conditions indicated good isolation of vane-to-case hooks from the hot gaspath flow. This can be seen in the finite element model results shown in Figures 5.2.5-13 and 5.2.5-14. Leading edge hooks are a nominal 26°C (80°F) cooler than trailing edge hooks because of the greater degree of gaspath isolation possible at the front of each vane. Temperatures shown would be approximately 17°C (30°F) higher for the integrated core/low spool.

A transient thermal response analysis of the case was conducted to assess the thermal behavior of the second stage vane and fourth stage vane outer airseal case hooks during snap acceleration/deceleration operation. The second and fourth stage vane locations were selected in order to be compatible with the locations selected for the rotor thermal analysis. The initial analysis was conducted without the use of active clearance control. Results of this analysis are shown in Figures 5.2.5-15 and -16. These figures show the degree to which the case hooks were effectively shielded from hot gaspath temperatures and also indicate the desired comparable thermal response at the front and rear hook locations. The second analysis was conducted to determine the degree of outer airseal radial deflection possible by exercising the active clearance control system during the same engine transient operation. Results of this analysis are shown in Figures 5.2.5-17 and -18. The deflection resulting from use of fifteenth stage high-pressure compressor bleed air only defines the maximum deflection possible, whereas the deflections resulting from use of eighth or tenth stage high-pressure compressor bleed air only define the minimum deflection possible. Deflections within these ranges can be accomplished by mixing the bleed air. It should be noted that use of all fifteenth stage bleed air is not possible at sea level takeoff conditions since this would elevate the temperatures at the case hooks above the capability of the Inconel 718 case material. Use of eighth stage bleed air provides a small improvement in deflection range at the second stage vane location and a significantly larger improvement at the fourth stage vane location.

5.2.5.4 Turbine Intermediate Case

Major features of the turbine intermediate case cooling air distribution system shown in Figure 5.2.5-19. These include:

- o Feather seals that bridge the inner and outer diameter chordal gaps between strut fairing segments and limit leakage to 0.25 percent of core engine flow.
- o Struts cooled internally by 0.35 percent of core engine flow from the tenth stage high-pressure compressor outer diameter bleed. (Because of the large surface area and high film coefficients involved, it is not practical to cool the strut fairing.)
- o An outer case with temperature controlled by spent air from the high-pressure turbine active clearance control system. The outer case has been thermally matched with the strut inner torque box with no additional cooling air required.



NOTE: IC/LS TEMPERATURES
 ≈ 17°C (30°F) HOTTER
 TEMPERATURES °C (°F)

Figure 5.2.5-13 Case Finite Element Model Showing Temperature Distribution at Steady-State Sea Level Takeoff Hot Day Operating Conditions

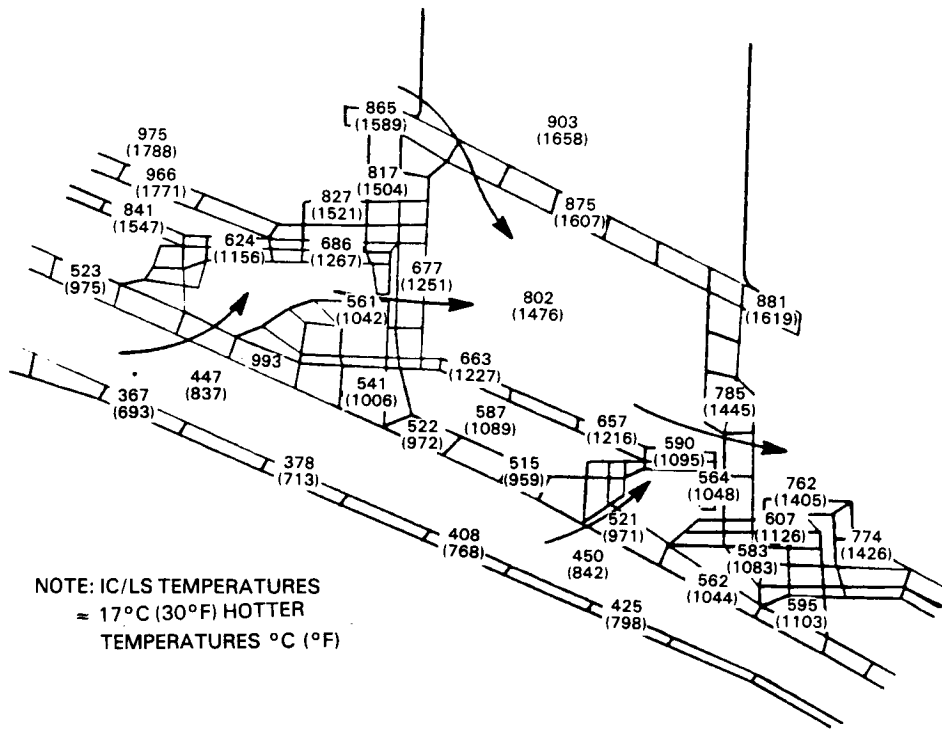


Figure 5.2.5-14 Temperature Distribution at Low-Pressure Turbine Third Vane Attachment at Steady-State Sea Level Takeoff Hot Day Operating Conditions

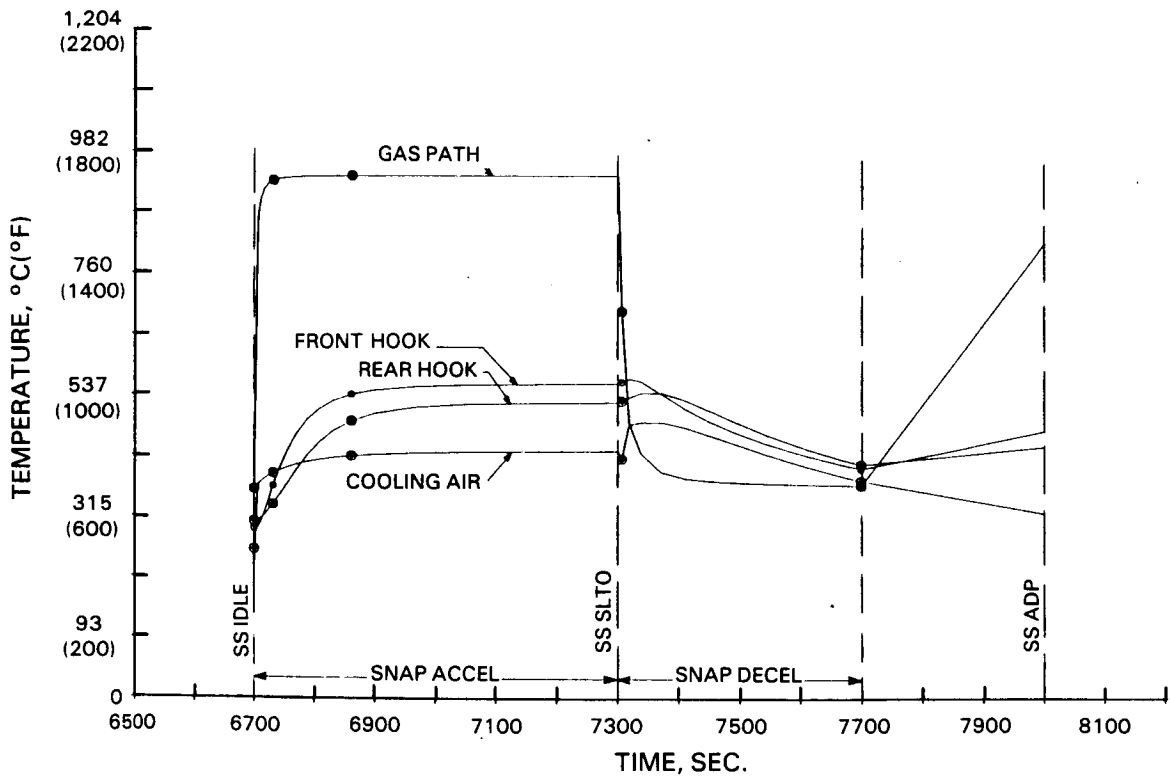


Figure 5.2.5-15 Temperature Versus Time History at Selected Second Stage Low-Pressure Turbine Vane/Outer Airseal Locations During Severe Engine Power Excursions

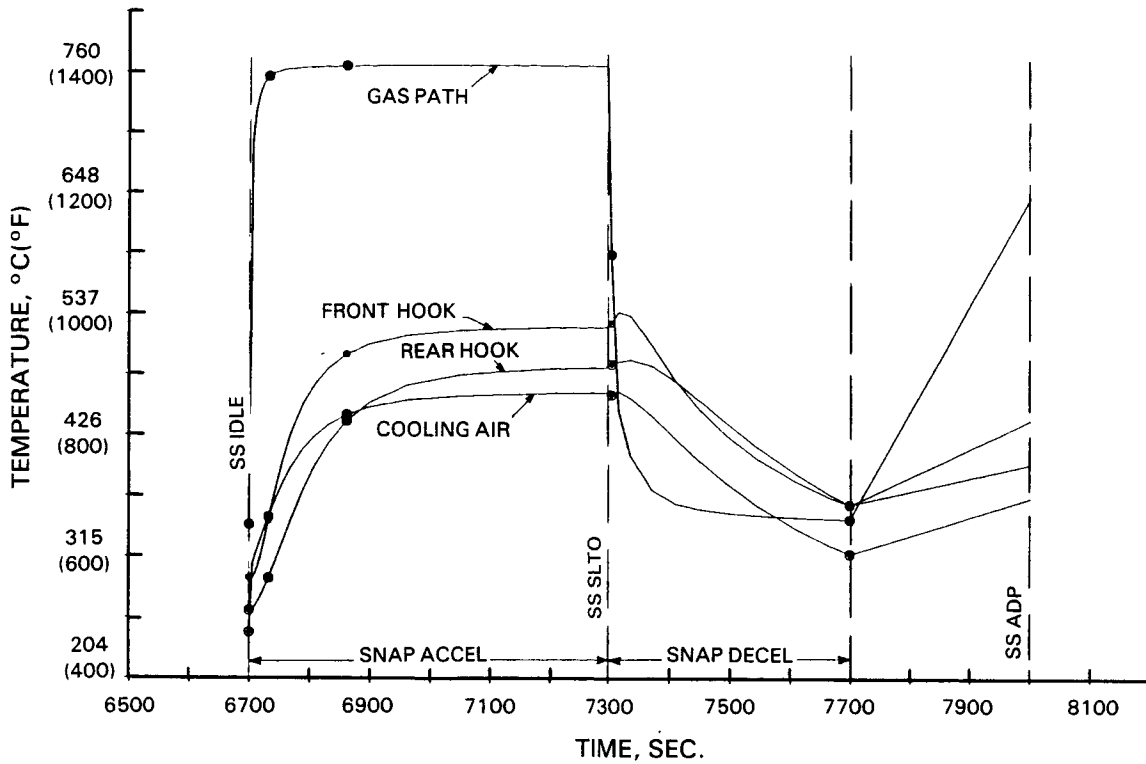


Figure 5.2.5-16 Temperature Versus Time History at Selected Fourth Stage Low-Pressure Turbine Vane/Outer Airseal Locations During Severe Engine Power Excursions

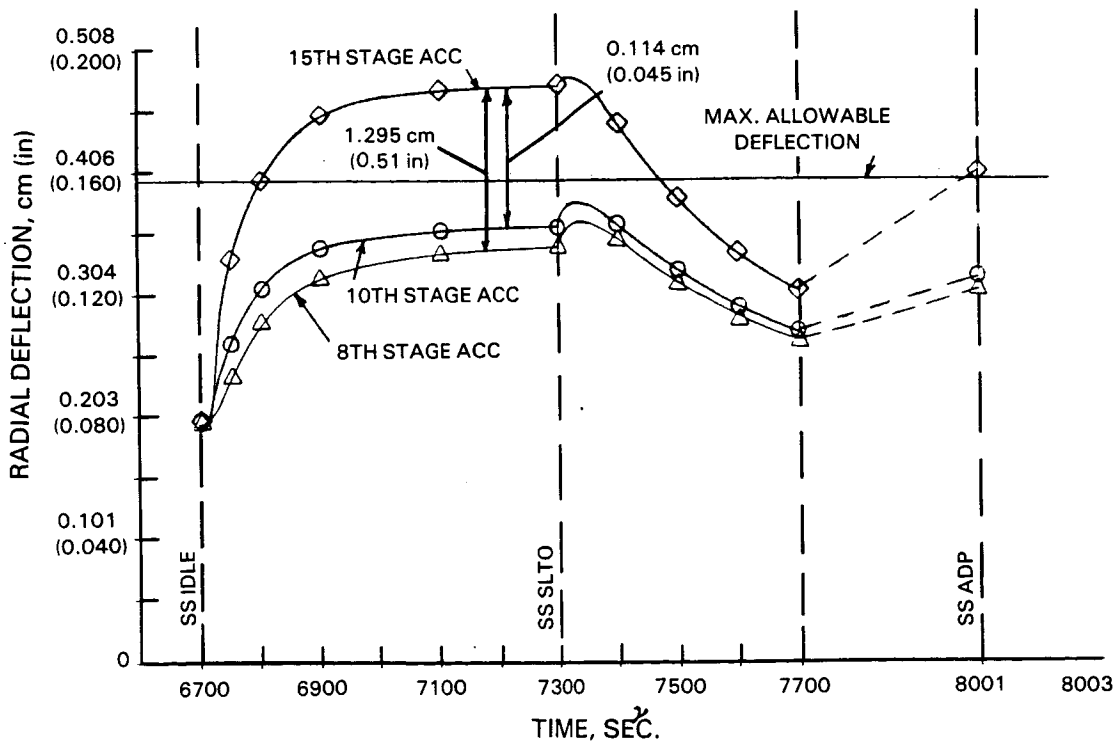


Figure 5.2.5-17 Low-Pressure Turbine Second Stage Outer Airseal Radial Deflection with Active Clearance Control in Operation

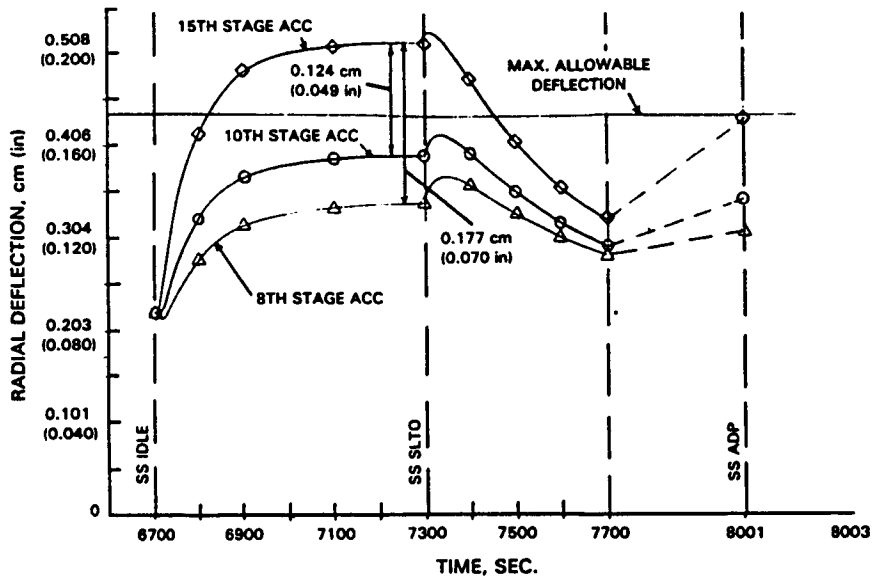


Figure 5.2.5-18 Low-Pressure Turbine Fourth Stage Outer Airseal Radial Deflection with Active Clearance Control in Operation

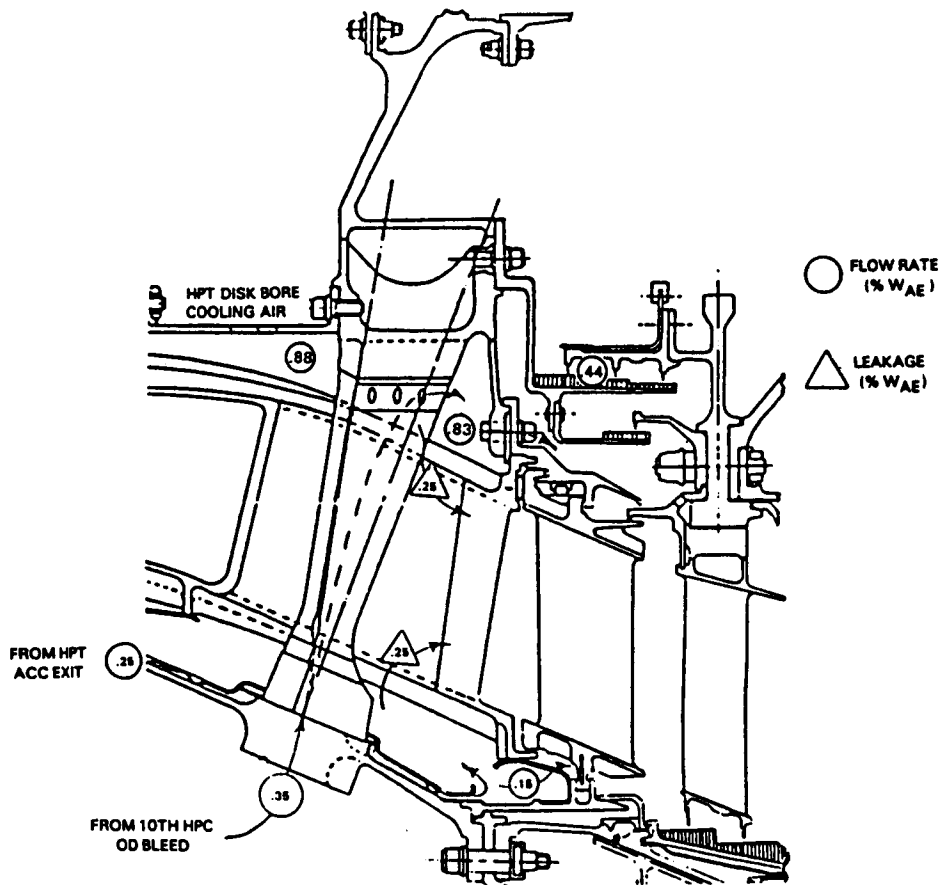


Figure 5.2.5-19 Turbine Intermediate Case Secondary Flow System

The temperature distribution in the integrated core/low spool turbine intermediate case structure was assessed at sea level takeoff engine operating conditions. Results of this assessment are shown in Figure 5.2.5-20 and indicate that the load carrying struts, inner diameter and outer diameter ring steady-state temperatures are all maintained at, or below, 551°C (1025°F).

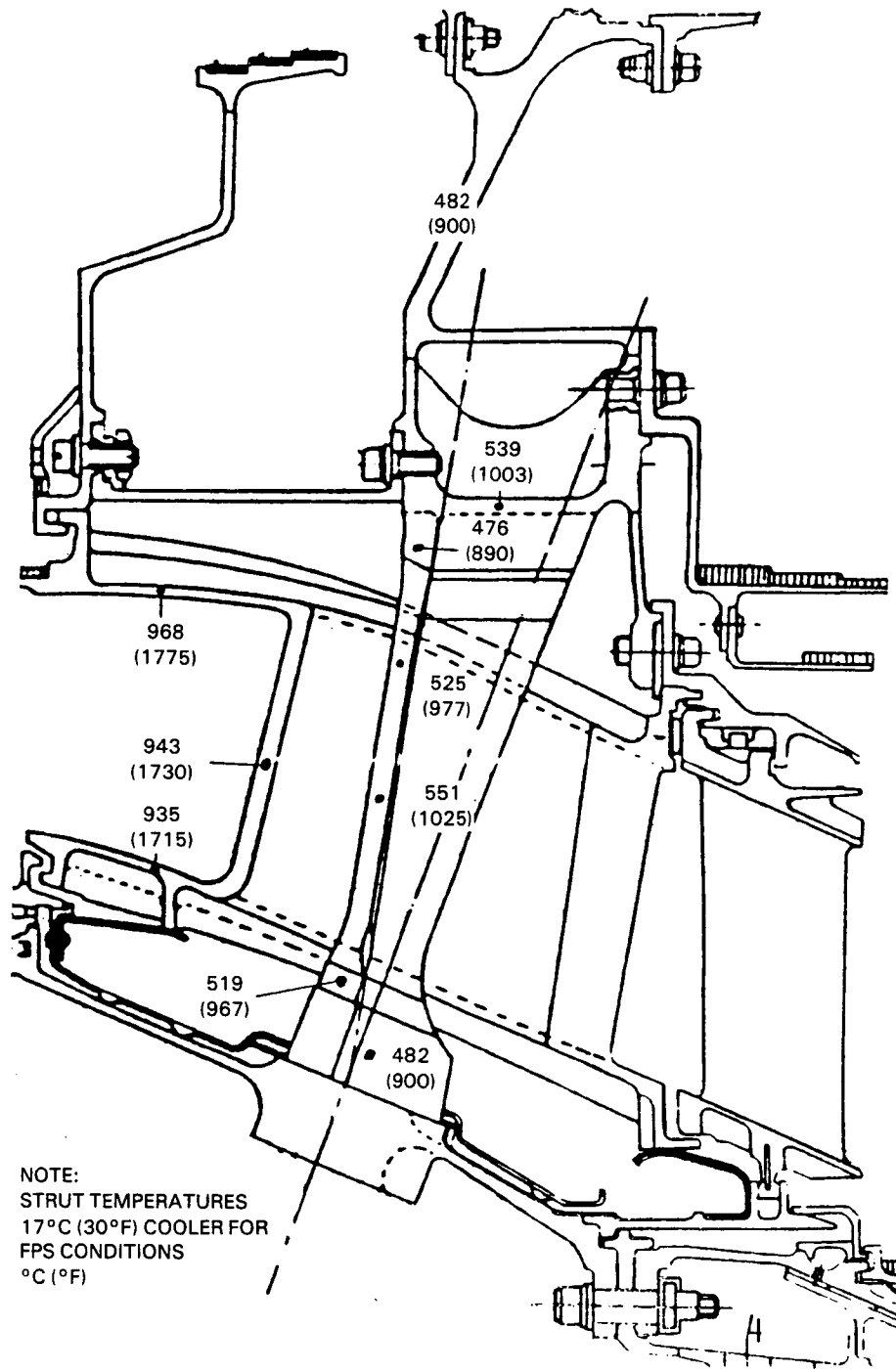


Figure 5.2.5-20 Integrated Core/Low Spool Turbine Intermediate Case Temperature Map at Sea Level Takeoff Engine Operating Conditions

The torque box-to-strut case structure represents a classic ring-strut-ring thermal stress problem. To minimize thermal stresses in this support structure during temperature excursions, it is desirable to thermally match the inner ring torque box and the outer case. This was accomplished by ducting 0.25 percent of core engine airflow from the high-pressure turbine active clearance control system along the outer case wall, as shown in Figure 5.2.5-19, and not cooling the torque box structure. The resultant time-temperature history in Figure 5.2.5-21 shows that the thermal response rates for the two rings were equalized, indicating that the desired thermal matching was achieved. The faster responding strut is permitted to expand by circumferential deflection of the rings relative to each other, utilizing the circumferential tilt of the struts to advantage (see Section 5.2.3.2.1 of the report for further discussion).

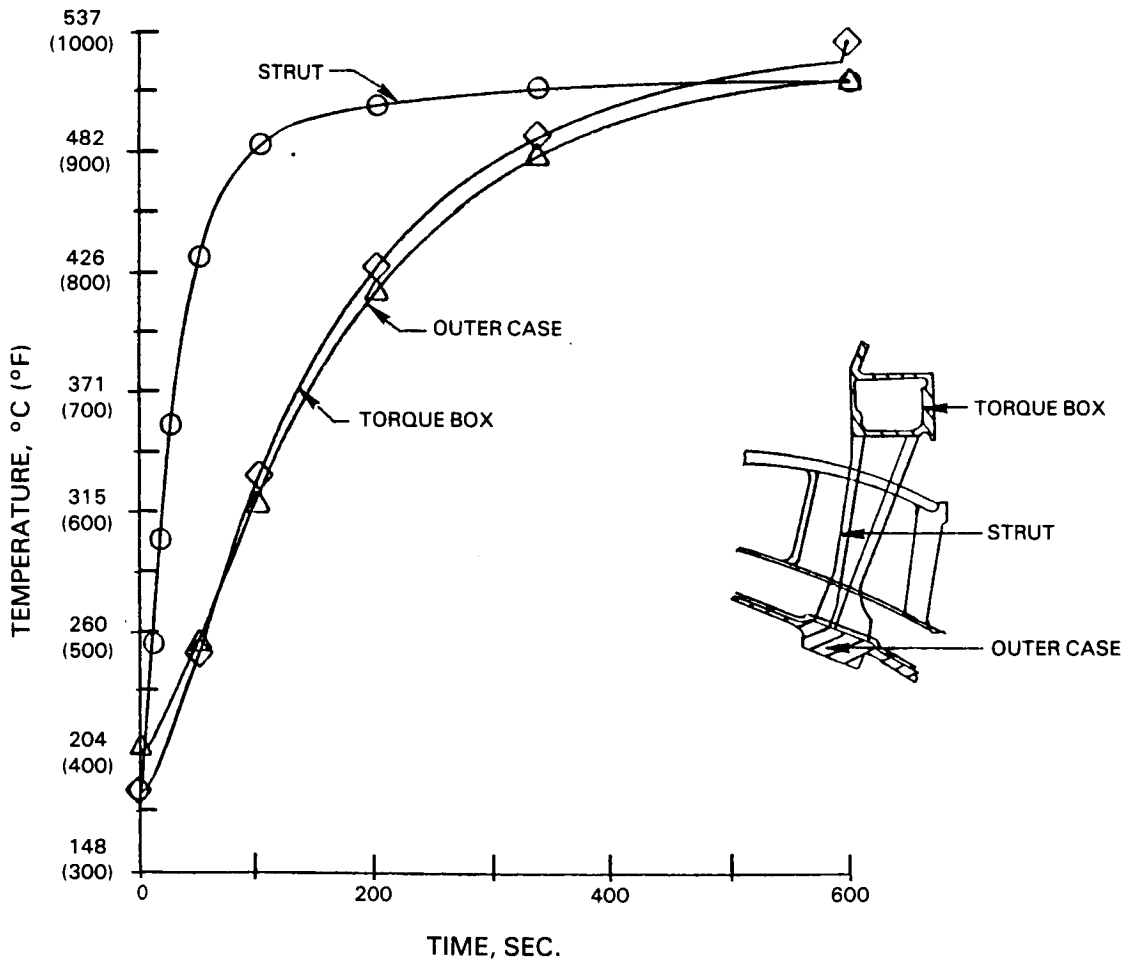


Figure 5.2.5-21 Temperature-Time History for Turbine Intermediate Case Torque Box-To-Strut Case Support Structure During Temperature Excursions

5.2.6 Turbine System Weight Summary

Preliminary weight analyses were conducted for the turbine intermediate case and low-pressure turbine as configured for the integrated core/low spool. Results of these analyses are presented in Table 5.2.6-I. A detailed weight assessment will not be performed until the final flight propulsion system preliminary design update.

TABLE 5.2.6-I
PRELIMINARY WEIGHT SUMMARY FOR INTEGRATED CORE/LOW SPOOL
TURBINE INTERMEDIATE CASE AND LOW-PRESSURE TURBINE COMPONENT

	<u>WEIGHT</u> Kg/(LB)
Turbine Intermediate Case	139.4 (307)
Low-Pressure Turbine Component	
Rotor	381.8 (841)
Case and Vanes	302.8 (667)
Exhaust Case	323.7 (713)
Shaft	114.9 (253)
TOTAL	1262.6 (2781)

SECTION 6.0 CONCLUDING REMARKS

The intermediate case and low-pressure turbine designs represent a positive step towards improving engine fuel efficiency on a component level through advances in aerodynamics, structure and materials. The turbine component, in particular, introduces several technical features to enhance performance and durability, while offering a substantial reduction in weight. Also, the designs are sensitive to the variables of cost and maintainability, which are fundamental requirements of the commercial market.

Overall, much of the technology is universally applicable to any engine of the next generation since it reflects refinements in aerodynamic and thermodynamic design techniques. Included are concepts for reducing gaspath leakage, active clearance control and high strength/high temperature capability materials.

Completion of the intermediate case, low-pressure turbine and turbine exit guide vane designs is a major accomplishment under Task 2 of the Energy Efficient Engine Program. The supporting technology programs have been successful in providing pertinent design information as well as substantiating the benefits of various advanced concepts. Technology verification on a system level is the next step, and this will be accomplished during the scheduled integrated core/low spool test program.

APPENDIXES

APPENDIX A

NASTRAN stress results for turbine intermediate case strut fairing.

- A-1: Platform and airfoil stress contours caused by pressure loads
- A-2: Platform and airfoil stress contours caused by hot spot thermals
- A-3: Platform and airfoil stress contours caused by transient thermals

APPENDIX A
NASTRAN STRESS ANALYSIS

APPENDIX A

NASTRAN stress results for turbine intermediate case strut fairing.

A-1: Platform and airfoil stress contours caused by pressure loads

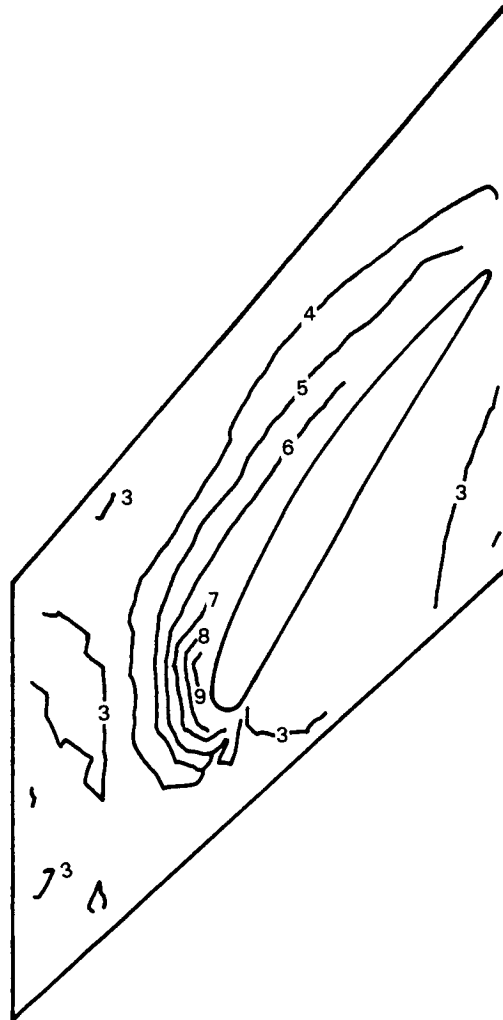
A-2: Platform and airfoil stress contours caused by hot spot thermals

A-3: Platform and airfoil stress contours caused by transient thermals

A-1

PLATFORM AND AIRFOIL STRESS CONTOURS CAUSED BY PRESSURE LOADS

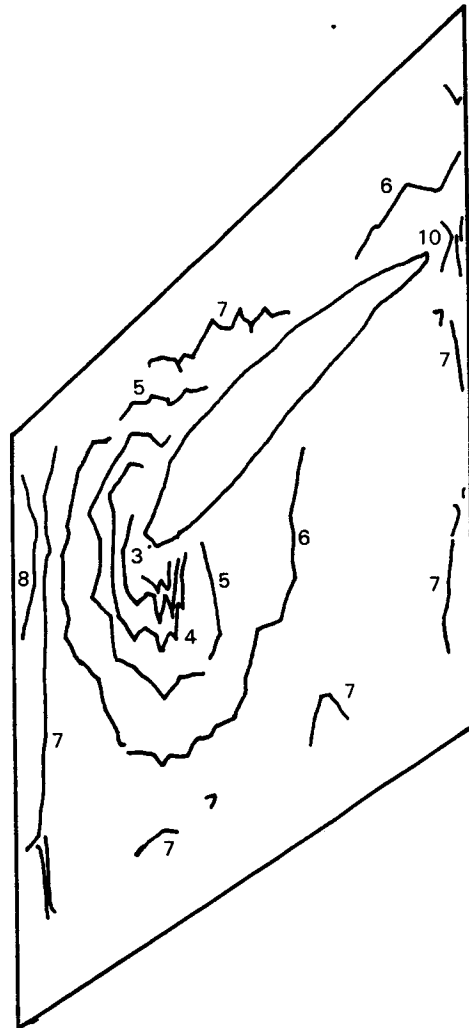
PLATFORM AND AIRFOIL STRESS CONTOURS CAUSED BY PRESSURE LOADS



SYMBOL	VALUE
1	-7.142109E+03
2	-3.817291E+03
3	-4.924727E+02
4	2.832346E+03
5	6.157164E+03
6	9.481920E+03
7	1.280680E+04
8	1.613161E+04
9	1.945643E+04
10	2.278126E+04

Inner Diameter Platform Stress Results - Pressure Load
(Integrated Core/Low Spool)

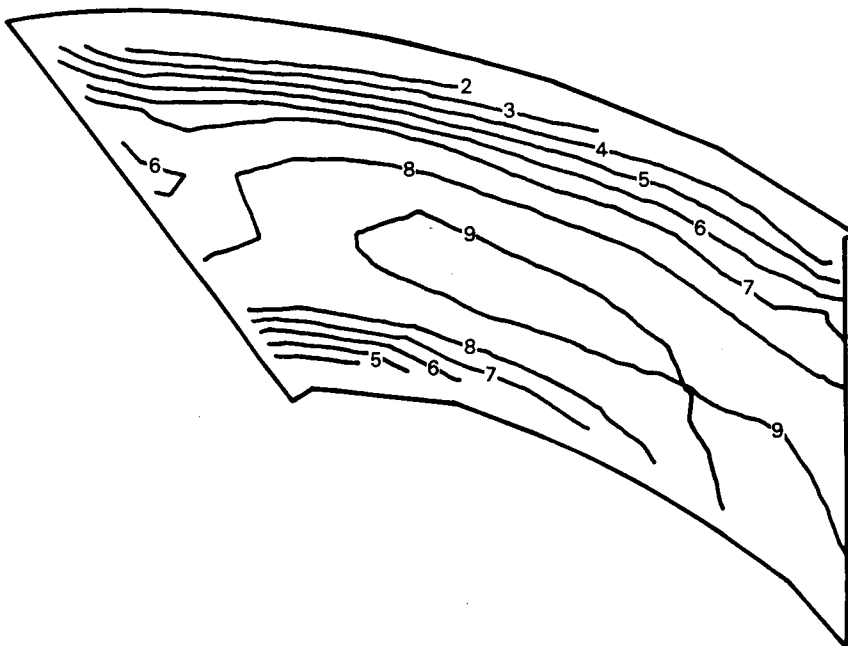
PLATFORM AND AIRFOIL STRESS CONTOURS CAUSED BY PRESSURE LOADS



SYMBOL	VALUE
1	-1.633836E+04
2	-1.349928E+04
3	-1.066021E+04
4	-7.821133E+03
5	-4.982059E+03
6	-2.142984E+03
7	6.960898E+02
8	3.535164E+03
9	6.374238E+03
10	9.213312E+03

Outer Diameter Platform Stress Results - Pressure Load
(Integrated Core/Low Spool)

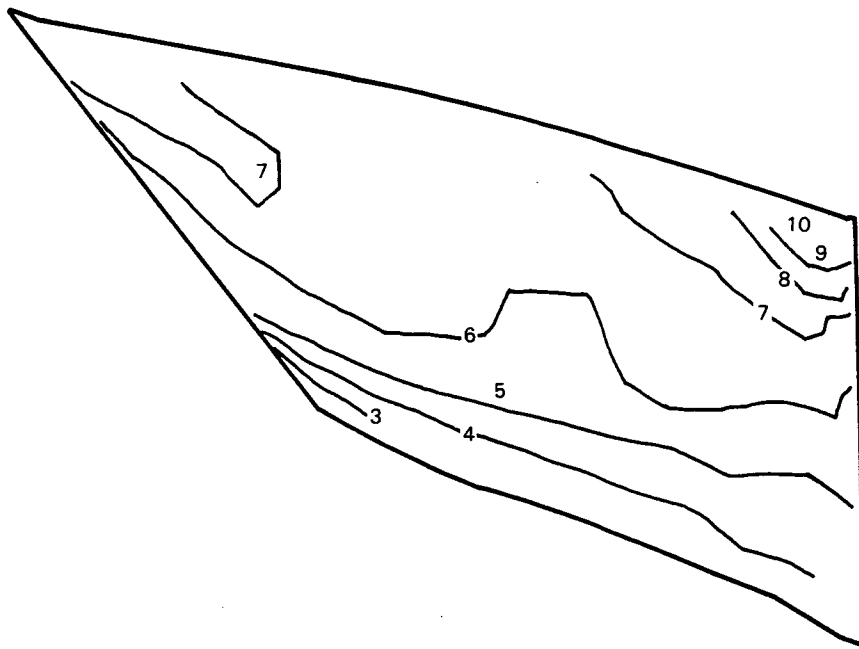
PLATFORM AND AIRFOIL STRESS CONTOURS CAUSED BY PRESSURE LOADS



SYMBOL	VALUE
1	-2.172700E+04
2	-1.898413E+04
3	-1.624126E+04
4	-1.349839E+04
5	-1.075552E+04
6	-8.012645E+03
7	-5.269773E+03
8	-2.526904E+03
9	2.159648E+02
10	2.958826E+03

Airfoil Suction Wall Stress Results - Pressure Load
(Integrated Core/Low Spool)

PLATFORM AND AIRFOIL STRESS CONTOURS CAUSED BY PRESSURE LOADS



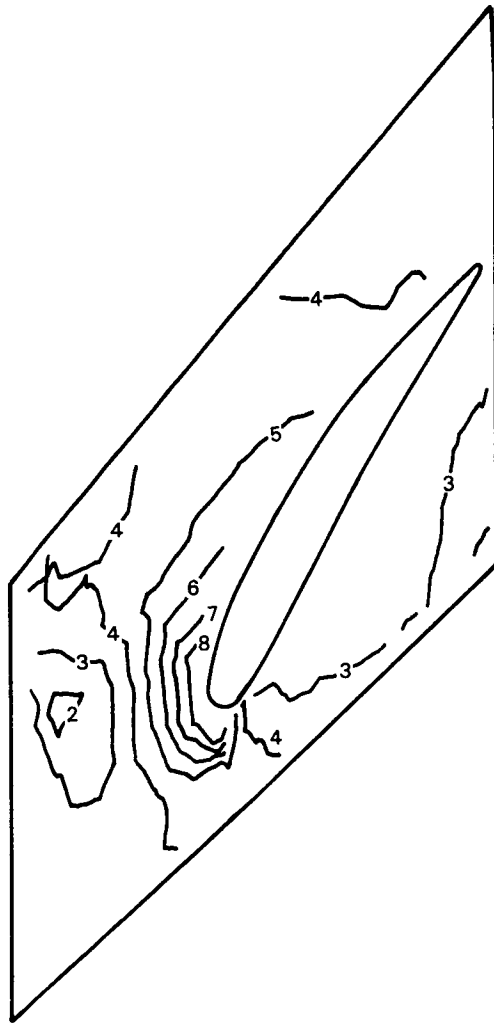
SYMBOL	VALUE
1	-9.281922E+03
2	-7.454176E+03
3	-5.626430E+03
4	-3.798684E+03
5	-1.970937E+03
6	-1.431914E+02
7	1.684555E+03
8	3.512301E+03
9	5.340047E+03
10	7.167793E+03

Airfoil Pressure Wall Stress Results - Pressure Load
(Integrated Core/Low Spool)

A-2

PLATFORM AND AIRFOIL STRESS CONTOURS CAUSED BY HOT SPOT THERMALS

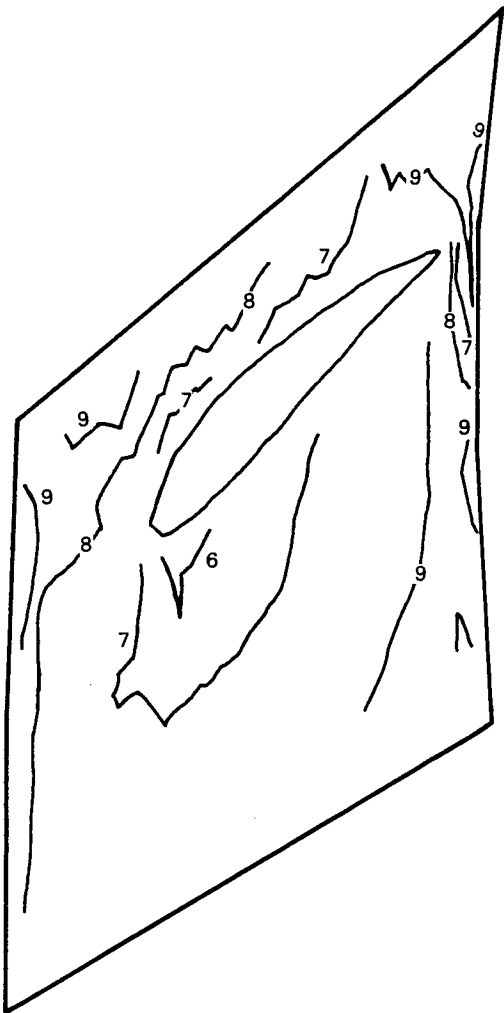
PLATFORM AND AIRFOIL STRESS CONTOURS CAUSED BY HOT SPOT THERMALS



SYMBOL	VALUE
1	-2.224739E+03
2	-1.192309E+03
3	-1.598794E+02
4	8.725503E+02
5	1.904980E+03
6	2.937410E+03
7	3.969839E+03
8	5.002266E+03
9	6.034695E+03
10	7.067129E+03

Inner Diameter Platform Stress Results - Hot Spot Thermals
(Integrated Core/Low Spool)

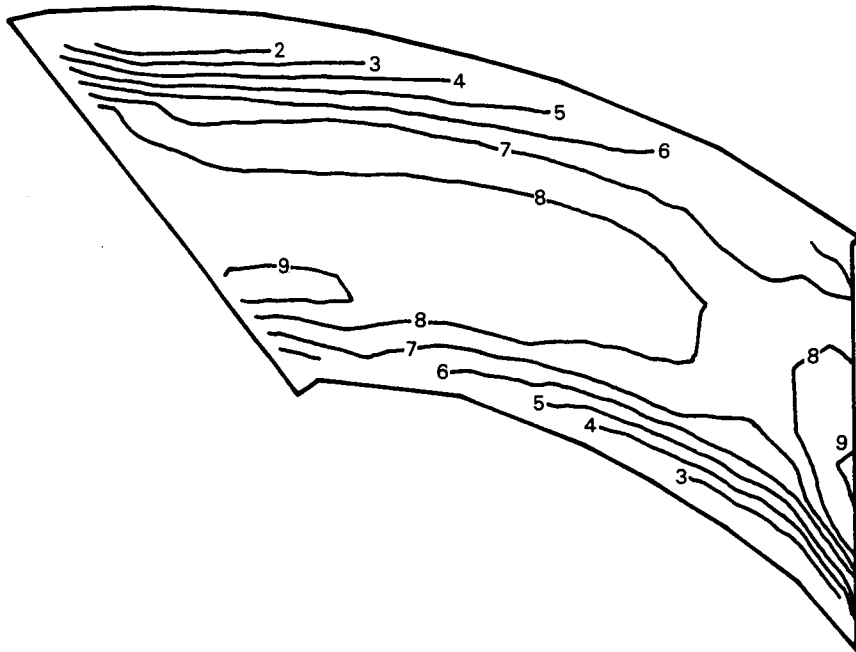
PLATFORM AND AIRFOIL STRESS CONTOURS CAUSED BY HOT SPOT THERMALS



SYMBOL	VALUE
1	-6.139207E+03
2	-5.222969E+03
3	-4.306730E+03
4	-3.390494E+03
5	-2.474258E+03
6	-1.558021E+03
7	-6.417852E+02
8	2.744512E+02
9	1.190687E+03
10	2.106922E+03

Outer Diameter Platform Stress Results - Hot Spot Thermals
(Integrated Core/Low Spool)

PLATFORM AND AIRFOIL STRESS CONTOURS CAUSED BY HOT SPOT THERMALS



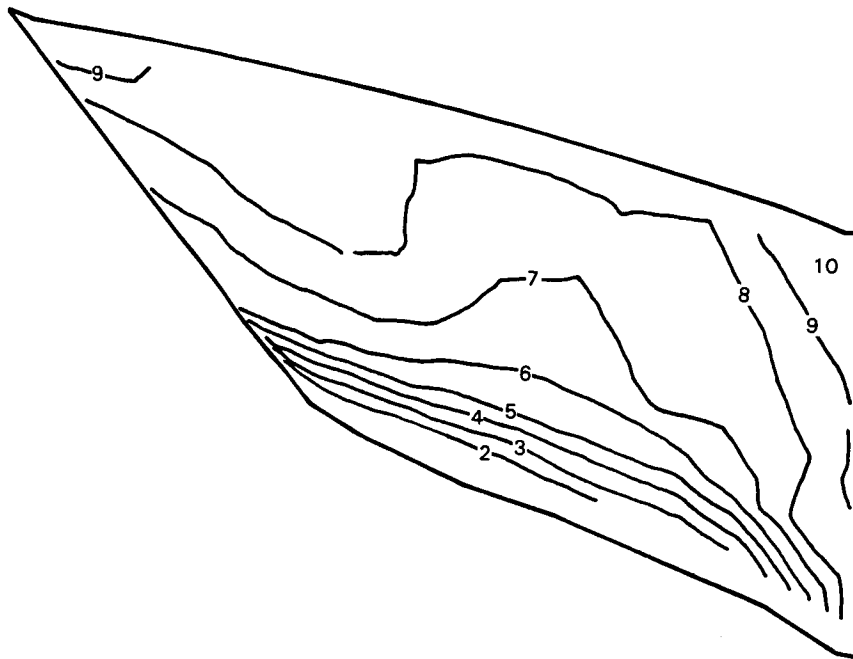
SYMBOL	VALUE
1	-5.293922E+03
2	-4.625516E+03
3	-3.957111E+03
4	-3.288706E+03
5	-2.620301E+03
6	-1.951896E+03
7	-1.283492E+03
8	-6.150869E+02
9	5.331787E+01
10	7.217253E+02

Airfoil Suction Wall Stress Results - Hot Spot Thermals
(Integrated Core/Low Spool)

A-3

PLATFORM AND AIRFOIL STRESS CONTOURS CAUSED BY TRANSIENT THERMALS

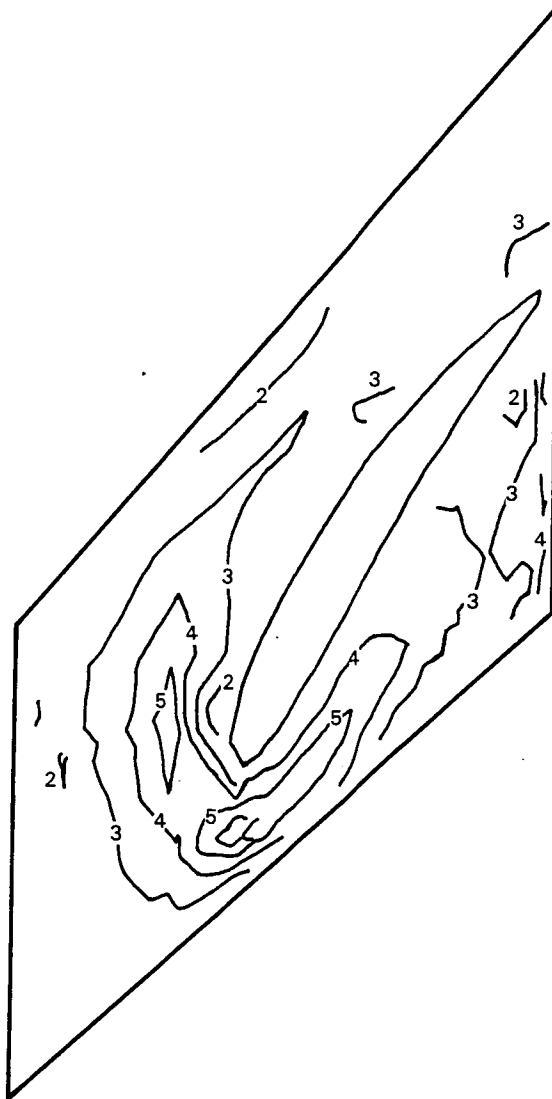
PLATFORM AND AIRFOIL STRESS CONTOURS CAUSED BY TRANSIENT THERMALS



SYMBOL	VALUE
1	-2.548554E+03
2	-2.150909E+03
3	-1.753265E+03
4	-1.355620E+03
5	-9.579751E+02
6	-5.603303E+02
7	-1.626855E+02
8	2.349592E+02
9	6.326040E+02
10	1,030250E+03

Airfoil Pressure Wall Stress Results - Hot Spot Thermals
(Integrated Core/Low Spool)

PLATFORM AND AIRFOIL STRESS CONTOURS CAUSED BY TRANSIENT THERMALS



SYMBOL	VALUE
1	-5.807805E+03
2	-3.497070E+02
3	5.108391E+03
4	1.056649E+04
5	1.602459E+04
6	2.148268E+04
7	2.694078E+04
8	3.239888E+04
9	3.785698E+04
10	4.331508E+04

Inner Diameter Platform Stress Results - Transient Thermal
(Integrated Core/Low Spool)

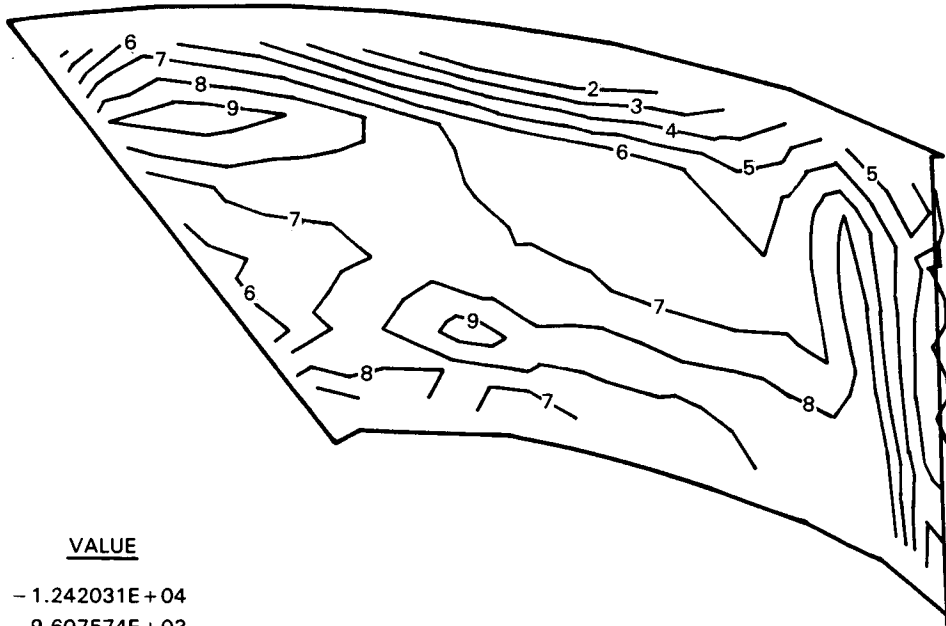
PLATFORM AND AIRFOIL STRESS CONTOURS CAUSED BY TRANSIENT THERMALS



SYMBOL	VALUE
1	-3.584471E+03
2	-1.034071E+03
3	1.516329E+03
4	4.066729E+03
5	6.617129E+03
6	9.167527E+03
7	1.171793E+04
8	1.426832E+04
9	1.681872E+04
10	1.936913E+04

Outer Diameter Platform Stress Results - Transient Thermal
(Integrated Core/Low Spool)

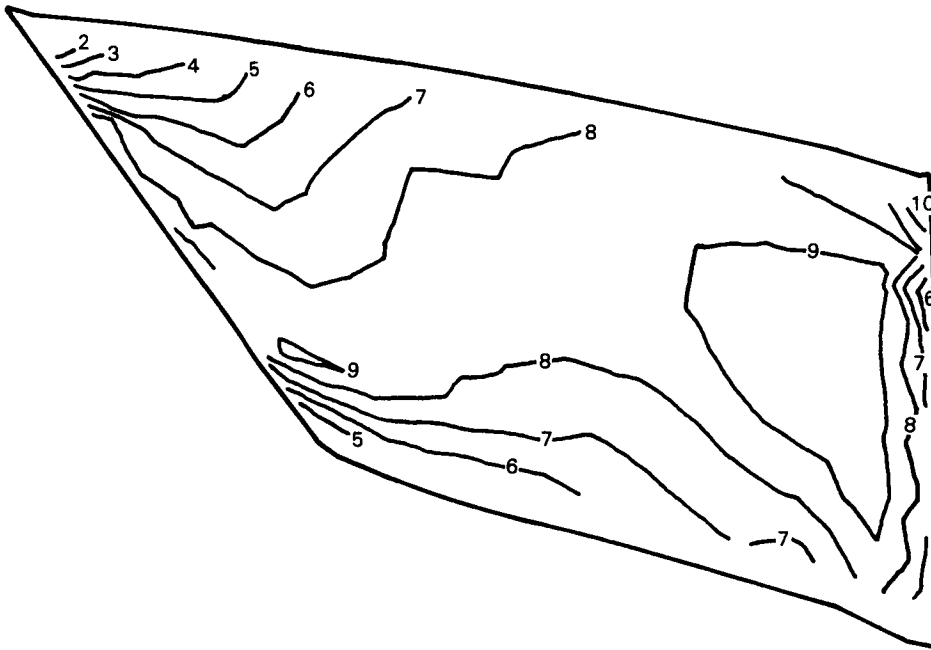
PLATFORM AND AIRFOIL STRESS CONTOURS CAUSED BY TRANSIENT THERMALS



<u>SYMBOL</u>	<u>VALUE</u>
1	-1.242031E+04
2	-9.607574E+03
3	-6.794836E+03
4	-3.982099E+03
5	-1.169361E+03
6	1.643376E+03
7	4.456113E+03
8	7.268848E+03
9	1.008158E+04
10	1.289432E+04

Airfoil Suction Wall Stress Results - Transient Thermal
(Integrated Core/Low Spool)

PLATFORM AND AIRFOIL STRESS CONTOURS CAUSED BY TRANSIENT THERMALS



SYMBOL	VALUE
1	-3.177446E+04
2	-2.764677E+04
3	-2.351907E+04
4	-1.939137E+04
5	-1.526367E+04
6	-1.113597E+04
7	-7.008270E+03
8	-2.880570E+03
9	1.247129E+03
10	5.374855E+03

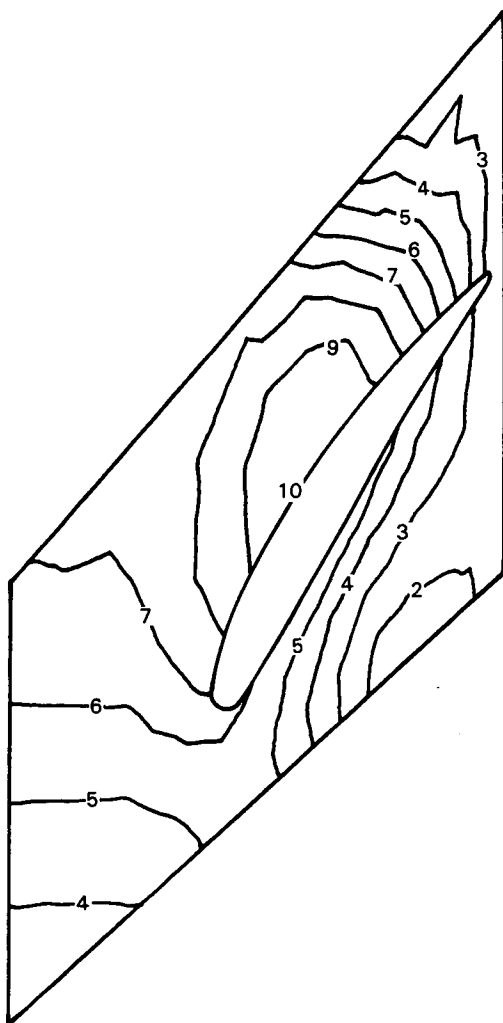
Airfoil Pressure Wall Stress Results - Transient Thermal
(Integrated Core/Low Spool)

APPENDIX B

TURBINE INTERMEDIATE CASE STRUT FAIRING PLATFORM
AND AIRFOIL DEFLECTION CONTOURS CAUSED BY PRESSURE LOADS

TURBINE INTERMEDIATE CASE STRUT FAIRING PLATFORM
AND AIRFOIL DEFLECTION CONTOURS CAUSED BY PRESSURE LOADS

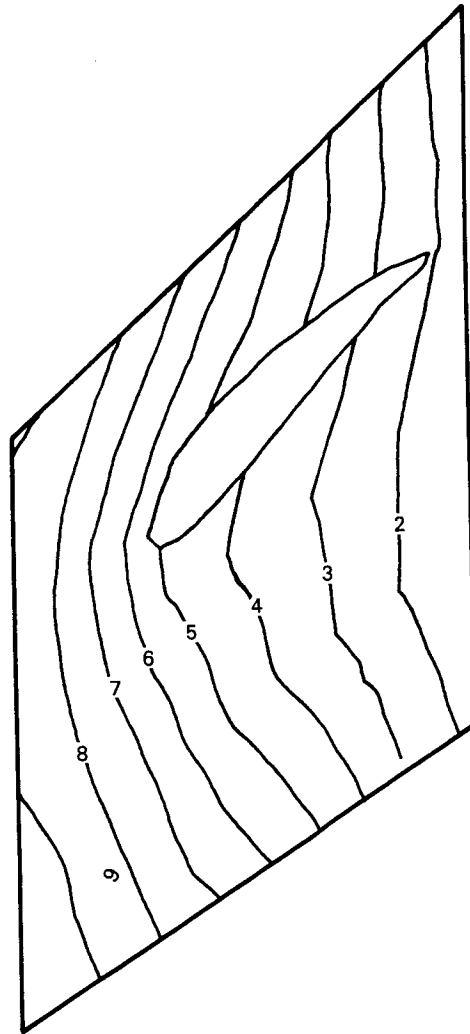
8



SYMBOL	VALUE
1	-7.503985E-04
2	-2.536122E-04
3	2.431741E-04
4	7.399605E-04
5	1.236747E-03
6	1.733533E-03
7	2.230319E-03
8	2.727106E-03
9	3.223892E-03
10	3.720682E-03

Inner Diameter Platform Radial Deflections - Pressure Load
(Integrated Core/Low Spool)

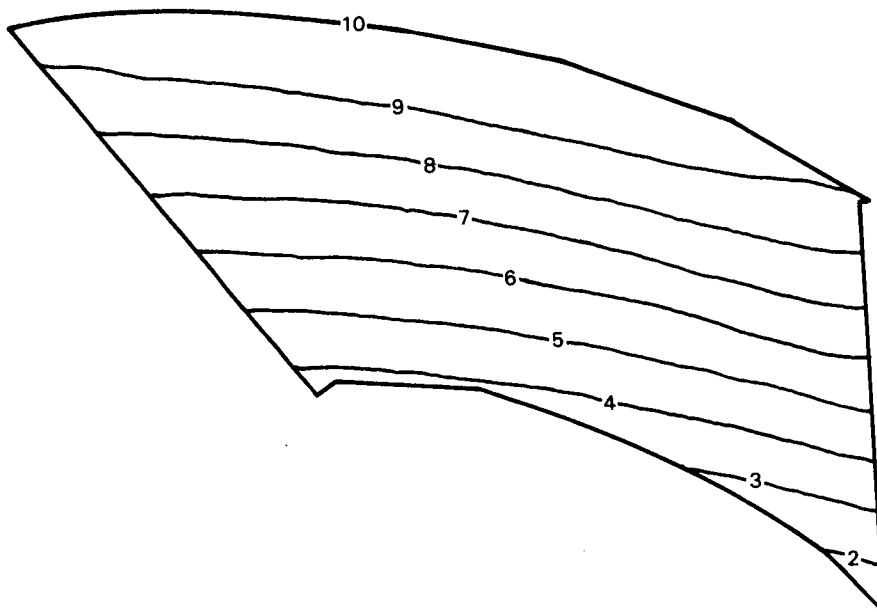
TURBINE INTERMEDIATE CASE STRUT FAIRING PLATFORM
AND AIRFOIL DEFLECTION CONTOURS CAUSED BY PRESSURE LOADS



SYMBOL	VALUE
1	-3.091799E -02
2	-2.786454E -02
3	-2.481109E -02
4	-2.175764E -02
5	-1.870418E -02
6	-1.565073E -02
7	-1.259728E -02
8	-9.543825E -03
9	-6.490372E -03
10	-3.436932E -03

Outer Diameter Platform Radial Deflections - Pressure Load
(Integrated Core/Low Spool)

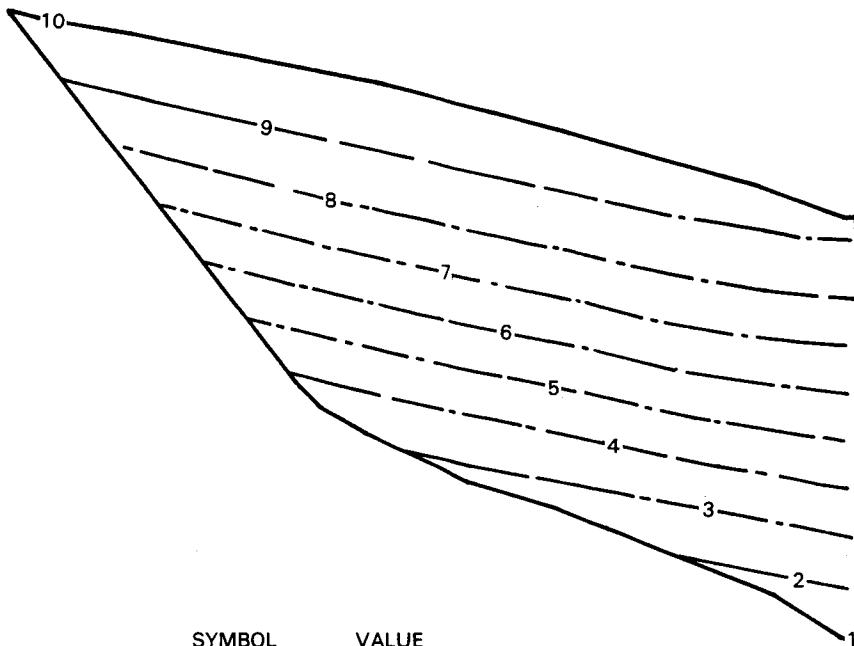
TURBINE INTERMEDIATE CASE STRUT FAIRING PLATFORM
AND AIRFOIL DEFLECTION CONTOURS CAUSED BY PRESSURE LOADS



SYMBOL	VALUE
1	-2.755137E-02
2	-2.407670E-02
3	-2.060202E-02
4	-1.712735E-02
5	-1.365267E-02
6	-1.017800E-02
7	-6.703321E-03
8	-3.228648E-03
9	2.460242E-04
10	3.720682E-03

Airfoil Suction Wall Transverse Deflections - Pressure Load
(Integrated Core/Low Spool)

TURBINE INTERMEDIATE CASE STRUT FAIRING PLATFORM
AND AIRFOIL DEFLECTION CONTOURS CAUSED BY PRESSURE LOADS



<u>SYMBOL</u>	<u>VALUE</u>
1	-2.755137E-02
2	-2.426654E-02
3	-2.098172E-02
4	-1.769689E-02
5	-1.441206E-02
6	-1.112724E-02
7	-7.842410E-03
8	-4.557583E-03
9	-1.272760E-03
10	2.012047E-03

Airfoil Pressure Wall Transverse Deflections - Pressure Load
(Integrated Core/Low Spool)

APPENDIX C
TURBINE INTERMEDIATE CASE STRUT FAIRING AIRFOIL COORDINATES

STRUT FAIRING 400 SERIES
(Section 1)

X/BX	SUCTION SIDE Y/BX	PRESSURE SIDE Y/BX
1.00000	1.49436	1.49436
0.99000	1.50131	1.47229
0.98000	1.49121	1.45161
0.97000	1.47953	1.43120
0.96000	1.46802	1.41086
0.94000	1.44469	1.37039
0.92000	1.42121	1.33022
0.88000	1.37374	1.25066
0.84000	1.32558	1.17166
0.80000	1.27682	1.09275
0.76000	1.22760	1.01407
0.72000	1.17804	0.93597
0.68000	1.12812	0.85870
0.64000	1.07774	0.78248
0.60000	1.02677	0.70747
0.56000	0.97514	0.63384
0.52000	0.92274	0.56172
0.48000	0.86947	0.49125
0.44000	0.81524	0.42254
0.40000	0.75998	0.35574
0.36000	0.70350	0.29104
0.32000	0.64558	0.22870
0.28000	0.58590	0.16909
0.24000	0.52391	0.11288
0.20000	0.45907	0.06048
0.16000	0.39076	0.01330
0.12000	0.31792	-0.02835
0.08000	0.23837	-0.05686
0.06000	0.19460	-0.06494
0.04000	0.14702	-0.06583
0.03000	0.12077	-0.06286
0.02000	0.09091	-0.05704
0.01000	0.05806	-0.04654
0.0	0.0	0.0

STRUT FAIRING 400 SERIES
(Section 2)

X/BX	SUCTION SIDE Y/BX	PRESSURE SIDE Y/BX
1.0000	1.10108	1.10108
0.99000	1.10790	1.08457
0.98000	1.10073	1.07015
0.97000	1.09321	1.05592
0.96000	1.08568	1.04170
0.94000	1.07043	1.01338
0.92000	1.05502	0.98520
0.88000	1.02369	0.92923
0.84000	0.99167	0.87347
0.80000	0.95902	0.81753
0.76000	0.92588	0.76136
0.72000	0.89235	0.70524
0.68000	0.85842	0.64935
0.64000	0.82399	0.59389
0.60000	0.78897	0.53898
0.56000	0.75327	0.48474
0.52000	0.71682	0.43131
0.48000	0.67954	0.37898
0.44000	0.64136	0.32744
0.40000	0.60216	0.27693
0.36000	0.56184	0.22758
0.32000	0.52025	0.17971
0.28000	0.47699	0.13378
0.24000	0.43152	0.09022
0.20000	0.38331	0.04961
0.16000	0.33179	0.01316
0.12000	0.27586	-0.01819
0.08000	0.21359	-0.03993
0.06000	0.17900	-0.04759
0.04000	0.14022	-0.04955
0.03000	0.11861	-0.04713
0.02000	0.09506	-0.04199
0.01000	0.06674	-0.03271
0.0	0.0	-0.0

STRUT FAIRING 400 SERIES
(Section 3)

X/BX	SUCTION SIDE Y/BX	PRESSURE SIDE Y/BX
1.0000	0.88068	0.88068
0.9900	0.88727	0.86652
0.9800	0.88177	0.85490
0.9700	0.87625	0.84343
0.9600	0.87065	0.83196
0.9400	0.85932	0.80914
0.9200	0.84782	0.78643
0.8800	0.82435	0.74136
0.8400	0.80021	0.69649
0.8000	0.77547	0.65145
0.7600	0.75028	0.60619
0.7200	0.72473	0.56091
0.6800	0.69880	0.51578
0.6400	0.67238	0.47096
0.6000	0.64540	0.42656
0.5600	0.61777	0.38268
0.5200	0.58945	0.33942
0.4800	0.56034	0.29700
0.4400	0.53039	0.25537
0.4000	0.49950	0.21449
0.3600	0.46758	0.17453
0.3200	0.43445	0.13575
0.2800	0.39974	0.09852
0.2400	0.36926	0.06328
0.2000	0.32370	0.03044
0.1600	0.28144	0.00115
0.1200	0.23519	-0.02408
0.0800	0.18335	-0.04066
0.0600	0.15432	-0.04537
0.0400	0.12156	-0.04700
0.0300	0.10341	-0.04471
0.0200	0.08349	-0.03971
0.0100	0.05988	-0.03059
0.0	0.0	0.0

STRUT FAIRING 400 SERIES
(Section 4)

X/BX	SUCTION SIDE Y/BX	PRESSURE SIDE Y/BX
1.00000	0.73531	0.73531
0.99000	0.74174	0.72222
0.98000	0.73716	0.71188
0.97000	0.73265	0.70170
0.96000	0.72805	0.69153
0.94000	0.71874	0.67132
0.92000	0.70929	0.65128
0.88000	0.68993	0.61164
0.84000	0.66999	0.57236
0.80000	0.64955	0.53310
0.76000	0.62876	0.49379
0.72000	0.60771	0.45462
0.68000	0.58635	0.41577
0.64000	0.56459	0.37734
0.60000	0.54234	0.33945
0.56000	0.51954	0.30217
0.52000	0.49614	0.26560
0.48000	0.47207	0.22988
0.44000	0.44726	0.19505
0.40000	0.42164	0.16115
0.36000	0.39511	0.12832
0.32000	0.36748	0.09677
0.28000	0.33843	0.06680
0.24000	0.30764	0.03878
0.20000	0.27477	0.01300
0.16000	0.23935	-0.00965
0.12000	0.20047	-0.02865
0.08000	0.15683	-0.04074
0.06000	0.13213	-0.04318
0.04000	0.10434	-0.04340
0.03000	0.08900	-0.04131
0.02000	0.07163	-0.03646
0.01000	0.04930	-0.02750
0.0	0.0	0.0

APPENDIX D
LOW-PRESSURE TURBINE VANE AND BLADE AIRFOIL COORDINATES

SECOND-STAGE VANE COORDINATES
 ROOT SECTION (HOT RADIUS = 16.39000)

PERCENT X	X	Y TOP	Y BOT
0.0	0.00209	2.29910	2.29910
0.010	0.01781	2.31407	2.25376
0.020	0.03354	2.30879	2.22621
0.030	0.04926	2.29923	2.20238
0.040	0.06498	2.28774	2.17851
0.050	0.08071	2.27433	2.15455
0.060	0.09643	2.26020	2.13065
0.070	0.11216	2.24533	2.10674
0.080	0.12788	2.23046	2.08285
0.090	0.14360	2.21553	2.05890
0.100	0.15933	2.20054	2.03505
0.125	0.19863	2.16276	1.97535
0.150	0.23794	2.12453	1.91567
0.175	0.27725	2.08583	1.85607
0.200	0.31656	2.04661	1.79639
0.225	0.35587	2.00683	1.73680
0.250	0.39518	1.96644	1.67723
0.275	0.43449	1.92538	1.61772
0.300	0.47380	1.88358	1.55824
0.325	0.51310	1.84097	1.49879
0.350	0.55241	1.79747	1.43937
0.375	0.59172	1.75300	1.38000
0.400	0.63103	1.70744	1.32066
0.425	0.67034	1.66068	1.26136
0.450	0.70965	1.61257	1.20210
0.475	0.74896	1.56296	1.14289
0.500	0.78827	1.51167	1.08370
0.525	0.82757	1.45850	1.02463
0.550	0.86688	1.40320	0.96556
0.575	0.90619	1.34548	0.90649
0.600	0.94550	1.28508	0.84756
0.625	0.98481	1.22178	0.78866
0.650	1.02412	1.15545	0.72977
0.675	1.06343	1.08607	0.67104
0.700	1.10274	1.01373	0.61235
0.725	1.14204	0.93862	0.55369
0.750	1.18135	0.86101	0.49515
0.775	1.22066	0.78117	0.43676
0.800	1.25997	0.69940	0.37852
0.825	1.29928	0.61597	0.32042
0.850	1.33859	0.53114	0.26245
0.875	1.37790	0.44513	0.20471
0.900	1.41721	0.35811	0.14734
0.910	1.43293	0.32307	0.12452
0.920	1.44865	0.28789	0.10178
0.930	1.46438	0.25259	0.07917
0.940	1.48010	0.21718	0.05669
0.950	1.49582	0.18167	0.03441
0.960	1.51155	0.14607	0.01247
0.970	1.52727	0.11037	-0.00902
0.980	1.54299	0.07460	-0.02337
0.990	1.55872	0.03873	-0.02382
1.000	1.57444	-0.00202	-0.00202

SECOND-STAGE VANE COORDINATES
MEAN SECTION (HOT RADIUS = 18.11501)

PERCENT X	X	Y TOP	Y BOT
0.0	0.00652	2.36065	2.36065
0.010	0.02218	2.37622	2.31705
0.020	0.03783	2.37197	2.29072
0.030	0.05349	2.36463	2.26651
0.040	0.06915	2.35471	2.24219
0.050	0.08481	2.34311	2.21787
0.060	0.10047	2.33083	2.19355
0.070	0.11613	2.31861	2.16912
0.080	0.13178	2.30620	2.14472
0.090	0.14744	2.29371	2.12046
0.100	0.16310	2.28111	2.09612
0.125	0.20225	2.24912	2.03537
0.150	0.24139	2.21642	1.97443
0.175	0.28054	2.18293	1.91366
0.200	0.31968	2.14862	1.85280
0.225	0.35883	2.11341	1.79198
0.250	0.39797	2.07725	1.73125
0.275	0.43712	2.04005	1.67052
0.300	0.47626	2.00174	1.60982
0.325	0.51541	1.96225	1.54914
0.350	0.55455	1.92146	1.48848
0.375	0.59370	1.87928	1.42784
0.400	0.63284	1.83561	1.36723
0.425	0.67199	1.79031	1.30664
0.450	0.71113	1.74327	1.24607
0.475	0.75028	1.69434	1.18553
0.500	0.78942	1.64339	1.12502
0.525	0.82857	1.59024	1.06458
0.550	0.86772	1.53473	1.00418
0.575	0.90686	1.47670	0.94368
0.600	0.94601	1.41595	0.88329
0.625	0.98515	1.35232	0.82300
0.650	1.02430	1.28566	0.76258
0.675	1.06344	1.21580	0.70231
0.700	1.10259	1.14263	0.64216
0.725	1.14173	1.06605	0.58200
0.750	1.18088	0.98599	0.52185
0.775	1.22002	0.90241	0.46171
0.800	1.25917	0.81529	0.40164
0.825	1.29831	0.72468	0.34171
0.850	1.33746	0.63065	0.28200
0.875	1.37660	0.53329	0.22242
0.900	1.41575	0.43273	0.16290
0.910	1.43141	0.39164	0.13918
0.920	1.44707	0.35006	0.11550
0.930	1.46272	0.30802	0.09188
0.940	1.47838	0.26552	0.06838
0.950	1.49404	0.22256	0.04503
0.960	1.50970	0.17918	0.02179
0.970	1.52536	0.13538	0.00088
0.980	1.54101	0.09115	-0.02006
0.990	1.55667	0.04652	-0.02222
1.000	1.57233	-0.00202	-0.00202

SECOND-STAGE VANE COORDINATES
TIP SECTION (HOT RADIUS = 19.84001)

PERCENT X	X	Y TOP	Y BOT
0.0	0.01019	2.56710	2.56710
0.010	0.02580	2.58257	2.52332
0.020	0.04141	2.57929	2.49703
0.030	0.05702	2.57211	2.47173
0.040	0.07264	2.56276	2.44679
0.050	0.08825	2.55330	2.42165
0.060	0.10386	2.54263	2.39654
0.070	0.11948	2.53186	2.37142
0.080	0.13509	2.52094	2.34628
0.090	0.15070	2.50988	2.32112
0.100	0.16631	2.49868	2.29595
0.125	0.20535	2.47006	2.23298
0.150	0.24438	2.44048	2.16990
0.175	0.28341	2.40988	2.10674
0.200	0.32244	2.37816	2.04348
0.225	0.36147	2.34526	1.98011
0.250	0.40051	2.31109	1.91663
0.275	0.43954	2.27553	1.85304
0.300	0.47857	2.23850	1.78934
0.325	0.51760	2.19988	1.72551
0.350	0.55664	2.15955	1.66155
0.375	0.59567	2.11739	1.59746
0.400	0.63470	2.07326	1.53323
0.425	0.67373	2.02704	1.46884
0.450	0.71276	1.97858	1.40431
0.475	0.75180	1.92774	1.33960
0.500	0.79083	1.87437	1.27474
0.525	0.82986	1.81833	1.20969
0.550	0.86889	1.75949	1.14444
0.575	0.90792	1.69768	1.07900
0.600	0.94696	1.63277	1.01334
0.625	0.98599	1.56460	0.94746
0.650	1.02502	1.49298	0.88134
0.675	1.06405	1.41775	0.81496
0.700	1.10308	1.33871	0.74832
0.725	1.14212	1.25564	0.68138
0.750	1.18115	1.16832	0.61415
0.775	1.22018	1.07653	0.54660
0.800	1.25921	0.98001	0.47869
0.825	1.29824	0.87849	0.41041
0.850	1.33728	0.77168	0.34172
0.875	1.37631	0.65925	0.27261
0.900	1.41534	0.54088	0.20302
0.910	1.43095	0.49180	0.17506
0.920	1.44657	0.44169	0.14700
0.930	1.46218	0.39050	0.11886
0.940	1.47779	0.33827	0.09064
0.950	1.49341	0.28491	0.06232
0.960	1.50902	0.23042	0.03391
0.970	1.52463	0.17478	0.00540
0.980	1.54024	0.11794	-0.01855
0.990	1.55586	0.05989	-0.02150
1.000	1.57147	-0.00198	-0.00198

SECOND-STAGE BLADE COORDINATES
 ROOT SECTION (HOT RADIUS = 16.94200)

PERCENT X	X	Y TOP	Y BOT
0.0	0.00171	0.43803	0.43803
0.010	0.01220	0.47115	0.42735
0.020	0.02269	0.49032	0.43075
0.030	0.03318	0.50825	0.43689
0.040	0.04367	0.52556	0.44465
0.050	0.05415	0.54228	0.45362
0.060	0.06464	0.55843	0.46294
0.070	0.07513	0.57401	0.47180
0.080	0.08562	0.58906	0.48017
0.090	0.09611	0.60357	0.48808
0.100	0.10660	0.61759	0.49557
0.125	0.13282	0.65048	0.51260
0.150	0.15905	0.68042	0.52740
0.175	0.18527	0.70758	0.54018
0.200	0.21149	0.73207	0.55114
0.225	0.23771	0.75400	0.56039
0.250	0.26394	0.77344	0.56802
0.275	0.29016	0.79045	0.57412
0.300	0.31638	0.80510	0.57875
0.325	0.34261	0.81741	0.58193
0.350	0.36883	0.82739	0.58371
0.375	0.39505	0.83508	0.58410
0.400	0.42127	0.84047	0.58309
0.425	0.44750	0.84353	0.58069
0.450	0.47372	0.84427	0.57687
0.475	0.49994	0.84265	0.57161
0.500	0.52617	0.83861	0.56483
0.525	0.55239	0.83209	0.55649
0.550	0.57861	0.82303	0.54650
0.575	0.60483	0.81131	0.53475
0.600	0.63106	0.79683	0.52109
0.625	0.65728	0.77945	0.50533
0.650	0.68350	0.75899	0.48725
0.675	0.70973	0.73525	0.46649
0.700	0.73595	0.70796	0.44264
0.725	0.76217	0.67681	0.41517
0.750	0.78840	0.64140	0.38383
0.775	0.81462	0.60130	0.34895
0.800	0.84084	0.55615	0.31132
0.825	0.86706	0.50568	0.27156
0.850	0.89329	0.44978	0.23014
0.875	0.91951	0.38850	0.18737
0.900	0.94573	0.32198	0.14342
0.910	0.95622	0.29400	0.12555
0.920	0.96671	0.26524	0.10752
0.930	0.97720	0.23575	0.08936
0.940	0.98769	0.20556	0.07106
0.950	0.99818	0.17469	0.05262
0.960	1.00867	0.14316	0.03406
0.970	1.01916	0.11102	0.01537
0.980	1.02964	0.07828	-0.00119
0.990	1.04013	0.04499	-0.00361
1.000	1.05062	-0.00920	-0.00920

SECOND-STAGE BLADE COORDINATES
QTR ROOT SECTION (HOT RADIUS = 17.87300)

PERCENT X	X	Y TOP	Y BOT
0.0	0.00941	0.48439	0.48439
0.010	0.01982	0.51936	0.47310
0.020	0.03023	0.53968	0.47671
0.030	0.04064	0.55879	0.48324
0.040	0.05106	0.57707	0.49151
0.050	0.06147	0.59457	0.50109
0.060	0.07188	0.61132	0.51100
0.070	0.08229	0.62738	0.52038
0.080	0.09271	0.64275	0.52922
0.090	0.10312	0.65750	0.53755
0.100	0.11353	0.67162	0.54542
0.125	0.13956	0.70438	0.56321
0.150	0.16559	0.73376	0.57859
0.175	0.19162	0.75999	0.59183
0.200	0.21765	0.78329	0.60312
0.225	0.24368	0.80382	0.61261
0.250	0.26971	0.82170	0.62042
0.275	0.29574	0.83705	0.62662
0.300	0.32177	0.84994	0.63127
0.325	0.34780	0.86045	0.63444
0.350	0.37383	0.86862	0.63616
0.375	0.39986	0.87448	0.63641
0.400	0.42589	0.87804	0.63523
0.425	0.45192	0.87933	0.63259
0.450	0.47795	0.87832	0.62848
0.475	0.50398	0.87499	0.62284
0.500	0.53002	0.86931	0.61562
0.525	0.55605	0.86122	0.60676
0.550	0.58208	0.85066	0.59613
0.575	0.60811	0.83754	0.58362
0.600	0.63414	0.82173	0.56903
0.625	0.66017	0.80312	0.55215
0.650	0.68620	0.78151	0.53264
0.675	0.71223	0.75670	0.51008
0.700	0.73826	0.72842	0.48383
0.725	0.76429	0.69632	0.45323
0.750	0.79032	0.66003	0.41857
0.775	0.81635	0.61921	0.38107
0.800	0.84238	0.57364	0.34175
0.825	0.86841	0.52325	0.30112
0.850	0.89444	0.46813	0.25948
0.875	0.92047	0.40850	0.21701
0.900	0.94650	0.34471	0.17385
0.910	0.95691	0.31811	0.15641
0.920	0.96733	0.29094	0.13887
0.930	0.97774	0.26322	0.12126
0.940	0.98815	0.23500	0.10354
0.950	0.99856	0.20628	0.08577
0.960	1.00897	0.17709	0.06792
0.970	1.01939	0.14746	0.04997
0.980	1.02980	0.11743	0.03914
0.990	1.04021	0.08700	0.03905
1.000	1.05062	-0.05368	-0.05368

SECOND-STAGE BLADE COORDINATES
MEAN SECTION (HOT RADIUS = 18.80299)

PERCENT X	X	Y TOP	Y BOT
0.0	0.00941	0.55491	0.55491
0.010	0.01982	0.59002	0.54357
0.020	0.03024	0.61044	0.54721
0.030	0.04065	0.62949	0.55377
0.040	0.05106	0.64758	0.56209
0.050	0.06147	0.66477	0.57172
0.060	0.07188	0.68113	0.58168
0.070	0.08230	0.69671	0.59105
0.080	0.09271	0.71154	0.59983
0.090	0.10312	0.72567	0.60809
0.100	0.11353	0.73914	0.61585
0.125	0.13956	0.77008	0.63328
0.150	0.16559	0.79743	0.64822
0.175	0.19162	0.82153	0.66090
0.200	0.21765	0.84260	0.67157
0.225	0.24368	0.86084	0.68036
0.250	0.26971	0.87641	0.68740
0.275	0.29574	0.88942	0.69276
0.300	0.32177	0.89999	0.69650
0.325	0.34781	0.90816	0.69869
0.350	0.37384	0.91402	0.69932
0.375	0.39987	0.91759	0.69841
0.400	0.42590	0.91889	0.69596
0.425	0.45193	0.91793	0.69192
0.450	0.47796	0.91471	0.68627
0.475	0.50399	0.90919	0.67893
0.500	0.53002	0.90134	0.66981
0.525	0.55605	0.89111	0.65880
0.550	0.58208	0.87841	0.64572
0.575	0.60811	0.86314	0.63037
0.600	0.63414	0.84518	0.61245
0.625	0.66017	0.82437	0.59153
0.650	0.68620	0.80051	0.56704
0.675	0.71223	0.77335	0.53821
0.700	0.73826	0.74257	0.50514
0.725	0.76429	0.70779	0.46916
0.750	0.79032	0.66870	0.43142
0.775	0.81635	0.62513	0.39248
0.800	0.84238	0.57711	0.35260
0.825	0.86841	0.52482	0.31200
0.850	0.89444	0.46859	0.27075
0.875	0.92047	0.40882	0.22899
0.900	0.94650	0.34596	0.18676
0.910	0.95691	0.32005	0.16974
0.920	0.96733	0.29374	0.15266
0.930	0.97774	0.26707	0.13552
0.940	0.98815	0.24004	0.11832
0.950	0.99856	0.21270	0.10106
0.960	1.00897	0.18505	0.08375
0.970	1.01939	0.15712	0.06637
0.980	1.02980	0.12892	0.05504
0.990	1.04021	0.10049	0.05473
1.000	1.05062	0.06915	0.06915

SECOND-STAGE BLADE COORDINATES
QTR TIP COORDINATES (HOT RADIUS = 19.73500)

PERCENT X	X	Y TOP	Y BOT
0.0	-0.00037	0.65325	0.65325
0.010	0.01014	0.68512	0.64294
0.020	0.02065	0.70346	0.64614
0.030	0.03116	0.72025	0.65197
0.040	0.04167	0.73618	0.65934
0.050	0.05218	0.75131	0.66786
0.060	0.06269	0.76568	0.67671
0.070	0.07320	0.77935	0.68506
0.080	0.08371	0.79234	0.69287
0.090	0.09422	0.80469	0.70018
0.100	0.10473	0.81643	0.70704
0.125	0.13101	0.84331	0.72233
0.150	0.15728	0.86688	0.73520
0.175	0.18356	0.88744	0.74592
0.200	0.20983	0.90518	0.75465
0.225	0.23611	0.92028	0.76150
0.250	0.26238	0.93287	0.76658
0.275	0.28866	0.94304	0.76995
0.300	0.31493	0.95089	0.77165
0.325	0.34121	0.95646	0.77171
0.350	0.36748	0.95979	0.77012
0.375	0.39375	0.96093	0.76686
0.400	0.42003	0.95984	0.76190
0.425	0.44630	0.95655	0.75517
0.450	0.47258	0.95102	0.74657
0.475	0.49885	0.94320	0.73599
0.500	0.52513	0.93304	0.72326
0.525	0.55140	0.92046	0.70815
0.550	0.57768	0.90534	0.69033
0.575	0.60395	0.88756	0.66935
0.600	0.63023	0.86694	0.64456
0.625	0.65650	0.84325	0.61534
0.650	0.68278	0.81622	0.58227
0.675	0.70905	0.78549	0.54685
0.700	0.73533	0.75064	0.50993
0.725	0.76160	0.71139	0.47199
0.750	0.78788	0.66768	0.43323
0.775	0.81415	0.61969	0.39382
0.800	0.84042	0.56777	0.35383
0.825	0.86670	0.51242	0.31338
0.850	0.89297	0.45414	0.27250
0.875	0.91925	0.39345	0.23124
0.900	0.94552	0.33075	0.18962
0.910	0.95603	0.30521	0.17288
0.920	0.96654	0.27941	0.15610
0.930	0.97705	0.25341	0.13928
0.940	0.98756	0.22719	0.12240
0.950	0.99807	0.20079	0.10548
0.960	1.00858	0.17422	0.08853
0.970	1.01909	0.14749	0.07151
0.980	1.02960	0.12061	0.05520
0.990	1.04011	0.09359	0.05186
1.000	1.05062	0.06412	0.06412

SECOND-STAGE BLADE COORDINATES
TIP SECTION (HOT RADIUS = 20.66600)

PERCENT X	X	Y TOP	Y BOT
0.0	-0.02208	0.79950	0.79950
0.010	-0.01135	0.82495	0.79054
0.020	-0.00062	0.83950	0.79250
0.030	0.01011	0.85206	0.79652
0.040	0.02083	0.86393	0.80174
0.050	0.03156	0.87516	0.80784
0.060	0.04229	0.88580	0.81426
0.070	0.05301	0.89586	0.82032
0.080	0.06374	0.90539	0.82595
0.090	0.07447	0.91439	0.83119
0.100	0.08519	0.92291	0.83606
0.125	0.11201	0.94218	0.84667
0.150	0.13883	0.95875	0.85518
0.175	0.16565	0.97283	0.86174
0.200	0.19246	0.98457	0.86644
0.225	0.21928	0.99411	0.86933
0.250	0.24610	1.00150	0.87045
0.275	0.27292	1.00685	0.86983
0.300	0.29973	1.01017	0.86746
0.325	0.32655	1.01152	0.86330
0.350	0.35337	1.01091	0.85729
0.375	0.38019	1.00832	0.84936
0.400	0.40700	1.00372	0.83938
0.425	0.43382	0.99709	0.82719
0.450	0.46064	0.98837	0.81255
0.475	0.48746	0.97746	0.79515
0.500	0.51427	0.96429	0.77454
0.525	0.54109	0.94868	0.75006
0.550	0.56791	0.93046	0.72115
0.575	0.59473	0.90941	0.68854
0.600	0.62154	0.88522	0.65373
0.625	0.64836	0.85746	0.61755
0.650	0.67518	0.82559	0.58038
0.675	0.70200	0.78903	0.54244
0.700	0.72881	0.74754	0.50389
0.725	0.75563	0.70130	0.46481
0.750	0.78245	0.65085	0.42527
0.775	0.80927	0.59692	0.38533
0.800	0.83608	0.54023	0.34503
0.825	0.86290	0.48141	0.30439
0.850	0.88972	0.42096	0.26346
0.875	0.91654	0.35923	0.22224
0.900	0.94335	0.29654	0.18076
0.910	0.95408	0.27124	0.16410
0.920	0.96481	0.24583	0.14741
0.930	0.97553	0.22033	0.13066
0.940	0.98626	0.19473	0.11390
0.950	0.99699	0.16904	0.09709
0.960	1.00771	0.14328	0.08026
0.970	1.01844	0.11745	0.06338
0.980	1.02917	0.09154	0.04649
0.990	1.03989	0.06561	0.03157
1.000	1.05062	0.03819	0.03819

THIRD-STAGE VANE COORDINATES
 ROOT SECTION (HOT RADIUS = 17.35500)

PERCENT X	X	Y TOP	Y BOT
0.0	-0.00041	0.65793	0.65793
0.010	0.01570	0.71300	0.64681
0.020	0.03181	0.75378	0.65750
0.030	0.04791	0.79133	0.67258
0.040	0.06402	0.82610	0.68799
0.050	0.08013	0.85845	0.70308
0.060	0.09624	0.88864	0.71782
0.070	0.11234	0.91690	0.73221
0.080	0.12845	0.94342	0.74625
0.090	0.14456	0.96835	0.75991
0.100	0.16067	0.99182	0.77319
0.125	0.20094	1.04471	0.80463
0.150	0.24121	1.09036	0.83342
0.175	0.28147	1.12975	0.85937
0.200	0.32174	1.16354	0.88228
0.225	0.36201	1.19225	0.90199
0.250	0.40228	1.21631	0.91832
0.275	0.44255	1.23601	0.93111
0.300	0.48282	1.25162	0.94023
0.325	0.52309	1.26331	0.94558
0.350	0.56336	1.27123	0.94707
0.375	0.60363	1.27550	0.94468
0.400	0.64390	1.27618	0.93839
0.425	0.68417	1.27331	0.92825
0.450	0.72443	1.26694	0.91430
0.475	0.76470	1.25702	0.89666
0.500	0.80497	1.24354	0.87545
0.525	0.84524	1.22642	0.85083
0.550	0.88551	1.20557	0.82295
0.575	0.92578	1.18086	0.79201
0.600	0.96605	1.15209	0.75818
0.625	1.00632	1.11904	0.72166
0.650	1.04659	1.08142	0.68262
0.675	1.08685	1.03884	0.64125
0.700	1.12712	0.99086	0.59773
0.725	1.16739	0.93700	0.55222
0.750	1.20766	0.87699	0.50487
0.775	1.24793	0.81077	0.45583
0.800	1.28820	0.73850	0.40526
0.825	1.32847	0.66054	0.35324
0.850	1.36874	0.57738	0.29993
0.875	1.40901	0.48960	0.24540
0.900	1.44928	0.39781	0.18977
0.910	1.46538	0.36010	0.16723
0.920	1.48149	0.32186	0.14453
0.930	1.49760	0.28314	0.12167
0.940	1.51371	0.24396	0.09867
0.950	1.52981	0.20436	0.07553
0.960	1.54592	0.16436	0.05224
0.970	1.56203	0.12400	0.02883
0.980	1.57814	0.08327	0.00528
0.990	1.59424	0.04223	-0.01343
1.000	1.61035	-0.00146	-0.00146

THIRD-STAGE VANE COORDINATES
 QTR ROOT SECTION (HOT RADIUS = 18.46500)

PERCENT X	X	Y TOP	Y BOT
0.0	-0.00007	0.83670	0.83670
0.010	0.01603	0.88372	0.82705
0.020	0.03214	0.91825	0.83617
0.030	0.04824	0.95080	0.84887
0.040	0.06434	0.98159	0.86175
0.050	0.08045	1.01077	0.87434
0.060	0.09655	1.03845	0.88662
0.070	0.11266	1.06475	0.89858
0.080	0.12876	1.08975	0.91023
0.090	0.14487	1.11355	0.92156
0.100	0.16097	1.13622	0.93256
0.125	0.20123	1.18828	0.95859
0.150	0.24149	1.23440	0.98240
0.175	0.28175	1.27514	1.00390
0.200	0.32201	1.31101	1.02298
0.225	0.36227	1.34231	1.03952
0.250	0.40253	1.36936	1.05341
0.275	0.44279	1.39235	1.06454
0.300	0.48306	1.41145	1.07279
0.325	0.52332	1.42679	1.07806
0.350	0.56358	1.43847	1.08025
0.375	0.60384	1.44655	1.07924
0.400	0.64410	1.45104	1.07495
0.425	0.68436	1.45197	1.06730
0.450	0.72462	1.44931	1.05622
0.475	0.76488	1.44300	1.04162
0.500	0.80514	1.43297	1.02346
0.525	0.84540	1.41909	1.00172
0.550	0.88566	1.40122	0.97634
0.575	0.92592	1.37915	0.94731
0.600	0.96618	1.35264	0.91466
0.625	1.00644	1.32135	0.87838
0.650	1.04670	1.28487	0.83852
0.675	1.08696	1.24264	0.79509
0.700	1.12722	1.19394	0.74818
0.725	1.16748	1.13787	0.69784
0.750	1.20775	1.07356	0.64415
0.775	1.24801	1.00035	0.58719
0.800	1.28827	0.91799	0.52706
0.825	1.32853	0.82663	0.46386
0.850	1.36879	0.72679	0.39769
0.875	1.40905	0.61933	0.32867
0.900	1.44931	0.50520	0.25692
0.910	1.46541	0.45789	0.22746
0.920	1.48152	0.40974	0.19760
0.930	1.49762	0.36081	0.16733
0.940	1.51373	0.31114	0.13667
0.950	1.52983	0.26078	0.10561
0.960	1.54593	0.20979	0.07416
0.970	1.56204	0.15822	0.04234
0.980	1.57814	0.10611	0.01015
0.990	1.59425	0.05348	-0.01343
1.000	1.61035	-0.00147	-0.00147

THIRD-STAGE VANE COORDINATES
 MEAN SECTION (HOT RADIUS = 19.57600)

PERCENT X	X	Y TOP	Y BOT
0.0	0.00028	1.02438	1.02438
0.010	0.01638	1.06534	1.01555
0.020	0.03248	1.09460	1.02322
0.030	0.04858	1.12231	1.03391
0.040	0.06468	1.14861	1.04470
0.050	0.08078	1.17360	1.05530
0.060	0.09688	1.19735	1.06567
0.070	0.11299	1.21996	1.07583
0.080	0.12909	1.24148	1.08576
0.090	0.14519	1.26199	1.09546
0.100	0.16129	1.28151	1.10493
0.125	0.20154	1.32636	1.12745
0.150	0.24179	1.36600	1.14827
0.175	0.28204	1.40089	1.16722
0.200	0.32229	1.43138	1.18414
0.225	0.36255	1.45774	1.19886
0.250	0.40280	1.48021	1.21118
0.275	0.44305	1.49893	1.22091
0.300	0.48330	1.51404	1.22784
0.325	0.52355	1.52563	1.23177
0.350	0.56381	1.53376	1.23246
0.375	0.60406	1.53848	1.22972
0.400	0.64431	1.53979	1.22335
0.425	0.68456	1.53766	1.21314
0.450	0.72481	1.53206	1.19894
0.475	0.76506	1.52292	1.18061
0.500	0.80532	1.51012	1.15803
0.525	0.84557	1.49354	1.13115
0.550	0.88582	1.47298	1.09992
0.575	0.92607	1.44822	1.06437
0.600	0.96632	1.41895	1.02455
0.625	1.00657	1.38478	0.98056
0.650	1.04683	1.34523	0.93254
0.675	1.08708	1.29963	0.88063
0.700	1.12733	1.24712	0.82502
0.725	1.16758	1.18669	0.76591
0.750	1.20783	1.11754	0.70352
0.775	1.24809	1.03910	0.63805
0.800	1.28834	0.95133	0.56972
0.825	1.32859	0.85457	0.49873
0.850	1.36884	0.74956	0.42529
0.875	1.40909	0.63726	0.34958
0.900	1.44934	0.51872	0.27180
0.910	1.46544	0.46977	0.24014
0.920	1.48155	0.42005	0.20819
0.930	1.49765	0.36962	0.17595
0.940	1.51375	0.31850	0.14343
0.950	1.52985	0.26678	0.11064
0.960	1.54595	0.21448	0.07761
0.970	1.56205	0.16165	0.04432
0.980	1.57815	0.10833	0.01079
0.990	1.59425	0.05455	-0.01343
1.000	1.61035	-0.00146	-0.00146

THIRD-STAGE VANE COORDINATES
QTR TIP SECTION (HOT RADIUS = 20.68600)

PERCENT X	X	Y TOP	Y BOT
0.0	0.00065	1.22253	1.22253
0.010	0.01675	1.25721	1.21416
0.020	0.03285	1.28096	1.22001
0.030	0.04894	1.30357	1.22831
0.040	0.06504	1.32510	1.23666
0.050	0.08114	1.34562	1.24485
0.060	0.09724	1.36517	1.25289
0.070	0.11333	1.38379	1.26075
0.080	0.12943	1.40156	1.26846
0.090	0.14553	1.41849	1.27597
0.100	0.16162	1.43461	1.28330
0.125	0.20187	1.47162	1.30074
0.150	0.24211	1.50421	1.31680
0.175	0.28235	1.53270	1.33131
0.200	0.32259	1.55734	1.34411
0.225	0.36284	1.57830	1.35497
0.250	0.40308	1.59577	1.36368
0.275	0.44332	1.60985	1.36997
0.300	0.48356	1.62061	1.37359
0.325	0.52381	1.62813	1.37422
0.350	0.56405	1.63243	1.37157
0.375	0.60429	1.63352	1.36532
0.400	0.64453	1.63139	1.35517
0.425	0.68478	1.62599	1.34080
0.450	0.72502	1.61728	1.32197
0.475	0.76526	1.60515	1.29848
0.500	0.80550	1.58948	1.27018
0.525	0.84574	1.57011	1.23698
0.550	0.88599	1.54683	1.19891
0.575	0.92623	1.51939	1.15608
0.600	0.96647	1.48745	1.10861
0.625	1.00671	1.45057	1.05677
0.650	1.04696	1.40823	1.00081
0.675	1.08720	1.35966	0.94104
0.700	1.12744	1.30392	0.87776
0.725	1.16768	1.24001	0.81130
0.750	1.20793	1.16714	0.74194
0.775	1.24817	1.08479	0.66999
0.800	1.28841	0.99289	0.59571
0.825	1.32865	0.89179	0.51934
0.850	1.36890	0.78221	0.44111
0.875	1.40914	0.66510	0.36120
0.900	1.44938	0.54147	0.27982
0.910	1.46548	0.49042	0.24688
0.920	1.48158	0.43855	0.21374
0.930	1.49767	0.38592	0.18040
0.940	1.51377	0.33258	0.14688
0.950	1.52987	0.27858	0.11319
0.960	1.54596	0.22398	0.07932
0.970	1.56206	0.16879	0.04528
0.980	1.57816	0.11309	0.01109
0.990	1.59425	0.05691	-0.01343
1.000	1.61035	-0.00146	-0.00146

THIRD-STAGE VANE COORDINATES
TIP SECTION (HOT RADIUS = 21.79700)

PERCENT X	X	Y TOP	Y BOT
0.0	0.00105	1.43534	1.43534
0.010	0.01715	1.46634	1.42696
0.020	0.03324	1.48687	1.43153
0.030	0.04933	1.50634	1.43818
0.040	0.06543	1.52483	1.44482
0.050	0.08152	1.54236	1.45132
0.060	0.09761	1.55900	1.45767
0.070	0.11370	1.57479	1.46387
0.080	0.12980	1.58975	1.46992
0.090	0.14589	1.60394	1.47579
0.100	0.16198	1.61739	1.48149
0.125	0.20222	1.64788	1.49492
0.150	0.24245	1.67422	1.50702
0.175	0.28268	1.69668	1.51764
0.200	0.32291	1.71548	1.52652
0.225	0.36315	1.73082	1.53346
0.250	0.40338	1.74282	1.53817
0.275	0.44361	1.75158	1.54032
0.300	0.48384	1.75718	1.53958
0.325	0.52408	1.75966	1.53557
0.350	0.56431	1.75907	1.52788
0.375	0.60454	1.75539	1.51611
0.400	0.64477	1.74862	1.49988
0.425	0.68501	1.73870	1.47881
0.450	0.72524	1.72556	1.45263
0.475	0.76547	1.70912	1.42117
0.500	0.80570	1.68925	1.38434
0.525	0.84594	1.66578	1.34221
0.550	0.88617	1.63851	1.29495
0.575	0.92640	1.60717	1.24284
0.600	0.96663	1.57142	1.18622
0.625	1.00686	1.53082	1.12548
0.650	1.04710	1.48482	1.06104
0.675	1.08733	1.43265	0.99329
0.700	1.12756	1.37336	0.92261
0.725	1.16779	1.30606	0.84935
0.750	1.20803	1.22990	0.77382
0.775	1.24826	1.14428	0.69632
0.800	1.28849	1.04895	0.61710
0.825	1.32872	0.94400	0.53634
0.850	1.36896	0.82988	0.45425
0.875	1.40919	0.70735	0.37100
0.900	1.44942	0.57729	0.28672
0.910	1.46551	0.52337	0.25274
0.920	1.48161	0.46845	0.21863
0.930	1.49770	0.41262	0.18439
0.940	1.51379	0.35590	0.15001
0.950	1.52989	0.29836	0.11552
0.960	1.54598	0.24006	0.08092
0.970	1.56207	0.18105	0.04621
0.980	1.57817	0.12136	0.01138
0.990	1.59426	0.06105	-0.01343
1.000	1.61035	-0.00146	-0.00146

THIRD-STAGE BLADE COORDINATES
 ROOT SECTION (HOT RADIUS = 17.53300)

PERCENT X	X	Y TOP	Y BOT
0.0	-0.00048	0.67741	0.67741
0.010	0.01282	0.70872	0.66855
0.020	0.02611	0.72689	0.67276
0.030	0.03940	0.74362	0.67956
0.040	0.05269	0.76008	0.68794
0.050	0.06598	0.77625	0.69717
0.060	0.07928	0.79213	0.70608
0.070	0.09257	0.80770	0.71455
0.080	0.10586	0.82297	0.72261
0.090	0.11915	0.83791	0.73026
0.100	0.13245	0.85253	0.73751
0.125	0.16568	0.88765	0.75402
0.150	0.19891	0.92063	0.76832
0.175	0.23214	0.95141	0.78057
0.200	0.26537	0.97992	0.79087
0.225	0.29860	1.00608	0.79932
0.250	0.33183	1.02983	0.80598
0.275	0.36506	1.05111	0.81092
0.300	0.39829	1.06984	0.81415
0.325	0.43152	1.08595	0.81573
0.350	0.46475	1.09935	0.81562
0.375	0.49799	1.10997	0.81387
0.400	0.53122	1.11770	0.81044
0.425	0.56445	1.12247	0.80530
0.450	0.59768	1.12414	0.79843
0.475	0.63091	1.12260	0.78974
0.500	0.66414	1.11773	0.77919
0.525	0.69737	1.10938	0.76666
0.550	0.73060	1.09738	0.75205
0.575	0.76383	1.08157	0.73521
0.600	0.79706	1.06174	0.71594
0.625	0.83029	1.03765	0.69396
0.650	0.86353	1.00906	0.66881
0.675	0.89676	0.97568	0.64006
0.700	0.92999	0.93716	0.60741
0.725	0.96322	0.89313	0.57020
0.750	0.99645	0.84313	0.52776
0.775	1.02968	0.78671	0.48043
0.800	1.06291	0.72352	0.42925
0.825	1.09614	0.65342	0.37511
0.850	1.12937	0.57654	0.31852
0.875	1.16260	0.49320	0.25994
0.900	1.19583	0.40390	0.19970
0.910	1.20912	0.36664	0.17517
0.920	1.22242	0.32857	0.15038
0.930	1.23571	0.28971	0.12544
0.940	1.24900	0.25014	0.10026
0.950	1.26229	0.20986	0.07489
0.960	1.27559	0.16893	0.04931
0.970	1.28888	0.12738	0.02357
0.980	1.30217	0.08526	-0.00236
0.990	1.31546	0.04259	-0.01495
1.000	1.32876	-0.00248	-0.00248

THIRD-STAGE BLADE COORDINATES
QTR ROOT SECTION (HOT RADIUS = 18.84399)

PERCENT X	X	Y TOP	Y BOT
0.0	-0.00046	0.68076	0.68076
0.010	0.01283	0.72322	0.66959
0.020	0.02612	0.74885	0.67625
0.030	0.03941	0.77326	0.68661
0.040	0.05271	0.79659	0.69933
0.050	0.06600	0.81891	0.71302
0.060	0.07929	0.84028	0.72594
0.070	0.09258	0.86073	0.73806
0.080	0.10587	0.88033	0.74943
0.090	0.11917	0.89909	0.76013
0.100	0.13246	0.91707	0.77019
0.125	0.16569	0.95872	0.79285
0.150	0.19892	0.99600	0.81230
0.175	0.23215	1.02923	0.82892
0.200	0.26538	1.05865	0.84297
0.225	0.29861	1.08448	0.85464
0.250	0.33184	1.10687	0.86410
0.275	0.36507	1.12593	0.87145
0.300	0.39830	1.14178	0.87676
0.325	0.43153	1.15450	0.88011
0.350	0.46476	1.16411	0.88152
0.375	0.49799	1.17067	0.88101
0.400	0.53122	1.17419	0.87858
0.425	0.56446	1.17464	0.87420
0.450	0.59769	1.17203	0.86782
0.475	0.63092	1.16630	0.85938
0.500	0.66415	1.15739	0.84878
0.525	0.69738	1.14522	0.83589
0.550	0.73061	1.12967	0.82053
0.575	0.76384	1.11062	0.80246
0.600	0.79707	1.08790	0.78132
0.625	0.83030	1.06129	0.75680
0.650	0.86353	1.03054	0.72845
0.675	0.89676	0.99533	0.69535
0.700	0.92999	0.95525	0.65587
0.725	0.96322	0.90979	0.60928
0.750	0.99645	0.85832	0.55753
0.775	1.02968	0.80024	0.50254
0.800	1.06291	0.73519	0.44533
0.825	1.09614	0.66307	0.38642
0.850	1.12937	0.58408	0.32619
0.875	1.16260	0.49870	0.26482
0.900	1.19583	0.40754	0.20247
0.910	1.20913	0.36963	0.17728
0.920	1.22242	0.33095	0.15198
0.930	1.23571	0.29157	0.12653
0.940	1.24900	0.25150	0.10097
0.950	1.26229	0.21082	0.07530
0.960	1.27559	0.16955	0.04953
0.970	1.28888	0.12774	0.02364
0.980	1.30217	0.08542	-0.00236
0.990	1.31546	0.04264	-0.01494
1.000	1.32876	-0.00247	-0.00247

THIRD-STAGE BLADE COORDINATES
MEAN SECTION (HOT RADIUS = 20.15401)

PERCENT X	X	Y TOP	Y BOT
0.0	-0.00023	0.73695	0.73695
0.010	0.01306	0.78223	0.72504
0.020	0.02635	0.81000	0.73230
0.030	0.03964	0.83638	0.74137
0.040	0.05293	0.86145	0.75749
0.050	0.06622	0.88529	0.77233
0.060	0.07951	0.90798	0.78620
0.070	0.09280	0.92959	0.79915
0.080	0.10609	0.95019	0.81126
0.090	0.11938	0.96980	0.82259
0.100	0.13267	0.98849	0.83322
0.125	0.16589	1.03143	0.85701
0.150	0.19911	1.06936	0.87728
0.175	0.23234	1.10272	0.89447
0.200	0.26556	1.13186	0.90889
0.225	0.29879	1.15704	0.92076
0.250	0.33201	1.17848	0.93026
0.275	0.36524	1.19634	0.93752
0.300	0.39846	1.21078	0.94262
0.325	0.43169	1.22190	0.94562
0.350	0.46491	1.22978	0.94656
0.375	0.49814	1.23447	0.94545
0.400	0.53136	1.23601	0.94229
0.425	0.56459	1.23441	0.93701
0.450	0.59781	1.22965	0.92956
0.475	0.63104	1.22172	0.91987
0.500	0.66426	1.21055	0.90777
0.525	0.69749	1.19606	0.89308
0.550	0.73071	1.17814	0.87563
0.575	0.76394	1.15665	0.85523
0.600	0.79716	1.13142	0.83155
0.625	0.83039	1.10221	0.80348
0.650	0.86361	1.06873	0.76915
0.675	0.89683	1.03061	0.72744
0.700	0.93006	0.98738	0.67944
0.725	0.96328	0.93842	0.62626
0.750	0.99651	0.88311	0.56977
0.775	1.02973	0.82096	0.51133
0.800	1.06296	0.75178	0.45152
0.825	1.09618	0.67570	0.39064
0.850	1.12941	0.59312	0.32892
0.875	1.16263	0.50466	0.26645
0.900	1.19586	0.41107	0.20330
0.910	1.20915	0.37237	0.17789
0.920	1.22244	0.33300	0.15240
0.930	1.23573	0.29303	0.12678
0.940	1.24902	0.25249	0.10111
0.950	1.26231	0.21142	0.07535
0.960	1.27560	0.16986	0.04953
0.970	1.28889	0.12785	0.02361
0.980	1.30218	0.08542	-0.00238
0.990	1.31547	0.04260	-0.01494
1.000	1.32876	-0.00246	-0.00246

THIRD-STAGE BLADE COORDINATES
QTR TIP SECTION (HOT RADIUS = 21.46500)

PERCENT X	X	Y TOP	Y BOT
0.0	0.00015	0.83054	0.83054
0.010	0.01343	0.87454	0.81895
0.020	0.02672	0.90126	0.82592
0.030	0.04001	0.92657	0.83677
0.040	0.05329	0.95056	0.85011
0.050	0.06658	0.97334	0.86438
0.060	0.07986	0.99498	0.87770
0.070	0.09315	1.01554	0.89011
0.080	0.10644	1.03511	0.90169
0.090	0.11972	1.05372	0.91248
0.100	0.13301	1.07142	0.92257
0.125	0.16622	1.11200	0.94502
0.150	0.19944	1.14772	0.96395
0.175	0.23265	1.17902	0.97979
0.200	0.26587	1.20623	0.99284
0.225	0.29908	1.22960	1.00333
0.250	0.33230	1.24933	1.01142
0.275	0.36552	1.26560	1.01721
0.300	0.39873	1.27851	1.02080
0.325	0.43195	1.28817	1.02221
0.350	0.46516	1.29465	1.02148
0.375	0.49838	1.29796	1.01859
0.400	0.53159	1.29816	1.01352
0.425	0.56481	1.29522	1.00618
0.450	0.59802	1.28911	0.99647
0.475	0.63124	1.27978	0.98428
0.500	0.66445	1.26718	0.96937
0.525	0.69767	1.25117	0.95149
0.550	0.73088	1.23165	0.93024
0.575	0.76410	1.20841	0.90497
0.600	0.79731	1.18125	0.87477
0.625	0.83053	1.14990	0.83877
0.650	0.86374	1.11396	0.79569
0.675	0.89696	1.07301	0.74515
0.700	0.93017	1.02642	0.69025
0.725	0.96339	0.97349	0.63312
0.750	0.99660	0.91365	0.57452
0.775	1.02982	0.84662	0.51476
0.800	1.06303	0.77247	0.45403
0.825	1.09625	0.69163	0.39247
0.850	1.12946	0.60477	0.33020
0.875	1.16268	0.51269	0.26731
0.900	1.19590	0.41619	0.20386
0.910	1.20918	0.37652	0.17835
0.920	1.22247	0.33631	0.15276
0.930	1.23575	0.29560	0.12706
0.940	1.24904	0.25442	0.10132
0.950	1.26233	0.21281	0.07549
0.960	1.27561	0.17081	0.04961
0.970	1.28890	0.12844	0.02365
0.980	1.30218	0.08574	-0.00239
0.990	1.31547	0.04271	-0.01494
1.000	1.32876	-0.00247	-0.00247

THIRD-STAGE BLADE COORDINATES
TIP SECTION (HOT RADIUS = 22.77499)

PERCENT X	X	Y TOP	Y BOT
0.0	0.00063	0.94790	0.94790
0.010	0.01391	0.98978	0.93692
0.020	0.02719	1.01483	0.94350
0.030	0.04047	1.03835	0.95372
0.040	0.05375	1.06054	0.96625
0.050	0.06703	1.08150	0.97972
0.060	0.08031	1.10134	0.99230
0.070	0.09360	1.12011	1.00398
0.080	0.10688	1.13790	1.01485
0.090	0.12016	1.15475	1.02495
0.100	0.13344	1.17071	1.03435
0.125	0.16664	1.20705	1.05510
0.150	0.19985	1.23872	1.07235
0.175	0.23305	1.26616	1.08650
0.200	0.26625	1.28969	1.09785
0.225	0.29946	1.30958	1.10659
0.250	0.33266	1.32603	1.11286
0.275	0.36586	1.33921	1.11677
0.300	0.39907	1.34921	1.11836
0.325	0.43227	1.35613	1.11767
0.350	0.46547	1.36005	1.11468
0.375	0.49868	1.36098	1.10935
0.400	0.53188	1.35893	1.10160
0.425	0.56508	1.35390	1.09132
0.450	0.59829	1.34585	1.07831
0.475	0.63149	1.33470	1.06233
0.500	0.66469	1.32038	1.04306
0.525	0.69790	1.30276	1.01999
0.550	0.73110	1.28167	0.99227
0.575	0.76430	1.25691	0.95848
0.600	0.79750	1.22821	0.91674
0.625	0.83071	1.19523	0.86815
0.650	0.86391	1.15750	0.81525
0.675	0.89711	1.11444	0.75933
0.700	0.93032	1.06526	0.70147
0.725	0.96352	1.00915	0.64231
0.750	0.99672	0.94556	0.58215
0.775	1.02993	0.87439	0.52110
0.800	1.06313	0.79592	0.45929
0.825	1.09633	0.71082	0.39680
0.850	1.12954	0.61996	0.33370
0.875	1.16274	0.52428	0.27006
0.900	1.19594	0.42463	0.20592
0.910	1.20922	0.38384	0.18012
0.920	1.22251	0.34256	0.15426
0.930	1.23579	0.30085	0.12831
0.940	1.24907	0.25874	0.10232
0.950	1.26235	0.21627	0.07625
0.960	1.27563	0.17346	0.05009
0.970	1.28891	0.13035	0.02392
0.980	1.30219	0.08695	-0.00235
0.990	1.31547	0.04329	-0.01495
1.000	1.32876	-0.00247	-0.00247

FOURTH-STAGE BLADE COORDINATES
 ROOT SECTION (HOT RADIUS = 17.65700)

PERCENT X	X	Y TOP	Y BOT
0.0	-0.00048	0.67553	0.67553
0.010	0.01281	0.70826	0.66642
0.020	0.02610	0.72740	0.67095
0.030	0.03939	0.74509	0.67819
0.040	0.05269	0.76240	0.68709
0.050	0.06598	0.77935	0.69692
0.060	0.07927	0.79591	0.70634
0.070	0.09256	0.81211	0.71527
0.080	0.10585	0.82791	0.72375
0.090	0.11915	0.84334	0.73178
0.100	0.13244	0.85838	0.73940
0.125	0.16567	0.89433	0.75670
0.150	0.19890	0.92787	0.77166
0.175	0.23213	0.95897	0.78448
0.200	0.26536	0.98761	0.79528
0.225	0.29859	1.01375	0.80416
0.250	0.33183	1.03735	0.81120
0.275	0.36506	1.05837	0.81646
0.300	0.39829	1.07677	0.81999
0.325	0.43152	1.09248	0.82182
0.350	0.46475	1.10543	0.82194
0.375	0.49798	1.11557	0.82038
0.400	0.53121	1.12281	0.81711
0.425	0.56444	1.12707	0.81211
0.450	0.59767	1.12825	0.80535
0.475	0.63090	1.12623	0.79674
0.500	0.66414	1.12091	0.78624
0.525	0.69737	1.11213	0.77374
0.550	0.73060	1.09975	0.75911
0.575	0.76383	1.08360	0.74219
0.600	0.79706	1.06348	0.72275
0.625	0.83029	1.03916	0.70056
0.650	0.86352	1.01039	0.67521
0.675	0.89675	0.97689	0.64624
0.700	0.92998	0.93829	0.61302
0.725	0.96322	0.89421	0.57482
0.750	0.99645	0.84418	0.53131
0.775	1.02968	0.78770	0.48308
0.800	1.06291	0.72442	0.43119
0.825	1.09614	0.65422	0.37647
0.850	1.12937	0.57720	0.31945
0.875	1.16260	0.49371	0.26055
0.900	1.19583	0.40425	0.20005
0.910	1.20912	0.36694	0.17544
0.920	1.22242	0.32882	0.15058
0.930	1.23571	0.28991	0.12558
0.940	1.24900	0.25029	0.10035
0.950	1.26229	0.20997	0.07495
0.960	1.27559	0.16901	0.04934
0.970	1.28888	0.12743	0.02358
0.980	1.30217	0.08529	-0.00236
0.990	1.31546	0.04260	-0.01495
1.000	1.32876	-0.00247	-0.00247

FOURTH-STAGE BLADE COORDINATES
 QTR ROOT SECTION (HOT RADIUS = 19.09200)

PERCENT X	X	Y TOP	Y BOT
0.0	-0.00044	0.68756	0.68756
0.010	0.01286	0.73111	0.67611
0.020	0.02615	0.75754	0.68301
0.030	0.03944	0.78272	0.69374
0.040	0.05273	0.80674	0.70691
0.050	0.06602	0.82968	0.72105
0.060	0.07932	0.85159	0.73437
0.070	0.09261	0.87253	0.74683
0.080	0.10590	0.89256	0.75853
0.090	0.11919	0.91169	0.76951
0.100	0.13248	0.92999	0.77984
0.125	0.16571	0.97227	0.80306
0.150	0.19894	1.00995	0.82298
0.175	0.23217	1.04337	0.83997
0.200	0.26540	1.07284	0.85433
0.225	0.29863	1.09859	0.86625
0.250	0.33186	1.12078	0.87591
0.275	0.36509	1.13955	0.88341
0.300	0.39832	1.15505	0.88885
0.325	0.43155	1.16735	0.89228
0.350	0.46478	1.17650	0.89375
0.375	0.49801	1.18256	0.89326
0.400	0.53124	1.18555	0.89081
0.425	0.56447	1.18546	0.88639
0.450	0.59770	1.18230	0.87992
0.475	0.63093	1.17601	0.87135
0.500	0.66416	1.16655	0.86058
0.525	0.69739	1.15384	0.84745
0.550	0.73062	1.13775	0.83181
0.575	0.76385	1.11818	0.81340
0.600	0.79708	1.09496	0.79188
0.625	0.83031	1.06785	0.76682
0.650	0.86354	1.03662	0.73754
0.675	0.89677	1.00092	0.70309
0.700	0.93000	0.96035	0.66208
0.725	0.96323	0.91436	0.61403
0.750	0.99646	0.86232	0.56106
0.775	1.02969	0.80364	0.50512
0.800	1.06292	0.73797	0.44718
0.825	1.09615	0.66523	0.38770
0.850	1.12938	0.58566	0.32704
0.875	1.16261	0.49977	0.26534
0.900	1.19584	0.40819	0.20276
0.910	1.20913	0.37014	0.17750
0.920	1.22242	0.33135	0.15213
0.930	1.23571	0.29186	0.12663
0.940	1.24900	0.25170	0.10103
0.950	1.26230	0.21095	0.07533
0.960	1.27559	0.16962	0.04954
0.970	1.28888	0.12777	0.02364
0.980	1.30217	0.08543	-0.00236
0.990	1.31546	0.04264	-0.01494
1.000	1.32876	-0.00247	-0.00247

FOURTH-STAGE BLADE COORDINATES
MEAN SECTION (HOT RADIUS = 21.24500)

PERCENT X	X	Y TOP	Y BOT
0.0	0.00008	0.81316	0.81316
0.010	0.01336	0.85744	0.80149
0.020	0.02665	0.88438	0.80852
0.030	0.03994	0.90993	0.81946
0.040	0.05322	0.93416	0.83290
0.050	0.06651	0.95718	0.84728
0.060	0.07980	0.97906	0.86071
0.070	0.09308	0.99987	0.87323
0.080	0.10637	1.01967	0.88490
0.090	0.11966	1.03851	0.89580
0.100	0.13294	1.05645	0.90599
0.125	0.16616	1.09758	0.92869
0.150	0.19938	1.13383	0.94786
0.175	0.23260	1.16561	0.96395
0.200	0.26581	1.19329	0.97726
0.225	0.29903	1.21709	0.98801
0.250	0.33225	1.23723	0.99636
0.275	0.36546	1.25387	1.00243
0.300	0.39868	1.26714	1.00630
0.325	0.43190	1.27713	1.00802
0.350	0.46511	1.28392	1.00761
0.375	0.49833	1.28753	1.00506
0.400	0.53155	1.28800	1.00036
0.425	0.56477	1.28533	0.99342
0.450	0.59798	1.27946	0.98415
0.475	0.63120	1.27038	0.97245
0.500	0.66442	1.25802	0.95809
0.525	0.69763	1.24225	0.94085
0.550	0.73085	1.22297	0.92038
0.575	0.76407	1.19999	0.89619
0.600	0.79728	1.17310	0.86754
0.625	0.83050	1.14204	0.83337
0.650	0.86372	1.10645	0.79194
0.675	0.89694	1.06590	0.74267
0.700	0.93015	1.01981	0.68861
0.725	0.96337	0.96749	0.63198
0.750	0.99659	0.90836	0.57366
0.775	1.02980	0.84210	0.51409
0.800	1.06302	0.76876	0.45350
0.825	1.09624	0.68871	0.39206
0.850	1.12945	0.60257	0.32989
0.875	1.16267	0.51110	0.26708
0.900	1.19589	0.41513	0.20369
0.910	1.20918	0.37563	0.17820
0.920	1.22246	0.33557	0.15264
0.930	1.23575	0.29501	0.12696
0.940	1.24903	0.25396	0.10125
0.950	1.26232	0.21246	0.07544
0.960	1.27561	0.17055	0.04957
0.970	1.28890	0.12826	0.02363
0.980	1.30218	0.08563	-0.00239
0.990	1.31547	0.04267	-0.01494
1.000	1.32876	-0.00247	-0.00247

FOURTH-STAGE BLADE COORDINATES
 QTR TIP SECTION (HOT RADIUS = 23.03799)

PERCENT X	X	Y TOP	Y BOT
0.0	0.00074	0.97496	0.97496
0.010	0.01402	1.01616	0.96415
0.020	0.02730	1.04072	0.97060
0.030	0.04058	1.06371	0.98061
0.040	0.05386	1.08540	0.99286
0.050	0.06714	1.10587	1.00606
0.060	0.08042	1.12523	1.01841
0.070	0.09370	1.14354	1.02986
0.080	0.10698	1.16087	1.04051
0.090	0.12026	1.17728	1.05040
0.100	0.13354	1.19282	1.05960
0.125	0.16674	1.22813	1.07987
0.150	0.19994	1.25883	1.09665
0.175	0.23314	1.28537	1.11036
0.200	0.26634	1.30804	1.12125
0.225	0.29954	1.32712	1.12954
0.250	0.33274	1.34281	1.13534
0.275	0.36594	1.35526	1.13878
0.300	0.39914	1.36458	1.13987
0.325	0.43234	1.37087	1.13865
0.350	0.46554	1.37418	1.13509
0.375	0.49874	1.37454	1.12916
0.400	0.53194	1.37195	1.12073
0.425	0.56515	1.36641	1.10970
0.450	0.59835	1.35788	1.09583
0.475	0.63155	1.34628	1.07886
0.500	0.66475	1.33154	1.05839
0.525	0.69795	1.31351	1.03384
0.550	0.73115	1.29202	1.00432
0.575	0.76435	1.26688	0.96847
0.600	0.79755	1.23779	0.92442
0.625	0.83075	1.20441	0.87361
0.650	0.86395	1.16626	0.81911
0.675	0.89715	1.12273	0.76242
0.700	0.93035	1.07300	0.70418
0.725	0.96355	1.01626	0.64469
0.750	0.99675	0.95198	0.58421
0.775	1.02995	0.88006	0.52288
0.800	1.06315	0.80082	0.46080
0.825	1.09635	0.71497	0.39808
0.850	1.12955	0.62340	0.33475
0.875	1.16275	0.52704	0.27091
0.900	1.19595	0.42676	0.20656
0.910	1.20923	0.38572	0.18068
0.920	1.22251	0.34422	0.15474
0.930	1.23579	0.30227	0.12871
0.940	1.24907	0.25995	0.10264
0.950	1.26235	0.21726	0.07649
0.960	1.27563	0.17424	0.05026
0.970	1.28892	0.13093	0.02401
0.980	1.30220	0.08732	-0.00234
0.990	1.31548	0.04347	-0.01495
1.000	1.32876	-0.00247	-0.00247

FOURTH-STAGE BLADE COORDINATES
TIP SECTION (HOT RADIUS = 24.83200)

PERCENT X	X	Y TOP	Y BOT
0.0	0.00164	1.19628	1.19628
0.010	0.01491	1.22908	1.18716
0.020	0.02818	1.24824	1.19170
0.030	0.04145	1.26550	1.19896
0.040	0.05472	1.28186	1.20788
0.050	0.06800	1.29739	1.21778
0.060	0.08127	1.31212	1.22713
0.070	0.09454	1.32609	1.23578
0.080	0.10781	1.33933	1.24378
0.090	0.12108	1.35188	1.25119
0.100	0.13435	1.36375	1.25803
0.125	0.16753	1.39065	1.27280
0.150	0.20071	1.41382	1.28452
0.175	0.23388	1.43350	1.29345
0.200	0.26706	1.44989	1.29973
0.225	0.30024	1.46314	1.30349
0.250	0.33342	1.47339	1.30479
0.275	0.36659	1.48071	1.30364
0.300	0.39977	1.48516	1.30004
0.325	0.43295	1.48680	1.29391
0.350	0.46613	1.48565	1.28515
0.375	0.49931	1.48169	1.27361
0.400	0.53248	1.47492	1.25902
0.425	0.56566	1.46529	1.24108
0.450	0.59884	1.45274	1.21925
0.475	0.63202	1.43718	1.19282
0.500	0.66519	1.41850	1.16060
0.525	0.69837	1.39654	1.12084
0.550	0.73155	1.37111	1.07328
0.575	0.76473	1.34196	1.02083
0.600	0.79790	1.30879	0.96547
0.625	0.83108	1.27119	0.90813
0.650	0.86426	1.22863	0.84928
0.675	0.89744	1.18042	0.78920
0.700	0.93061	1.12580	0.72807
0.725	0.96379	1.06415	0.66605
0.750	0.99697	0.99512	0.60321
0.775	1.03015	0.91870	0.53966
0.800	1.06332	0.83526	0.47546
0.825	1.09650	0.74539	0.41066
0.850	1.12968	0.64988	0.34528
0.875	1.16286	0.54954	0.27946
0.900	1.19604	0.44515	0.21311
0.910	1.20931	0.40241	0.18642
0.920	1.22258	0.35918	0.15968
0.930	1.23585	0.31549	0.13286
0.940	1.24912	0.27137	0.10600
0.950	1.26239	0.22686	0.07907
0.960	1.27566	0.18198	0.05205
0.970	1.28893	0.13677	0.02497
0.980	1.30220	0.09124	-0.00216
0.990	1.31548	0.04542	-0.01491
1.000	1.32875	-0.00244	-0.00244

FOURTH-STAGE VANE COORDINATES
 ROOT SECTION (HOT RADIUS = 17.60899)

PERCENT X	X	Y TOP	Y BOT
0.0	-0.00153	0.62329	0.62329
0.010	0.01315	0.67021	0.61219
0.020	0.02782	0.70165	0.62070
0.030	0.04250	0.73134	0.63345
0.040	0.05718	0.75944	0.64829
0.050	0.07186	0.78606	0.66294
0.060	0.08654	0.81131	0.67718
0.070	0.10122	0.83529	0.69099
0.080	0.11590	0.85807	0.70437
0.090	0.13058	0.87971	0.71732
0.100	0.14526	0.90029	0.72982
0.125	0.18196	0.94739	0.75910
0.150	0.21866	0.98885	0.78548
0.175	0.25536	1.02517	0.80886
0.200	0.29205	1.05681	0.82918
0.225	0.32875	1.08407	0.84634
0.250	0.36545	1.10722	0.86029
0.275	0.40215	1.12646	0.87099
0.300	0.43885	1.14197	0.87839
0.325	0.47555	1.15388	0.88249
0.350	0.51225	1.16227	0.88326
0.375	0.54894	1.16722	0.88071
0.400	0.58564	1.16879	0.87486
0.425	0.62234	1.16699	0.86575
0.450	0.65904	1.16181	0.85343
0.475	0.69574	1.15324	0.83794
0.500	0.73244	1.14123	0.81937
0.525	0.76914	1.12572	0.79780
0.550	0.80583	1.10661	0.77330
0.575	0.84253	1.08376	0.74599
0.600	0.87923	1.05704	0.71595
0.625	0.91593	1.02620	0.68329
0.650	0.95263	0.99100	0.64812
0.675	0.98933	0.95111	0.61054
0.700	1.02602	0.90613	0.57068
0.725	1.06272	0.85559	0.52862
0.750	1.09942	0.79926	0.48449
0.775	1.13612	0.73711	0.43838
0.800	1.17282	0.66946	0.39039
0.825	1.20952	0.59677	0.34062
0.850	1.24622	0.51967	0.28918
0.875	1.28291	0.43879	0.23612
0.900	1.31961	0.35477	0.18157
0.910	1.33429	0.32041	0.15935
0.920	1.34897	0.28564	0.13690
0.930	1.36365	0.25052	0.11424
0.940	1.37833	0.21507	0.09136
0.950	1.39301	0.17932	0.06828
0.960	1.40769	0.14327	0.04498
0.970	1.42237	0.10697	0.02150
0.980	1.43705	0.07042	-0.00219
0.990	1.45173	0.03366	-0.01803
1.000	1.46641	-0.00572	-0.00572

FOURTH-STAGE VANE COORDINATES
QTR ROOT SECTION (HOT RADIUS = 19.178500)

PERCENT X	X	Y TOP	Y BOT
0.0	-0.00069	0.72757	0.72757
0.010	0.01398	0.77184	0.71714
0.020	0.02865	0.80178	0.72508
0.030	0.04332	0.83055	0.73693
0.040	0.05800	0.85821	0.75058
0.050	0.07267	0.88480	0.76412
0.060	0.08734	0.91038	0.77747
0.070	0.10201	0.93498	0.79059
0.080	0.11668	0.95865	0.80348
0.090	0.13135	0.98140	0.81614
0.100	0.14602	1.00328	0.82855
0.125	0.18270	1.05434	0.85846
0.150	0.21938	1.10050	0.88669
0.175	0.25605	1.14205	0.91306
0.200	0.29273	1.17925	0.93744
0.225	0.32941	1.21230	0.95965
0.250	0.36609	1.24137	0.97954
0.275	0.40276	1.26658	0.99688
0.300	0.43944	1.28802	1.01153
0.325	0.47612	1.30579	1.02325
0.350	0.51280	1.31995	1.03186
0.375	0.54947	1.33050	1.03716
0.400	0.58615	1.33748	1.03894
0.425	0.62283	1.34087	1.03702
0.450	0.65950	1.34062	1.03124
0.475	0.69618	1.33672	1.02143
0.500	0.73286	1.32908	1.00749
0.525	0.76954	1.31761	0.98930
0.550	0.80621	1.30218	0.96681
0.575	0.84289	1.28263	0.94000
0.600	0.87957	1.25877	0.90888
0.625	0.91625	1.23036	0.87351
0.650	0.95292	1.19712	0.83398
0.675	0.98960	1.15866	0.79039
0.700	1.02628	1.11454	0.74292
0.725	1.06296	1.06417	0.69170
0.750	1.09963	1.00693	0.63695
0.775	1.13631	0.94215	0.57883
0.800	1.17299	0.86937	0.51757
0.825	1.20967	0.78819	0.45335
0.850	1.24634	0.69847	0.38638
0.875	1.28302	0.60024	0.31685
0.900	1.31970	0.49379	0.24496
0.910	1.33437	0.44898	0.21557
0.920	1.34904	0.40297	0.18584
0.930	1.36371	0.35578	0.15580
0.940	1.37838	0.30745	0.12542
0.950	1.39305	0.25802	0.09474
0.960	1.40772	0.20754	0.06376
0.970	1.42239	0.15605	0.03248
0.980	1.43707	0.10359	0.00094
0.990	1.45174	0.05020	-0.01802
1.000	1.46641	-0.00572	-0.00572

FOURTH-STAGE VANE COORDINATES
 MEAN SECTION (HOT RADIUS = 20.74800)

PERCENT X	X	Y TOP	Y BOT
0.0	0.00055	0.88029	0.88029
0.010	0.01521	0.92137	0.87052
0.020	0.02987	0.94894	0.87772
0.030	0.04453	0.97547	0.88848
0.040	0.05918	1.00101	0.90071
0.050	0.07384	1.02561	0.91282
0.060	0.08850	1.04930	0.92475
0.070	0.10316	1.07210	0.93651
0.080	0.11782	1.09405	0.94806
0.090	0.13248	1.11518	0.95943
0.100	0.14714	1.13550	0.97060
0.125	0.18378	1.18296	0.99754
0.150	0.22043	1.22587	1.02302
0.175	0.25708	1.26448	1.04687
0.200	0.29372	1.29900	1.06895
0.225	0.33037	1.32957	1.08904
0.250	0.36701	1.35633	1.10696
0.275	0.40366	1.37939	1.12250
0.300	0.44031	1.39882	1.13540
0.325	0.47695	1.41468	1.14542
0.350	0.51360	1.42700	1.15232
0.375	0.55025	1.43579	1.15580
0.400	0.58689	1.44105	1.15561
0.425	0.62354	1.44276	1.15149
0.450	0.66019	1.44085	1.14318
0.475	0.69683	1.43527	1.13047
0.500	0.73348	1.42593	1.11318
0.525	0.77013	1.41270	1.09118
0.550	0.80677	1.39544	1.06440
0.575	0.84342	1.37395	1.03282
0.600	0.88006	1.34802	0.99648
0.625	0.91671	1.31734	0.95548
0.650	0.95336	1.28157	0.90999
0.675	0.99000	1.24028	0.86020
0.700	1.02665	1.19290	0.80634
0.725	1.06330	1.13875	0.74866
0.750	1.09994	1.07714	0.68745
0.775	1.13659	1.00737	0.62294
0.800	1.17324	0.92899	0.55543
0.825	1.20988	0.84161	0.48515
0.850	1.24653	0.74517	0.41238
0.875	1.28318	0.63974	0.33730
0.900	1.31982	0.52574	0.26016
0.910	1.33448	0.47785	0.22877
0.920	1.34914	0.42869	0.19708
0.930	1.36380	0.37834	0.16511
0.940	1.37846	0.32681	0.13289
0.950	1.39311	0.27418	0.10040
0.960	1.40777	0.22046	0.06766
0.970	1.42243	0.16573	0.03469
0.980	1.43709	0.11002	0.00148
0.990	1.45175	0.05338	-0.01803
1.000	1.46641	-0.00572	-0.00572

FOURTH-STAGE VANE COORDINATES
 QTR TIP SECTION (HOT RADIUS = 22.31750)

PERCENT X	X	Y TOP	Y BOT
0.0	0.00201	1.06069	1.06069
0.010	0.01666	1.10085	1.05108
0.020	0.03130	1.12797	1.05804
0.030	0.04594	1.15384	1.06846
0.040	0.06059	1.17855	1.08004
0.050	0.07523	1.20214	1.09149
0.060	0.08988	1.22470	1.10272
0.070	0.10452	1.24626	1.11375
0.080	0.11916	1.26688	1.12457
0.090	0.13381	1.28659	1.13517
0.100	0.14845	1.30543	1.14553
0.125	0.18506	1.34895	1.17036
0.150	0.22167	1.38770	1.19353
0.175	0.25828	1.42201	1.21486
0.200	0.29489	1.45216	1.23416
0.225	0.33150	1.47837	1.25122
0.250	0.36811	1.50080	1.26583
0.275	0.40472	1.51960	1.27774
0.300	0.44133	1.53486	1.28668
0.325	0.47794	1.54668	1.29238
0.350	0.51455	1.55507	1.29459
0.375	0.55116	1.56009	1.29302
0.400	0.58777	1.56171	1.28740
0.425	0.62438	1.55993	1.27747
0.450	0.66099	1.55468	1.26304
0.475	0.69760	1.54592	1.24392
0.500	0.73421	1.53353	1.21999
0.525	0.77082	1.51738	1.19116
0.550	0.80743	1.49731	1.15747
0.575	0.84404	1.47310	1.11893
0.600	0.88065	1.44449	1.07567
0.625	0.91726	1.41113	1.02786
0.650	0.95387	1.37259	0.97574
0.675	0.99048	1.32831	0.91949
0.700	1.02709	1.27757	0.85945
0.725	1.06370	1.21948	0.79582
0.750	1.10031	1.15320	0.72893
0.775	1.13692	1.07794	0.65902
0.800	1.17353	0.99314	0.58638
0.825	1.21014	0.89852	0.51120
0.850	1.24675	0.79414	0.43379
0.875	1.28336	0.68030	0.35429
0.900	1.31997	0.55768	0.27293
0.910	1.33461	0.50633	0.23990
0.920	1.34926	0.45375	0.20661
0.930	1.36390	0.40001	0.17307
0.940	1.37854	0.34514	0.13930
0.950	1.39319	0.28924	0.10529
0.960	1.40783	0.23232	0.07105
0.970	1.42248	0.17447	0.03661
0.980	1.43712	0.11572	0.00194
0.990	1.45176	0.05615	-0.01804
1.000	1.46641	-0.00572	-0.00572

FOURTH-STAGE VANE COORDINATES
TIP SECTION (HOT RADIUS = 23.88699)

PERCENT X	X	Y TOP	Y BOT
0.0	0.00370	1.26887	1.26887
0.010	0.01833	1.30908	1.25925
0.020	0.03296	1.33632	1.26619
0.030	0.04758	1.36182	1.27653
0.040	0.06221	1.38575	1.28780
0.050	0.07684	1.40825	1.29879
0.060	0.09146	1.42944	1.30949
0.070	0.10609	1.44943	1.31990
0.080	0.12072	1.46829	1.33001
0.090	0.13534	1.48609	1.33980
0.100	0.14997	1.50291	1.34927
0.125	0.18654	1.54098	1.37143
0.150	0.22311	1.57392	1.39132
0.175	0.25967	1.60223	1.40872
0.200	0.29624	1.62633	1.42346
0.225	0.33281	1.64651	1.43531
0.250	0.36938	1.66301	1.44406
0.275	0.40595	1.67601	1.44948
0.300	0.44251	1.68564	1.45136
0.325	0.47908	1.69200	1.44948
0.350	0.51565	1.69518	1.44366
0.375	0.55222	1.69522	1.43368
0.400	0.58878	1.69211	1.41940
0.425	0.62535	1.68584	1.40069
0.450	0.66192	1.67638	1.37747
0.475	0.69849	1.66366	1.34965
0.500	0.73505	1.64757	1.31726
0.525	0.77162	1.62799	1.28030
0.550	0.80819	1.60472	1.23887
0.575	0.84476	1.57753	1.19306
0.600	0.88133	1.54612	1.14303
0.625	0.91789	1.51008	1.08892
0.650	0.95446	1.46889	1.03097
0.675	0.99103	1.42185	0.96935
0.700	1.02759	1.36800	0.90431
0.725	1.06416	1.30622	0.83602
0.750	1.10073	1.23544	0.76477
0.775	1.13730	1.15464	0.69071
0.800	1.17387	1.06320	0.61409
0.825	1.21043	0.96087	0.53507
0.850	1.24700	0.84788	0.45387
0.875	1.28357	0.72485	0.37063
0.900	1.32014	0.59279	0.28555
0.910	1.33476	0.53767	0.25103
0.920	1.34939	0.48134	0.21624
0.930	1.36402	0.42388	0.18120
0.940	1.37864	0.36536	0.14591
0.950	1.39327	0.30587	0.11038
0.960	1.40790	0.24543	0.07462
0.970	1.42253	0.18415	0.03863
0.980	1.43715	0.12206	0.00243
0.990	1.45178	0.05922	-0.01805
1.000	1.46641	-0.00573	-0.00573

FIFTH-STAGE BLADE COORDINATES
 ROOT SECTION (HOT RADIUS = 17.74400)

PERCENT X	X	Y TOP	Y BOT
0.0	-0.00015	0.47744	0.47744
0.010	0.01372	0.50415	0.46878
0.020	0.02758	0.51946	0.47154
0.030	0.04144	0.53334	0.47653
0.040	0.05531	0.54674	0.48284
0.050	0.06917	0.55966	0.48921
0.060	0.08304	0.57211	0.49518
0.070	0.09690	0.58411	0.50078
0.080	0.11076	0.59565	0.50602
0.090	0.12463	0.60674	0.51089
0.100	0.13849	0.61739	0.51543
0.125	0.17315	0.64213	0.52534
0.150	0.20781	0.66421	0.53332
0.175	0.24247	0.68372	0.53947
0.200	0.27713	0.70072	0.54390
0.225	0.31179	0.71524	0.54670
0.250	0.34644	0.72736	0.54793
0.275	0.38110	0.73710	0.54766
0.300	0.41576	0.74450	0.54593
0.325	0.45042	0.74958	0.54279
0.350	0.48508	0.75238	0.53830
0.375	0.51974	0.75291	0.53247
0.400	0.55440	0.75118	0.52534
0.425	0.58906	0.74721	0.51693
0.450	0.62372	0.74098	0.50726
0.475	0.65838	0.73251	0.49634
0.500	0.69303	0.72179	0.48419
0.525	0.72769	0.70881	0.47081
0.550	0.76235	0.69355	0.45620
0.575	0.79701	0.67600	0.44038
0.600	0.83167	0.65613	0.42332
0.625	0.86633	0.63391	0.40503
0.650	0.90099	0.60930	0.38549
0.675	0.93565	0.58227	0.36469
0.700	0.97031	0.55276	0.34261
0.725	1.00496	0.52073	0.31923
0.750	1.03962	0.48610	0.29453
0.775	1.07428	0.44883	0.26845
0.800	1.10894	0.40889	0.24097
0.825	1.14360	0.36631	0.21204
0.850	1.17826	0.32113	0.18162
0.875	1.21292	0.27343	0.14962
0.900	1.24758	0.22330	0.11600
0.910	1.26144	0.20259	0.10206
0.920	1.27530	0.18153	0.08786
0.930	1.28917	0.16011	0.07336
0.940	1.30303	0.13835	0.05857
0.950	1.31690	0.11626	0.04348
0.960	1.33076	0.09384	0.02808
0.970	1.34462	0.07111	0.01236
0.980	1.35849	0.04806	-0.00369
0.990	1.37235	0.02473	-0.01471
1.000	1.38621	-0.00228	-0.00228

FIFTH-STAGE BLADE COORDINATES
 QTR ROOT SECTION (HOT RADIUS = 19.79700)

PERCENT X	X	Y TOP	Y BOT
0.0	0.00188	0.44382	0.44382
0.010	0.01532	0.47595	0.43483
0.020	0.02877	0.49497	0.43923
0.030	0.04221	0.51299	0.44630
0.040	0.05565	0.53038	0.45494
0.050	0.06910	0.54718	0.46389
0.060	0.08254	0.56338	0.47252
0.070	0.09598	0.57899	0.48083
0.080	0.10943	0.59404	0.48883
0.090	0.12287	0.60851	0.49652
0.100	0.13631	0.62244	0.50389
0.125	0.16992	0.65488	0.52091
0.150	0.20353	0.68404	0.53591
0.175	0.23714	0.71002	0.54883
0.200	0.27075	0.73291	0.55967
0.225	0.30436	0.75278	0.56839
0.250	0.33797	0.76969	0.57498
0.275	0.37157	0.78371	0.57940
0.300	0.40518	0.79486	0.58166
0.325	0.43879	0.80318	0.58172
0.350	0.47240	0.80871	0.57959
0.375	0.50601	0.81143	0.57527
0.400	0.53962	0.81136	0.56874
0.425	0.57323	0.80850	0.56002
0.450	0.60683	0.80283	0.54910
0.475	0.64044	0.79433	0.53601
0.500	0.67405	0.78298	0.52074
0.525	0.70766	0.76872	0.50333
0.550	0.74127	0.75152	0.48377
0.575	0.77488	0.73130	0.46211
0.600	0.80849	0.70800	0.43837
0.625	0.84209	0.68153	0.41257
0.650	0.87570	0.65177	0.38475
0.675	0.90931	0.61862	0.35494
0.700	0.94292	0.58192	0.32317
0.725	0.97653	0.54153	0.28949
0.750	1.01014	0.49726	0.25393
0.775	1.04374	0.44896	0.21653
0.800	1.07735	0.39661	0.17733
0.825	1.11096	0.34024	0.13639
0.850	1.14457	0.27999	0.09373
0.875	1.17818	0.21606	0.04941
0.900	1.21179	0.14869	0.00348
0.910	1.22523	0.12085	-0.01535
0.920	1.23867	0.09253	-0.03441
0.930	1.25212	0.06374	-0.05373
0.940	1.26556	0.03450	-0.07329
0.950	1.27900	0.00484	-0.09308
0.960	1.29245	-0.02523	-0.11312
0.970	1.30589	-0 5568	-0.13339
0.980	1.31933	-0 8652	-0.15390
0.990	1.33278	-0 1770	-0.16470
1.000	1.34622	-0. 5184	-0.15184

FIFTH-STAGE BLADE COORDINATES
 MEAN SECTION (HOT RADIUS = 21.85100)

PERCENT X	X	Y TOP	Y BOT
0.0	0.00882	0.46390	0.46390
0.010	0.02180	0.50030	0.45401
0.020	0.03479	0.52243	0.45930
0.030	0.04777	0.54355	0.46764
0.040	0.06075	0.56374	0.47783
0.050	0.07374	0.58306	0.48853
0.060	0.08672	0.60151	0.49903
0.070	0.09971	0.61915	0.50931
0.080	0.11269	0.63600	0.51936
0.090	0.12567	0.65208	0.52916
0.100	0.13866	0.66743	0.53871
0.125	0.17112	0.70269	0.56145
0.150	0.20358	0.73376	0.58240
0.175	0.23604	0.76090	0.60139
0.200	0.26850	0.78433	0.61825
0.225	0.30096	0.80419	0.63276
0.250	0.33342	0.82064	0.64474
0.275	0.36588	0.83379	0.65399
0.300	0.39834	0.84375	0.66032
0.325	0.43080	0.85058	0.66355
0.350	0.46326	0.85435	0.66354
0.375	0.49572	0.85510	0.66013
0.400	0.52818	0.85286	0.65328
0.425	0.56064	0.84766	0.64290
0.450	0.59310	0.83947	0.62903
0.475	0.62556	0.82831	0.61168
0.500	0.65802	0.81414	0.59096
0.525	0.69048	0.79691	0.56698
0.550	0.72294	0.77660	0.53991
0.575	0.75540	0.75312	0.50990
0.600	0.78786	0.72637	0.47716
0.625	0.82032	0.69626	0.44188
0.650	0.85278	0.66264	0.40426
0.675	0.88524	0.62537	0.36449
0.700	0.91770	0.58424	0.32275
0.725	0.95016	0.53902	0.27924
0.750	0.98262	0.48952	0.23410
0.775	1.01508	0.43560	0.18748
0.800	1.04754	0.37725	0.13953
0.825	1.08000	0.31457	0.09037
0.850	1.11246	0.24774	0.04013
0.875	1.14492	0.17702	-0.01112
0.900	1.17738	0.10274	-0.06328
0.910	1.19037	0.07210	-0.08437
0.920	1.20335	0.04097	-0.10559
0.930	1.21633	0.00936	-0.12693
0.940	1.22932	-0.02269	-0.14838
0.950	1.24230	-0.05517	-0.16995
0.960	1.25529	-0.08806	-0.19164
0.970	1.26827	-0.12135	-0.21342
0.980	1.28125	-0.15499	-0.23503
0.990	1.29424	-0.18899	-0.24045
1.000	1.30722	-0.22597	-0.22597

FIFTH-STAGE BLADE COORDINATES
 QTR TIP SECTION (HOT RADIUS = 23.90401)

PERCENT X	X	Y TOP	Y BOT
0.0	-0.01089	0.55933	0.55933
0.010	0.00229	0.59048	0.55036
0.020	0.01548	0.60895	0.55441
0.030	0.02866	0.62642	0.56104
0.040	0.04184	0.64312	0.56914
0.050	0.05502	0.65910	0.57748
0.060	0.06820	0.67437	0.58563
0.070	0.08138	0.68895	0.59357
0.080	0.09456	0.70286	0.60133
0.090	0.10774	0.71614	0.60886
0.100	0.12092	0.72878	0.61617
0.125	0.15388	0.75774	0.63343
0.150	0.18683	0.78309	0.64908
0.175	0.21978	0.80499	0.66296
0.200	0.25273	0.82360	0.67489
0.225	0.28569	0.83903	0.68467
0.250	0.31864	0.85140	0.69208
0.275	0.35159	0.86077	0.69694
0.300	0.38455	0.86722	0.69904
0.325	0.41750	0.87078	0.69816
0.350	0.45045	0.87148	0.69415
0.375	0.48340	0.86935	0.68683
0.400	0.51636	0.86438	0.67610
0.425	0.54931	0.85658	0.66190
0.450	0.58226	0.84591	0.64419
0.475	0.61522	0.83233	0.62300
0.500	0.64817	0.81580	0.59840
0.525	0.68112	0.79625	0.57052
0.550	0.71407	0.77358	0.53949
0.575	0.74703	0.74769	0.50552
0.600	0.77998	0.71845	0.46879
0.625	0.81293	0.68571	0.42951
0.650	0.84588	0.64925	0.38789
0.675	0.87884	0.60886	0.34413
0.700	0.91179	0.56425	0.29842
0.725	0.94474	0.51517	0.25095
0.750	0.97770	0.46143	0.20190
0.775	1.01065	0.40295	0.15140
0.800	1.04360	0.33972	0.09961
0.825	1.07655	0.27185	0.04665
0.850	1.10951	0.19951	-0.00737
0.875	1.14246	0.12298	-0.06232
0.900	1.17541	0.04255	-0.11814
0.910	1.18859	0.00937	-0.14069
0.920	1.20177	-0.02436	-0.16336
0.930	1.21495	-0.05861	-0.18614
0.940	1.22814	-0.09338	-0.20903
0.950	1.24132	-0.12861	-0.23202
0.960	1.25450	-0.16432	-0.25513
0.970	1.26768	-0.20047	-0.27832
0.980	1.28086	-0.23703	-0.30162
0.990	1.29404	-0.27399	-0.32131
1.000	1.30722	-0.31281	-0.31281

FIFTH-STAGE BLADE COORDINATES
 TIP SECTION (HOT RADIUS = 25.95799)

PERCENT X	X	Y TOP	Y BOT
0.0	-0.01771	0.66940	0.66940
0.010	-0.00446	0.69252	0.66053
0.020	0.00879	0.70548	0.66188
0.030	0.02204	0.71746	0.66520
0.040	0.03529	0.72900	0.66941
0.050	0.04854	0.74011	0.67360
0.060	0.06178	0.75081	0.67771
0.070	0.07503	0.76109	0.68172
0.080	0.08828	0.77095	0.68563
0.090	0.10153	0.78040	0.68945
0.100	0.11478	0.78944	0.69315
0.125	0.14791	0.81023	0.70190
0.150	0.18103	0.82847	0.70980
0.175	0.21415	0.84418	0.71671
0.200	0.24728	0.85737	0.72243
0.225	0.28040	0.86804	0.72676
0.250	0.31352	0.87617	0.72941
0.275	0.34665	0.88176	0.73010
0.300	0.37977	0.88479	0.72845
0.325	0.41289	0.88523	0.72412
0.350	0.44602	0.88303	0.71668
0.375	0.47914	0.87816	0.70578
0.400	0.51226	0.87055	0.69108
0.425	0.54539	0.86015	0.67241
0.450	0.57851	0.84688	0.64972
0.475	0.61163	0.83064	0.62309
0.500	0.64476	0.81133	0.59278
0.525	0.67788	0.78884	0.55910
0.550	0.71100	0.76302	0.52245
0.575	0.74413	0.73372	0.48322
0.600	0.77725	0.70073	0.44178
0.625	0.81037	0.66384	0.39846
0.650	0.84350	0.62280	0.35357
0.675	0.87662	0.57737	0.30735
0.700	0.90974	0.52748	0.26001
0.725	0.94287	0.47317	0.21172
0.750	0.97599	0.41465	0.16262
0.775	1.00911	0.35221	0.11285
0.800	1.04224	0.28624	0.06249
0.825	1.07536	0.21714	0.01162
0.850	1.10848	0.14531	-0.03966
0.875	1.14161	0.07113	-0.09134
0.900	1.17473	-0.00506	-0.14334
0.910	1.18798	-0.03604	-0.16422
0.920	1.20123	-0.06727	-0.18515
0.930	1.21448	-0.09875	-0.20612
0.940	1.22773	-0.13045	-0.22713
0.950	1.24098	-0.16236	-0.24817
0.960	1.25422	-0.19448	-0.26926
0.970	1.26747	-0.22677	-0.29037
0.980	1.28072	-0.25924	-0.31152
0.990	1.29397	-0.29188	-0.33208
1.000	1.30722	-0.32610	-0.32610

FIFTH-STAGE VANE COORDINATES (WANGEA2)
 ROOT SECTION (HOT RADIUS = 17.70000)

PERCENT X	X	Y TOP	Y BOT
0.0	-0.00044	0.38687	0.38687
0.010	0.01400	0.42832	0.37688
0.020	0.02845	0.45635	0.38404
0.030	0.04289	0.48317	0.39480
0.040	0.05733	0.50884	0.40691
0.050	0.07177	0.53342	0.41870
0.060	0.08622	0.55696	0.43011
0.070	0.10066	0.57950	0.44113
0.080	0.11510	0.60109	0.45179
0.090	0.12955	0.62176	0.46206
0.100	0.14399	0.64157	0.47195
0.125	0.18009	0.68741	0.49504
0.150	0.21620	0.72840	0.51582
0.175	0.25231	0.76487	0.53429
0.200	0.28841	0.79710	0.55047
0.225	0.32452	0.82533	0.56439
0.250	0.36063	0.84976	0.57607
0.275	0.39673	0.87056	0.58552
0.300	0.43284	0.88786	0.59276
0.325	0.46895	0.90178	0.59781
0.350	0.50505	0.91240	0.60069
0.375	0.54116	0.91980	0.60141
0.400	0.57727	0.92404	0.59999
0.425	0.61337	0.92515	0.59645
0.450	0.64948	0.92318	0.59080
0.475	0.68559	0.91812	0.58306
0.500	0.72169	0.90999	0.57324
0.525	0.75780	0.89876	0.56135
0.550	0.79391	0.88442	0.54742
0.575	0.83001	0.86692	0.53145
0.600	0.86612	0.84621	0.51347
0.625	0.90223	0.82221	0.49346
0.650	0.93833	0.79484	0.47148
0.675	0.97444	0.76397	0.44749
0.700	1.01054	0.72951	0.42156
0.725	1.04665	0.69126	0.39365
0.750	1.08276	0.64904	0.36379
0.775	1.11886	0.60266	0.33201
0.800	1.15497	0.55201	0.29829
0.825	1.19108	0.49700	0.26266
0.850	1.22718	0.43772	0.22513
0.875	1.26329	0.37422	0.18571
0.900	1.29940	0.30671	0.14441
0.910	1.31384	0.27861	0.12737
0.920	1.32828	0.24993	0.11002
0.930	1.34272	0.22068	0.09238
0.940	1.35717	0.19085	0.07444
0.950	1.37161	0.16050	0.05619
0.960	1.38605	0.12962	0.03766
0.970	1.40049	0.09825	0.01884
0.980	1.41494	0.06638	-0.00030
0.990	1.42938	0.03405	-0.01370
1.000	1.44382	-0.00135	-0.00135

FIFTH-STAGE VANE COORDINATES
 QTR ROOT SECTION (HOT RADIUS = 19.66000)

PERCENT X	X	Y TOP	Y BOT
0.0	-0.00006	0.58849	0.58849
0.010	0.01438	0.62893	0.57871
0.020	0.02882	0.65625	0.58563
0.030	0.04326	0.68240	0.59604
0.040	0.05770	0.70745	0.60769
0.050	0.07214	0.73145	0.61902
0.060	0.08658	0.75444	0.62998
0.070	0.10102	0.77648	0.64057
0.080	0.11546	0.79759	0.65080
0.090	0.12989	0.81782	0.66067
0.100	0.14433	0.83719	0.67015
0.125	0.18043	0.88204	0.69224
0.150	0.21653	0.92212	0.71198
0.175	0.25262	0.95773	0.72937
0.200	0.28872	0.98913	0.74434
0.225	0.32482	1.01654	0.75692
0.250	0.36091	1.04014	0.76706
0.275	0.39701	1.06005	0.77477
0.300	0.43311	1.07642	0.78002
0.325	0.46921	1.08931	0.78282
0.350	0.50530	1.09881	0.78314
0.375	0.54140	1.10498	0.78100
0.400	0.57750	1.10785	0.77637
0.425	0.61359	1.10742	0.76926
0.450	0.64969	1.10371	0.75970
0.475	0.68579	1.09671	0.74764
0.500	0.72188	1.08637	0.73314
0.525	0.75798	1.07267	0.71618
0.550	0.79408	1.05553	0.69677
0.575	0.83018	1.03486	0.67493
0.600	0.86627	1.01057	0.65067
0.625	0.90237	0.98250	0.62402
0.650	0.93847	0.95051	0.59500
0.675	0.97456	0.91438	0.56361
0.700	1.01066	0.87388	0.52990
0.725	1.04676	0.82870	0.49387
0.750	1.08285	0.77852	0.45556
0.775	1.11895	0.72299	0.41500
0.800	1.15505	0.66199	0.37223
0.825	1.19114	0.59546	0.32724
0.850	1.22724	0.52359	0.28011
0.875	1.26334	0.44664	0.23083
0.900	1.29944	0.36502	0.17948
0.910	1.31388	0.33116	0.15836
0.920	1.32831	0.29665	0.13691
0.930	1.34275	0.26153	0.11514
0.940	1.35719	0.22583	0.09304
0.950	1.37163	0.18956	0.07062
0.960	1.38607	0.15277	0.04789
0.970	1.40051	0.11549	0.02483
0.980	1.41495	0.07773	0.00147
0.990	1.42939	0.03952	-0.01370
1.000	1.44382	-0.00135	-0.00135

FIFTH-STAGE VANE COORDINATES
 MEAN SECTION (HOT RADIUS = 21.62000)

PERCENT X	X	Y TOP	Y BOT
0.0	0.00032	0.78462	0.78462
0.010	0.01475	0.82168	0.77540
0.020	0.02919	0.84611	0.78149
0.030	0.04362	0.86963	0.79073
0.040	0.05806	0.89226	0.80106
0.050	0.07249	0.91404	0.81115
0.060	0.08693	0.93500	0.82095
0.070	0.10136	0.95516	0.83046
0.080	0.11580	0.97455	0.83969
0.090	0.13023	0.99318	0.84861
0.100	0.14467	1.01109	0.85723
0.125	0.18076	1.05278	0.87739
0.150	0.21684	1.09030	0.89554
0.175	0.25293	1.12382	0.91158
0.200	0.28902	1.15355	0.92541
0.225	0.32511	1.17962	0.93696
0.250	0.36119	1.20212	0.94614
0.275	0.39728	1.22118	0.95285
0.300	0.43337	1.23686	0.95703
0.325	0.46946	1.24920	0.95860
0.350	0.50554	1.25824	0.95749
0.375	0.54163	1.26399	0.95362
0.400	0.57772	1.26647	0.94696
0.425	0.61381	1.26564	0.93743
0.450	0.64990	1.26148	0.92499
0.475	0.68598	1.25395	0.90962
0.500	0.72207	1.24295	0.89129
0.525	0.75816	1.22843	0.86999
0.550	0.79425	1.21024	0.84570
0.575	0.83033	1.18826	0.81845
0.600	0.86642	1.16232	0.78824
0.625	0.90251	1.13219	0.75509
0.650	0.93860	1.09765	0.71908
0.675	0.97468	1.05834	0.68019
0.700	1.01077	1.01394	0.63853
0.725	1.04686	0.96390	0.59412
0.750	1.08295	0.90770	0.54706
0.775	1.11903	0.84479	0.49740
0.800	1.15512	0.77491	0.44523
0.825	1.19121	0.69796	0.39062
0.850	1.22730	0.61422	0.33366
0.875	1.26338	0.52409	0.27444
0.900	1.29947	0.42822	0.21305
0.910	1.31391	0.38841	0.18790
0.920	1.32834	0.34783	0.16242
0.930	1.34278	0.30653	0.13663
0.940	1.35721	0.26455	0.11050
0.950	1.37165	0.22193	0.08407
0.960	1.38608	0.17871	0.05734
0.970	1.40052	0.13493	0.03029
0.980	1.41495	0.09063	0.00296
0.990	1.42939	0.04585	-0.01369
1.000	1.44382	-0.00134	-0.00134

FIFTH-STAGE VANE COORDINATES
 QTR TIP SECTION (HOT RADIUS = 23.58000)

PERCENT X	X	Y TOP	Y BOT
0.0	0.00067	0.97251	0.97251
0.010	0.01511	1.00440	0.96384
0.020	0.02954	1.02469	0.96844
0.030	0.04397	1.04427	0.97568
0.040	0.05840	1.06316	0.98359
0.050	0.07283	1.08137	0.99133
0.060	0.08726	1.09892	0.99886
0.070	0.10169	1.11580	1.00620
0.080	0.11613	1.13205	1.01334
0.090	0.13056	1.14767	1.02027
0.100	0.14499	1.16269	1.02698
0.125	0.18107	1.19761	1.04276
0.150	0.21715	1.22893	1.05702
0.175	0.25323	1.25678	1.06965
0.200	0.28930	1.28124	1.08047
0.225	0.32538	1.30241	1.08938
0.250	0.36146	1.32034	1.09620
0.275	0.39754	1.33512	1.10078
0.300	0.43362	1.34673	1.10295
0.325	0.46970	1.35524	1.10255
0.350	0.50578	1.36062	1.09941
0.375	0.54186	1.36288	1.09339
0.400	0.57793	1.36201	1.08430
0.425	0.61401	1.35794	1.07204
0.450	0.65009	1.35065	1.05648
0.475	0.68617	1.34005	1.03751
0.500	0.72225	1.32608	1.01508
0.525	0.75833	1.30860	0.98913
0.550	0.79441	1.28750	0.95965
0.575	0.83048	1.26263	0.92667
0.600	0.86656	1.23380	0.89024
0.625	0.90264	1.20076	0.85044
0.650	0.93872	1.16327	0.80738
0.675	0.97480	1.12096	0.76116
0.700	1.01088	1.07345	0.71196
0.725	1.04696	1.02021	0.65990
0.750	1.08304	0.96073	0.60517
0.775	1.11911	0.89453	0.54791
0.800	1.15519	0.82132	0.48832
0.825	1.19127	0.74092	0.42651
0.850	1.22735	0.65342	0.36269
0.875	1.26343	0.55902	0.29698
0.900	1.29951	0.45815	0.22955
0.910	1.31394	0.41609	0.20211
0.920	1.32837	0.37310	0.17443
0.930	1.34280	0.32923	0.14651
0.940	1.35723	0.28451	0.11835
0.950	1.37167	0.23897	0.08996
0.960	1.38610	0.19268	0.06136
0.970	1.40053	0.14563	0.03256
0.980	1.41496	0.09789	0.00353
0.990	1.42939	0.04949	-0.01370
1.000	1.44382	0.00135	-0.00135

FIFTH-STAGE VANE COORDINATES
TIP SECTION (HOT RADIUS = 25.53999)

PERCENT X	X	Y TOP	Y BOT
0.0	0.00094	1.11157	1.11157
0.010	0.01537	1.13977	1.10297
0.020	0.02980	1.15724	1.10632
0.030	0.04423	1.17407	1.11196
0.040	0.05865	1.19025	1.11797
0.050	0.07308	1.20583	1.12388
0.060	0.08751	1.22079	1.12968
0.070	0.10194	1.23518	1.13537
0.080	0.11637	1.24899	1.14093
0.090	0.13080	1.26222	1.14638
0.100	0.14523	1.27491	1.15169
0.125	0.18130	1.30427	1.16435
0.150	0.21737	1.33038	1.17604
0.175	0.25344	1.35335	1.18664
0.200	0.28952	1.37326	1.19597
0.225	0.32559	1.39019	1.20389
0.250	0.36166	1.40419	1.21019
0.275	0.39773	1.41532	1.21467
0.300	0.43380	1.42358	1.21706
0.325	0.46988	1.42901	1.21709
0.350	0.50595	1.43156	1.21445
0.375	0.54202	1.43125	1.20885
0.400	0.57809	1.42803	1.19992
0.425	0.61416	1.42187	1.18736
0.450	0.65024	1.41269	1.17086
0.475	0.68631	1.40041	1.15016
0.500	0.72238	1.38494	1.12506
0.525	0.75845	1.36613	1.09546
0.550	0.79452	1.34386	1.06136
0.575	0.83060	1.31791	1.02281
0.600	0.86667	1.28808	0.98001
0.625	0.90274	1.25406	0.93320
0.650	0.93881	1.21554	0.88267
0.675	0.97489	1.17206	0.82873
0.700	1.01096	1.12312	0.77175
0.725	1.04703	1.06803	0.71201
0.750	1.08310	1.00624	0.64985
0.775	1.11917	0.93720	0.58553
0.800	1.15525	0.86060	0.51933
0.825	1.19132	0.77628	0.45144
0.850	1.22739	0.68440	0.38211
0.875	1.26346	0.58523	0.31146
0.900	1.29953	0.47930	0.23970
0.910	1.31396	0.43517	0.21070
0.920	1.32839	0.39008	0.18155
0.930	1.34282	0.34410	0.15226
0.940	1.35725	0.29724	0.12283
0.950	1.37168	0.24957	0.09326
0.960	1.38611	0.20112	0.06357
0.970	1.40054	0.15195	0.03376
0.980	1.41496	0.10207	0.00383
0.990	1.42939	0.05154	-0.01369
1.000	1.44382	-0.00134	-0.00134

APPENDIX E
LOW-PRESSURE TURBINE EXIT GUIDE VANE AIRFOIL COORDINATES

ROOT LEADING EDGE SECTION
(HOT RADIUS = 17.82300)

PERCENT X	X	Y TOP	Y BOT
0.0	0.0	-1.58466	-1.58466
0.010	0.06332	-1.50484	-1.62788
0.020	0.12664	-1.44639	-1.59315
0.030	0.18996	-1.38943	-1.55836
0.040	0.25328	-1.33392	-1.52401
0.050	0.31660	-1.27980	-1.49010
0.060	0.37992	-1.22703	-1.45662
0.070	0.44324	-1.17558	-1.42357
0.080	0.50656	-1.12540	-1.39095
0.090	0.56988	-1.07646	-1.35877
0.100	0.63320	-1.02872	-1.32699
0.125	0.79150	-0.91445	-1.24940
0.150	0.94980	-0.80707	-1.17439
0.175	1.10810	-0.70621	-1.10193
0.200	1.26640	-0.61151	-1.03198
0.225	1.42470	-0.52269	-0.96451
0.250	1.58300	-0.43948	-0.89948
0.275	1.74130	-0.36166	-0.83688
0.300	1.89960	-0.28903	-0.77668
0.325	2.05790	-0.22139	-0.71885
0.350	2.21620	-0.15860	-0.66338
0.375	2.37450	-0.10051	-0.61024
0.400	2.53280	-0.04699	-0.55942
0.425	2.69110	0.00207	-0.51091
0.450	2.84940	0.04678	-0.46469
0.475	3.00770	0.08722	-0.42075
0.500	3.16600	0.12347	-0.37908
0.525	3.32430	0.15560	-0.33967
0.550	3.48260	0.18366	-0.30253
0.575	3.64090	0.20771	-0.26763
0.600	3.79920	0.22780	-0.23499
0.625	3.95750	0.24395	-0.20460
0.650	4.11580	0.25620	-0.17645
0.675	4.27410	0.26456	-0.15056
0.700	4.43240	0.26905	-0.12693
0.725	4.59070	0.26968	-0.10556
0.750	4.74900	0.26644	-0.08645
0.775	4.90730	0.25934	-0.06963
0.800	5.06560	0.24835	-0.05509
0.825	5.22390	0.23347	-0.04286
0.850	5.38220	0.21465	-0.03294
0.875	5.54050	0.19187	-0.02535
0.900	5.69880	0.16509	-0.02011
0.910	5.76212	0.15325	-0.01868
0.920	5.82544	0.14075	-0.01763
0.930	5.88876	0.12760	-0.01696
0.940	5.95208	0.11379	-0.01667
0.950	6.01540	0.09931	-0.01676
0.960	6.07872	0.08417	-0.01725
0.970	6.14204	0.06835	-0.01812
0.980	6.20536	0.05185	-0.01938
0.990	6.26868	0.03467	-0.02104
1.000	6.33200	-0.00001	-0.00001

ROOT TRAILING EDGE SECTION
(HOT RADIUS = 19.46600)

PERCENT X	X	Y TOP	Y BOT
0.0	-0.08780	-1.87726	-1.87726
0.010	-0.02360	-1.78131	-1.92093
0.020	0.04060	-1.70450	-1.87492
0.030	0.10480	-1.63028	-1.82752
0.040	0.16900	-1.55849	-1.78086
0.050	0.23320	-1.48901	-1.73498
0.060	0.29740	-1.42172	-1.68980
0.070	0.36160	-1.35652	-1.64535
0.080	0.42580	-1.29332	-1.60161
0.090	0.49000	-1.23201	-1.55858
0.100	0.55420	-1.17254	-1.51624
0.125	0.71470	-1.03136	-1.41341
0.150	0.87520	-0.90014	-1.31479
0.175	1.03570	-0.77806	-1.22026
0.200	1.19620	-0.66445	-1.12975
0.225	1.35670	-0.55871	-1.04316
0.250	1.51720	-0.46037	-0.96040
0.275	1.67770	-0.36900	-0.88140
0.300	1.83820	-0.28425	-0.80608
0.325	1.99870	-0.20579	-0.73439
0.350	2.15920	-0.13335	-0.66627
0.375	2.31970	-0.06670	-0.60164
0.400	2.48020	-0.00564	-0.54046
0.425	2.64070	0.05004	-0.48269
0.450	2.80120	0.10047	-0.42827
0.475	2.96170	0.14581	-0.37717
0.500	3.12220	0.18616	-0.32935
0.525	3.28270	0.22164	-0.28476
0.550	3.44320	0.25234	-0.24338
0.575	3.60370	0.27832	-0.20518
0.600	3.76420	0.29965	-0.17013
0.625	3.92470	0.31638	-0.13820
0.650	4.08520	0.32855	-0.10938
0.675	4.24570	0.33619	-0.08354
0.700	4.40620	0.33931	-0.06096
0.725	4.56670	0.33792	-0.04134
0.750	4.72720	0.33201	-0.02476
0.775	4.88770	0.32159	-0.01120
0.800	5.04820	0.30660	-0.00066
0.825	5.20870	0.28702	0.00687
0.850	5.36920	0.26281	0.01138
0.875	5.52970	0.23391	0.01289
0.900	5.69020	0.20024	0.01140
0.910	5.75440	0.18542	0.00996
0.920	5.81860	0.16981	0.00804
0.930	5.88280	0.15342	0.00564
0.940	5.94700	0.13623	0.00275
0.950	6.01120	0.11824	-0.00061
0.960	6.07540	0.09944	-0.00446
0.970	6.13960	0.07982	-0.00879
0.980	6.20380	0.05937	-0.01361
0.990	6.26800	0.03809	-0.01891
1.000	6.33220	-0.00001	-0.00001

1/4 ROOT TRAILING EDGE SECTION

(HOT RADIUS = 21.36050)

PERCENT X	X	Y TOP	Y BOT
0.0	-0.16555	-1.88512	-1.88512
0.010	-0.12037	-1.78847	-1.92837
0.020	-0.05519	-1.71107	-1.88160
0.030	0.00999	-1.63627	-1.83386
0.040	0.07517	-1.56392	-1.78689
0.050	0.14035	-1.49390	-1.74068
0.060	0.20553	-1.42608	-1.69520
0.070	0.27071	-1.36037	-1.65048
0.080	0.33589	-1.29667	-1.60647
0.090	0.40107	-1.23488	-1.56319
0.100	0.46625	-1.17492	-1.52062
0.125	0.62920	-1.03262	-1.41724
0.150	0.79215	-0.90036	-1.31812
0.175	0.95510	-0.77731	-1.22317
0.200	1.11805	-0.66278	-1.13227
0.225	1.28100	-0.55620	-1.04531
0.250	1.44395	-0.45708	-0.96223
0.275	1.60690	-0.36498	-0.88293
0.300	1.76985	-0.27956	-0.80734
0.325	1.93280	-0.20049	-0.73540
0.350	2.09575	-0.12751	-0.66703
0.375	2.25870	-0.06035	-0.60216
0.400	2.42165	0.00117	-0.54077
0.425	2.58460	0.05723	-0.48279
0.450	2.74755	0.10801	-0.42816
0.475	2.91050	0.15364	-0.37687
0.500	3.07345	0.19423	-0.32885
0.525	3.23640	0.22990	-0.28409
0.550	3.39935	0.26072	-0.24253
0.575	3.56230	0.28679	-0.20417
0.600	3.72525	0.30814	-0.16896
0.625	3.88820	0.32485	-0.13690
0.650	4.05115	0.33694	-0.10795
0.675	4.21410	0.34443	-0.08211
0.700	4.37705	0.34735	-0.05935
0.725	4.54000	0.34570	-0.03967
0.750	4.70295	0.33947	-0.02304
0.775	4.86590	0.32865	-0.00948
0.800	5.02885	0.31321	0.00103
0.825	5.19180	0.29312	0.00850
0.850	5.35475	0.26831	0.01291
0.875	5.51770	0.23874	0.01427
0.900	5.68065	0.20431	0.01257
0.910	5.74583	0.18916	0.01103
0.920	5.81101	0.17322	0.00900
0.930	5.87619	0.15648	0.00648
0.940	5.94137	0.13892	0.00347
0.950	6.00655	0.12055	-0.00004
0.960	6.07173	0.10135	-0.00404
0.970	6.13691	0.08131	-0.00854
0.980	6.20209	0.06044	-0.01353
0.990	6.26727	0.03870	-0.01901
1.000	6.33245	-0.00001	-0.00001

MEAN TRAILING EDGE SECTION
(HOT RADIUS = 23.25500)

PERCENT X	X	Y TOP	Y BOT
0.0	-0.28730	-1.75474	-1.75474
0.010	-0.22110	-1.66533	-1.79712
0.020	-0.15490	-1.59619	-1.75500
0.030	-0.08870	-1.52907	-1.71295
0.040	-0.02250	-1.46387	-1.67149
0.050	0.04370	-1.40051	-1.63065
0.060	0.10990	-1.33893	-1.59040
0.070	0.17610	-1.27906	-1.55075
0.080	0.24230	-1.22083	-1.51168
0.090	0.30850	-1.16419	-1.47320
0.100	0.37470	-1.10908	-1.43529
0.125	0.54020	-0.97769	-1.34301
0.150	0.70570	-0.85489	-1.25421
0.175	0.87120	-0.74010	-1.16884
0.200	1.03670	-0.63282	-1.08681
0.225	1.20220	-0.53260	-1.00807
0.250	1.36770	-0.43910	-0.93256
0.275	1.53320	-0.35197	-0.86023
0.300	1.69870	-0.27095	-0.79103
0.325	1.86420	-0.19577	-0.72492
0.350	2.02970	-0.12622	-0.66185
0.375	2.19520	-0.06212	-0.60179
0.400	2.36070	-0.00329	-0.54470
0.425	2.52620	0.05042	-0.49055
0.450	2.69170	0.09914	-0.43932
0.475	2.85720	0.14298	-0.39098
0.500	3.02270	0.18204	-0.34550
0.525	3.18820	0.21642	-0.30287
0.550	3.35370	0.24618	-0.26307
0.575	3.51920	0.27138	-0.22608
0.600	3.68470	0.29208	-0.19189
0.625	3.85020	0.30833	-0.16050
0.650	4.01570	0.32015	-0.13189
0.675	4.18120	0.32756	-0.10606
0.700	4.34670	0.33059	-0.08300
0.725	4.51220	0.32922	-0.06272
0.750	4.67770	0.32347	-0.04521
0.775	4.84320	0.31331	-0.03049
0.800	5.00870	0.29873	-0.01854
0.825	5.17420	0.27968	-0.00939
0.850	5.33970	0.25614	-0.00305
0.875	5.50520	0.22804	0.00048
0.900	5.67070	0.19533	0.00118
0.910	5.73690	0.18094	0.00066
0.920	5.80310	0.16579	-0.00032
0.930	5.86930	0.14988	-0.00175
0.940	5.93550	0.13320	-0.00365
0.950	6.00170	0.11575	-0.00600
0.960	6.06790	0.09752	-0.00882
0.970	6.13410	0.07850	-0.01210
0.980	6.20030	0.05869	-0.01585
0.990	6.26650	0.03808	-0.02006
1.000	6.33270	-0.00000	-0.00000

1/4 TIP TRAILING EDGE SECTION
(HOT RADIUS = 25.14900)

PERCENT X	X	Y TOP	Y BOT
0.0	-0.33605	-1.40187	-1.40187
0.010	-0.31886	-1.32629	-1.44336
0.020	-0.25167	-1.27422	-1.41314
0.030	-0.18448	-1.22332	-1.38327
0.040	-0.11729	-1.17356	-1.35377
0.050	-0.05010	-1.12493	-1.32462
0.060	0.01709	-1.07739	-1.29582
0.070	0.08428	-1.03092	-1.26737
0.080	0.15147	-0.98551	-1.23927
0.090	0.21866	-0.94111	-1.21151
0.100	0.28585	-0.89773	-1.18410
0.125	0.45382	-0.79354	-1.11705
0.150	0.62180	-0.69524	-1.05212
0.175	0.78977	-0.60258	-0.98925
0.200	0.95775	-0.51533	-0.92844
0.225	1.12572	-0.43330	-0.86966
0.250	1.29370	-0.35632	-0.81288
0.275	1.46167	-0.28421	-0.75810
0.300	1.62965	-0.21684	-0.70529
0.325	1.79762	-0.15408	-0.65444
0.350	1.96560	-0.09580	-0.60554
0.375	2.13357	-0.04192	-0.55858
0.400	2.30155	0.00767	-0.51355
0.425	2.46952	0.05305	-0.47045
0.450	2.63750	0.09429	-0.42926
0.475	2.80547	0.13146	-0.39000
0.500	2.97345	0.16461	-0.35265
0.525	3.14142	0.19380	-0.31722
0.550	3.30940	0.21907	-0.28372
0.575	3.47737	0.24046	-0.25214
0.600	3.64535	0.25800	-0.22249
0.625	3.81332	0.27171	-0.19478
0.650	3.98130	0.28161	-0.16902
0.675	4.14927	0.28773	-0.14522
0.700	4.31725	0.29005	-0.12340
0.725	4.48522	0.28859	-0.10357
0.750	4.65320	0.28334	-0.08576
0.775	4.82117	0.27429	-0.06998
0.800	4.98915	0.26144	-0.05624
0.825	5.15712	0.24476	-0.04459
0.850	5.32510	0.22421	-0.03504
0.875	5.49307	0.19978	-0.02764
0.900	5.66105	0.17142	-0.02240
0.910	5.72824	0.15897	-0.02092
0.920	5.79543	0.14587	-0.01980
0.930	5.86262	0.13214	-0.01903
0.940	5.92981	0.11776	-0.01863
0.950	5.99700	0.10273	-0.01859
0.960	6.06419	0.08704	-0.01891
0.970	6.13138	0.07070	-0.01960
0.980	6.19857	0.05370	-0.02067
0.990	6.26576	0.03603	-0.02212
1.000	6.33295	-0.00000	-0.00000

TIP TRAILING EDGE SECTION
(HOT RADIUS = 27.04300)

PERCENT X	X	Y TOP	Y BOT
0.0	-0.48680	-0.63221	-0.63221
0.010	-0.41860	-0.57440	-0.67660
0.020	-0.35040	-0.54937	-0.66821
0.030	-0.28220	-0.52477	-0.65984
0.040	-0.21400	-0.50061	-0.65148
0.050	-0.14580	-0.47687	-0.64312
0.060	-0.07760	-0.45356	-0.63478
0.070	-0.00940	-0.43067	-0.62645
0.080	0.05880	-0.40820	-0.61813
0.090	0.12700	-0.38615	-0.60982
0.100	0.19520	-0.36452	-0.60152
0.125	0.36570	-0.31224	-0.58084
0.150	0.53620	-0.26253	-0.56023
0.175	0.70670	-0.21534	-0.53972
0.200	0.87720	-0.17065	-0.51930
0.225	1.04770	-0.12844	-0.49899
0.250	1.21820	-0.08869	-0.47880
0.275	1.38870	-0.05136	-0.45874
0.300	1.55920	-0.01644	-0.43882
0.325	1.72970	0.01608	-0.41905
0.350	1.90020	0.04622	-0.39945
0.375	2.07070	0.07401	-0.38004
0.400	2.24120	0.09945	-0.36083
0.425	2.41170	0.12256	-0.34184
0.450	2.58220	0.14335	-0.32310
0.475	2.75270	0.16182	-0.30463
0.500	2.92320	0.17799	-0.28645
0.525	3.09370	0.19186	-0.26859
0.550	3.26420	0.20344	-0.25109
0.575	3.43470	0.21274	-0.23397
0.600	3.60520	0.21975	-0.21726
0.625	3.77570	0.22449	-0.20099
0.650	3.94620	0.22694	-0.18520
0.675	4.11670	0.22712	-0.16992
0.700	4.28720	0.22501	-0.15517
0.725	4.45770	0.22062	-0.14098
0.750	4.62820	0.21394	-0.12736
0.775	4.79870	0.20498	-0.11433
0.800	4.96920	0.19371	-0.10190
0.825	5.13970	0.18013	-0.09005
0.850	5.31020	0.16424	-0.07879
0.875	5.48070	0.14603	-0.06811
0.900	5.65120	0.12547	-0.05797
0.910	5.71940	0.11659	-0.05407
0.920	5.78760	0.10734	-0.05025
0.930	5.85580	0.09770	-0.04651
0.940	5.92400	0.08769	-0.04285
0.950	5.99220	0.07729	-0.03926
0.960	6.06040	0.06652	-0.03575
0.970	6.12860	0.05536	-0.03232
0.980	6.19680	0.04382	-0.02895
0.990	6.26500	0.03190	-0.02566
1.000	6.33320	-0.00001	-0.00001

TIP LEADING EDGE SECTION
(HOT RADIUS = 26.07001)

PERCENT X	X	Y TOP	Y BOT
0.0	-0.43455	-1.08479	-1.08479
0.010	-0.36687	-1.01759	-1.12716
0.020	-0.29919	-0.97742	-1.10632
0.030	-0.23152	-0.93803	-1.08567
0.040	-0.16384	-0.89942	-1.06524
0.050	-0.09617	-0.86158	-1.04500
0.060	-0.02849	-0.82451	-1.02495
0.070	0.03919	-0.78818	-1.00511
0.080	0.10686	-0.75260	-0.98546
0.090	0.17454	-0.71774	-0.96600
0.100	0.24222	-0.68361	-0.94674
0.125	0.41141	-0.60138	-0.89943
0.150	0.58060	-0.52348	-0.85333
0.175	0.74979	-0.44977	-0.80841
0.200	0.91898	-0.38015	-0.76468
0.225	1.08817	-0.31453	-0.72213
0.250	1.25736	-0.25280	-0.68075
0.275	1.42655	-0.19487	-0.64055
0.300	1.59574	-0.14067	-0.60151
0.325	1.76493	-0.09014	-0.56364
0.350	1.93412	-0.04318	-0.52694
0.375	2.10331	0.00024	-0.49141
0.400	2.27250	0.04018	-0.45706
0.425	2.44169	0.07670	-0.42391
0.450	2.61088	0.10983	-0.39193
0.475	2.78007	0.13962	-0.36117
0.500	2.94926	0.16609	-0.33162
0.525	3.11845	0.18927	-0.30329
0.550	3.28764	0.20920	-0.27622
0.575	3.45683	0.22591	-0.25040
0.600	3.62602	0.23939	-0.22586
0.625	3.79521	0.24967	-0.20260
0.650	3.96440	0.25676	-0.18067
0.675	4.13359	0.26067	-0.16006
0.700	4.30278	0.26139	-0.14082
0.725	4.47197	0.25894	-0.12296
0.750	4.64116	0.25330	-0.10650
0.775	4.81036	0.24447	-0.09147
0.800	4.97955	0.23245	-0.07786
0.825	5.14874	0.21721	-0.06572
0.850	5.31793	0.19873	-0.05506
0.875	5.48712	0.17700	-0.04590
0.900	5.65631	0.15199	-0.03826
0.910	5.72398	0.14106	-0.03563
0.920	5.79166	0.12960	-0.03326
0.930	5.85933	0.11761	-0.03112
0.940	5.92701	0.10508	-0.02924
0.950	5.99469	0.09201	-0.02761
0.960	6.06236	0.07840	-0.02623
0.970	6.13004	0.06424	-0.02511
0.980	6.19772	0.04955	-0.02424
0.990	6.26539	0.03430	-0.02365
1.000	6.33307	-0.00001	-0.00001

LIST OF ABBREVIATIONS AND SYMBOLS

ACC	active clearance control
ADP	aerodynamic design point
Al	aluminum
B	constant for the law of the wall
bx	axial chord
c	Celsius (centegrade)
c/a	cooling airflow
C _f	skin friction, $2 \tau_w / \rho U_\infty^2$
Cl	climb
cm	centimeter
C _p	pressure coefficient
cps	cycle per second
Cr	cruise
C _x /U	ratio of throughflow velocity to wheel speed
deg	degree, angle
EGV	exit guide vane
F	Fahrenheit
FI	flight idle
FPS	flight propulsion system
ft	feet
Δh	specific work
H	shape factor, δ^*/θ
HPC	high-pressure compressor
HPT	high-pressure turbine
$\Delta h/U^2$	work factor
I	idle
IC/LS	integrated core/low spool
ID	inner diameter
IGV	inlet guide vane
in	inch
k	Von Karman's constant
K	spring rate

LIST OF ABBREVIATIONS AND SYMBOLS (Cont'd)

L	length
lb	pound
LE	leading edge
L/H	length to height ratio
LPC	low-pressure compressor
L _{pg}	platform gap
LPT	low-pressure turbine
m	meter
M ₁	airfoil inlet Mach number
M ₂	airfoil exit Mach number
M _n	mach number
N	Newton
N ₁	low-pressure rotor speed, rpm
OD	outer diameter
PDR	Preliminary Design Review
P _s	static pressure
P _t	total pressure
P _{t3}	pressure at station 3
ΔP _T /P _T	total pressure loss
$\overline{q^2}$	turbulence energy, $\overline{u^2} + \overline{v^2} + \overline{w^2}$
R	radius
Re _θ	Reynolds number, $U_\infty \theta / \nu$, Boundary Layer Momentum Loss Thickness
rpm	revolutions per minute
s	surface distance
SLTO	sea level takeoff
ss	steady state
T	temperature
TE	trailing edge
TLPR	Transient Liquid Phase
Ti	titanium
T/O	takeoff

LIST OF ABBREVIATIONS AND SYMBOLS (Cont'd)

u	fluctuating streamwise component of velocity
$\frac{u}{v^*}$	Dimensionless turbulence intensity $\sqrt{u^2}/v^*$
u^2	streamwise component of turbulence intensity
U^+	dimensionless velocity, U/v^*
U	wheel speed
v	fluctuating velocity perpendicular to test wall
$\frac{v}{v^*}$	normal component of turbulence intensity
V_m	Velocity Ratio, mean - Relationship between the blade wheel speed and amount of turbine work output
	$V_m = \sqrt{\frac{U^2 (\text{No. of Stages})}{2gJ \Delta h}}$
v^*	friction velocity $\sqrt{\tau \omega / \rho}$
$\overline{w^2}$	traverse component of turbulence intensity
w_{acc}	active clearance control flow
w_{ae}	core engine airflow
w_p	platform axial width
y	normal distance from wall
y^+	dimensionless distance from wall, $y v^* / \nu$
α	angle
α_G	platform gap angle
α_T	taper angle
β_1	airfoil inlet angle
β_2	airfoil exit angle
δ	boundary layer thickness
δ_{aero}	Aerodynamic damping
Δ	difference
ρ	density
σ_B	bending stress
σ_{Brg}	bearing stress
σ_C	compression stress
σ_H	hoop stress
Θ	angle
Θ	Boundary Layer Momentum Loss Thickness
ν	Kinematic viscosity
$\tau \omega$	wall shear stress
ω	frequency

REFERENCES

1. Leach, K. and Thulin, R.: "Energy Efficient Engine Turbine Transition Duct Model Test Program Technology Report", February 1982, pending publication.
2. Sharma, O. P. et al: "Energy Efficient Engine Low-Pressure Turbine Subsonic Cascade Technology Report", January 1982; NASA CR-165592 (PWA 5594-167).
3. Gardner, W.B.: "Energy Efficient Engine Low-Pressure Turbine Boundary Layer Technology Report", April 1981; NASA CR-165338 (PWA 5594-141).



DISTRIBUTION LIST

GOVERNMENT AGENCIES

NASA Headquarters
600 Independence Ave., SW
Washington, D.C. 20546
Attention: RTP-6/R.S. Colladay
 RTP-6/C.C. Rosen
 RTP-6/L. Harris
 RRP-6/J. Facey
 Library

NASA-Lewis Research Center
21000 Brookpark Road
Cleveland, OH 44135

Attention: D. L. Nored	MS 301-2
C. C. Ciepluch	MS 301-4 (20 copies)
J. W. Schaefer	MS 301-4
P. G. Batterton	MS 301-4
G. K. Sievers	MS 301-2
Library	MS 60-3 (2 copies)
Report Control Office	MS 5-5
Tech Utilization Office	MS 3-19
M. A. Beheim	MS 3-5
M. J. Hartmann	MS 5-3
R. A. Rudey	MS 60-4
R. A. Weber	MS 500-127
W. C. Strack	MS 501-10
T. P. Moffitt	MS 77-2
J. E. Rohde	MS 77--2
R. L. Dreshfield	MS 105-1
A. Long	MS 500-305
W. M. Braithwaite	MS 500-208
L. Reid	MS 5-9
AFSC Liaison Office	MS 501-3
Army R&T Propulsion Lab	MS 302-2

DISTRIBUTION LIST (Cont'd)

NASA-Lewis Research Center 21000 Brookpark Road Cleveland, Ohio 44135 Attention: D.L. Nored	MS 301-2	NASA-Lewis Research Center 21000 Brookpark Road Cleveland, Ohio 44135 Attention: R.J. Weber	MS 500-127
NASA-Lewis Research Center 21000 Brookpark Road Cleveland, Ohio 44135 Attention: C.C. Ciepluch	MS 301-4 20 Copies	NASA-Lewis Research Center 21000 Brookpark Road Cleveland, Ohio 44135 Attention: W.C. Strack	MS 501-10
NASA-Lewis Research Center 21000 Brookpark Road Cleveland, Ohio 44135 Attention: J.W. Schaefer	MS 301-4	NASA-Lewis Research Center 21000 Brookpark Road Cleveland, Ohio 44135 Attention: T.P. Moffitt	MS 77-2
NASA Lewis Research Center 21000 Brookpark Road Cleveland, Ohio 44135 Attention: P.G. Batterton	MS 301-4	NASA-Lewis Research Center 21000 Brookpark Road Cleveland, Ohio 44135 Attention: J.E. Rohde	MS 77-2
NASA-Lewis Research Center 21000 Brookpark Road Cleveland, Ohio 44135 Attention: G.M. Sievers	MS 301-2	NASA-Lewis Research Center 21000 Brookpark Road Cleveland, Ohio 44135 Attention: R. L. Dreshfield	MS 105-1
NASA-Lewis Research Center 21000 Brookpark Road Cleveland, Ohio 44135 Attention: Library	MS 60-3 2 Copies	NASA-Lewis Research Center 21000 Brookpark Road Cleveland, Ohio 44135 Attention: A. Long	MS 500-305
NASA-Lewis Research Center 21000 Brookpark Road Cleveland, Ohio 44135 Attention: Report Control Office	MS 5-5	NASA-Lewis Research Center 21000 Brookpark Road Cleveland, Ohio 44135 Attention: W.M. Braithwaite	MS 500-208
NASA-Lewis Research Center 21000 Brookpark Road Cleveland, Ohio 44135 Attention: Tech Utilization Office	MS 3-19	NASA-Lewis Research Center 21000 Brookpark Road Cleveland, Ohio 44135 Attention: L. Reid	MS 5-9
NASA-Lewis Research Center 21000 Brookpark Road Cleveland, Ohio 44135 Attention: M.A. Beheim	MS 3-5	NASA-Lewis Research Center 21000 Brookpark Road Cleveland, Ohio 44135 Attention: AFSC Liaison Office	MS 501-3
NASA-Lewis Research Center 21000 Brookpark Road Cleveland, Ohio 44135 Attention: M.J. Hartmann	MS 3-7	NASA-Lewis Research Center 21000 Brookpark Road Cleveland, Ohio 44135 Attention: Army R&T Propulsion	MS 302-2
NASA-Lewis Research Center 21000 Brookpark Road Cleveland, Ohio 44135 Attention: R.A. Rudey	MS 86-5	NASA Ames Research Center Moffett Field, CA 94035 Attention: 202-7/M. H. Waters Library	

DISTRIBUTION LIST (Cont'd)

NASA Langley Research Center
Langley Field, VA 23365
Attention: R. Leonard
D. Maiden
L. J. Williams
Library

NASA Dryden Flight Research Center
P.O. Box 273
Edwards, CA 93523
Attention: J. A. Albers
Library

NASA Scientific and Technical Information
Facility
P.O. Box 8757
B.W.I. Airport, MD 21240
Attention: Acquisition Branch (10 copies)

Department of Defense
Washington, D.C. 20301
Attention: R. Standahar 3D1089 Pentagon

Wright-Patterson Air Force Base
Dayton, Ohio 45433
Attention: APL Chief Scientist AFWAL/PS

Wright-Patterson Air Force Base
Dayton, Ohio 45433
Attention: E.E. Abell ASD/YZE

Wright-Patterson Air Force Base
Dayton, Ohio 45433
Attention: H.I. Bush AFWAL/POT

Wright-Patterson Air Force Base
Dayton, Ohio 45433
Attention: E.E. Bailey (NASA Liaison)
AFWAL/NASA

Wright-Patterson Air Force Base
Dayton, Ohio 45433
Attention: R.P. Carmichael ASD/XRHI

Wright-Patterson Air Force Base
Dayton, Ohio 45433
Attention: R. Ellis ASD/YZN

Wright-Patterson Air Force Base
Dayton, Ohio 45433
Attention: W.H. Austin, Jr. ASD/ENF

Eustis Directorate
U.S. Army Air Mobility
R&D Laboratory
Fort Eustis, VA 23604
Attention: J. Lane, SAVDL-EU-Tapp

Navy Department
Naval Air Systems Command
Washington, D. C. 20361
Attention: W. Koven AIR-03E

Navy Department
Naval Air Systems Command
Washington, D. C. 20361
Attention: J.L. Byers AIR-53602

Navy Department
Naval Air Systems Command
Washington, D. C. 20361
Attention: E.A. Lichtman AIR-330E

Navy Department
Naval Air Systems Command
Washington, D. C. 20361
Attention: G. Derderian AIR-5362C

NAVAL AIR Propulsion Test Center
Trenton, NJ 08628
Attention: J. J. Curry
A. A. Martino

U.S. Naval Air Test Center
Code SY-53
Patuxent River, MD 20670
Attention: E. A. Lynch

USAVRAD Command
PO Box 209
St. Louis, MO 63166
Attention: Robert M. Titus (ASTIO)

Department of Transportation
NASA/DOT Joint Office of Noise Abatement
Washington, D.C. 20590
Attention: C. Foster

Federal Aviation Administration
Noise Abatement Division
Washington, D.C. 20590
Attention: E. Sellman AEE-120

Environmental Protection Agency
1835 K Street, NW
Washington, D.C. 20460
Attention: J. Schettino
J. Tyler

Environmental Protection Agency
2565 Plymouth Road
Ann Arbor, MI 48105
Attention: R. Munt

DISTRIBUTION LIST (Cont'd)

Federal Aviation Administration
12 New England Executive Park
Burlington, MA 18083
Attention: Jack A. Sain, ANE-200

Curtiss Wright Corporation
Woodridge, NJ 07075
Attention: S. Lombardo
S. Moskowitz

Detroit Diesel Allison Div. G.M.C.
P.O. Box 894
Indianapolis, IN 46206
Attention: W. L. McIntire

Cummins Engine Co.
Technical Center
500 S. Poplar
Columbus, IN 47201
Attention: J. R. Drake

AVCO/Lycoming
550 S. Main Street
Stratford, CT 06497
Attention: H. Moellmann

Detroit Diesel Allison Div. G.M.C.
333 West First Street
Dayton, Ohio 45402
Attention: F. H. Walters

The Garrett Corporation
AIRResearch Manufacturing Co.
Torrance, CA 90509
Attention: F. E. Faulkner

The Garrett Corporation
AIRResearch Manufacturing Co.
402 S. 36 Street
Phoenix, AZ 85034
Attention: Library

General Electric Co./AEG
One Jimson Road
Evendale, Ohio 45215
Attention: R.W. Bucy (3 copies)
T. F. Donohue

Pratt & Whitney Aircraft Group/UTC
Government Products Division
P.O. Box 2691
West Palm Beach, FL 33402
Attention: B. A. Jones

The Garrett Corporation
AIRResearch Aviation Co.
19201 Susana Road
Compton, CA 90221
Attention: N. J. Palmer

AIRResearch Manufacturing Co.
111 South 34th Street
P.O. Box 5217
Phoenix, AZ 85010
Attention: C. E. Corrigan
(93-120/503-4F)

Williams Research Co.
2280 W. Maple Road
Walled Lake, MI 48088
Attention: R. VanNimwegen
R. Horn

Teledyne CAE, Turbine Engines
1330 Laskey Road
Tolendo, Ohio 43612
Attention: R. H. Gaylord

General Electric Co./AEG
1000 Western Ave.
Lynn, MA 01910
Attention: R. E. Neitzel

Pratt & Whitney Aircraft Group/UTC
Commercial Products Division
East Hartford, Ct 06108
Attention: W. Gardner
I. Mendelson

Boeing Commercial Airplane Co.
P.O. Box 3707
Seattle, WA 98124
Attention: P. E. Johnson MS 9H-46
D. C. Nordstrom MS 73-01

Boeing Aerospace Co.
P.O. Box 3999
Seattle, Wa 98124
Attention: D. S. Miller MS 40-26
H. Higgins

The Boeing Co., Wichita Division
Wichita, KS 67210
Attention: D. Tarkelson

Douglas Aircraft Company
McDonnell Douglas Corp.
3855 Lakewood Boulevard
Long Beach, CA 90846
Attention: R. T. Kawai Code 36-41
M. Klotzsche

DISTRIBUTION LIST (Cont'd)

Lockheed California Co. Burbank, CA 91502 Attention: J. F. Stroud, Dept. 75-42 R. Tullis, Dept. 75-21 J. I. Benson	Pan American World Airways, Inc. JFK International Airport Jamica, NY 11430 Attention: J. G. Borger A. MacLarty
General Dynamics Convair P. O. Box 80847 San Diego, CA 92138 Attention: S. Campbell, MZ 632-00	United Airlines San Francisco International Airport Maint. Operations Center San Francisco, CA 94128 Attention: J. J. Overton
Rockwell International International Airport Los Angeles Division Los Angeles, CA 90009 Attention: A. W. Martin	Hamilton Standard Bradley Field Windsor Locks, CT 06096 Attention: P. J. Dumais, MS 1A-3-1 A. T. Reiff, MS 1-2-2
Gates Learjet Corp. P. O. Box 7707 Wichita, KS 67277 Attention: E. Schiller	Fluidyne Engineering Corp. 5900 Olson Memorial Highway Minneapolis, MN 55422 Attention: J. S. Holdhusen
McDonnell Aircraft Co. McDonnell Douglas Corp. P. O. Box 516 St. Louis, MO 63166 Attention: F. C. Claser Dept. 243	Rohr Corporation P.O. Box 878 Foot & H Street Chula Vista, CA 92012 Attention: Library
Lockheed Georgia Co. Marietta, GA 30060 Attention: H. S. Sweet	Solar Division International Harvester 2200 Pacific Highway San Diego, CA 92112 Attention: Library
Grumman Aerospace Corp. South Oyster Bay Road Bethpage, New York 11714 Attention: C. Hoeltzer	Gas Dynamics Laboratories Aerospace Engineering Building University of Michigan Ann Arbor, MI 48109 Attention: Dr. C. W. Kaufmann
American Airlines Maint. & Engr. Center Tulsa, OK 74151 Attention: W. R. Neeley	Massachusetts Inst. of Technology Dept. of Astronautics & Aeronautics Cambridge, MA 02139 Attention: Jack Kerrebrock
Eastern Airlines International Airport Miami, FL 33148 Attention: A. E. Fishbein	Massachusetts Inst. of Technology Dept. of Structural Mechanics Cambridge, MA 02139 Attention: James Mar
Delta Airlines, Inc. Hartsfield-Atlanta International Airport Atlanta, GA 30320 Attention: C. C. Davis	Westinghouse Electric Corp. P.O. Box 5837 Beulah Road Pittsburgh, PA 15236 Attention: Library
TransWorld Airlines 605 Third Avenue New York, NY 10016 Attention: A. E. Carrol	

DISTRIBUTION LIST (Cont'd)

University of Tennessee
Space Institute
Tullahoma, TN 37388
Attention: Dr. V. Smith

TRW Equipment Group
TRW Inc.
23555 Euclid Ave.
Cleveland, OH 44117
Attention: I. Toth

Aerospace Corporation
R & D Center
Los Angeles, CA 90045
Attention: Library

George Shevlin
P.O. Box 1925
Washington, D.C. 20013

Brunswick Corporation
2000 Brunswick Lane
Deland, FL 32720
Attention: A. Erickson

Pennsylvania State University
Department of Aerospace Engineering
233 Hammond Building
University Park, Pennsylvania 16802
Attention: Dr. B. Lakshminarayana

Iowa State University
Department of Mechanical Engineering
Ames, Iowa 50011
Attention: Dr. Patrick Kavanagh

Detroit Diesel Allison
P.O. Box 894
Indianapolis, Indiana 46206
Attention: Mr. Robert Delanie
Speed Code U29A
Mr. H. L. Stocker
Speed Code U21A

KVB Inc*
18006 Skypark Blvd.
P.O. Box 19518
Irvine CA 92714
Attention: A. M. Mellor